The University Of Sheffield.

Development and Optimisation of Analytical Techniques for Non-Woven Flue Gas Filtration Media

Daniel Francis Curry

A thesis submitted in partial fulfilment of the requirements for the degree of Doctor of Engineering (EngD)

The University of Sheffield
Faculty of Engineering
School of Mechanical Engineering

Submission Date

13th December 2022

- This Page is Intentionally Left Blank -

Abstract

Combustion of solid fuels produces solid and gaseous emissions which are harmful to the environment. Filtration, in combination with additional process such as sorbent injection aim to reduce the concentration of these emissions before being released into the atmosphere. Bag house filtration composes of multiple bags of filtration media that collects the solids from gas streams. In power generation, these units collect fly ash and other solids from the flue gas, depositing them into a hopper for disposal.

Industrially new and used filtration media from various sites were examined. Analytical techniques such as air permeability, mass/density, and thickness were used to determine the variation within a defined sample size. Whilst the British Standards were used as the baseline methodology, they required a significantly small surface area for analysis in comparison to surface area of a flue gas filtration bag. When the sample size was increased, results suggested a relationship between the data and the diameter of the bag for air permeability, mass/density, and thickness. In addition, a preliminary longevity study was explored using new and industrially used media. This study used μCT, SEM, air permeability, mass/density, and thickness measurements to illustrate how the media changed once it had reached a pre-defined end point. Whilst these results are preliminary, the critical evaluation of the data suggested how longevity may be calculated.

As the sample size increases, so does the time required to perform analysis. The work presented in this thesis demonstrated the potential variation in a sample and illustrated relationships about the circumference of the bag. These relationships could be investigated without severely impacting the sample turnaround time. This work is being discussed with members of the British Standard Working Group 7 to update their standards to better reflect and understand the potential variation across air permeability, mass/density, and thickness analysis.

- This Page is Intentionally Left Blank -

Declaration of Authorship

The author of this body of work hereby declares their awareness to the University of Sheffield's guidelines on the use of unfair means (published: https://www.sheffield.ac.uk/new-students/unfair-means). The work has not been submitted for an award at any establishment, in both academic and industrial settings. Furthermore, the author confirms that the submitted work is their own. Where joint authorship has led to the publication, each authors contribution and appropriate accreditation of their work towards the publication is explicitly stated below.

Conference Papers

Paper 1: "High Resolution Permeability Study of Used Non-woven Filtration Media from a U.K. Energy from Waste Combustion Site" -[1]

Description: This paper focused on part of research conducted in Chapter/Section 6. The study focused largely on the analysis of the air permeability variation across the as received, post cleaned, filtrate/cake, and difference between new and cleaned media. Furthermore, the paper presented a brief statistical summary of the fixed machine variable cross direction variation.

The aim of this paper was to highlight the potential variation across the full filtration bag, and the effect that selecting three sample points in each vertical third could have on the reported air permeability. The study used the British standards as a baseline but assessed a total surface area of >10%, as opposed to the standard which tested <1%. Thus, the study illustrated the variation across the bag more accurately.

Contribution: Daniel Curry (Carried out research and wrote up findings 85%), Ben Dannatt (Reviewed 5%), Jane Howarth (Reviewed 5%), Willian Nimmo (Reviewed 5%)

Conference Presentations

1st Feria conference in Nottingham, United Kingdom dated April 2021 (presentation)

Title: Evaluation of Depth Filtration in Non-woven Filtration Media Using Micro-Computed Tomography (μCT) Techniques – A Case Study from a Power Generation Site located in Teesside, United Kingdom

Description: Utilisation of industrial relevant samples taken at fixed positions to determine the porosity variation across the thickness of the sample.

Contribution: Daniel Curry (Carried out research and wrote up findings 85%), Ben Dannatt (Reviewed 5%), Jane Howarth (Reviewed 5%), Willian Nimmo (Reviewed 5%)

Filtech 2022 in Cologne Germany dated March 2022 (presentation)

Title: High Resolution Permeability Study of Used Non-woven Filtration Media from a U.K. Energy from Waste Combustion Site

Description: Presentation of the research and findings published in paper 1 [1].

The aim of this study was to assess how the air permeability of a used filtration bag varied. Analysis was performed in the as received (AR) state and post cleaned (PC) state. Results suggested a parabolic like relationship across the fixed machine, variable cross direction of the bag. The resultant air permeability was visually shown to vary, depending on where the sample point was taken. This study showed the industry and wider audience that taking three samples may not be fully representative of the actual air permeability of the bag.

Contribution: Daniel Curry (Carried out research and wrote up findings 85%), Ben Dannatt (Reviewed 5%), Jane Howarth (Reviewed 5%), Willian Nimmo (Reviewed 5%)

Other Presentations

Fuel and Energy Research Meeting in Sheffield, United Kingdom dated April 2022 (presentation)

Title: Air Permeability Variation Across a Used, Non-woven, Filter Media Bag

Description: Based off the research and analysis of paper 1 [1], the presentation depicted further analysis of the variation, which included preliminary analysis of both axial variations. The work detailed the potential air permeability variation across a known sample size utilising current standards through statistical analysis.

The overall aim was to show that when considering standards, an understanding of the potential variation is needed. The recommendation was that the reporting of the confidence interval should not be voluntary.

Contribution: Daniel Curry (Carried out research and wrote up findings 85%), Ben Dannatt (Reviewed 5%), Jane Howarth (Reviewed 5%), Willian Nimmo (Reviewed 5%)

39th International Symposium on Combustion in Vancouver, Canada dated July 2022 (poster presentation)

Title: Understanding the Impact Particulate Matter has on Filtration Media (work in progress)

Description: This poster presentation presented the current work and findings using the filtration test rig which was commissioned for operation circa. June 2022. The current, ongoing study is to ascertain if ultimate failure can be determined using industrial relevant samples. To do so, a baseline is required which is currently defined as a new, unused sample of the same media and expected filtration and cleaning characteristics.

The ultimate aim is to develop this further, using the pilot scale fluidised bed to generate our own samples to further support and improve the model to improve accuracy and surrounding methodologies.

Contribution: Daniel Curry (Carried out research and wrote up findings 80%), Peter Cole (Observed experiment and Reviewed 5%) Ben Dannatt (Reviewed 5%), Jane Howarth (Reviewed 5%), Willian Nimmo (Reviewed 5%)

Acknowledgments

First, I would like to thank my academic and industrial supervisors, Professor Bill Nimmo, Dr. Ben Dannatt, Dr. Jane Howarth, and Barry Goulden. Their support, discussions, and guidance throughout the past four years have been insightful and helped me shape into the researcher I am now. Whilst working with the industrial partner company, Durham Filtration, I learnt a valuable insight into the world outside academia. Given the chance to work on various analytical/consultancy projects across the country, provided me with a unique perspective of how my research could impact the community. I am grateful of their support during the EngD.

Next, the EPSRC Centre for Doctoral Training (CDT) in Carbon Capture and Storage and Cleaner Fossil Energy (CCSCFE), led by Professor Colin Snape, for providing me with the opportunity to learn, develop, and grow my knowledge of a wide range of topics (from energy policies to various power generation technologies). Particular thanks go to Amnael Orozco (Department of Oncology & Metabolism, University of Sheffield) and Stuart Micklethwaite (Leeds Electron Microscopy and Spectroscopy Centre, University of Leeds) for their tuition and guidance about performing sample evaluation. My friends, particularly James Harman-Thomas and Thomas Carr deserve a special thanks for their support through every twist and turn on this journey.

Last, but not least, is my gratitude and thankfulness to my parents and family members. Many of whom have often endured listening to me sound out ideas and concepts (particularly my nephews Bailey, Harry, and Daisy the cockapoo, who had no choice but to listen to me and provide emotional support). Without my families support and dedication, this work would not have been possible.

Contents

List of Figures

List of Tables

List of Equations

Nomenclature

Abbreviations

Abbreviation	Definition	Abbreviation	Definition
AR	As Received	NIR	Near Infrared
ASTM	American Society for Testing Materials	NOx	Nitrogen Oxides
BS	British Standard	MWe	Megawatt Electrical
BSI	British Standard Institute	OPC	Optical Particle Counter
CCS	Carbon Capture Storage	PACT	Pilot Advanced-Scale Capture Technology National Facilities
CFD	Computational Fluid Dynamics	PAH	Polycyclic Aromatic Hydrocarbons
CoD	Cleaning on Demand	PC	Post Cleaned
CoT	Cleaning on Time	PM	Particulate Matter
CT	Computer Tomography	PPS	Polyphenylene Sulphide
DIN	German Institute for Standardisation (Deutsches Institute für Normung)	PSD	Particle Size Distribution
DP	Differential Pressure	PTFE	Polytetrafluoroethylene
EDX	Energy Dispersive X-ray	P84	Type of Fibre
EFW	Energy from Waste	SEM	Scanning Electron Microscopy
ESP	Electrostatic Precipitator	SFT	Single Fibre Theory
FAR	Filter Assessment Rig	SOx	Sulphur Oxides
FCVM	Fixed Cross, Variable Machine	TGA	Thermo-Gravimetric Analysis
FMVC	Fixed Machine, Variable Cross	UK	United Kingdom
HCL	Hydrogen Chloride	VDI	Verein Deutscher Ingenieure – association of German engineers that promotes advancements in technologies and produce standards
HF	Hydrogen Fluoride	VN	Virgin/New
HU	Hounsfield Unit	VOC	Volatile Organic Compounds
ISO	International Standards Organisation	XRD	X-Ray Diffraction
LCCC	Low Carbon Combustion Centre	XRF	X-Ray Fluorescence

Greek Alphabet

Symbol	Description	Unit
α	Packing density	[-]
Δe	Percentage error	[-]
ΔL	Change in length	[M]
ΔP	Pressure drop across a given point	$[ML^{-1}T^{-2}]$
∇P	Pressure gradient	$[ML^{-2}T^{-2}]$
ΔP_m	Pressure drop across the media	$[ML^{-1}T^{-2}]$
ΔP_c	Pressure drop across the filtration cake	$[ML^{-1}T^{-2}]$
ϵ	Porosity in the defined volume	[-]
η_d	Collection efficiency due to diffusion	[-]
η_g	Collection efficiency due to gravity	[-]
η_i	Collection efficiency due to inertia	[-]
η_{id}	Collection efficiency due to direct interception	[-]
η_T	Total Collection efficiency	[-]
μ	Dynamic Viscosity of the fluid/gas	$[ML^{-1}T^{-1}]$
π	Pi – constant	[-]
ρ_f	Fibre density	$[ML^{-3}]$
ρ_g	Gaseous density	$[ML^{-3}]$
ρ_p	Particle/filtrate density	$[ML^{-3}]$
σ	Tensile strength	$[MLT^{-2}]$
φ_{AR}	Air permeability in the as received state	$[L^3L^{-2}T^{-1}]$
φ_{PC}	Air permeability in the post cleaned state	$[L^3L^{-2}T^{-1}]$

Roman Alphabet

Symbol	Description	Unit
A	Surface Area	$[M^2]$
A_{bag}	Surface area of the filtration bag	$[M^2]$
$A_{collector}$	Surface area of the collector	$[M^2]$
Cd	Parameter for the diffusional efficiency	[-]
$C_{m,x}$	Mass concentration of subject "x"	$[ML^{-3}]$
Cr	Parameter for the direct interception efficiency	[-]
D	Mean equivalent pore diameter	[L]
D_{eq}	Equivalent diameter	[L]
D_f (or d_f)	Fibre diameter	[L]
D_p (or d_p)	Particle diameter	[L]
E	Collection efficiency	[-]
F	Fibre diameter	[M]
F	Force	$[MLT^{-2}]$
G	Gravity – assumed constant at 9.81	$[LT-^{2}]$
H	Height (also defined thickness by some research)	[M]
K	Permeability tensor	$[L^2]$
k_c	Flow resistivity through the filtration cake	$[L^{-2}T^{-1}]$
k_m	Flow resistivity through the filter media	$[L^{-1}]$
K_p	Flow permeability coefficient	$[M^2]$
Ku	Kuwabara factor	[-]
L	Length (also defined the thickness by some research)	[L]
M_{sample}	Sample Mass	[M]
N_{bag}	Number of filtration bags in the collector	[-]
Nre	Reynolds Number	[-]
P	Penetration efficiency	[-]
Pe	Peclet number	[-]
Q	Volumetric flowrate	$[L^3T^{-1}]$
q	Fluid flux	$[L^3T^{-1}L^{-2}]$
Q_{in}	Volumetric flow of fluid into the filtration unit	$[L^3T^{-1}]$
R	Ratio of the particle diameter over the fibre diameter	[-]
Re	Reynolds number	[-]
St	Stokes number	[-]
T	Time	[T]
T	Thickness	[L]
t_{width}	Width of the sample used during tensile testing	[L]
U	Uniformity	[-]
v_{can}	Can velocity	$[LT^{-1}]$
v_i	Velocity at location "i"	$[LT^{-1}]$
v_s	Superficial velocity of the fluid (Also denoted as V_o, U_o, U_m)	$[LT^{-1}]$
v_t	Settling velocity of a particle within a fluid	$[LT^{-1}]$
W	Deposited mass on the filter	[M]

Chapter 1: Introduction

1.1 Introduction

Analytical techniques are often employed to evaluate the overall health of bag house filtration media. Air permeability [2], [3], mass/density [4], [5], thickness [6], [7], and tensile testing [8], [9] are some of the most common methods used to evaluate flue gas filtration media. Other techniques are available to aid analysis, such as free moisture content determination [10], [11], or imaging techniques Scanning Electron Microscopy (SEM) [12], [13] and microcomputed tomography (μCT) [14], [15] for example. The main challenge faced when performing large scale evaluation of filtration media stems from the cost/benefit analysis. Tomographic and microscopic imaging is expensive, particularly when performed over potentially hundreds of samples. Moisture determination could take over an hour to dry and the capacity of the drying oven limited the number of samples evaluated at any given time. Lastly, the required turnaround time needed to isolate, remove, analyse, and interpretation of data is dependent on the number of samples analysed. As the sample number increases, so does the required analysis time. Consequently, the focal point of most analytical studies, from an industrial perspective, utilised air permeability, mass, and thickness to evaluate the health of the media.

Techniques laid out by the British Standard Institute (BSI) in BS 22031:2021 “Sampling and test method for cleanable filter media taken from filters of systems in operation” [16] included air permeability, but also mentioned some of the above techniques. Whilst the aim of this thesis is not to critically evaluate the standard, it provided a benchmark for the development and optimisation of specific analytical methods used on nonwoven filtration media from the energy sector.

Therefore, the aim of this thesis is to enhance the understanding of the resultant potential variation within various analytical techniques. From this, optimisation/development of analytical methods could account for the variation and establish the effect it may have on the resultant data. Section 1.5 provided a more comprehensive breakdown of this aim, with specific reference to each chapters aims, outputs, and impact on industrial practices.

1.2 Background Theory

1.2.1 Energy Sector

According to the United Kingdom (U.K.)'s government, our energy is sourced primarily from the following: Coal, Natural Gas, Bioenergy and Waste, Nuclear, and Wind/Solar/Hydro [17]. In recent years, the use of coal as a fuel for energy production has decreased [18], largely due to the negative environmental impacts such as CO_2,SO_x,NO_x, and particulate matter (PM) emissions [19], [20]. This reduction transpired due to events such as the 1952 London Smog incident. A review of this incident by Bell and Davis [21] suggested that increased coal burning in the city led to increased SO_x/air pollution and therefore an increased mortality within the population. In recent years, the use of coal has been reduced, due to switching to other forms of energy, reducing the reliance on of coal for power generation [22], [23]. The end of coal power has recently been brought forward to October 2024 [24]. With the reduction of coal from the energy mix, the use of natural gas has increased over recent years to ensure the energy availability of flexibility in the energy generation is followed [17]. One limitation of natural gas is that it is still a non-renewable source of energy being a fossil fuel. Combustion of natural gas primarily produced CO_2 emissions, which negatively impact the environment. One potential way to limit this impact is the use of Carbon Capture Storage (CCS) of the emissions post combustion to reduce this impact [25]. Without CCS, the use of natural gas will have to decline in order to limit global warming [26]. Consequently, a decrease in fossil fuel (non-renewable) sources for energy production will require alternative energy sources such as solar, wind, hydro, nuclear, and biomass to become more prevalent in the energy mix.

Energy sources such as wind, solar, and nuclear are increasing in prevalence within the U.K.'s energy mix [17], [27]. One benefit of wind and solar is that it utilises an energy stream which is seemingly limitless. However, they work on the basis that either a strong enough wind is flowing to spin the turbine blades, or that there is minimal cloud coverage for the suns solar rays to hit the solar panels. This creates a degree of intermittency within the generated power, particularly for solar which is limited to daytime only. Solar power is further dependent on multiple factors such as the capacity and efficiency of the chosen solar panels, square footage needed to meet energy demand, and additional infrastructure such as battery storage [28]–[30]. Resistance to wind power can be further characterised by the "nimbyism" effect, where members of the public are resistant to installation within their community for fear of visual impact and disruption to bird migration paths for example [31]–

[33]. Whilst nuclear power addressed the intermittency of wind and solar, it too faces several barriers to the deployment within the U.K. [34]. Factors such as waste disposal [35], previous process safety [36], and trust and perceived risk factors [37], [38] are examples of factors effecting public opinion and perception to the technology. Biomass and energy from waste (or waste to energy) offered a solution to the intermittency issues.

Biomass combustion uses organic matter from various sources such as virgin wood, waste wood and energy crops to generate power [39]–[42]. The use of a renewable source promotes security in fuel source. The term biomass encompasses variation in the chemical composition dependent on the fuel source/mix [43]. There is debate over the sustainability of biomass, given importation of biomass contributes to global CO_2 emissions [44], which may be reduced by sourcing the fuel more local to the power plant [41]. In addition, the combustion released previously captured CO_2 emissions, along with any by-products such as SO_x, NO_x, acidic compounds, and particulate matter [45]–[47]. Energy from waste (EfW) combustion also suffers from associated emission problems. According to the waste hierarchy, the combustion of waste is only one stage better than the worst, which is to send it to landfill sites [48][49]. EfW encompasses the municipal Solid Waste (MSW) generated by a populous and just like biomass, can vary in composition as illustrated by Habib et al,. [50], Amber et al,. [51], and Sharma et al,. [52]. Therefore, whilst both biomass and EfW combustion processes aid to address the variability associated with wind and solar power generation, (regardless of fuel variation) they still can have associated negative impacts on the environment.

Combustion of solid fuel produces both solid and gaseous emissions. By-products of the combustion process, such as Volatile Organic Compounds (VOC), Polycyclic aromatic hydrocarbons (PAH), and Particulate Matter (PM), but also CO_2, NO_x, SO_x, and other acidic compounds negatively impact the environment (such as global warming and acid rain) [40], [45], [53], [54]. In addition, exposure to emissions such as PM have negative impacts on personal health. Conditions such as cardiac [55]–[57] and pulmonary effects [58]–[60] contribute to the morbidity and mortality [61]–[64] across the population due to particulate matter. Studies such as [64]–[67], have examined the exposure duration, proximity, and impact on health. The economic impact associated with these conditions increased the burden on health services [68]–[70]. A reduction in the amount of solid particulate matter, emitted to the atmosphere, would contribute towards reducing the frequency of new cases associated with the exposure to solid particulate matter.

1.2.2 Flue Gas Chemistry

Burning a fuel to produce heat is a chemical reaction, whereby the fuels combustible fractions undergo oxidation, releasing energy. This is a thermochemical process. Other processes are pyrolysis, gasification, and liquefication, which produce either charcoal, liquid/oil, or fuel gas [40].Various processes, such as boilers and flue gas treatment systems, are used as part of the overall combustion process. In power generation, various types and sources of biomass, and municipal wastes can be burned to produce heat [51], [71]–[73]. An example of the combustion process, showing key parts such as the heat recovery and boiler system, but also the downstream processes such as the flue gas treatment and sorbent/treatment injection is shown in Figure 1 [74]. The exact set-up is site dependent and can vary. For example, Figure 1 [74] shows a rotatory kiln to dry the fuel before combustion, but both plants evaluated by Maeda et al,. [75] had the fuel injected directly to the furnace for combustion. The use of a kiln likely formed part of a fuel treatment process which dried the fuel before combustion. The useful product from combustion is heat, which can be recovered for power generation, used for heat at another site, or combined heat and power (CHP) which is the most common approach [76].

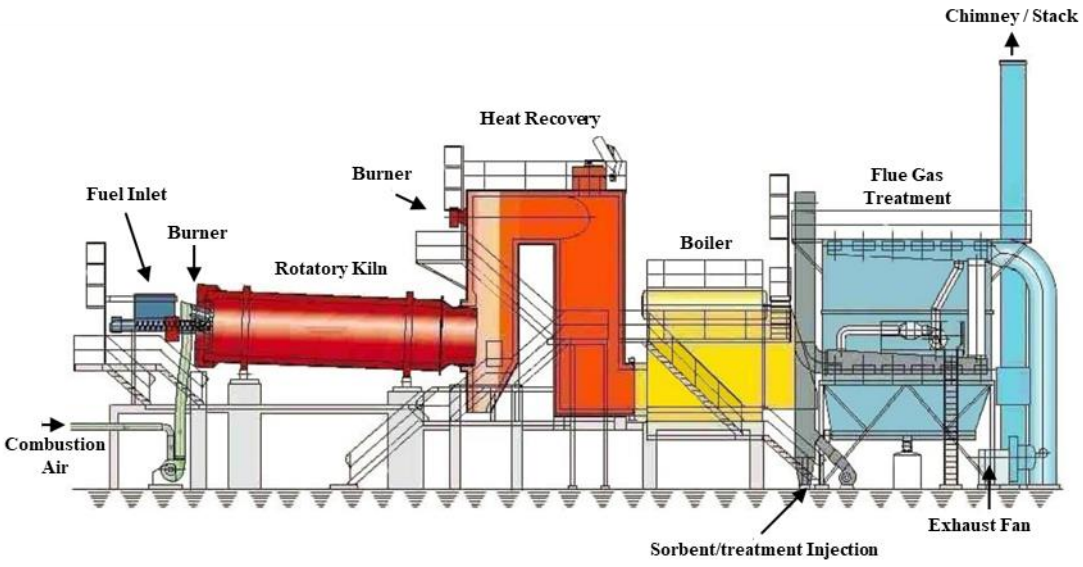

Figure 1: Example Layout of the Combustion Process, Including Flue Gas Treatment [74]

Apart from the release of energy, the main products of combustion are gaseous, and solids released as the fuel combusts. For example, bottom ash is one example of solid particulate matter that remains at the combustion chamber, often consisting of mineral impurities from the fuel, heavy metals, and some of the combustion bed material that wasn't entrained in the flue gas stream [40], [77]. Some ash is entrained in the flue gas stream, where it travels

downstream in particulate form. This is known as fly ash and is carried downstream in the flue gas which formed the gaseous compounds produced during combustion.

The flue gas composition is dependent on the chemical composition of the fuel but can be approximated based on the ultimate analysis of the fuel and volume of combustion air used. Often, excess air is delivered to aid complete combustion, and is often denoted as (λ) in literature [78]. Multiple authors have described the ultimate analysis of multiple fuels (both biomass and waste), which can be used to calculate the gaseous chemical composition of the flue gas [79]–[83]. One study evaluated the variation in waste wood over nine years [84], which suggested the potential variation within the fuel source, during combustion. The resultant chemical composition of the flue gas composes of CO_2, H_2O, NO_x, SO_x, and O_2, but can also contain acidic compounds such as HCL and HF if present in the fuel [83], [85], [86]. The environmental impact of NO_x, SO_x, and acidic compounds has been discussed extensively in literature [40], [47], [53]. To reduce the concentration of certain compounds such as HCL and SO_x, sorbents can be injected into the flue gas which facilitate reactions allowing them to be collected.

Calcium hydroxide ($Ca(OH)_2$), sodium bicarbonate ($NaHCO_3$), and powder activated carbon (PAC) are some examples of flue gas treatment. PAC injections aim to adsorb heavy metals such as mercury and various organic compounds present from the flue gas [83], [87], [88]. Sodium bicarbonate undergoes thermal degradation to produce sodium carbonate (Na_2CO_3) [89]. Sodium carbonate then reacts with gaseous compounds such as SO_2, HCL, and to some extent HF so that they can be separated from the flue gas physically and solid particulates as opposed to gaseous [83], [89], [90]. Calcium hydroxide can also act as the sorbent to reduce gaseous compounds such as HCL and HF, but can also mitigate SO_x emissions [83]. The selected sorbent or combinations of sorbents is dependent on the fuel's composition and the resultant gaseous chemicals produced from the combustion process.

Example chemical pathways for sodium bicarbonate and calcium hydroxide are illustrated in Equation 1 [89], [90] and Equation 2 [85] respectively. Another addition could be gaseous ammonia (NH_3) [91], which reacts with the NO_x components to produce nitrogen and water as shown in Equation 3 [83]. These exampled reaction pathways illustrate some of the potential reactions possible. Injection of sodium bicarbonate and/or calcium hydroxide facilitated sorption of the pollutant into the solid phase. Additional products of water or

carbon dioxide are also produced but remain gaseous. The resultant solids (such as Na_2CO_3, $NaCl(s), CaCl_2\ (s)$) remain in the flue gas.

$$2NaHCO_3(s) \xrightarrow{thermal\ decomposition} Na_2CO_3(s) + CO_2(g) + H_2O\ (g)$$
$$Na_2CO_3(s) + 2HCl(g) \rightarrow 2NaCl(s) + CO_2(g) + H_2O(g)$$
$$Na_2CO_3(s) + SO_2(g) \rightarrow Na_2SO_3(s) + CO_2(g)$$

Equation 1: Sodium Bicarbonate Reaction Pathway Examples [89], [90]

$$Ca(OH)_2\ (s) + 2HCl\ (g) \rightarrow CaCl_2\ (s) + 2H_2O\ (g)$$
$$Ca(OH)_2\ (s) + 2HF\ (g) \rightarrow CaF_2(s) + 2H_2O\ (g)$$

Equation 2:Calcium Hydroxide Reaction Pathway Examples [85]

$$4NO + 4NH_3 \rightarrow 4N_2 + 6H_2O$$
$$2NO_2 + 4NH_3 \rightarrow 3N_2 + 6H_2O$$

Equation 3: Ammonia Reaction Pathway Examples [83]

A solid emission from the combustion process is fly ash. Fly ash is the term given to ash which is below a certain size/density which allowed it to remain entrained within the flue gas [92]. The physical transformation from fuel to ash has been studied by researchers such as Williams et al., [81], Fuller et al., [93], and Bryers [94]. Chemical variation in the fuel resulted in the chemical composition of the ash varying. Studies such as Vassilev et al., [43], Masia et al., [95], and Vassilev et al., [96] have demonstrated the variability in ash composition when different fuels are used in the combustion process. The chemical composition of the fly ash is solid oxides, such as SiO_2, Al_2O_3, FE_2O_3, etc. In addition, the introduction of solid sorbents to the flue gas will mix and impact the chemical composition. Consequently, any fly ash collected from the combustion process, through separation processes after sorbent injection, will contain a mixture of fly ash and sorbents, with their respective solid products.

1.2.3 Separation Processes

Flue gas filtration is the removal process of solid particulate matter from the flue gas stream. Technologies such as cyclones, electrostatic precipitators, and bag filters are common processes to capture the solid particulate matter. For gaseous emissions that have not been effectively treated, such as remaining SO_x, acidic compounds, mercury, dioxins, or NOx abatement (for example), wet or dry scrubbers may be deployed to bring the emitted concentrations down [88], [97], [98]. As discussed in section 1.2.2, the addition of sorbents to

the flue gas post combustion aided to reduce specific emissions. Some examples of dry sorbents that can be injected into the stream are powdered activated carbon and lime, which react with specific chemical components of the flue gas to reduce their concentration [54], [85], [99], [100]. Solid additions to treat the flue gas will therefore affect the particle size distribution, chemical compound complexity, concentration, and bulk density.

Cyclone

Cyclones use centrifugal forces to remove dense particles from the gas stream [53]. Cyclones are typically tapered cylinder shapes, where the gas inlet is tangential to vertical top. The centrifugal forces increase as the gas spirals down the length of the cyclone. The exerted force on the particle causes it to fall out of suspension vertically downwards in the direction of gravity where it is collected. The gas then travels out of the cyclone at the vertical top. Cyclones have no moving parts, or consumables, which reduces the operational cost and are inherently easy to manage. One limitation of cyclone usage is their inability to handle micro and nano sized particles effectively, which is currently being addressed in studies such as [101]–[104]. Studies such as Xiong et al., [101] tend to agree that the cyclone collection efficiency can reach 99% with particles bigger than 10µm in diamiter, thought his number is dependent of the properties of the fluid and solids such as density, solidity, and humidity [101]–[104]. Due to the lower collection efficiencies noted at smaller particle sizes, other separation techniques which are capable of collecting these particle sizes are more efficient, such as electrostatic precipitators and/or bag filters, at removing these smaller particle sizes [105].

Electrostatic precipitation (ESP)

ESP is a method to collect filtrate that uses an electrostatic charge [97], [106], [107]. The ESP only provides a charge to the filtrate. The charged particles are then drawn towards collection plates of the opposite charge, without affecting the fluid flow path. The collected filtrate is then removed when the charge of the plate is neutralised, which caused the filtrate to drop due to gravimetric affects into a collection system. On issue noted with ownership is the collection of larger particle size. As the size increases, the collection efficiency decreased as shown by Sarkar et al,.[108]. However, as suggested by George et al,. [109], it is possible to combine a cyclone and ESP separator to improve collection efficiency, given these techniques complement each other in terms of limitations. Further information on ESP's can be found in [110], [111].

Fabric filtration

Fabric filtration is used to collect solid particulates from gas streams from various industries such as power generation [54], [88]. The selected fabric acted as a physical barrier for the filtrate laden flue gas stream, where once the gas had passed through the barrier it had effectively been cleaned. Separation of the solids occurred due to the fabric. The fabric used can be woven or nonwoven, and is characterised by its manufacturing process, surface treatment, porosity, area density, and thickness for example [54], [112]–[114]. Operation of fabric filtration is limited to temperatures below the maximum operational temperature of the fabric in use, and above the acidic dew point temperature [115]. The solid particulate can be captured through various mechanisms, such as impaction, diffusion, interception, gravity, and sieving [116], [117]. The efficiency of these collection mechanisms is dependent on the flow characteristics and properties of the filtrate. Overall, the collection efficiency of fabric filtration can achieve high collection efficiencies for a wide range of particle sizes, particularly for smaller micrometre sizes [88], [97], [118].

Nonwoven bag filters are one of the most common fabric filters, with various designs as illustrated in Figure 2 [54]. They are highly efficient at collecting solid particulate material, typical values range between >1 μm particle size at flow rates >1m^3hr^{-1} [112]. The fabric is commonly stitched together using a three-needle chain, which then be laminated or sealed [54]. Some other designs exist, such as cassette, ceramic, and pleated filters [118].

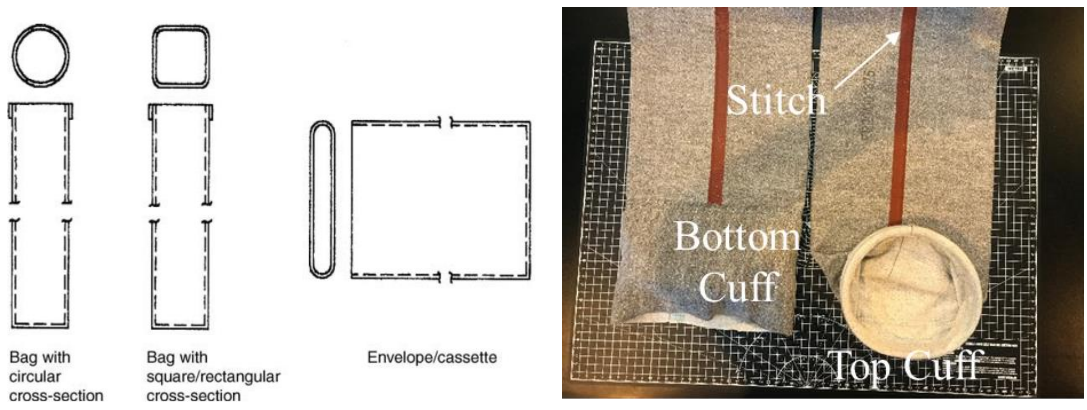

Figure 2: Illustration of Various Bag Filters [54] (left) and Example Circular Bag (right) showing the Top and Bottom Cuff

The design of the fabric filter is dependent on the cleaning mechanism. There are three key designs [119], [120]:

- Shaker:

The fabric filter is shaken, by a motor which drives supporting frame back and forth to cause the filtrate to dislodge from the inside of the filter bag [115]. The time for completion is dependent on how many oscillations are required, but typically last between 30 seconds to a few minutes [53]. This method is more efficient when the gas stream is isolated, but can be done as part of a continuous process [112]. The fabric needs to be resilient to the movement and is usually heavier to mitigate against accelerated wear due to cleaning [115]. This additional weight increased stress on the supporting mechanism [115]. Compared to the cleaning methods reverse air and pulse jet, there is also an associated increased risk of breakdown given the level of moving parts.

- Reverse air:

Like the shaker cleaning method, the top of the filter media is suspended at the vertical top and closed. The filtrate is collected inside the filter bag. Ambient air is then passed through the outside of the bag towards the inside where the collected filtrate is to facilitate its removal [54]. This cleaning must be conducted offline, which may require the system to be compartmentalised if continuous operation is needed [54]. The filter bags can be longer leading to a smaller footprint requirement than the pulse jet or shaking cleaning method, and have an increased longevity [53]. This cleaning method is more gentle than shaking, which allows more delicate/fragile media to be used [115]. Due to this, needle felted filtration media cannot be used as the resultant clean is ineffective at removing the filtrate [54].

- Pulse jet:

Unlike the cleaning methods reverse air and shaker, collection of filtrate occurs on the outside of the filter bag for pulse jet cleaning [112]. Each bag is suspended on a tube sheet and is kept open through the use of a support cage [54]. Cleaning is achieved by delivering a pressurised pulse of compressed air on the inside of the bag, which usually lasts for a fraction of a second [53], [112]. As the pulse of compressed air travels vertically down towards the sealed bottom of the filter bag, it causes the bag to expand, which releases the filtrate from the bag [118]. This cleaning method can happen online and offline [53]. Whilst online cleaning meant allowed for a continuous process to be achieved, it also facilitated redeposition through re-entrained filtrate [53], [54], [113]. The cleaning sequence depends on site preference, but can occur individually, in small groups, or all at the same time [112].

Wang et al., [115] provided a direct comparison between the cleaning methods mentioned above. An example schematic of pulse jet fabric filtration which was the selected cleaning mechanism owing to its prevalence in industry is illustrated in Figure 3 [88]. An illustration of the pulse jet cleaning mechanism in action is illustrated in Figure 4 [112].

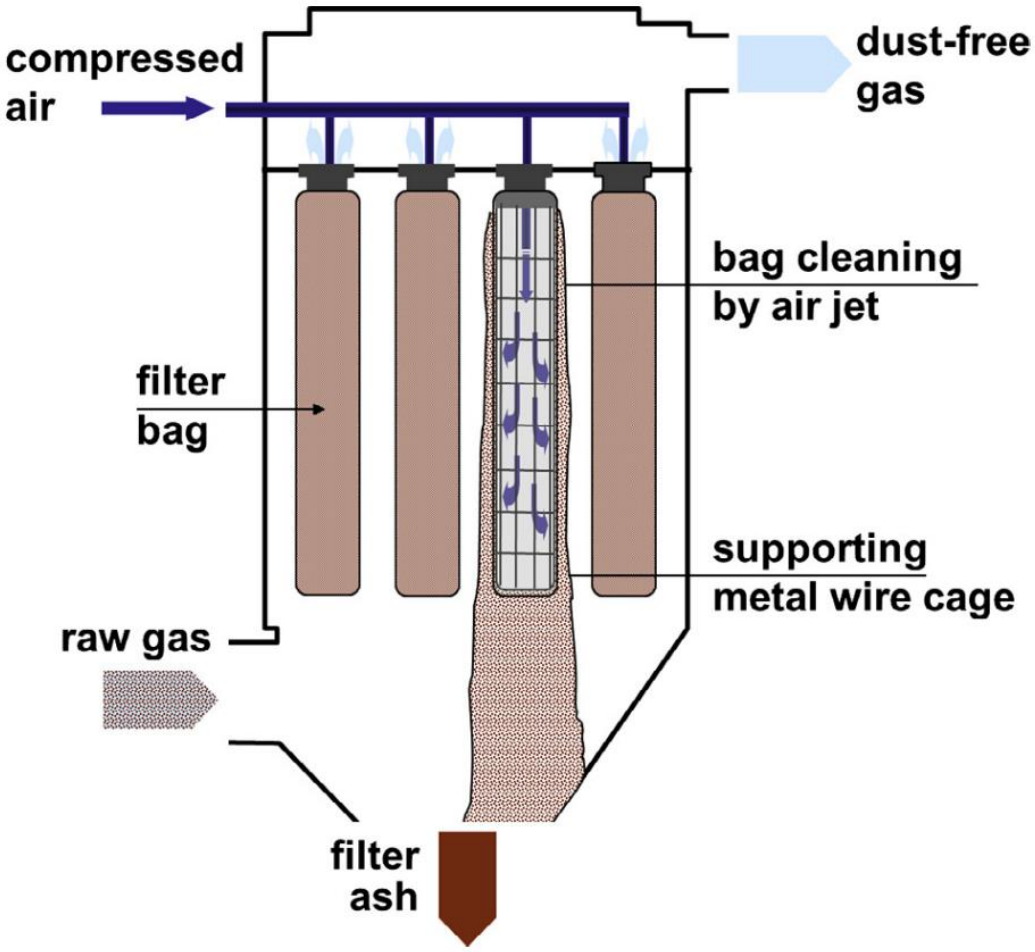

Figure 3: Pulse Jet Fabric Filtration Schematic [88]

The air to cloth ratio is defined as the flow rate of flue gas over the available collection surface area and is used during the design phase to help decide the number of filtration bags needed for the filtration process [53], [115].For pulse jet filtration, the ratio is reported to equal 5 for fly ash [115]. This design tool suggested the size and therefore the number of filtration bags needed. Collectively, a group of filtration bags is often referred to as a bag house, which can constitute a single compartment or chamber, or multiple depending on the design requirements [53], [54], [112]. The effects of varying this value are discussed in further detail by Wang et al,. [53], Mukhopadyay [54], and Sutherland [112]. For commissioned and operational bag houses, this parameter is fixed and can only be changed if major retrofitting/conversion processes happen.

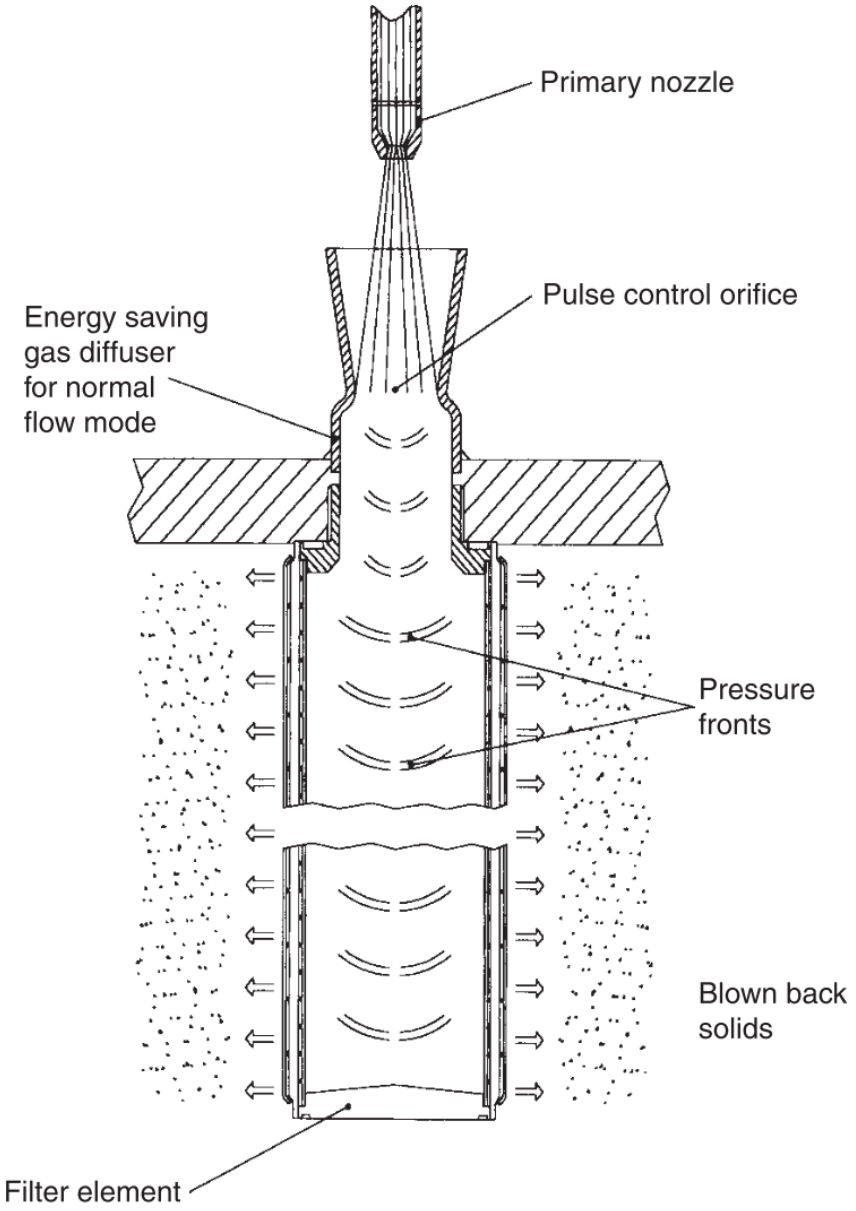

Figure 4: Schematic of Pulse Jet Cleaning In Action [112]

Typically, depending on usage and suitability, the filtration bag can have a lifespan greater than two years [115], though Wang et al,.[53] stated it can remain in-situ for longer time periods depending on its performance during operation.

In all cases, the flue gas is driven through the filtration media by an induced draft (ID) fan or forced draft (FD) fan which is located downstream and upstream respectively of the filtration unit. The demand placed on the fan is a function of the desired volume throughput of the flue gas and the system pressure drop [115], [121].

1.3 Analytical Technique Methods

Plant data provides the operator with a limited view of the condition of the bag house unit, which is dependent on the resolution of the data. If a site only recorded global values between the inlet and the outlet of the filtration unit, then identification of a region where failure is more prominent is more unlikely to be noticed. Industrial bag houses often contain hundreds of filter bags, within multiple compartments or cells. Representation of each cell through a global value, may still be unable to note any particular region within the cell, although comparative analysis between each other cell may indicate something is incorrect within a given cell. Reliance, therefore, is on the operator(s) to understand the data and act accordingly. As the number of datapoints increases, so does the complexity of understanding the data.

Offline analysis of each compartment affords a window into how the filtration media is performing. Selection of bags to withdraw can occur two ways: strategically or based on visual observations. The former required division of the tube sheet into equal parts, where removal of at least one filtration bag per part transpired. Subsequent analysis yields information across the entire tube sheet, at the resolution determined by the number of parts afforded to the tube sheet. BS 22031:2021 “Sampling and test method for cleanable filter media taken from filters of systems in operation” [16] provided a clear methodology to perform this task. However, if upon inspection of the cell there appeared a region where failure occurred (such as filtrate on the clean side, discolouration to the air exit side of the filtration media, significant moisture, etc) bags may be withdrawn in the area to determine if failure has occurred, and how widespread it is in the affected area. On the whole, industrial sampling of filtration bags appeared not to follow a structured approach where some samples are presented for evaluation with little to no further information. Omission of further information about the sample, except (sometimes) of the filtration bag’s original location within the cell, inadvertently performed blind analysis, with the resultant report only discussing the particular region examined – not the full cell. Sometimes, leading to general comments about a cell, owing to the samples retrieved having no locational information.

This inability to control sampling, through disconnect between sampling and analysis calls into question the current methodology used during the analysis of a used filtration media bag. Chapter 2 discussed these techniques in further detail. This led to the question:

“Do the current analytical methods represent the full sample/filtration bag?”

Economic considerations, from both the site and analysts' point of view are a major factor in the number of filtration bags that are evaluated. From A sites perspective, the cost to replace each filtration bag, labour, frequency, cost of being offline, and analyst costs factor into the decision to perform analysis. Apart from laboratory consumables the analyst's time is the biggest cost in performing the evaluation. Using current methods, a full filtration bag required two hours to complete the analysis. For each workday, this could equate to 3.5 full filtration bags per analyst. Consequently, as the number of bags sent for analysis increased, so did the turnaround time to complete the evaluation, interpret, and report the results. Sites therefore may choose to limit the number of samples evaluated, in favour of a quicker turnaround time (to get the site operational again) and limit expenses. This led to the expansion of the previous question, into parts:

"Do the current analytical methods represent the full sample/filtration bag?"

1. What is the difference between the current method, against a larger sample size from the filter bag?
2. Is the current method representative of the overall filtration bag?
3. Can any more information about the filtration bag, without having to extend the turnaround time too severely, occur from performing further analysis?
    a. If so, can the conduction of further analysis transpire after original testing and supplied to the site as an appendix, or kept internally to aid future sample evaluation.

Chapters 2,4,5,6, and 7 discussed this question, and answered it in Chapter 8.

1.4 Durham Filtration

For the Engineering Doctorate (EngD) project, Durham Filtration became the industrial partners. Durham Filtration provided access to a range of used bag house filtration media from multiple combustion sites across the United Kingdom. Throughout this thesis, the use of industrially relevant samples facilitated an easy transfer of the results into industry. At their site in Jarrow, Newcastle -Upon-Tyne, an analytics laboratory provided an opportunity to gain first-hand experience of the variability of not only filtrate and filtration media used, but also how sites prepare and select filtration media for analysis. Over the past two years, under the supervision and direction of the author, the laboratory has expanded and developed to allow for more analytical techniques; furthering the understanding of variation of a particular datum such as free lime and moisture determination. Appendix E summarised reports/work

performed for Durham filtration, including preliminary results towards the application of μCT across a full, used, filter bag.

1.5 Thesis aim, outcome, and structure

The overall aim of this thesis was to enhance the understanding of the resultant potential variation within various analytical techniques. From this, optimisation/development of analytical methods such as air permeability, mass/density determination, filter media thickness, and porosity, could account for the variation and establish the effect it can have on the resultant data. If the data used to evaluate the media is not representative, this can impact the decision to leave the media in or change it. If the media is changed when it could remain in-situ for longer, there is an increased economic burden to the site. If the media remains in-situ but requires changing, this could cause increased emissions or increased operational costs due to an increased cleaning frequency for example. Therefore, it is important to understand how the results vary over a given sample, to allow for a more informed decision on the media condition.

The thesis focused on common analytical techniques such as air permeability, mass, and thickness, but also considered sample preparation. These techniques were highlighted in BS 22031:2021 "Sampling and test method for cleanable filter media taken from filters of systems in operation" [16] alongside a cleaning method, which was also assessed as part of this thesis. This allowed for differential analysis between the as received sample (with filtrate) and just the filtration media (no filtrate). Preliminary testing was performed using a newly acquired (2022) filter assessment rig (FAR) to develop a methodology to evaluate the remaining longevity of filtration media under site specific operational parameters.

Chapter 1 presented the background theory surrounding ownership and discussed subjects such as energy, flue gas chemistry, and filtration theory. The aim of this chapter was to provide the reader with enough knowledge of the energy sector and background theory towards filtration, without going into specifics, before the discussion on specific topics in Chapter two.

Chapter 2 afforded the reader with a literature review on key topics surrounding analytical techniques, available methods, longevity assessment, and new/emerging technologies. This provided adequate background information which allowed for the understanding of the research chapters presented in Chapter 4-7 inclusive. Chapters 4 to 6 stemmed from the review conducted for BS 22031:2021 "Sampling and test method for cleanable filter media

taken from filters of systems in operation" [16]. Chapter 7 used the FAR to begin longevity studies and determine if a method to suggest the remaining longevity of filtration media was possible. Chapter 7 also explored the use of X-ray imaging and μCT as an analytical tool. The work presented in Chapters 4-7 was the result of Chapter 2, which identified concepts in literature which had previously not been examined.

Chapter 3 summarised the methodologies applied in Chapters 4-7, each chapter supplied details about its respective method. This increased the readability of each chapter by allowing each chapter to be read in isolation. Chapter 3 Section 3.2 presented the selection and commission of the FAR. It detailed information about the operation and made provisions for future upgrades. The review presented in section 3.2 provided future researchers with a clear understanding of how the rig operated, potential issues they may face, and a selection of improvements they may wish to undertake. Chapter 3 laid the foundations for each subsequent chapter.

Chapter 4 presented the research around the cleaning method mentioned in BS 22031:2021 "Sampling and test method for cleanable filter media taken from filters of systems in operation" [16]. The aim of this study was to determine the most appropriate method to sufficiently clean the filtration media to allow for analysis in the post cleaned state.

Chapter 5 aimed to demonstrate the variability of the mass and thickness readings from a definitive sample size. Likewise, Chapter 6 aimed to demonstrate the variability of air permeability across the full filtration bag, not just at a fixed sample size. The expansion from a small defined surface area to a full filtration bag occurred due to the noted variability concluded in chapter 5. Both chapters used (different sites) industrially derived material, to afford a better understanding of how modifications to the current method may impact analysis and interpretation of their results.

Lastly, Chapter 7 aimed to critically evaluate the preliminary data obtained from performing two longevity tests. The initial aim for this work was to identify if used filtration media could be evaluated in the FAR to determine the remaining longevity of the filtration media under near replicable industrial conditions. The chapter evaluated the data critically, making recommendations on how future researchers may take the presented ideas and develop them further.

At the heart of the thesis, was the implications towards large scale industrial evaluation of nonwoven filtration media. Given the impact that each chapter potentially had on current practices, each chapter also aimed to minimise the disturbance to standard practices. Increasing the number of samples evaluated per filtration bag, or number of repeats, increased the time required to complete analysis. Chapter's 4 to 6 inclusive extensively considered this in their results and discussion. Chapter 7 showcased new and potential methodologies and technologies to evaluate the filtration media.

Appendices to the thesis provided an overview of other work conducted throughout the four-year period of this project. Where applicable, anonymization has taken place. Additional, SEM imaging and μCT work are also presented, along with material data sheets and a brief overview of the air permeability variation on new, virgin filtration media.

Chapter 2: Literature Review

2.1 Introduction

This chapter provided an overview of the current literature that surrounded bag house filtration for flue gas filtration in the energy sector. The aim of this chapter was to provide a detailed overview of the characteristics associated with the ownership of these systems. Topics such as flue gas treatment [89], [91], [118], [122], economic factors [121], [123], [124], utilisation of fly ash [125]–[127], and associated health impacts [46], [55], [68], [128], [129] are discussed in Chapter 1. Therefore, the subsequent review focused on three distinct topics:

- The filtration Process:

This topic focused on the interaction between the flue gas filtration media and the particulate matter, also referred to as filtrate or fly ash.

- The Cleaning Process:

Periodical removal of surface filtrate allowed regulated the media which allowed for further collection of the filtrate. Section 2.3 characterised the associated equipment and operational conditions of the pulse jet cleaning process. This cleaning method was the most common found within industry during the project.

- Analytical Techniques:

One limitation of global data is the inability to identify areas where filtration media may have failed, to a specified definition, and needs replacing. Subsequently, periodical inspection and removal of filtration media occurred to allow for offline evaluation.

2.2 Filtration Process

Filtration is the process of separating solid particulates from a fluid. In flue gas filtration, filtration media facilitated this separation. Solid particulates in the flue gas comprise of fly ash [111] and any solid upstream pre-treatment chemicals such as calcium carbonate [130], sodium carbonate [89], activated carbon [91], or a combination. The combination of fly ash and pre-treatment chemicals is referred to as filtrate. The filtrate is drawn through the

filtration media either by an induced draft (ID) or forced draft (FD) fan. The filtrate is then collected by the fabric until it is either replaced or cleaned, depending on the unit design.

Nonwoven filtration media is a common fabric used as a filter for the removal of the filtrate from the flue gas. Some of the common fabrics used to construct the filter bag are presented in Table 1 [53], [115], [131]. Various properties such as fibre diameter, needle penetration depth, punch density, and stroke frequency will impact the resultant properties media [9], [132]–[134]. Information on manufacturing and different types of media can be found in the following literature sources [53], [120].The selected filtration media will have a set of parameters specific to its design. Air permeability, thickness, areal density, and porosity are example parameters which will influence the process [3], [135], [136].

Table 1: Various Fabric Operating Characteristics [53], [115], [131]

Fabric	Max surge temperature	Max continuous temperature	abrasion	Fluoride resistance	alkali resistance	flex abrasion resistance	mineral acids	organic acids
Cotton	225°C	180°C	VG	P	G	VG	P	G
Polypropylene	190°C	190°C	E	P	E	VG	E	E
Dacron	325°C	275°C	VG	P/F	G	VG	G	G
Nomex	425°C	400°C	E	G	E	E	F	G
Teflon	500°C	450°C	F/G	P/F	E	F	E	E
Fibreglass	550°C	500°C	F/G	P	F/G	F	G	G
Wool	250°C	200°C	F/G	P	P/F	F/G	VG	VG

Where: P = Poor, F = Fair, G = Good, VG = Very Good, and E = excellent.

Depth, Surface, and Cake Filtration

Depth filtration is characterised by the internal deposition of particulate inside the media. Over time, the saturation of the filter becomes significant enough that deposition tends towards the surface pores of the media. Collection of the filtrate at the surface is often referred to as surface filtration: suspension of filtrate at the surface of the media. Once the accumulation of filtrate at the surface becomes significant, a layer of filtrate is formed at the surface, which increase in thickness over time and is referred to as a cake. Various authors such as Li et al., [137], Kanaoka [138], Thomas et al,. [139], and li et al,. [140] have discussed these filtration steps in their studies/experiments.

The relationship between the pore size/porosity and the filtrate particle size played a crucial part in the transaction between filtration phases. One study by Li et al,. [137] evaluated this against three particle sizes, which conformed to previous studies, however they noted that the particles larger than the pore size largely remained at the surface [137]. Whereas particles

smaller than the pore size more readily travelled internally and promoted depth filtration. Another study by Li et al,. [140] characterised these filtration steps in terms of pressure drop. For depth filtration, the pressure drop rate accelerated. Once depth filtration was sufficient, the pressure drop rate deceleration as surface filtration become the dominant filtration mechanism until a sufficient surface layer of filtrate had formed. Lastly, the pressure drop exhibited a near constant increase, which suggested cake filtration had become dominant. Another study by Thomas et al,. [139] examined a singular filtrate, but changed the filtration velocity. The study by Thomas et al,. [139] suggested that as this velocity increased, the number of smaller particles deposited internally increased. This was characterised by a significant increase in pressure drop across the filter at any given time during the experimental test.

Filtrate deposited internally is difficult to remove and once deposited generally remains within the media [141]. Therefore, depth filtration should be avoided in order to promote the longevity of the filtration media. Cake filtration uses already collected particulate to collect the filtrate, meaning that it acted as a barrier to the filter media. Depending on the efficiency of filtrate removal during cleaning, cake filtration can re-occur quickly, so long as enough surface filtrate remained. Over cleaning would remove the surface filtrate, resulting in depth and surface filtration, dependent on the severity of the over clean. Therefore, to mitigate the depth filtration, cleaning should aim to remove the bulk of the cake, without significantly compromising the surface filtrate. Whilst this would lead to a slightly elevated pressure drop immediately after cleaning, it would reduce depth filtration and therefore promote the longevity of the media.

Differential pressure

Differential pressure is the directional change in pressure between a specific upstream and downstream measuring point. Various studies have illustrated different locations where the measurements could be taken. Illustrated in Table 2 are various studies which have measured the differential pressure. Measuring the differential pressure between the flange inlet and outlet provided a global overview of the differential pressure exhibited across the unit. However, the global value cannot identify regions of higher or lower differential pressure across the filter. This would require multiple sensors between the filtration media, which for large scale units could require thousands of data probes. Realistically, whilst small scale studies can effectively measure across the filtration media, as the size of the unit increases,

there is a tendency to use a more global value which assumes that the differential pressure across the filtration media is equal, regardless of any locational variations.

Table 2: Various Studies Demonstrating Various Differential Pressure Measuring Points

Measurement Source	Description	Literature Sources
Tube sheet	From the dirty, to the clean side of the tube sheet	[142–146]
Overall System	From the inlet to the outlet, flange	[121,147-149]
Fabric and filtration cake	Across the filtration media and cake	[99], [136], [150]–[152]

Various studies have applied the Ergun equation [153] to characterize the differential pressure across the bag house and is illustrated in Equation 4 [136], [152], [154], [155]. The equation characterised the overall differential pressure as a function of the filtration media (ΔP_m) and filtrate/cake deposited (ΔP_c). Davies law described the flow of fluid through a porous medium, which characterized the differential pressure further in terms of the velocity of the fluid (v_s), flow resistivities (k_m, k_c), and the deposited mass (W) [156]. The mass deposited on the filter is defined by the multiplication of the mass feed per unit time and total filtration time, over the filtration area($W = Qt/A$) [156].

$$\Delta P = \Delta P_m + \Delta P_c = k_m v_s + k_c v_s W$$

Equation 4: Total Differential Pressure [136], [152], [154], [155]

An equation referred to as the Kozeny-Carman equation is shown in Equation 5 [157]. This equation has been modified and adapted to suit experimental studies, examples of which are illustrated in Equation 6 [158] and Equation 7 [159]. Deployment of the Kozeny-Carman equation against experimental data relied on the use of various assumptions discussed by Tien et al,. [159], which evaluated the use of the equation to determine porosity (ϵ). The assumptions discussed by Tien et al,. [159] focused on translation between spherical particles for packed beds to cake filters, constant velocity flow, representative particle size, and consistent gas density, which led to some studies such as Aguiar and Coury [146], Hsiao et al,. [158], and Tien and Ramarao [159] having to implement corrections, or defining the equation slightly different based on their research. This isn't to say that their studies are incorrect or misleading, it merely illustrated the complexity of using theoretical equations to model experimental results.

For Equation 5 [157], Equation 6 [158], and Equation 7 [159], the particle diameter is denoted as (D_p) and (d_{eq}), fluid velocity as (U_m) and (U_o), the Reynolds number of the flow as (N_{Re}), Gravity constant as (g_c), filter thickness as (L), and gas viscosity as (μ).

$$\frac{\Delta P g_c}{L} \cdot \frac{D_p}{G U_m} \cdot \frac{\epsilon^3}{1-\epsilon} = 150 \cdot \frac{1-\epsilon}{N_{Re}} + 1.75$$

Equation 5: Kozeny-Carman Equation developed by Ergun[157]

$$\frac{\Delta P}{L} = U_o \mu \cdot \frac{A s_v^2 (1-\epsilon)^2}{\epsilon^3}$$

Equation 6: Representation of the Kozeny-Carman Equation [158]

$$\frac{\Delta P}{\Delta L} = A \cdot \frac{(1-\epsilon)^2}{\epsilon^3} \cdot \frac{\mu u_s}{d_{eq}^2}$$

Equation 7: Representation of the Kozeny-Carman Equation [159]

Deployment of any form of the Kozeny-Carman equation to describe large scale flue gas filtration media is difficult. Doing so would rely on knowing the velocity at any given point, evolution of thickness over time, porosity deviation, to name a few parameters that would be assumed constant but may not be at larger scales. Studies agree with the theory, that as the porosity decreased, the pressure drop increased. However, the evaluation of porosity is dependent on knowing the thickness at any given time, which would require removal and offline testing. Therefore, Equation 4 sufficiently described the differential pressure at a given filtration cycle. Whilst ΔP_m described the differential pressure of the new filtration media, it also accounted for any filtrate deposited internally at any given point during operation. Consequently, the term ΔP_m is a function of the new media and any internal or remaining deposits post clean. As a result, ΔP_m described the baseline differential pressure immediately after the completion of cleaning.

Consideration should also be given to other factors, such as particle size, velocity, temperature, humidity, and concentration. These factors would affect the resultant thickness of the cake as well as internal deposition. These interactions have an effect on the rate of differential pressure exhibited by the filtration media. The illustrated the complexity of flue gas filtration, showing the difficulty towards modelling. Extrapolation of this from small scale to industrial scale could lead to more extensive deviations in the model. Understanding the interactions between the filtrate, flue gas, and media is critical to evaluate the resultant

pressure drop experienced on the system, and to further explain its evolution as the process continued.

Operational Parameter Influence

One study performed by Wang et al., [148] considered the effect of cake structure based on the concentration presented at the filter. Their work suggested that under a constant velocity, an increased filtrate concentration led to a slower rate increase of differential pressure. They attributed this down to the structural formation of the cake, where at an increased concentration, there was a reduced probability of it becoming organized, denser, and therefore result in a higher differential pressure. The study by Wang et al., [148] presented two cakes evaluated, showing their results in Figure 5 [148]. Another study by Hsiao et al., [158] stated that the increased concentration led to an increased rate of pressure drop, which contradicted the findings of Wang et al., [148]. Experimental variation between the two studies could have contributed to the difference in results. Whilst the study by Hsiao et al., [158] simulated a more representative bag filtration set-up, Wang et al., [148] used a parallel delivery system, meaning particle separation could not effectively take place. Furthermore, the filtration velocity differed from 0.1-0.2ms^{-1} for Wang et al., [148] and 0.035ms^{-1} for Hsiao et al.,[158]. The particle size distribution could have also played a role, given smaller particles will more readily block the filter, leading to an increased differential pressure as previously discussed. Consequently, the difference between studies further demonstrated the complexity of the filtration process.

Another study by Miguel [160] experimented on the filtration velocity, experimentally showing that as the velocity increased, so did the rate of differential pressure increase [160]. Other studies by Rogozinski et al., [143], and Saleem et al., [161] both demonstrated that the increase of velocity on new/virgin filtration media led to higher differential pressure readings due to compression of the media under forces. Regardless of the type of filtrate or media, studies indicated that an increased velocity led to increased differential pressures, but also a reduced porosity [143], [148], [161]. If the increase in velocity leads to an increased differential pressure rate, it could be suggested that the velocity across the unit should be as low as possible. One point not considered with a change in velocity is the potential effect on the particle size and therefore the collection efficiency.

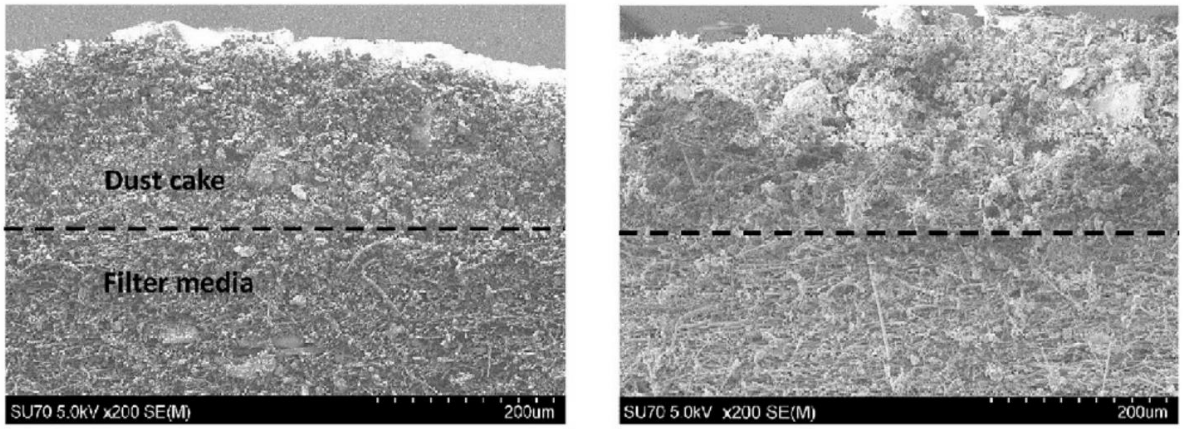

Figure 5: Demonstration of the Filtration Cake Structure at 0.32µgcm^{-3} (left) and 7.08µgcm^{-3} (right) [148]

At operational temperatures above 100°C the water present in the gas stream will be gaseous. Various studies have examined the effect of moisture on the pressure drop rate. A study by Boudhan et al., [162] evaluated the difference between a fully dry gas stream and one with 73gm^{-3} ambient humidity. Their study found that the moisture presence contributed to the formation of capillary bridges on the filtrate, which resulted in an increased differential pressure rate on filtration bags. Another study by Joubert et al., [163] presented similar results over two differing filtrates and various relative humidity's. Their work suggested an increased pressure drop rate with increased humidity but correlated this to increased blinding due to the capillary bridge formed between the particulates which restricted fluid flow. Other studies have found similar results with various moisture contents and filtrate [164], [165]. Moisture sorption is affected by the composition of the filtrate which will impact the resultant differential pressure rate [81], [166], [167]. Performing moisture analysis offline would afford an insight into the sorption effect of moisture onto/into the filtrate, thereby suggesting the interaction during operation.

Collection Efficiency

Overall, the aim of the filtration process is to efficiently collect the filtrate. This is achieved through various collection mechanisms, such as: gravity, impaction, interception, and diffusion. These collection mechanisms have been studied extensively within literature, often summarized by the single fibre theory (SFT) [168]–[170]. The SFT, evaluated particle size against a single fibre, before extrapolating it to the filtration media. The filtration media is characterized by its thickness, the fibre diameter, and either the packing density/solidity (α) or porosity (ϵ). Both the packing density/solidity and porosity are a decimal between zero and one and can be changed to the other by their subtraction from unity. The single fibre

efficiency (E) is calculated based on the addition of the calculated efficiencies for each mechanism as shown in Equation 8.Consequently the collection efficiency can be calculated using Equation 9 [171]. One alternative way is to calculate the penetration efficiency (P(n)) using Equation 10following form of Equation 10 [169]. These equations equated the collection efficiencies against the filter's fibre diameter (D_f) and the thickness of the filter (H) or (L) against the porosity (ϵ) or packing density (α).

$$\left(\eta = \eta_{gravity} + \eta_{diffusion} + \cdots\right)$$

Equation 8: Summation of all collection efficiencies to get the overall efficiency value

$$E = 1 - \exp\left(-\frac{4(1-\epsilon)H\eta}{\pi\epsilon D_f}\right)$$

Equation 9: Collection Efficiency [171]

$$P(n) = \exp\left[-\frac{4\alpha L\eta_T(n)}{\pi D_F(1-\alpha)}\right]$$

Equation 10: Penetration Efficiency [169]

Each collection mechanism is based on the interaction between the filtrate particle size, and the fibre diameter. The collection mechanisms evaluated as part of this literature review is illustrated in Figure 6 [115]. Whilst electrostatic collection exists, it is not uncommon for fabric filtration to not have an electrical charge applied to the media. Studies such as Jaworek et al., [111], Visser [172] and Lathrache and Fissan [173] explored this collection mechanism, defining the interactions between the media and filtrate. The complexity of modelling the electric charge of each individual particle against its material composition, and the filter itself lead to most studies inadvertently assuming that the electrostatic efficiency is negligible in comparison to other mechanism. For large scale combustion, this would require significant time and experimental expertise to define not only the chemical composition, but to then classify it in terms of particle size and resultant charge. As such electrostatic collection was not considered. Regardless, the both the fibre diameter and particle size will have an impact on all collection mechanisms.

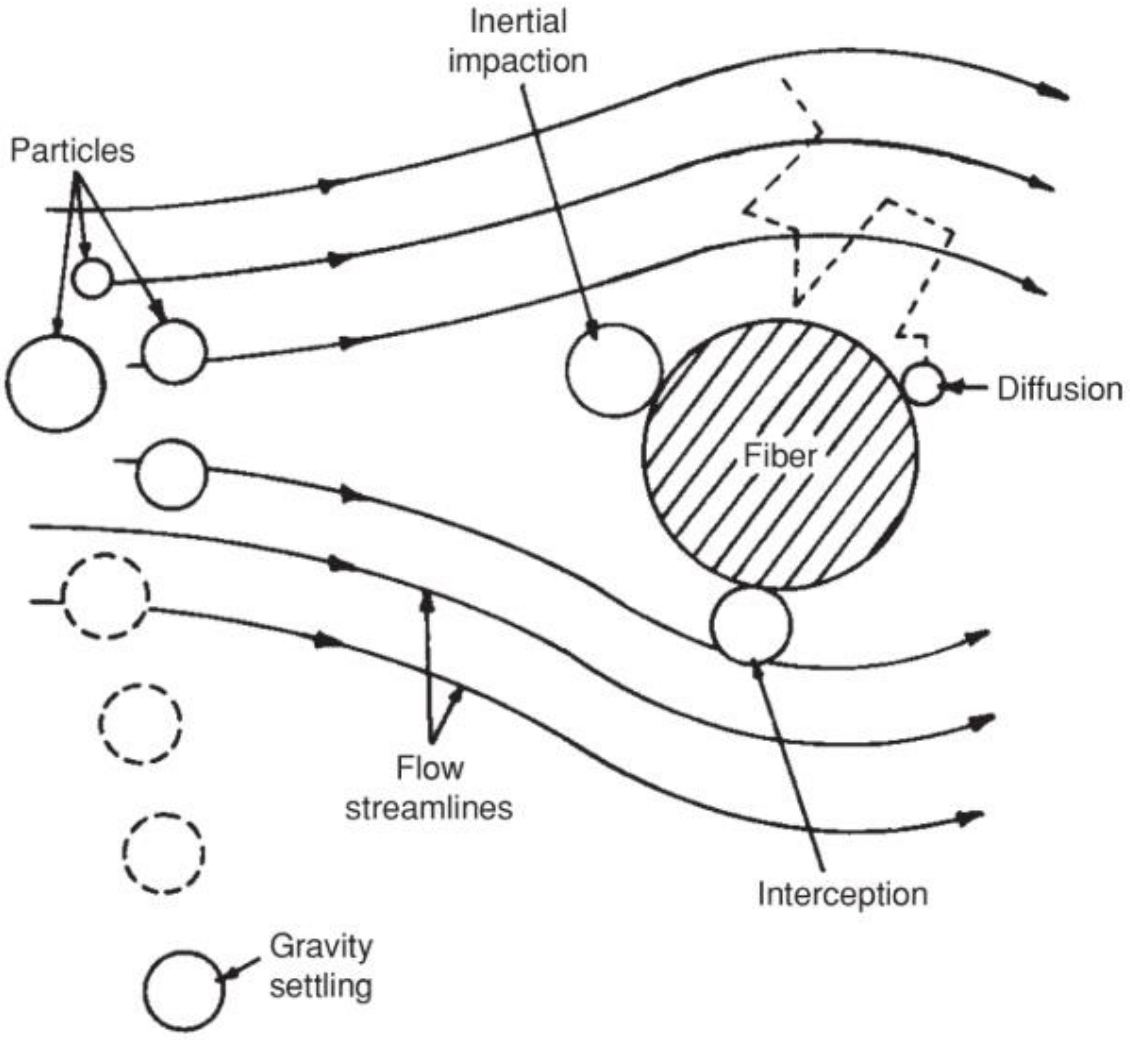

Figure 6: Illustration of Collection Mechanisms [115]

Fibre diameter is one parameter for discussion. One study by Kang et al., [147] presented four ways to calculate the diameter following the arithmetic mean, geometric mean, the volume-surface mean, and the effective diameter [147]. The definition of the diameter assumes fibre sphericity, coupled with the assumption that the distribution of the fibre diameters is narrow which allows for a singular fibre diameter to be used. Various studies such as Jackiewicz et al., [15], Kang et al., [147], and Barros et al., [156] have shown that for non-woven filtration media, the fibre diameter is variable. This assumption appeared to hold true for some studies such as Kang et al., [147] and Barros et al., [156], but had a large deviation between the theoretical and experimental results in some studies such as Steffens et al., [171], and Podgorski et al.,[174]. Whilst some variation was noted between the experimental and theoretical studies, they illustrated that the method used to define the fibre diameter impacted on the validation between the two methods.

Definition of the equivalent particle size could also affect validation between the experimental and theoretical data. A study conducted by Hinds [168] discussed the difference between the aerodynamic diameter and stokes equivalent spheres, which determined the particle size under the assumption of being perfectly spherical. They further discussed the irregularity of a particle, accounting for it which they suggested could be accounted for using a dynamic shape factor/constant depending on the material [168] .Experimental work by Podgorski et al., [174] applied the theoretical differences and showed the variation between the theoretical and experimental efficiencies. Table 3 illustrated various fly ash's from different combustion process, which illustrated that spherical assumption may under or overestimate the efficiency of collection.

Table 3: Fly Ash Studies

Reference	Brief Description	Application
[136]	Review of research related to filtrate collection, presenting theoretical models to define the efficiency of collection based on fly ash parameters.	Bag, cartridge, HEPA, ULPA, high performance filters.
[175]	Examination of fly ash and bottom ash from biomass.	Concrete production.
[176]	Considered the properties of 19 unconventional fly ashes.	Concrete production.
[177]	Ash formed from the combustion of pulverized grape pomace	Combustion systems

Application of the SFT to determine the theoretical efficiency has been widely applied, under various conditions, particle sizes, and filtration media, in literature for fabric filtration. Equation 11 [156] presented a specimen method to determine the collection efficiency. Reviews on the constants and calculation steps can be found in numerous papers. Whilst there appeared to be agreement between the experimental and theoretical, studies such as Tang et al., [6], Kang et al., [147], and Barros et al., [156] represented the experimental collection based on the ratio between the downstream and upstream concentrations such as Equation 12 [6]. Use of this method allowed for the entire collection efficiency of the unit to be calculated, without assumptions about the filter, filtrate, or operating conditions.

In Equation 11 [156], the efficiencies calculated are: diffusion (η_d), direct interception (η_{id}), inertia (η_i), and gravity (η_g). Dimensionless numbers such as the stokes number (St), Kuwabara factor (Ku), Peclet number (Pe), and ratio between the fibre and particle diameter (R) aid to calculate these efficiencies. For Equation 12 [6], this used the ratio between the

particulate concentration upstream over the particulate concentration downstream to calculate the efficiency (E).

$$\eta_d = 1.6\left(\frac{1-\alpha}{Ku}\right)^{1/3} Pe^{-2/3} C_d$$
$$\eta_{id} = 0.6\left(\frac{1-\alpha}{Ku}\right)\cdot\frac{R^2}{1+R}C_r$$
$$\eta_i = \frac{St^3}{St^3 + 0.77St^2 + 0.22}$$
$$\eta_g = \frac{(1-\epsilon)^{2/3} v_t}{v_s}$$
$$\eta_t = \eta_d + \eta_{id} + \eta_i + \eta_g$$
$$E = 1 - \exp\left[\frac{4L\alpha\eta_t}{\pi(1-\alpha)d_f}\right]$$

Equation 11: Application of the SFT to determine collection efficiency [156]

$$E(d_p) = 1 - \frac{C_{downstream}(d_p)}{C_{upstream}(d_p)}$$

Equation 12: Efficiency Based on Upstream and Downstream Filtrate Concentrations [6]

Lastly, as suggested by Equation 11 [156], the stream flow conditions affected the collection efficiency. The Peclet number, and Stokes number influenced deposition of a given particle size upon the fibre. For larger experimental apparatus, the can velocity, defined in Equation 13 [179] can be applied to suggest the velocity at any given point on the filtration media [117], [179]. This assumed that the flow stream was distributed equally and by extension the filtrate.

Each particle of a given size exhibited a unique settling velocity based on its size and density in relation to the gas stream conditions. Equation 13 [179] and Equation 14 [6] defined the settling velocities. In both cases, the settling velocity (V_{st}) or (v_t) defined the minim velocity required to keep the particle suspended in the stream. If the can velocity (V_{can}) was lower than the settling velocity for a given particle, it would begin to settle out of stream due to gravimetric forces. This phenomenon leads to a proportion of the larger filtrate being removed. As discussed previously, this could impact not only increase the differential pressure rate but lead to more internal deposition/blinding of the media. Furthermore, Equation 13 [179] accounted for the total area of the collector ($A_{collector}$), as well as the number of bags (N_{bag}) and area of said bags (A_{bag}), as opposed to Equation 14 [6] which didn't consider this. Given the differences noted between Equation 13 [179] and Equation 14 [6], it demonstrated potential further variation with the theoretical model given the use of

assumed spherical particles and constants based on idealist experiments, especially for Equation 13 [179] which used experimentally derived constants.

$$V_{can} = \frac{Q_{in}}{A_{collector} - N_{bag} \cdot A_{bag}}$$

$$V_{st} = \left(\frac{\mu}{\rho_g D_p}\right) \exp\left[-3.07 + 0.9935 \times \ln\left(\frac{4\rho_p \rho_g D_p^3 g}{3\mu^2}\right) - 0.0178 \times \ln\left(\frac{4\rho_p \rho_g D_p^3 g}{3\mu^2}\right)^2\right]$$

Equation 13: Can and Settling Velocity as Defined by [179]

$$v_t = \frac{d_p^2 g(\rho_p - \rho)}{18\mu}$$

Equation 14: Definition of Settling Velocity [6]

Although the SFT has been widely applied, it required considerate reading and experimentation before a model could be deployed to validate specific experimental conditions/data. Furthermore, the model only defined new/virgin media, given the porosity value remained constant. In practice, studies have shown that this value changes over time, with particle migrating through the media [141], which would therefore affect the model. In addition, assumptions made during extrapolation between the single fibre and media assumed the porosity was equally distributed, which may not be the case unless examined through imaging. The velocity profile across the filter was also assumed constant, along with other flow conditions such as temperature and viscosity. Studies have shown the potential impact on some of these conditions varying during use which affected collection efficiency [147], [180]. For larger scale filtration units, the assumption of equal flow distribution may not be correct. As a result, Equation 12 [6] can be used to determine the efficiency of the entire process, without using the assumptions made for the SFT.

Flue gas distribution

Flow distribution is characterized by the velocity profile within the filtration unit. The uniformity, as calculated in Equation 15 [181], is based on the velocity profile (V_i) and global velocity (V_{avg}). Unity defined the profile as uniform which meant the incoming flue gas and filtrate was equally distributed. As the uniformity (U) value increased, it demonstrated an unequal distribution of the flue gas. This resulted in regions where velocity is greater or lesser than the average, impacting the rate of failure and pressure drop evolution [149], [181]. One method to improve the distribution of flue gas is the use of flow distribution systems, or baffles, as suggested by Chen [149] and Chen and Cheng [181]. Their work evaluated various

baffle designs to promote a more uniform distribution of the velocities within the bag house. Their experimental work demonstrated that an increased uniformity of the velocity led to reduced pressure drop increase. This suggested that the cycle durations would also be positively affected, leading to both longer filtration cycles and a reduced cleaning frequency.

$$U = \sum_{i=1}^{n} \frac{\left(V_i - V_{avg}\right)^2}{n-1}$$

Equation 15: Uniformity of Flow Distribution as Proposed by [181]

Experimental determination of uniformity is reliant on there being enough data ports measuring the flow at specific points to determine a representative uniformity. Therefore, Computational Fluid Dynamics (CFD) allows for a higher number of datapoints to be obtained for a given unit. Application of a CFD model allowed for the evaluation of multiple designs, without having to perform multiple experimental tests. This reduced the design phase and associated economic considerations. Table 4 illustrated studies which evaluated the distribution of gases in(to) the bag house.

For large-scale flue gas filtration units, the application of CFD provided a way to evaluate various designs and alterations, without having to commit to experimental examination. One potential limitation is the accuracy of the 3D model and specified flow conditions when using CFD. If the parameters used are not representative, nor cover variability, the results may be impacted. Therefore, whilst analysts such as those in Table 4 have demonstrated the application and breadth, their results are limited to their specific studies. Therefore, their results are suggestive of what could occur when evaluation a different design. However, their methodologies provide a wide range of potential areas to improve the flow distribution to promote media longevity.

Table 4: Flue Gas Distribution Studies

Reference	Study Aims and Outcomes	Application
[182]	Evaluated flow performance of a manifold with multiple rectangular exit points (common in large scale bag houses). Their study evaluated the aspect ratio between of the rectangular exit and found that as the Reynolds number of the gas flow increased, so did the pressure drop across the manifold. However, when this is constant, the pressure drop doesn't significantly increase when the aspect ratio is above a set value.	Their work provided a basis to study the outlet design of the manifold, which feeds each chamber of the bag house. Their CFD model can readily be re-deployed using industrially relevant geometry and designs to investigate the distribution of the flue gas.
[183]	Evaluated both the hopper distribution and central plenum of a 14-compartment bag house using CFD.	Demonstrated the application of CFD on large scale industrial bag houses.
[184]	Examined a manifold with longitudinal tapering.	Illustrated that a tapered manifold, with singular series of outlets, yielded a more uniform distribution of flow.
[185]	Considered different locations of inlets to the bag house unit under CFD conditions	Indicated the effect of flow distribution onto the filtration media and described the resultant filtrate loading. Results indicated that whilst the flow distribution increased, there was still some preferential loading.
[186]	Evaluated a multi-compartment bag house with flow distribution plates in the hopper. Illustrated the variation of flow in the horizontal and vertical axis.	Industrially relevant simulation of a large-scale bag house filtration unit. Suggested regions of increased/decreased flow which would impact media.

Deformation

Deformation of the filtration media is divisible into two factors: chemical [8], [187] and mechanical [154], [188] degradation. Chemical degradation is the result of molecular reactions between the fabric material, flue gas composition, filtrate, and any pre-treatment chemicals [91], [187]. Mechanical degradation occurs due to media movement during filtration and cleaning and pore blockage [141], [189] within the media. Extent to which deformation occurs is dependent on these factors and their resultant interactions, though the longevity of the filtration media is expected to be within years [190]. Factors such as electrical sparks causing ignition [54], [112], ill-fitted media, and ripped media during installation (for example) are ways in which the media can fail. Failure can therefore be classified into two distinct occurrences: failure through increased downstream emissions, or significantly high baseline differential pressure within the filtration unit.

Increased emissions can be the result of holed filtration media [191], [192] or fully blinded/saturated media [123], [193]. For an increase in gaseous emissions, such as HCL, this

may be the result of inefficient treatment processes upstream, though models do exist to determine the minimum [89], [194], [195]. In practice, sites often overdose to ensure treatment but also to allow for any variation in the fuel which may increase the concentration within the stream. If the filtration media develops holes, this creates region(s) of low flow resistivity, promoting flow through the hole and therefore resulted in increased emissions [196], [197]. Holes develop due either improper instillation resulting in ripped media, or due to the expansion, contraction, and flexing [198]–[200] against the support cage causing wear marks which result in the formation of holes and therefore allow filtrate through.

Significantly high baseline pressure drop is the result of both ineffective cleaning and/or internal deposition [5], [12]. Cleaning efficiency is discussed further in section 2.3 but can be surmised whereby an ineffective cleaning cycle leaves a high volume of filtrate at the surface of the media which resulted in an artificially high baseline differential pressure. In contrast, the build-up of filtrate on the surface, that promotes cake filtration [138] required sufficient blockage of pores near the surface. Whilst there is some trade-off between leaving some filtrate on the surface to promote better efficacy, over time, particulate migration through the filter will occur. Over time, the amount of filtrate migrating through the filter will naturally increase [141], [189] and contribute to the increase of baseline differential pressure. Consequently, it is diagnostically important to understand these phenomena to evaluate used filtration media. The movement of the media during normal operation is illustrated in Figure 7 [201].

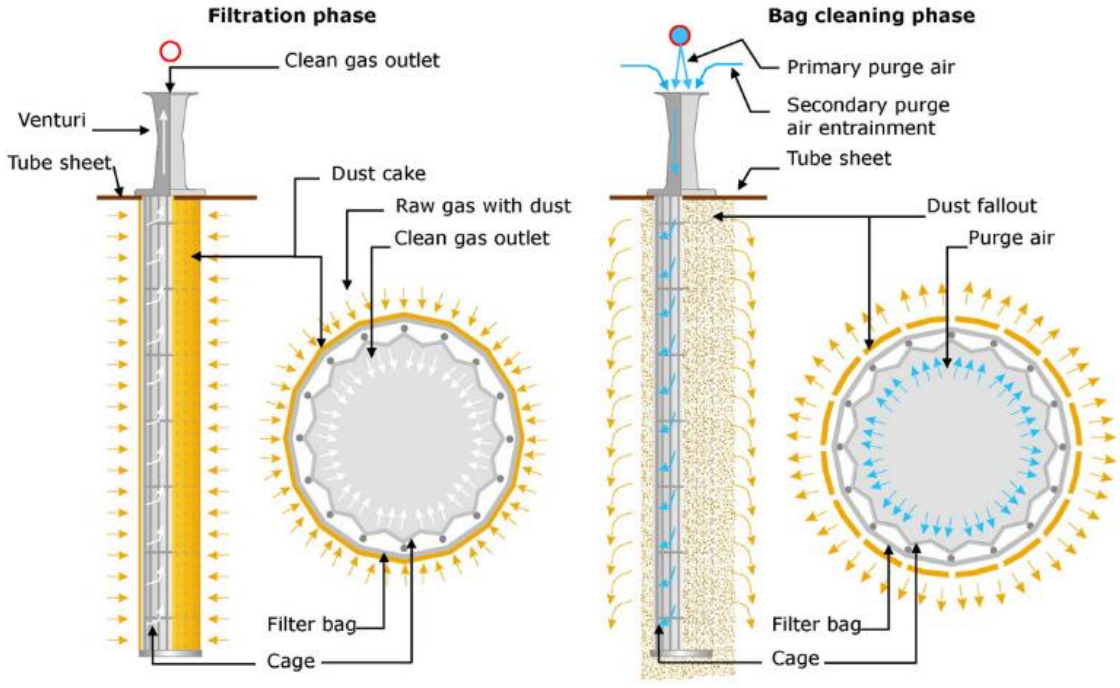

Figure 7: Illustration of Fabric Movement During Filtration and Cleaning Process [201]

Prior to the instillation of new or different filtration media, it is important to determine what effect it may have during operation. Section 2.4 evaluated British Standards (BS) such as BS11057:2011 "Air Quality – Test method for filtration characterization of cleanable filter media" [202] and BS16891:2016 "Test methods for evaluation degradation of characteristics of cleanable filter media" [203] which were specifically designed to evaluate the mechanical and chemical degradation of cleanable filtration media respectively. A detailed discussion on these and other standards can be found within said section. Furthermore, a detailed discussion towards other technical analytical equipment is also presented in Section 2.4.

2.3 Cleaning Process

Pulse jet cleaning comprised of a short pulse of compressed air that is delivered to the inside of the filtration bag [201]. This pulse of compressed air then travelled vertically down the bag. The pressure difference between the pulse and the bag resulted in a directional flow, which forced the filtration bag to expand [141]. As the air passed through, the resultant force between the filtrate and the fibres/filtrate where overcome, which led to dislodgment [193]. Once filtrate has been deposited internally, it is difficult to remove. In contrast, filtrate at the surface of the media can be easily removed. Upon removal, gravimetric forces deliver the bulk of the filtrate towards the hopper for removal. However, re-deposition of filtrate is possible, depending on various characteristics [204]. Cleaning allowed for the filtration bag/media to be regenerated, ready to collect more filtrate from the process without having to shut down for cleaning.

This section discussed the key aspects of the cleaning process. A clear illustration of what a large scale pulse jet cleaning system looks like in reality is shown in Figure 8 [201]. Compressed air is fed into a tank, also known as the header tank. When the demand for cleaning is met, the valve opens for a set period of time which delivers a pulse of air into the purge tubes. These tubes in turn deliver the pulse of air to the vertical top of the filtration bag. Operational and design parameters towards the ownership of pulse jet cleaning are subsequently discussed.

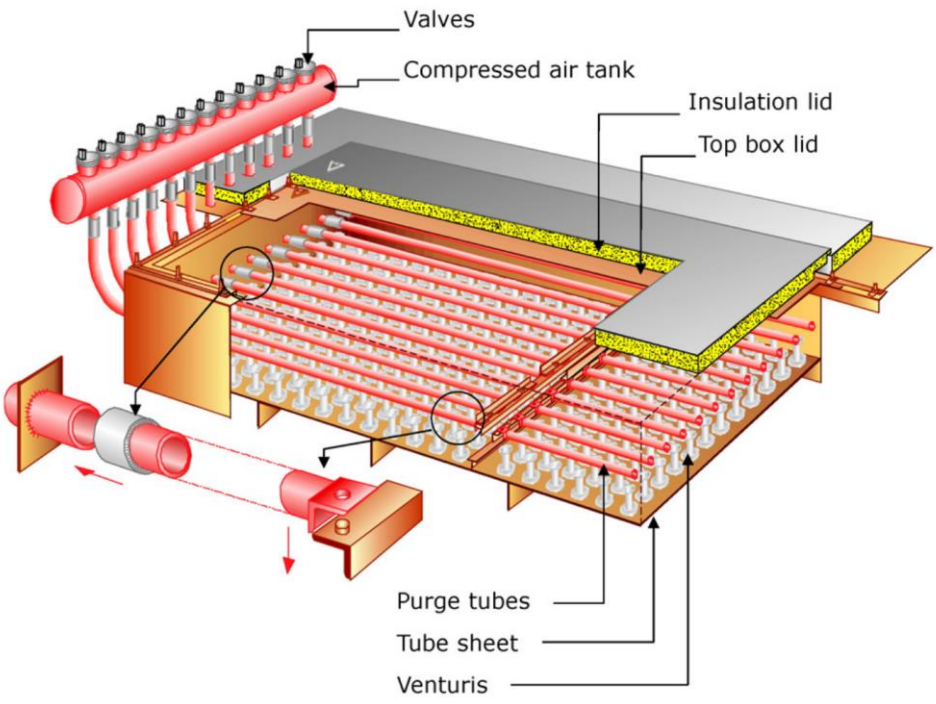

Figure 8: Example Layout of Large Scale Flue Gas Filtration Compartment [201]

Cleaning on Time (CoT) vs. Cleaning on demand (CoD)

Cleaning can either occur at specific time intervals (CoT / cleaning on time) or when a set pressure drop is reached (CoD / cleaning on demand). For CoT, the pressure drop across the filter that can take place is variable and cleaning will only happen when the time interval is reached. CoD is the opposite of CoT, where the maximum pressure drop is defined, and the time interval is variable. The pressure drop curves for CoT and CoD demonstrate the behaviour across the lifespan of the filter are illustrated in Figure 9 [193].

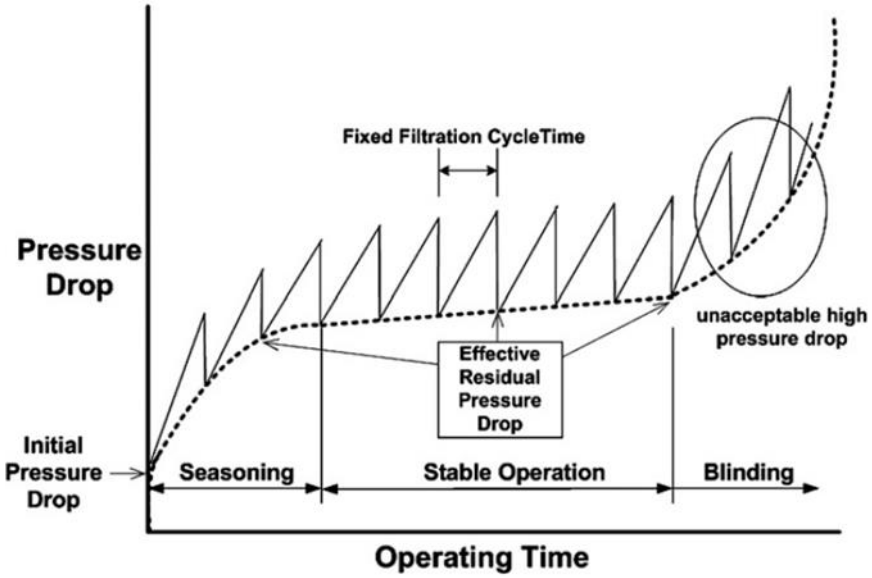

Clean-on-time mode.

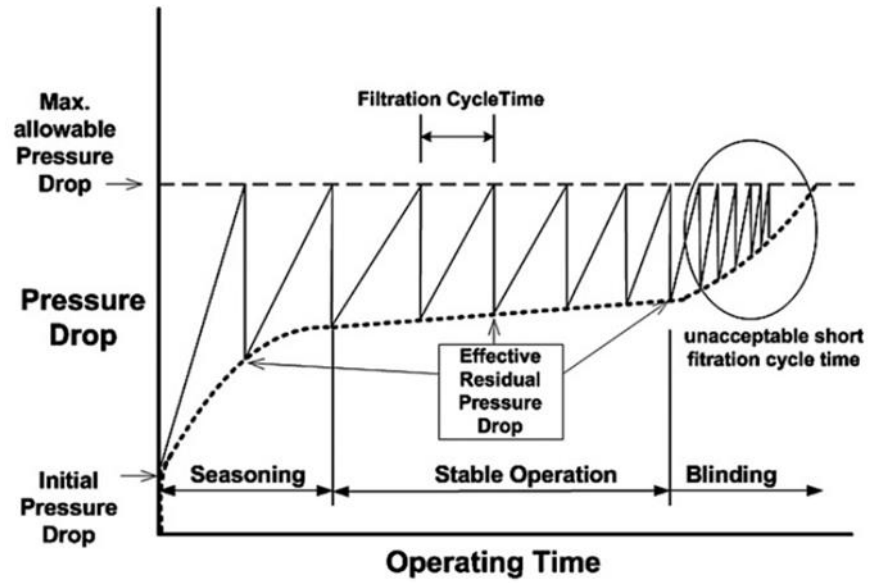

Clean-on-demand mode.

Figure 9: Illustration of CoT (top) and CoD (bottom) [193]

One study that compared the filtration cycle difference between the two methods, with respect to fine (0-15um), medium (15-35um), and large (35-75um) particle sizes [137]. Their experimental study demonstrated that the at the time interval, the pressure drop across the sample was larger than the set cleaning pressure for medium and fine particulate sizes [137]. For CoD, the medium and fine particulate size also had more cycles than the CoT, given that the pressure drop across the filter reached the desired cleaning pressure [137]. For the larger particle size, both cleaning methods where comparable, although the first CoT cycle exhibited a slightly lower pressure drop than the desired pressure for CoD [137]. For the finer particulate matter, the baseline pressure drop for CoD appeared to increase more rapidly than the larger size, which indicated a higher amount of blinding within the filter. Whilst this also occurred for the CoT, its rise wasn't as fast, given more filtrate was collected at or above the surface. Each modes respective 4^{th} cycle appeared to have a near similar baseline pressure drop. This experimental study illustrated the effect of size variation on the cleaning modes, but as it was time restricted, it only suggested the impact of size given it failed to reach an unacceptably high pressure drop/ blinding point.

Studies have experimentally discussed the point at which filter blinding becomes so substantial, that it resulted in a high baseline differential pressure. Studies such as Lo et al., [193] and Schuberth et al., [205] discussed how the cleaning pulse interacted with the filtration. Lo et al., [193] and Schuberth et al., [205] performed CoT studies until an exceptionally high pressure drop across the filter media occurred. Under a fixed cleaning pressure, both authors showed that as the pressure drop increased, the effect of the cleaning pulse reduced [193], [205]. The cleaning pulse is the driving force to clean the media and has to first overcome the initial pressure drop before any cleaning can transpire. Once this is overcome, the cleaning pulse is pressure driven upstream and allowed for cleaning to transpire. This is known as overpressure. As the pressure drop across the filter increased, the intensity of the overpressure decreased, which affected the efficiency of removing the filtrate/cleaning the media. This effect is due to a larger percentage of the cleaning pulse being needed to overcome the initial pressure drop across the filter. Evolution of the overpressure for a full CoT study is shown in Figure 10 [205].

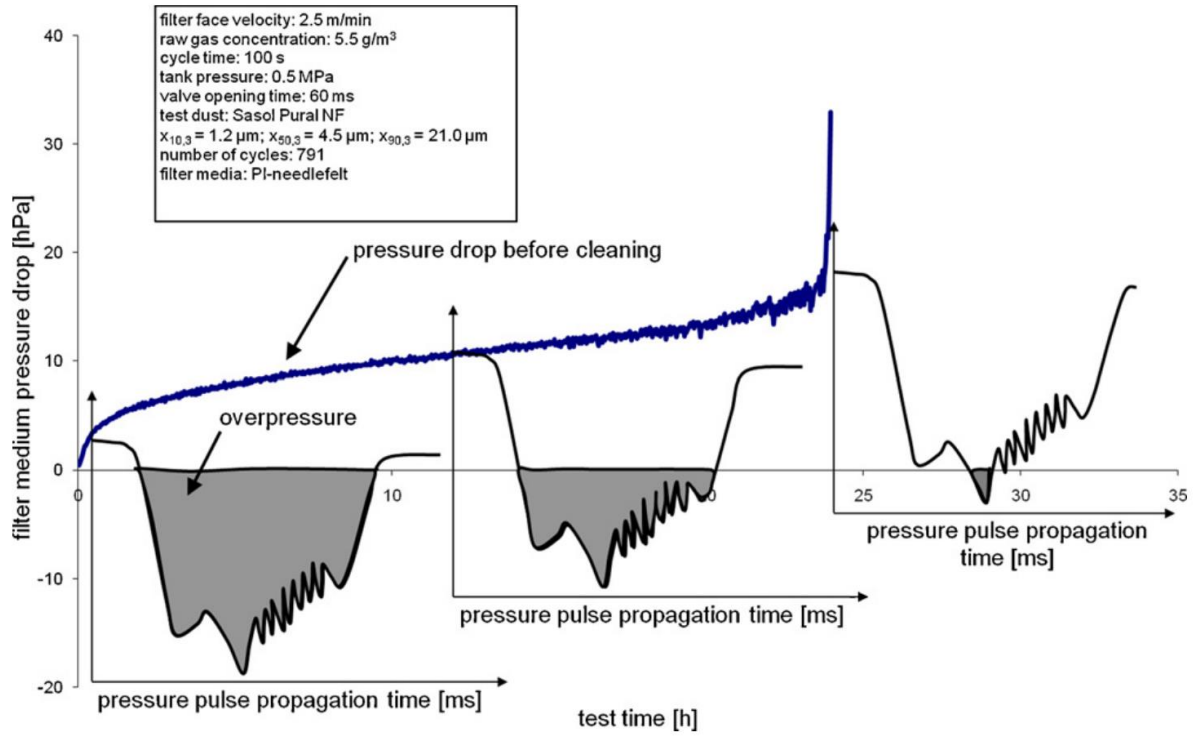

Figure 10:Cleaning on Time (CoT) Example of How the Peak Pressure interacted with the Filter Media [205]

For CoD, the overpressure is constant as the maximum pressure before cleaning is defined by the operator. This resulted in the filtration cycle time being a variable as opposed to CoT where it is constant, regardless of the pressure drop. As the baseline pressure drop increases, the filtration cycle time is reduced due which required more cleaning within a given timeframe. Removal of the surface filtrate still occurred, but as a proportion has been deposited internally, its removal is more difficult which resulted in the increase in said increase.

Filtrate Dislodgment

Removal of filtrate from the surface is a result of the overpressures interaction with the surface filtrate. The directional force of the overpressure, applied to the surface filtrate, caused dislodgment when the adhesion forces are overcome. Various studies such as Tanabe et al., [136], Kim et al., [144], and Kanaoka and Kishima [206] have examined the effects of thickness, cake porosity, cleaning velocity, and cleaning efficiency. The heterogeneity exhibited for particulate and filter media can lead to simplified models being used to estimate the overall adhesion forces. Visser [172] provided a review on the governing adhesion forces and further discussed the limitations between real world complexities and applied assumptions. One other consideration is the moisture present within the stream and its effect of resultant forces. Boudhan et al., [162] examined this and showed that increased humidity

yielded poorer removal of the filtrate through an increased pressure drop post cleaning. Upon completion of the cleaning pulse and removal of filtrate, the pressure drop across the filter media to reduce and allowed for a new filtration cycle to commence.

Parameters such as the retained mass fraction and cleaning velocity have been previously studied by Tanabe et al,. [136]. The retained mass fraction is defined by the mass per unit area of filtrate that has remained post cleaning, compared to the mass per unit area of filtrate just prior to cleaning. As the cleaning efficiency increases, the ratio value tends to zero. Furthermore, Tanabe et al,. [136] also indicated that as the pressure drop across the filter increased, the required cleaning velocity also increased. Another study by Kanaoka and Kishima [206] showed that the efficiency of cleaning increased as the porosity of the cake increased. This was further shown to increase when the overpressure increased, which allowed for an improved clean. Another study by Scoble [207] discussed how patchy cleaning led to a higher residual pressure drop, which required more cleaning, which was also mentioned experimentally by Tanabe et al., [136] through the filtration media being varied which showed differing degrees of internal deposition.

Filtrate dislodgment from the surface of a cylindrical filtration bag over specific time intervals is demonstrated in Figure 11 [144]. This illustration suggested how the filtrate is removed from the surface, first in agglomerate like structures, but transitioning into a finer powder like substance as time increases. Closer inspection of the 40ms snapshot in Figure 11 [144] suggested that some filtrate appeared to remain close to the surface and only partially broke away from the filter. Though it is difficult to verify this, given no further time frames of animation, it demonstrated the movement of filtrate away from the surface of the filter media.

One resultant phenomenon in literature is patchy cleaning which is characterised by retained filtrate post cleaning [208]–[210]. Retention of filtrate leads to an undistributed load on the filtration media. This can be visually observed when areas of the media still present filtrate after cleaning and others do not [210]. This retention negatively impacts the pressure drop, which leads to the filtration cycle duration decreasing and therefore potentially impacting the service life of the filtration bag [208]. Li et al., [208] emphasised the effects of patchy cleaning through classification. However, their study focused on the filtrate and filter being parallel with gravity, which is a less accurate representation of real world use. One issue with modelling and classification of patchy cleaning is the removal, analysis, and classification of

the properties. If the filter is not evaluated to completion, experimental studies only provide a snapshot into patchy cleaning. Therefore, although patchy cleaning is a known phenomenon, its negative effect on pressure drop post cleaning led to exploratory studies on reducing this phenomenon to improve cleaning efficiency.

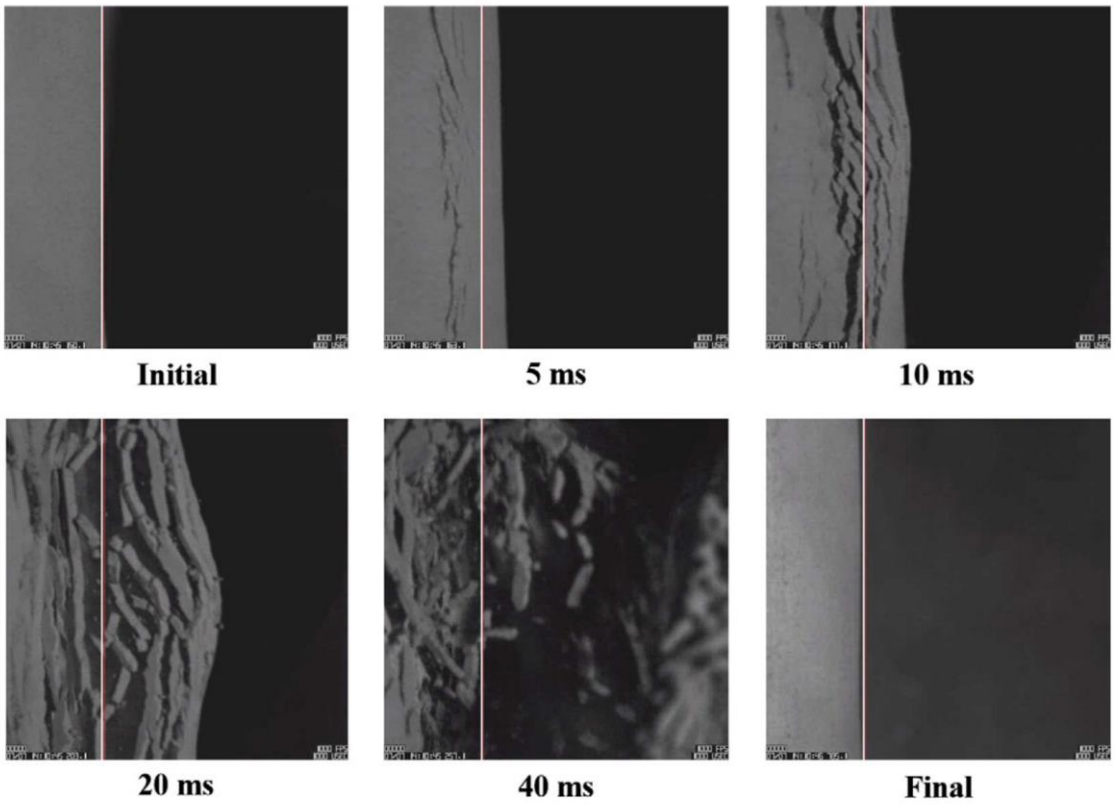

Figure 11: Dust Cake Dislodgment During Cleaning [144]

Another phenomenon which contributed to the effectiveness of cleaning is re-entrainment of previously collected filtrate. Re-entrainment could explain the observations made for Figure 11 [144], whereby it appeared that some of the filtrate broke away from the surface but remaining. Various studies such as Jackiewicz et al., [15], Kurtz et al., [191], and Bulejko [211] have suggested that some filtrate can be re-introduced due to flow conditions and particulate size and density. Consequently, any redeposition will negatively impact the pressure drop. Re-entrainment can occur on both the same filtration bag and/or on a neighbouring filtration bag. If deposited onto a neighbouring filtration bag which isn't being cleaned at the same time as the original bag, then the re-entrained filtrate will affect the pressure drop during the filtration cycle. In both instances, the re-entrained filtrate will decrease the available filtration cycle time, which will lead to an increased cleaning frequency and consequentially a potential reduction in life span of the media, depending on its severity.

Cleaning Pulse Characteristics

Tank pressure and pulse duration are two parameters which influence the efficiency of the clean. One study explored pulse duration and reported that for their study, the duration of the pulse had no effect on the baseline pressure drop post cleaning [212]. Whilst this was supported by the work conducted by Simon et al., [141], other studies such as Lo et al., [193] and Bakke [214] suggested that an increased duration can better recover the baseline pressure drop, but only up to a certain point before reverting back to support Litchwark et al., [212]'s work. Increased duration would increase the volume of compressed air used. This would increase the associated costs of usage. Furthermore, Litchwark et al., [212] discussed the impact of blinding at increased durations, which was a result of over cleaning which allowed more particulates to deposit internally. Therefore, the duration of the pulse needs to be sufficient enough to clean the media, but not too long as to over clean and contribute to blinding.

Kurtz et al., [213] and Kurtz et al.,[196] experimented with the overpressure between 2 Bar and 8 Bar (inclusive). Their work suggested that the flow resistivity increased with age. At lower pressures, this rate was higher, which was attributed to cleaning efficiency. This was further supported by the evolution of cycle time at specific ages of the media, which exhibited a shorter duration for lower over pressures. In contrast, they demonstrated that at higher pressures, the filtrate mass emitted downstream also increased [196], [213]. They stated this was due to the expansion of the pores within the filter, which momentarily allowed for the increased emission. Over the duration of the test, this emission value plateaued. The increased mass of emissions will also contribute to the blinding. Therefore, their work highlighted that for their study, an optimal over pressure existed between effective cleaning (which affected resistance to flow) and emission of filtrate.

Vertical Height Effect (Pulse Jet Uniformity)

Once a pulse is delivered to the top of the filtration bag, it travels vertically downwards to the bottom of the bag. Various experimental studies have examined the evolution of the overpressure across the vertical height of various filtration bags. Table 5 provided example studies which explored the effect of overpressure on various styles of media and conditions. These studies examined various filters and pulse conditions. These studies demonstrated that the overpressure varies along the vertical height of the filter. As the pulse travels vertically down the bag, some travels through the media towards the filtrate on the surface. This caused

the bag to expand due to the resultant pressure gradient between the pulse and the media which facilitated the removal of filtrate from the surface.

Table 5: Studies That Examined the Evolution of Overpressure Against the Vertical Height of the Filter

Reference	Type of Filter	Parameters	Observations
[210]	Cartridge	Types of cones at various distances and diameters	"No cone" – pressure increased down the height of the cartridge across the three pressure sample points. "Normal Cone" - pressure increased down the height of the cartridge across the three pressure sample points. "Cylindrical Cone" – Largely exhibited a local maximum pressure at the middle pressure sample point.
[217]	Fabric Bag	Various On-line Pressures	Parabolic like nature whose focal width decreased with an increase of peak pressure. Cleaning efficiency also appeared to hit a minimum at about the 1.4m height before tending back to >90% efficiency
[218]	Ceramic	Various pulse pressures against nozzle diameter sizes	Two pressure readings, "Top" pressure reading at 200mm below vertical top and "Bottom" pressure reading at 1500mm below vertical top. "Bottom" pressure reading displayed a greater peak pressure than "Top"
[219]	Fabric Bag	Different overpressure values	Considered the dust areal density at the end of experimentation, showed greater densities towards the vertical top and bottom, with the middle showing the lowest density.

In addition, a noted phenomenon in literature is the pulse rebounding of the vertical bottom and travelling vertically upwards. Studies have shown that this rebound effect increased with pulse intensity, and acted as a secondary clean, until the pressures equalised [210], [215], [216]. The effect of this rebound is therefore based on the peak pressure during the rebound phase. During the rebound, the peak pressure will reduce until it equalises with the pressure drop. This reduction will therefore limit the cleaning effectiveness of the rebound. It could however be sufficient enough to re-open pores and promote particulate transgression through which would impact emissions.

Purge Tube Length

As shown in Figure 8 [201], the purge tubes can consist of multiple rows of filtration bags. Various studies such as Andersen et al., [201], Li et al., [216], and Li et al., [220] have examined the effect on the overpressure on various purge tube lengths, each with a distinct number of filters. Studies have shown that the peak pressure varies with the number of nozzles. The peak pressure at the nozzle closest to the header tank appeared to be the lowest, but after increased incrementally until the end of the purge tube. These studies examined

various number of nozzles on the purge tube, which corroborated this increase in peak pressure. One negative impact is the potential for both over and under cleaning of the filtration media. To address this, optimisation across the purge tube length would attempt to reduce the variation, profiting a more consistent and effective clean.

Emission Spike Post Clean

Studies such as Li et al., [137], Li et al., [140], Li et al., [210], and Li et al., [220] have shown that at the point of administering a cleaning pulse, there is a PM emission spike. Both cleaning on demand and cleaning on time exhibited this phenomenon as shown by Li et al., [137]. Their work characterised particulate emissions based on the size of the particulates. Results showed that for all particle sizes (0-75 um) an emission spike occurred downstream of the filter [137]. This study only considered a short operational time of 50 minutes, which equated to four cycles on CoT. This meant that their study only portrayed an insight into the emission spike behaviour as a function of number of cycles. Whilst the CoD exhibited more cycles than the CoT, it again did not reach blinding and therefore only illustrated the emission peak due to cleaning.

The effect of cone design inside the filtration bag and its resultant effect on emissions was considered by [210]. Their study evaluated three designs: without a cone, a normal cone, and cylindrical cone. Results suggested that a cylindrical cone shape yielded a reduced emission from 0.899mgm^{-3} (without a cone) to 0.794mgm^{-3} (cylindrical cone). In comparison, the normal cone yielded a higher emission average of 0.899mgm^{-3} [210]. Whilst the cylindrical cone reduced the emission average by 12%, the results only represented a single dust type and media. Further studies around this would be needed before deployment. A study by Li et al., [140] considered the effect on water on solid emissions and found it increased the baseline emissions. Furthermore, additional hardware (the cone) would alter the current set up of the site, owing to the need to develop a way to install and remove the cone as needed to access the bag.

Unit Optimisation

Various authors have studied ways in which to improve the cleaning pulse. Various authors have aimed to improve pulse jet cleaning, some studies are shown in Table 6. These studies provided insight into how large scale pulse cleaning may be optimised. Through a combination of small scale and pilot scale studies, under various conditions, provides evidence and confidence to suggest initial testing at larger scale, before full deployment.

Table 6: Various Studies Which Looked into the Optimisation of Pulse Jet Cleaning

Reference	Study Title	Study Outcome (s)
[210]	Effect of cone installation in a pleated filter cartridge during pulse-jet cleaning	Considered the installation of a cone inside the filtration bag. A cylindrical cone led to increased filtration cycle duration which translated into reduced cleaning frequency. Pulse jet uniformity also increased with the cylindrical cone. Lower average solid emissions were achieved in comparison to the design without a cone.
[218]	Optimization of Nozzle Design for Pulse Cleaning of Ceramic Filter	Suggested a convergent nozzle displayed a more optimal clean, before evaluating the optimum outer diameter before suggesting an optimal design.
[221]	On the forming mechanism of the cleaning airflow of pulse-jet fabric filters	Demonstrated that a rectifier tube (venturi) at the vertical top of a cylindrical bag led to approximately 1.4 times greater cleaning intensity. Theoretical results were validated through their experimental work suggesting a model for future research.
[222]	Design and performance evaluation of novel colliding pulse jet for dust filter cleaning	Novel study showing colliding pulse-jet cleaning led to an increase in overpressure intensity, but patchy cleaning still occurred despite the increased consumption of compressed air

2.3.1 Cleaning Process Conclusions

Removal of surface filtrate is facilitated by a pulse of compressed air. However, the efficiency of filtrate removal is dependent on the over pressure delivered, to the filtration bag. Furthermore, consideration should be given to the purge tube length and relative position of the bag, given this can vary from the set point. To counteract this, studies have contemplated the use of nozzles, tubes, and additional structures to promote uniformity across both the vertical height and purge tube. Therefore, there is a degree of variation across the vertical height of the filtration bag, which could impact the pressure drop immediately after cleaning, which in turn would reduce the longevity of the media.

Studies have shown that the peak pressure at a given vertical height will vary, coupled with the position on the purge tube, this will dictate the effectiveness of the clean. Therefore, a study around the vertical height variation would provide evidence towards the cleaning efficacy and help in addressing this gap and also contribute to the understanding of how the variation effects the filtration media.

2.4 Analytical Techniques

British Standards

Conformity to standards, such as those laid out by the British Standard Institute (BSI), promotes quality assurance, efficiency, and for testing methods can lead to a reduction in economic costs without compromising on productivity and efficiency. For years, implementation of British Standards (BS) has provided reassurance to clients that the reported/presented data is accurate by conforming to a strict methodology. Other standard institutes exist, such as ISO, VDI, ASTM, and DIN standards. Naturally, there may be slight discrepancies between standards. However, regardless of the selected standards, conformity to which increases the perceived quality of the product/service. This work focused solely on the BSI, commonly accredited by the International Standard Organisation (ISO). This international accreditation further certified that regardless of where internationally the performance of the test occurred, it followed specific guidelines which resulted in increased and consistent data for the client.

Nonwoven flue gas filtration media evaluation can be classified into three distinct BS's:

- BS ISO 22031:2021 titled "Sampling and test method for cleanable filter media taken from filters of systems in operation" [16].
- BS ISO 11057:2011 titled "Air Quality – Test method for filtration characterization of cleanable filter media" [202].

And,

- BS ISO 16891:2016 titled "Test methods for evaluation degradation of characteristics of cleanable filter media" [203].

BS ISO 16891:2016 "Test methods for evaluation degradation of characteristics of cleanable filter media" [202] and BS ISO 11057:2011 "Air Quality – Test method for filtration characterization of cleanable filter media" [203] laid out a methodology to evaluate filtration media under different conditions.

BS ISO 16891:2016 "Test methods for evaluation degradation of characteristics of cleanable filter media"[202] focused on a systematic method to characterise degradation through exposure to corrosive gases such as NO_x and SO_x [202], but also HCL, moisture, HF, etc which may be present in flue gas conditions [83], [85], [86]. The standard aimed to simulate flue gas chemistry conditions in an augmented manner to simulate more rapidly prolonged

exposure. From which, the use of tensile testing characterised the degradation. Previous literature has applied the methodology to characterise different media. Rozy et al,. [8] and Fukui et al., [223] characterised the degradation of polyphenylene sulphide (PPS) filter media using this method at NO_2 at various temperatures. They demonstrated the effect of NO_2 concentration over a specified duration and heat, in turn demonstrating the impact that the standard can have on testing samples.

BS ISO 11057:2011 "Air Quality – Test method for filtration characterization of cleanable filter media" [203] afforded an example test rig and evaluation method to evaluate the mechanical deformation through emission and blocking [203]. The aim of this standard was to evaluate the new test filter media quickly and efficiently, without undertaking a long-term study which could last months or years. A detailed description and evolution of this experimental rig can be found in Pham et al., [224]. Previous researchers such as Hoppe et al., [225] and Schuberth et al., [205] have used the ideologies presented within the standard to evaluate filtration media. Hoppe et al., focused on depth filter media and compared the standards efficacy with the results from their experimental methods. They showed agreement between the two results and demonstrated a µCT model to show local variation within the sample as opposed to a global value [225]. Schuberth et al., [205] argued that the aging phase had a influence on the subsequent data of the test method. They demonstrated that after a certain aging time, the differential pressure across the media increased significantly. Their study, over various filtration velocities and valve opening times through a clean on time method, demonstrated the differential impact that the cycle ageing phase can have on subsequent results.

The two aforementioned British Standards demonstrated a method to evaluate filtration media for its chemical and mechanical degradation respectfully. Use of accelerated conditions aimed to reduce the test time, instead of prolonged testing given the media may actually be in operation for years. They afforded tests to a given specification and analytics which could evaluate various media and function as a tool to aid selection of said filtration media. Their inclusion of standards in literature (studies such as [8], [138], [180], [223], [225]–[227]) demonstrated the impact and versatility of the presented methods. Whilst they achieved this aim, limitation of the results tended towards specific degradation and not a combination which less representative of flue gas filtration systems.

Evaluation of a singular degradation mechanism limited the translation between academic and industrial studies. In flue gas filtration, exposure of the media to combustion gases and filtrate will dictate the overall degradation. However, pilot scale studies such as [143], [150], [162], [189], [228] provided evidence, showing that although a combination of the two can be made, the speed at which a similar methodology in terms of number of cycles is drastically increased from minutes/hours to days. This time increase therefore restricted subsequent analysis in terms of an increased timeframe and inadvertent economical factor (labour, supplies, etcetera). Consequently, although the separation of the two degradations limited the translation, it afforded the ability to evaluate multiple different samples in a quick manner in comparison.

Adaptation of both standards could yield a method to bridge the aforementioned limitation. A combination of standardised flue gas chemistry simulation, coupled with standardised test dust over pre-defined intervals would allow for better representation of industrial settings, without the time constraint. Therefore, research in this area would determine if this were a viable option and allow for a study to directly compare the two standards in isolation, with the proposed new method, focusing still on the reduced experimental time.

BS ISO 22031:2021 "Sampling and test method for cleanable filter media taken from filters of systems in operation" [16] aimed at providing a clear, precise method for sample retrieval and analysis from flue gas filtration bag houses. This comprehensive standard illustrated withdrawal positions of the media from a compartment/cell, their subsequent division into three distinct sections, and subsequent required and additional evaluation. The standard aimed to achieve a uniform methodology to evaluate filtration media. It achieved this by providing specific instructions towards the subsequent tests required such as visual observations (eye and microscopy), tensile strength and elongation ration, air permeability, and mention towards mass and thickness [16]. It also made mention of the state of the media, requiring cleaning before (in parts) and after analysis. This comprehensive standard was the first of its kind that attempted to regulate the testing of cleanable filtration media.

Although comprehensive, the standards linguistical structure in parts limited the clarity of the desired methodology. For example, in Section 5.5.4 the method to clean the filtration media achieved through "brushing" or "a cleaner" so long as it does not damage the filter [16]. Yet, in the previous section 5.4 it also included "vacuum cleaner" "air jet" and/or "scraping" [16] as a possible cleaning method. Furthermore, Page 8 of the standard [16] detailed the thickness

measurements as optional, yet the example test report on Page 18 [16] required these measurements. Also, the methodology presented for these readings, including mass readings, where omitted yet still required. Consequently, the presented language presented a degree of uncertainty within application of the standard which could result in compliance issues and limited the standards ease of compliance.

Given this limitation, to use of additional standards may provide assurance to the client that the subsequent analysis fully complied, regardless of the observed limitations. Whilst research is required around the expected difference of cleaning methods, BS ISO 22031:2021 "Sampling and test method for cleanable filter media taken from filters of systems in operation" [16] made reference to the BS ISO 9273:1995 [229] standard for air permeability determination. Provision allowed for the use any other suitable standards. This included the nonwoven textile standards BS ISO 29073 and BS9073 which characterised various parameters on nonwoven textiles. To address the aforementioned limitations, BS ISO 29073-1:1992 "Determination of mass per unit area" [230], BS ISO 29073-2:1997 "Determination of thickness"[231], and BS ISO 9073-15:2008 "Determination of air permeability" [232] where consulted.

BS ISO 29073-1:1992 "Determination of mass per unit area" [230]

A standard for the determination of mass per square centimetre of a nonwoven, which required a minimum of three samples of surface area greater than 50,000mm. If required and determined prior to the commencement of the evaluation, the coefficient of variation required five samples and reported to the nearest percentage of 0.1%. Any sample size, such as 250mm by 200mm, so long as the size was equal to/greater than 50,000mm^2 ensured conformity. In addition, the standard referred to its method accounting for the anisotropy of nonwovens which accounted for this by requiring the sample size be no smaller than 50,000mm^2.

BS ISO 29073-2:1997 "Determination of thickness"[231]

A standard to determine the thickness of a nonwoven, using a pressure foot of 25,000mm^2 and reference plate larger than 25,000mm^2. The sample surface area size should be greater than 25, 000mm^2.The samples sits between these two plates and the pressure foot exerted a vertical pressure of 0.1kPa until equilibrium, whose definition is at ten seconds after no movement of the footer. The resultant distance between the two plates indicated the thickness of the sample. Repetition of this method occurred through a minimum of ten different

samples, reporting the subsequent arithmetic mean and the coefficient of variation to 0.1% (if required).

BS ISO 9073-15:2008 "Determination of air permeability" [232]

A standard for air permeability which provided a numerical value to the volume of air passing perpendicularly through a given surface area at a pre-defined pressure. Compliance with the standard required that the evaluated surface area be either: $20cm^2$, $38.3cm^2$, or $50cm^2$, which corresponded to a minimum sample square size of 50mm, 70mm, or 80mm, respectively. The standard preferred large sample sizes but could accommodate for a sample size of 100mm by 100mm. Once place over the test area, and clamped to ensure tautness, the sample is ready for evaluation. The sample incurred a pre-defined pressure drop across it at either 125Pa, 150Pa, or 200Pa. This pressure drop happened due to a blower located downstream, which forced the air through the sample. Once achieved, the display indicated the air permeability result. Repetition of the sample occurred five times as a minimum, or through the number of repeats agreed prior to the start of evaluation. To ensure compliance, calculation of the resultant arithmetic mean and confidence variation to the nearest 0.1%, alongside reference to the standard's section eight, defined the resultant report.

Further Consideration Points for BS ISO 22031:2021 "Sampling and test method for cleanable filter media taken from filters of systems in operation" [16]

The standard aimed to provide a comprehensive methodology to assess cleanable filtration media, such as the nonwoven bag house filtration media used within the energy sector. It presented not only a sample withdrawal and periodical testing framework, but also a method to evaluate each subsequent sample. To do so, division of the sample into three distinct sup-samples as recommended by the standard for compliance. Subsequent testing yielded information about each distinct third and once collected, which made allowance for further analysis. To complement this, information about the original/new/virgin filtration media, within the report, afforded a direct comparison between the new and used data. The methods required to evaluate the sample where also provided and discussed within the standard. Overall, the standard further aimed to provide a comprehensive method to evaluate the media, without compromising of the time taken to perform said analysis.

One assumption was that the sample taken from each vertical third was representative of its original location, irrespective of the overall vertical height. The vertical height of flue gas filtration media varies depending on the exact set-up. Observations made during this project

saw, on average, four to six meter bags in the vertical height. Isolation of samples in each representative third at the millimetre scale casted uncertainty as to whether or not these samples where representative of their vertical thirds. By only evaluating in thirds, the total evaluation time reduced. This reduction allowed for better suitability from a practicality perspective, given a site may not want to have prolonged periods of downtime to complete evaluation. A study surrounding this assumption would provide either supportive evidence or counter evidence towards its suitability as an assumption.

Furthermore, the obscurity surrounding the thickness and measurement methods inadvertently may lead to variation amongst analysts. Though the required analytical methods such as air permeability are exampled in BS ISO 22031:2021 "Sampling and test method for cleanable filter media taken from filters of systems in operation" Appendix B1 [16] and C1 [16], it only illustrated what is to be examined and not the number of repeats or variation noted. The person performing the analysis could rely on the BS 29073 standards for mass and thickness, respectively. However, the person performing the analysis could simply choose to follow another method and still comply to the standard. The standard did however reference BS 29073:2008 [232] for air permeability. This could suggest the former point is more appropriate for compliance. The requirement to report the coefficient of variation is only for air permeability. Even if the mass and thickness standards were complied with, it is still an optional point for analysts. Consequently, the aforementioned obscurity may yield variations in the report produced for each sample.

To address these points, research conducted would determine a suitable method for mass and thickness for a given sample size, incorporation of a suitable methodology, and show the variation, all without impacting on the original aim of the standard. Given the standard omitted large sections and assumed representation, a study across the surface area of the filtration media would show the potential variation in the results. If the aforementioned studies were performed, it would provide a basis to demonstrate the potential variability across multiple analytical techniques, which would aid analysts when evaluating nonwoven filtration media from bag houses.

Air Permeability

Air permeability is an analytical technique which defines the volume of air passing through a given area within a defined unit of time, under a set pressure across the sample. Dimensions for permeability, can be reported in $(Ldm^{-2}min^{-1})$ or similar variations [233], [234].

However, other forms of air permeability can be found in literature which have units of (m^2) [148] or (cms^{-1}) [4] . The specific unit is dependent on the method used to evaluate the permeability of a sample.

$$q = -\frac{\boldsymbol{K}}{\mu}\nabla P$$

Equation 16: Flow Field Through a Porous Sample [235]

Fluid flow, through a porous sample can be described by Equation 16 [235] (Darcy's law). The fluid flux (q) is a function of the permeability tensor $(\boldsymbol{K})$ over the fluid viscosity (μ), multiplied by the pressure gradient (∇P) [235]. Consequently, for a given sample, at a known pressure gradient and fluid flux, calculation of the permeability is possible. Whilst Equation 16 [235] is capable to define the air permeability at a given point in time, it is difficult to account for particle deposition and the resultant porosity deviation. Derivation of Darcy's law yielded a calculation to determine the permeability and is shown in Equation 17 [236].

$$q = \frac{Q}{At} = \frac{k_p \Delta P}{\mu L} \; or \; Q = A \cdot T \cdot \frac{k_p \Delta P}{\mu L}$$

Equation 17: Example of the Derived Darcy's Law to Determine Permeability [236]

Section 2.2 discussed the permeability during operation, with a particular focus on the debate on the use of the Kozeny-Carman equation to determine porosity or cake resistivity (permeability) [145], [150], [159]. For offline sampling, the use of an air permeability machine uses the principle of Darcy's law to determine the permeability of a sample. Though instead of the units being an inverse length, representation as a volume flow over a given surface area made the parameter more relatable and clearer to understand/interpret the results.

In Equation 17 [236], the fluid flux (q) is defined by volumetric flowrate (Q), over a given area and time. Alternatively, the multiplication of the flow permeability (k_p) and the differential pressure over the fluid viscosity and thickness of the filter also gives the fluid flux.

Evaluation of air permeability required the use of a machine such as the one used by Ince [233]. Ince [233] performed a study which evaluated the difference between having multiple layers of nonwoven filtration media. Though Ince [233] varied the pressure drop across the filter, and the surface area under investigation, they demonstrated that as the number of layers (thickness) increased, the air permeability decreased. Thus, inadvertently illustrating the

effect of thickness on air permeability. They later justified the change of test area by demonstrating no statistical significance between the $20cm^2$ and $38cm^2$. The change in pressure drop did however show a statistical difference, which showed that the air permeability increases with pressure drop. The study by Ince [233] accounted for this due to the Bernoulli equation, affording the increase due to energy increase drawn through the sample. This study therefore provided evidence towards why different filters exhibit different air permeabilities, though Ince [233] did not consider this due to properties, only by an increase of thickness.

Zhu et al., [236] expanded the idea of parameter variation in fabrics, evaluating the effects of thickness, porosity, and density on air permeability Their study corroborated the findings of Ince [233], showing that as the thickness increased, the air permeability decreased. In contrast, as the pressure drop across the sample increased, so did the air permeability. Their study expanded by considering the density of the fibres and the porosity. Zhu et al., [236] method to calculate porosity (ϵ), which was then used to determine the mean pore volume is shown in Equation 18 [236].

$$D = \frac{\pi f}{4(1-\epsilon)} \; where \; \epsilon = \left(1 - \frac{\rho_n}{\rho_f}\right) \cdot 100$$

Equation 18: Steps to Determine Effective Pore Diameter [236]

As the pore size decreased (D), and the porosity decreased, so did the air permeability.

Humidity in the air is another condition that may impact the air permeability. Miguel [160] performed a study which examined the pressure drop evolution of cleanable fabrics with a humidity variation in the gas stream. This work reported the air permeability at 23%, 53%, 61% an 90% humidity. Reported in units of m^{-2}, the resultant air permeability difference for the evaluated humidities was $0.14 \cdot 10^{-11}$ which suggested that the humidity did not necessarily affect the air permeability. However, the study by Miguel [160] was to determine the effect of humidity during filtration, which did have an impact on the rate at which the pressure drop increased. This suggested that although under clean conditions it may not impact the air permeability, it could affect the longevity of the media which will, in turn, affect the air permeability.

Section 2.2 discussed the impact of humidity and other factors that affect the longevity, such as the dust concentration, which will determine not only how the air permeability evolves, but

how the pressure drop across the filter evolves too. For example, Wang et al., [148] conducted such a study which investigated cake formation at different concentrations. Another study by Silva et al., [145] illustrated the how the porosity (ϵ), particle size (d_p), and particle density (ρ_p), can affect the cake resistivity to flow (permeability) (k_c) and is exampled in Equation 19 [145] which also used the fluid viscosity of the gas (μ_g).

$$k_c = \frac{150(1-\epsilon)}{\epsilon^3} \cdot \frac{\mu_g}{\rho_p d_p^2}$$

Equation 19: Example Equation Which Described the Flow Resistivity Caused By Particulate Density, Size and Cake Porosity [145]

Consideration should be given towards the fabrication process parameters, such as punch density, penetration depth, and stroke frequency [133] which affect the areal density, thickness, and resultant porosity for large scale fabrication of nonwoven filtration media [132]. Inherent process variation during the production will therefore impact the air permeability. Studies conducted by Fukasawa et al., [4],[237] and Kanaoka [138] addressed this gap by performing a controlled air permeability study. These studies illustrated the air permeability variation as heat maps across the surface area of new filtration media. Therefore, they addressed and demonstrated the impact of the fabrication process at a larger scale than previously done. Although one limitation to their studies is that they only considered new, unused filtration media. Appendix B examined the air permeability variation across a piece of virgin media.

One limitation across all studies is the static nature, coupled with the locational variation of the new media. Exhibition of this variation on the filtration bag would impact the variation during usage. Whilst previous studies have shown that the permeability evolves over usage, they omitted the variation aspect across the full surface area of the filtration bag. Consequently, a literature gap exists whereby evaluation of the full surface area of a filtration bag for air permeability to determine localised variation. This in turn will aid to understand the variation over a large surface area and aid in developing how researchers evaluate filtration media which has a significantly larger surface area than the prescribed test area.

Consideration must also occur towards the time required to process such a large surface area. Larger studies that evaluate variation in new media, such as those shown in Fukasawa et al., [4], Thomas et al., [138], and Fukasawa et al., [237], were likely not to be under any significant time constraints. In contrast to industrially derived samples from large scale

combustion sites, a similar study would require discontinuing standard analysis in favour of an exploratory study. Currently, standard analysis required the bad to be divided into three sections, a sample removed from each section, and air permeability performed over three distinct locations as shown in BS ISO 22031:2021 "Sampling and test method for cleanable filter media taken from filters of systems in operation" [16]. This method made provisions for the evaluation of multiple samples in a quick and timely manner. Doing so, allowed for a quicker transition between offline to online. If a large mapping study occurred on the remove filtration media, not only would the data focus only on air permeability only, but the time required would increase exponentially. Therefore, an exploratory study on a used filtration bag would address the literature gap, allow for exploration of the variation, and examine if the standard is adequate to represent any said variation.

Gültekin et al., [3] appraised porosity and air permeability measurement using machine learning and light microscopy. Their study required the use of image processing techniques and neural networks to establish a model to evaluate the aforementioned parameters. Whilst there was a good agreement between the predicted and actual results, they only evaluated one specific type of new media. Nazarov et al., [134] also presented a model to predict air permeability, again using only new filtration media. However, the complexity to evaluate the air permeability, in contrast to the manual method, was higher which reduced the likelihood of pick up into industrial practice. Furthermore, they only validated their respective models based on new media. Resultantly, whilst the idea of evaluation air permeability visually is possible, further studies around used media would ascertain the validity of the technique. In addition, the automation of the process and comparison between traditional techniques would further support or denounce the technique in relation to deployment into an industrial setting.

Mass and Thickness

Mass and thickness determination of a sample is a standard analytical technique used to help evaluate filtration media in studies such as Chang et al., [238], and Sikorska et al.,[239].

Evaluation of the mass, in comparison to a baseline value, allowed for the determination of the mass of deposition within/on the filter. Liu et al., [5] demonstrated this by comparing five different filters, which predominantly collect either through surface or depth filtration. Three of their examined filters demonstrated that the deposited mass post clean where higher in comparison to the two surface filters which where comparatively lower. Whilst their comparison was static and therefore did not consider the deposition variation over time, it did

highlight the key differences between surface and depth filtration through pressure drop and collection efficacy. The depth filters showed a comparatively lower baseline pressure drop. This is due to the increased pore volume which allowed for the deposition to occur. Conversely, surface filtration promotes surface and cake formation. Given that the removal of cake filtrate is possible, this resulted in a significantly lower pressure drop upon cleaning. Filtrate deposited internally is difficult to remove without intensive treatment. Therefore, their study provided an insight into the benefits of this method.

Another study, conducted by Chang et al., [139] demonstrated the mass evolution over a single filtration cycle. Their study considered experimental and theoretical data and showed that both corroborated for a single cycle for both collection efficacy and pressure drop. Whilst Chang et al., [139] demonstrated the evolution of depositional mass against depth, surface, and cake phases, its consideration of only one cycle did not illustrate how the depth filtrate may evolve over time and impact the pressure drop. As shown in various studies Tanabe et al., [136], Li et al., [140], Boudhan et al., [162], and Kim et al.,[240], The resultant increase in baseline differential pressure post clean is associated with particulate retention. Therefore, whilst their study confirmed it possible to model the evolution of deposition mass, it was only valid for the single filtration cycle which limited the application when considering multiple filtration cycles.

One limitation with the study conducted by Liu et al., [5] is the fixed sample position which inadvertently described the surrounding media. Studies by Fukasawa et al., [4], [237] mapped the fibre mass distribution of new nonwoven media and with a resin and membrane finish [4]. Although their study only considered new filtration media, it addressed the localized sample gap in the study by Lie et al., [5] through the evaluation of a significantly large surface area. Their study combined the mass, with thickness and air permeability to further demonstrate the variation. However, their study ceased at this point and did not consider any variation due to filtrate loading. Localized variation during operation will impact the resultant values obtained from mass (thickness and air permeability) analysis.

Apart from the studies conducted in Fukasawa et al., [4], Rozy et al., [8], Fukasawa et al., [237], and Lie et al., [241], thickness measurement appeared static and used to aid the description of studies such as the single fibre theory (SFT) [135], [242] or flow considerations through the sample [147], [155]. Studies by Fukasawa et al,. [4] and Fukasawa et al, [237] considered the thickness deviation over a large surface area. The study conducted

by Rozy et al. [8], demonstrated that the thickness evolves over time. Their study focused solely on chemical degradation and did not determine if the mass of the sample also evolved over time. However, this is the closest study found during the project which demonstrates the evolution of thickness over time.

The study by Liu et al., [241] used computational fluid dynamics (CFD) to evaluate both the deposition mass and dust cake thickness. Their study on a ceramic candle filter demonstrated the possibility of simulating samples using pilot scale experimental facilities. The study simulated 120s of filtration before the computational filter results presented a results map similar to that of [4], [237]. Limitations within this study centred towards a specific time period and, coupled with the use of ceramic rather than fibrous filters, reduced the impact in terms of comparison to nonwoven filtration media. Comparison to experimental is also difficult, requiring evaluation of the ceramic as a function of its cylindrical nature as opposed to flat as it is within the computational result.

Subsequent studies could therefore utilize this literature gap, combine mass, and thickness studies over new and used filtration samples to determine the variation over a large sample area. If possible, samples from an industrially setting over incremental periods would address the evolution aspect of the gap, whilst a large scale surface area evaluation would identify the variation. This would help to address the literature gap, yield industrially relevant data which could help understand operational performance at a site level. The study would therefore aid to understand the variation across the surface area of a large sample and how it could impact site decisions to replace or retain the filtration media.

Additional available techniques

A multitude of experimental techniques are available for use to aid in understanding both the filtration media and filtrate. Discussed below, a discussion on the aims, advantages, and limitations of the selected techniques is available such as moisture, particle size distribution, and tensile testing. However, it is important to note, that this list is not extensive and is based on those seen within literature during the project and within industry.

Moisture

Normal practice is to have an operational bag house temperature greater than 150°C [54] which is above the acid dew point. Below this, condensation of acidic compounds Previous studies by Rozy et al,. [8], and Cai and Hu [243] have shown the effect of chemical

deformation on filtration media when the temperature is reduced. Naturally, the acidic dew point is dependent on the chemical compounds present in the flue gas and is affected by the efficacy of any pre-treatment processes such as calcium carbonate [194] or sodium carbonate [89]. At this temperature, the water molecules present in the flue gas and filtrate will be gaseous, unless a temperature region below 100°C had occurred anywhere within.

Removal of filtrate and filtration media from the combustion site, allowed for water to condensate and absorb on the fly ash. The amount of absorption is governed by the hydrophilicity of the ash within a given sample, with further absorption possible due to any charge imbalance of the element [93]. Therefore, moisture analysis aimed to identify the hydrophilic (and inadvertently hydrophobic) nature of the filtrate, which is therefore a function of the chemical composition of each respective sample. The sample size will therefore impact the variation in the result. Expectation therefore is that as the sample size volume evaluated increased, a more representative result would ensue.

Thermogravimetric analysis (TGA) and moisture determination through a drying oven are the two most common methods presented within literature. Other techniques, such as the use of a microwave sensor [244], or a portable NIR spectrometer [10] have been used to determine moisture. One concern with the use of specialist equipment and techniques is partly the capital and expertise, but the effect that the filtrate inflicted on said equipment. As a result, literature tended towards known, easily repeatable methods such as TGA and moisture determination through oven drying. One study compared nineteen different fly ash samples with TGA and oven drying [176]. Their results illustrated the difference between a sample size of 2-4g for oven and 30-50mg for TGA had on the resultant moisture content.

One benefit of the TGA method allowed for a clear, more defined determination of the moisture within the sample. The weight deviation record occurred internally during operation [126], unlike the oven method which required withdrawal from the oven and weight. This withdrawal from the oven would potentially re-introduce moisture into the sample given the temperature reduction and therefore affect the accuracy of the method. One limitation of the TGA method though is the sample size evaluated in comparison to the oven method, coupled with the inability to evaluate multiple samples simultaneously. The sample mass in literature for the oven method centred around the 5g-10g region per sample, placed into the oven at a temperature of ≈105°C±2°C [43], [245]–[247]. The simplicity of the oven drying method, which allowed multiple samples of a greater representation to the bulk chemical composition

saw prevalence within literature. The calculation used to determine the moisture percentile ($m_{moisture}$) based on the original/wet (m_w) and dry (m_d) basis is shown in Equation 20 [248], [249].

$$m_{moisture} = \left(\frac{m_w - m_d}{m_w}\right)$$

Equation 20: Example Calculation Method to Determine Moisture Content [248], [249]

Particle Size Distribution

Particle diameter affects not only the rate of pressure drop [137], but is included in models such as the SFT [135] to predict the efficacy of collection. If the test dust/filtrate used is in a powder form (fed into the experimental apparatus), then the distribution of size can be determined through the use of laser diffraction. Equipment such as the Mastersizer 3000, produced by Malvern Panalytical (U.K.) appeared frequently within literature in studies such as Fuller et al., [93], Mukhopadhyay [113], Joe et al., [117], Cirqueira et al., [189], and Hoppe et al., [225]. Other equipment, such as the aerosol spectrometer "Welas digital 3000H" by Palas, Germany [204] operated on a similar principle through the use of light scattering techniques to identify particle sizes. The difference being that although both used powder form dusts, the Welas analyser measured downstream of the test filter, as opposed to the bulk/upstream. Downstream measurements provided an understanding towards the collection efficacy and allowed for the characterisation of emission spikes caused through cleaning [137], [213].

In controlled studies, the characterisation and evolution of particle size distribution is possible, owing to ease of access and methodical experimental methods. In contrast, determination of particle size relied on previously collected filtrate. Either from the surface of the filtration media, at the hopper, or particulate on the clean side of the tube sheet. The latter of which would suggest failure and potentially yield biased results. Sampling is therefore only a representation of a given particle size based on its observation point, which increased the difficulty in obtaining the true representative PSD in the flue gas without in-line sensors.

Porosity

Rawal [250] presented comprehensive work which compared the experimental method of liquid extrusion porosimitry to evaluate the pore diameter against theoretical models [250]. Other techniques such as nitrogen adsorption isotherm [93] are possible to evaluate the pore

volume. The use of specialist equipment limited the deployment through literature. More common is the use of mathematical representations such as Equation 21 [145] which provided an example of how previous research has determined the porosity (ϵ). Other authors, such as Hsiao et al,. [158], Tien and Ramarao [159], and Kim et al,. [251], have used similar equations to determine the cake porosity. Filtration media can also be determined this way, as shown by Bian et al., [135] and Tanabe et al., [136]. One of the limitations of this method, unlike that of the experimental techniques which can account for this, is the inability to account for internal deposition as a secondary material. For Equation 21 [145], the mass per unit area (M), is calculated using both internal filtrate deposits and fibres under approximate conditions. Given the filtrate density (ρ_p) is higher, the resultant calculation would yield a lower porosity as a result. Chapter 7 discussed this in further detail and suggested a way in which to account for this.

$$M = LA\rho_p(1-\epsilon)$$

Equation 21:Example Calculation of Porosity for a Single Material [145]

Scanning Electron Microscopy (SEM)

Scanning electron microscopy provided imaging of a sample and elemental composition through energy dispersive X-ray/spectroscopy (EDX/EDS). SEM imaging provided illustrative examples of the morphology of both the filtrate and fibres as exampled in Rozy et al., [8], Roy and Ishtiaque [133],Bian et al.,[135], Tanabe et al., [136], Podgorski et al., [174], and Cirqueia et al., [189]. Studies by Suárez-Peña et al., [12], Barros et al., [156], and Cirqueira et al., [189] illustrated the evolution of internal deposition through Imaging techniques. Some studies that have used SEM-EDX/EDS Fuller et al., [93], Fukui et al., [223], Mahmoud et al., [252], and Esteves et al., [253] have examined the elemental composition of various filtrates and fibres. Whilst the technique of SEM-EDX afforded an indication of the chemical composition, it did not necessarily yield a definitive composition. In addition, like the TGA method, the volumetric amount studied is small, which would increase the variation. Finally, the economical consideration towards the use of the equipment is significant, which may restrict the volume of samples evaluated.

Tensile Testing

A test whereby an applied directional load to a filter sample resulted in a load displacement curve. The maximum force exerted on the sample, prior to breakage occurred at the peak of

this curve, also noted is the elongation of the sample. Equation 22 [9] provided an example calculation to determine the tensile strength of a sample (T_{ensile}), calculated by the applied force (F) over the multiplication of the sample mass per area (m_{sample}) and sample thickness/width (t_{width}). Performance of tensile testing usually occurred in two directions: the machine direction and cross direction. Studies such as Çinçik and Koç's [9] and Değirmenci and Çoruh's [254] explored and discussed the variation in the machine and cross direction showing the difference when analysing in both directions. Other studies, such as Fukui et al., [223] and Rozy et al., [8] illustrated the evolution of the tensile strength over different periods of operation. In their studies, both discussed the effect of NO_2 at various temperatures and exposure times in the machine and cross direction. One limitation of these studies has been the exclusivity to gaseous streams only. They also made reference to the standard BS ISO 16891:2016 "Test methods for evaluation degradation of characteristics of cleanable filter media" [203], which laid out a clear methodology for their work. Addressing this limitation would see the evaluation of particulate laden samples being evaluated similar to samples evaluated by Rozy et al., [8], and Fukui et al., [223] from industrial sites. Whilst this data would take years to completed due to the requirement for the sample to be placed under industrial conditions (and therefore could be in place for years to achieve a single datapoint), it would provide a unique, more accurate and representative, insight into the evolution of tensile strength over greater periods of time. From this, a more accurate model at the site level, would be feasible, aiding a model for longevity prediction.

$$T_{ensile} = \frac{F}{t_{width} \cdot m_{sample}} = \frac{N}{(mm) \cdot (gm^{-2})} = \left(\frac{N}{tex}\right) = \left(\frac{GPa}{gcm^3}\right) \; or = 1 \; Mega \; Yuri$$

Equation 22: Calculation of the Tensile Strength of a Sample [9]

X-ray Diffraction (XRD) and X-ray Fluorescence (XRF)

Utilization of XRD determined the mineralogical phases present in the sample, whilst XRF evaluated the oxide composition. Both XRD [255], [256] and XRF [175], [257], [258] have evaluated the use of fly ash as a product in cement for example. In terms of flue gas filtration, whilst these techniques provided an insight into the filtrate, the results assume a representative mean, regardless of the sample origin spatially across both the filtration bag, and from the hopper (depending on sample origin). It would further assume that the fuel variation upstream is insignificant enough to cause significant variation in the results.

Consequentially, these techniques have limited in routine testing, but are useful as a fault diagnosis technique when something has gone awry during operation for example.

2.5 Literature Gap

Subsequent analysis of the literature revealed areas whereby research had yet to be performed. Of particular note, were those identified during the review of the analytical techniques in section 2.4, such as air permeability, mass/density determination, material thickness. The close nature with industrial partners within this project afforded a great platform to address the following knowledge gaps through a combination of industrially derived samples and academic research methods.

1. BS22031:2021 “Sampling and test method for cleanable filter media taken from filters of systems in operation” [16] recommended analysts to clean the filtration media to evaluate how it had faired since instillation. It provided multiple methods to perform this clean, including an allowance to use any method under the proviso that it did not damage the fibres. However, it assumed that regardless of the method, the resultant clean would not be dissimilar in terms of the obtained analysis results. Inclusion of multiple methods ensured that analysts could perform this step, but still comply with their own risk assessments. The standard did not comment on the potential variation across different methods.

   Research in this area would focus on the use of industrial samples and performing various cleaning steps (such as brushing, scraping, shaking, compressed air blowing, vacuuming, and washing) to ascertain the expected variation which could arise through use of different cleaning methods.

2. Mass and thickness evaluation is a common analytical method throughout literature and required by BS22031:2021 “Sampling and test method for cleanable filter media taken from filters of systems in operation” [16]. Literature achieved this result through either standards such as “BS EN 29073-1:1992 Nonwovens — Part 1: Determination of mass per unit area.” [230], and " BS EN 29073-2:1997 Nonwovens — Part 2: Determination of thickness" [231] which laid out the specified equipment and methodologies, or through the use of specific instruments, without stating the variation. Some work, such as Fukasawa et al., [4], and Fukusawa et al., [237], illustrated the variability of filtration media, achieving a better understanding of how this varied across the machine and cross direction of the filtration media. Although

literature is emerging to demonstrate the variation, the literature review found no research that combined both the British standards and resultant variation across used flue gas filtration bags.

Research in this area would illustrate the variation across industrially relevant used filtration media, incorporating the results of the previous gap to identify how the reported results in BS22031:2021 "Sampling and test method for cleanable filter media taken from filters of systems in operation" [16] would be affected.

3. Air permeability is another analytical method commonly used to evaluate filtration media. Again, previous works such as Fukasawa et al., [4], and Fukusawa et al., [237] have illustrated variation on new media, which provided a basis for future research, but consideration to used media in the as received and post cleaned state required research to ascertain the variation and resultant effect on the analysis.

   Research towards identifying the variation across a used, industrially relevant, nonwoven filtration bag would aid to address this literature gap and subsequently help to guide the analytical methods and subsequent data analysis.

4. Lastly, the lifespan/longevity of the filtration media is a critical consideration factor when improving systems or selecting the media. Whilst studies have shown the effect of parameters such as flow characteristics [142], [259] and media properties [13] on longevity, they have not considered the impact of longevity in an operational setting. Reduction of this identified literature gap would combine industrially used filtration media, site specific settings, and running samples until they reach a specified failure point.

   Research aimed at this literature gap would allow for the development of a novel way to predict the longevity of industrial bag house filtration media, through testing relevant samples (along with new samples to function as a baseline) at near site conditions until the occurrence of failure. This is needed to better understand the changes that occur to the media during operation. Removal of filtrate media for analysis requires the bag house to be offline which affects the overall performance of the site and has a negative impact on economic factors. Consequently, if longevity can be accurately predicted then it may be possible to reduce the required site downtime and any negative impacts associated with the downtime.

Consequently, to address the aforementioned knowledge gaps, conduction of the following studies aimed to address these gaps (in ascending order):

- Chapter 4: Determination of an Appropriate Cleaning Method
- Chapter 5: Understanding Mass and Thickness Variation
- Chapter 6: Understanding Air Permeability Variation on a Full Filtration Bag
- Chapter 7: Critical Self-Evaluation of Longevity Study

Chapter 3: Methodology

3.1 Introduction

This chapter explored two aspects of this thesis: the acquisition and commissioning phase of a Filtration Assessment Rig (FAR) in Section 3.2. Section 3.3 looked at each chapter specifically, Chapter 4 used various cleaning methods such as washing, vacuuming, brushing, shaking, and scraping to change the state of the filter from the as received (AR) state to the post cleaned (PC) state. Chapter 5 explored the mass/density and thickness variation using samples of size 5cm by 5cm's across a large overall surface area. Chapter 6 used air permeability at 200Pa to explore the air permeability variation cross the surface of a full filtration bag. Lastly, Chapter 7 used a combination of offline measurements for air permeability, mass/density, thickness, porosity (calculated an through μCT) and online measurements to evaluate the samples.

3.2 MMTC200 Filtration Assessment Rig (FAR)

3.2.1 Acquisition

Various studies such as Schuberth et al,. [205], Pham et al,. [224], and Fukui et al,. [225] have referenced BS11057:2011 "Air Quality – Test method for filtration characterization of cleanable filter media" [202] as their experimental set up. These studies suggested two companies that manufactured filtration assessment rigs: Palas GmbH [225], [227] and Topas GmbH [148], [226]. An additional potential manufacturer, FilTEq, was identified outside of literature through an internet search. To aid in the selection process of an appropriate design, a decision matrix allowed for each design to be evaluated against a set of criteria shown in Table 7. Each criterion's weight percentile depended on the importance of future research and activities that may surround the final selected design. From this, a point-based award system, which was from zero to one hundred, allowed for evaluation of the options available.

Consequently, the awarded points where then multiplied with the weighting percentage to yield an overall score which could then be added together to suggest a preferred design when comparing all options. Subsequently, each option was ranked accordingly, which aided in the selection of a suitable Filter Assessment Rig (FAR).

Weighting Selection

The weight associated with each criteria point is shown in Table 7. Sixty-five percent of the overall weight assessed the functionality of the designs. Operational Parameter Ranges for filtration and cleaning summarised the ranges in which a user can define parameters such as filtration velocity and pulse pressure. As the rig required flexibility in operational parameters, the filtration cycle and cleaning cycle operational ranges were scored at twenty-five percent each, with the dust dispersion rate awarded fifteen percent. This allowed for the consideration towards the performance of the FAR outside the initial requirements of the standard. If the design is restrictive, the rangeability of programmable operational parameters will be low, which would yield a low score. Conversely, as the range increased, the resultant score would increase. Compliance to British standard BS11057:2011 "Air Quality – Test method for filtration characterization of cleanable filter media" [202] is desired for preliminary studies, which saw this criterion awarded fifteen percent. However, future studies may deviate from this methodology, which meant a higher weighting was needed for filtration and cleaning cycle Operational Parameter Ranges. Lasty, 10% and 5% where attributed to the ease of moveability and overall size of the rig, respectively.

Table 7: Decision Matrix of Suppliers Following Critical Assessment

Decision Matrix Comparing All Quotations and Products Sourced					
Created By: Daniel Curry Date: 18/03/2021					
		Companies / Products / Options			
Criterion	Weight	FilTEq	Topas AFC 133	Topas AFC 131	FIL/Palas MMTC 2000
Filtration Cycle Operational Parameter Ranges	25%	15	85	90	85
Cleaning Cycle Operational Parameter Ranges	25%	0	75	50	75
Dust Dispersion Rate	15%	0	10	50	75
Conformity to Testing standard	15%	100	100	100	100
Moveability	10%	0	0	80	80
Size	5%	50	40	75	75
Cost (weighted from cheapest to the most expensive)	5%	80	40	90	60
Total:	100%	25.25%	60.5%	73.75%	83%

Operational Parameter Ranges (Filtration and Cleaning)

The operational parameter ranges of the user specified values needed to be adequate to allow for representative industrial tests, but also wider academic studies. To determine this, the baseline values selected where defined by the parameters in BS11057:2011 "Air Quality – Test method for filtration characterization of cleanable filter media" [202] such as: Filtration velocity, dust concentration, cleaning pulse duration, pulse pressure where considered. Greater ranges offered a more favourable weighting to the design. This was due to the ability to perform wider studies, leading to the potential for research to be performed outside bag house filtration. At this stage, any modifications post-delivery where not considered.

Both the Topas AFC 133 and Palas MMTC2000 performed similarly, offering only a slight difference between the filtration and cleaning parameters. The Topas AFC131 afforded a slightly wider range for filtration face velocity, however the cleaning cycle rangeability was less, due to the maximum differential pressure across the filter and pulse duration time being lower in comparison. Consequently, Topas AFC131 yielded a lower number of points for cleaning cycle rangeability.

Dust Dispersion Rate

Definition of the dust dispersion rate is the quantity of test dust/powder/aerosol delivered to the test chamber. The FilTEq design resulted in a zero due to the omittance of any information pertaining to this characteristic. Although AFC 131 provided a range of 1-260gm^{-3}, questions over the potential accuracies arose, particularly for the test which require a small incremental change in a value. Furthermore, with the lowest achievable value of 1 gm^{-3}, any potential tests which required a low dispersion rate are unobtainable. Topas AFC 133 exhibited the same, which had an operable range of 1-34 gm^{-3}, whilst having potentially better accuracy control, it suffered from the same problem. The main difference was that the AFC 131 generated its own test dust through aerosolization. This restricted the number of dust available for analysis to a singular particle type and size, which significantly reduced variability. Resultantly, given the MMTC2000 afforded a lower minimum of 0.2 gm^{-3}, resulted in a larger score as opposed to others which had a higher minimum.

Section 3.2.2 discussed the method in which dust dispersion occurred in further detail.

Conformity to Standard

The design should be capable of complying initially to the assessment method within BS11057:2011 "Air Quality – Test method for filtration characterization of cleanable filter media" [202] irrespective of future studies . All designs stated compliance to the methodology which saw the maximum awardable number of points afforded to the criterion.

Moveability and Size

Whilst size and ease of moving the rig are not operationally critical, they determined the minimum space needed for the rig in terms of heigh, width, and depth. Depending on the design, if the rig is supported on rollers, this would make moving it around easier. Images of the options therefore suggested how easy it may be to move the equipment. Consideration of the required foot space and height allowed for the evaluation of the overall size of the rig.

Both FilTEq and Topas AFC 133 had a design fully compliant to BS11057:2011 "Air Quality – Test method for filtration characterization of cleanable filter media" [202] which saw the height of the entire unit extend over 2 meters tall. This restricted a number of spaces, given the need for overhead clearance to access the top of the rig, reducing the weighting. Furthermore, if relocated, the relocation area would need a minimum similar size to accommodate the rig. This restricted the ease or relocation and potentially moving the rig, given the potential need for additional clearance. The height of the AFC133 was higher than the FilTEq due to extra clearance needed for the dust dispersion. As such, it scored a slightly lower percentile than the FilTEq.

Both the AFC 131 and MMTC2000 had a shorter height due to their designs. Unlike the design shown in BS11057:2011 "Air Quality – Test method for filtration characterization of cleanable filter media" [202], they comprised of the horizontal section only, opting for an inline dust dispersion as opposed to a partial separation of a larger gas stream. These designs conformed to VDI2936 [225] and the methodology presented in BS11057:2011 "Air Quality – Test method for filtration characterization of cleanable filter media" [202] This significantly reduced the height requirement making both more viable in terms of size and moveability. In addition, both designs were set on wheels/ rollers located on the underside of the entire rig, which further increased their percentile score.

Cost

Overall, the general average cost to acquire the filtration assessment rig was ≈£100,000. Current testing requires multiple analytical techniques (such as air permeability, mass/density, thickness, tensile testing etc.) to be used over many samples and requires a large investment in terms of labour costs and laboratory upkeep.

At the point of assessment, no academic discounts were considered. Because of the cost similarity between the units, the units were ranked based on cheapest, to most expensive. An overall weighting of 5% was given due to the cost similarity, but also due to the available budget allowing for the acquisition of the required equipment.

Testing filtration media is a critical tool to ensure that the filtration media is performing well. If the media is not performing well, this could lead to increased emissions at the stack, which could lead to breaches in emissions regulations, leading to fines or other punishments. In addition, it could lead to the site performing increased cleaning if the media is blinded, which increases the operational cost. Whilst the upfront cost of ≈£100,000 (plus labour to test) may seem high, if the site must unexpectedly shut down and perform an unexpected bag change it could cost them significantly more. Therefore, periodical testing to understand the media is vital.

Decision Matrix Results

Conclusion of the operability criterion surrounding each option led to a total weight of 65% of the decision matrix. Overall, the MMTC200 obtained 79% of the total available percentile. Followed closely by both the Topas units AFC131 and AFC133 at 73.75% and 60.50% respectively. Lastly, the FilTEq option received 25.25%. This apparent low score was the result of a lack of information provided during the consideration phase. Given it conformed to the standard, the likelihood was that it had some operational parameter range, though it was unknown to what extent. However, give the omission of key information around the operational parameter ranges, it was difficult to quantify this value. The lowest score during operational parameter ranges was for the FilTEq design given the omitted information. In contrast, the overall range affordable to the MMTC2000, and ability to use different test dusts led to it achieving the highest awarded score at 79% of the total available percentile of sixty-five (cumulatively).

Both FilTEq and Topas AFC131 failed to score well for moveability and size due to the significant height, and apparent fixed positions. Their size reduced their moveability and ease of redeployment into a different/smaller laboratory. Consequently, this led to the AFC131 and MMTC2000 scoring higher. This was down to a combination of their minimalistic height, and their equipment frame which incorporated wheels which allowed it to move about more freely. Thus, the transportation of the experimental rig and its redeployment into another laboratory was advantageous and saw it awarded a substantial proportion of the points for these categories.

Cost weighting for the options were based on least to most expensive given the similarity in cost values. Whilst the Topas AFC131 and FilTEq options where the cheaper two options, their total overall score was lower than the MMTC2000 and Topas AFC133 options. Upon evaluation of the decision matrix in Table 7, the best option appeared to be the MMTC2000 option.

To supply the MMTC 2000 with compressed air, a silenced, oil free and dry compressor was sourced. This compressor had a maximum working pressure of 8Bar(g) and a reservoir of ≈250L of compressed air. The pressure within the reservoir was determined by an adjustable gauge but was set to a pressure of 6.5Bar(g) as a minimum. As part of the commissioning phase and subsequent hand over, an internally published standard operating procedure allowed other users of the equipment and readily benefit from the findings of this work. Discussed further in Section 3.2.2. The filtration assessment rig (FAR) in operation is shown in Figure 12, a simplified schematic is also shown in Figure 13 [225].

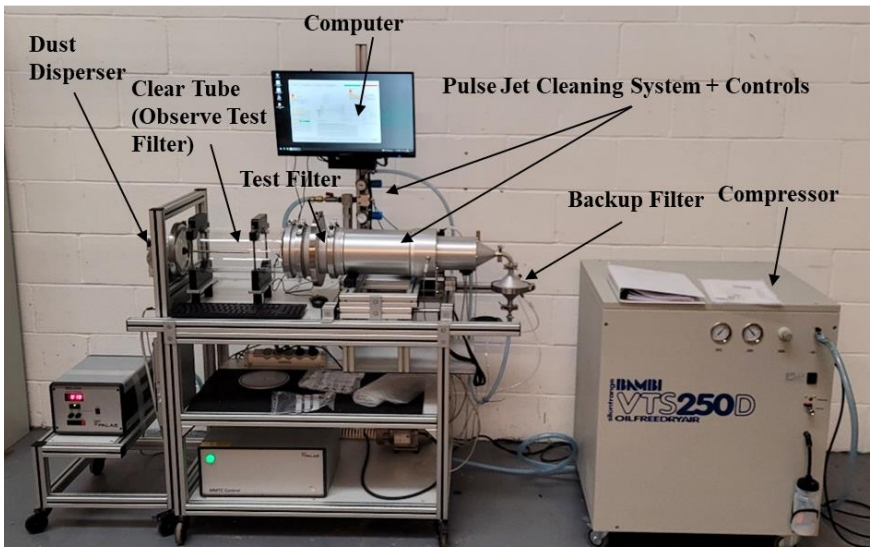

Figure 12: The Filtration Assessment Rig (FAR) In-situ

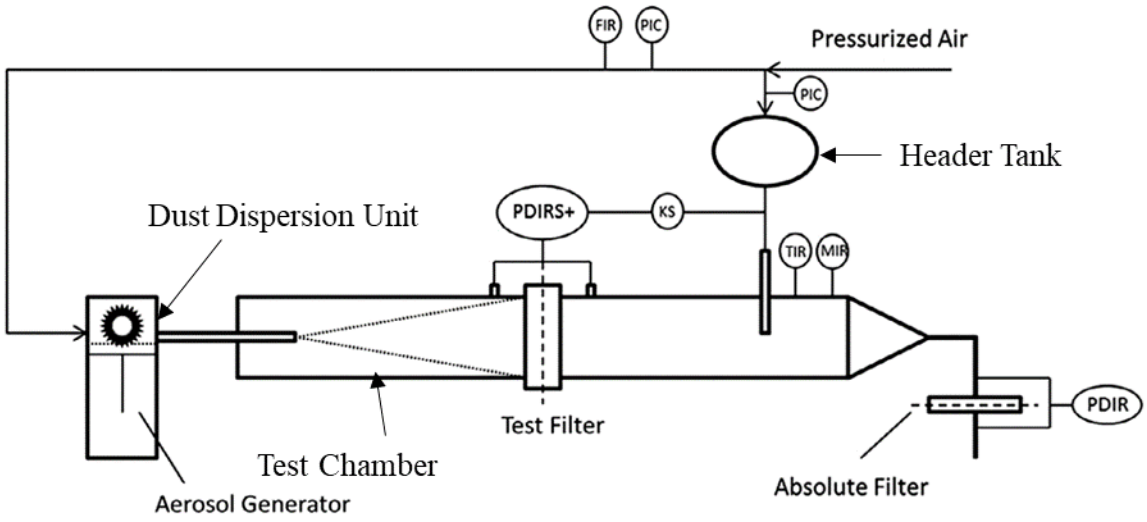

Figure 13: Schematic Showing Instrumentation and Key Aspects of the MMTC2000 [225]

3.2.2 Commissioning Phase

Commissioning required specific tests to ascertain that the rig was fully functional before conducting any experimental tests.

The first test ran compressed air only through the aerosol generator (dust dispersion unit) and into the header tank. The total airflow through the test chamber, with the air for dust dispersion was set at 180 mhr^{-1} or 45 $lmin^{-1}$. Assessment of the rig's capability to maintain a consistent flow rate saw this test ran uninterrupted for ten minutes. This determined flow variation across the filter, which was deemed to occur at 45.10±0.18 $Lmin^{-1}$. Repetition of the test transpired for a duration of 35 minutes and yielded comparable results of 45.10±0.19 $Lmin^{-1}$. In both circumstances, every second exhibited a singular datapoint. This test established the following:

- Any incorrect fittings, couplings, or other seals:

Incorrect fittings or seals could lead to filtrate and air leakage which would affect the quality of the test. At the setpoint of 45$lmin^{-1}$ the flowrate only deviated slightly at 0.1±0.18 $lmin^{-1}$, which suggested that the set-up was complete.

- The expected deviation in flowrate when running a test:

The tests conducted, where no filtrate was present, demonstrated the variability for both the flowrate and the differential pressure across the test filter. Prior to the commencement of any test, this test is run to determine the original baseline differential pressure across the filter, but

also the variation in the flowrate. The latter acted as a check to ensure seals and fixtures where complete.

Next, a test dust was introduced to examine the aerosol generator fully/dust dispersion unit. Introduction of test dust into the system allowed for the evaluation of the cleaning system and the dust dispersion unit. To do so, the header tanks was manually set to 0.6Mpa through a manual gauge. A pressure indicator also displayed the reading on the computer which allowed for any minor adjustments to the pressure, such that the pressure was at the desired setpoint. Upstream, the minimum pressure in the compressor was set to 6.5Mbar, which allowed for the header tank to efficiently repressurize following use by the pressure gradient. A solenoid and diaphragm valve, downstream of the header tank controlled the pulse duration and deliverance. This was set electronically before a test. This test used a 200ms opening time. A set differential pressure of 1.80mbar. A total of ten cycles were conducted on a clean on demand basis.

The selected test dust for commissioning was talcum powder (talc). Cost effective, the powder is cheap and readily available. Furthermore, the powder had a Mohs hardness rating of one, meaning it would not damage the metalwork or glass. Upon filling the piston with the powder, a weight measurement was taken and used to determine the compact density of the powder. This is then programmed into the software in gcm^{-3} which used the value to determine the piston federate. The rate at which this piston velocity, determined the mass concentration out of the aerosol generator. For the study, the feed was $5gm^{-3}$ at the test filter's interface. Dispersion of the dust occurred through a rotatory wire brush, which brushes against the interface of the piston. The test dust is then blown off from the brush by the compressed air which passed over it. It is then delivered into the FAR/test chamber.

Once the software observed a differential pressure across the test filter >1.8mBar, a signal allowed for the cleaning cycle to begin. Conversely, if the differential pressure value recorded showed <1.8mBar, the cleaning cycle would not operate. Upon completion of the cleaning pulse, the differential pressure across the test filter reduced back towards the original baseline differential pressure. Due to the data resolution, it was impossible to record the duration of the cleaning pulse. However, upon pulse completion, the header tank did automatically refill to the correct pressure due to the pressure gradient from the compressor.

All other sensors, including the differential pressure sensor at the absolute filter and temperature probe appeared to work normally and record data at the same resolution of one

datapoint every second. The following sections are related to the commissioning as they discussed any identified potential complications that may arise through usage.

Filling of the Dust Piston

The images presented in Figure 14 illustrated the piston at full extension (A) demonstrated it filled with PuralNF (B) and illustrated the slot mechanism used to guide the piston into place (C). Once inserted into the aerosol generator, a plate was inserted between rim of the piston and shelf to allow a metal-metal seal to form and ensured the piston housing remained secured and sealed during testing.

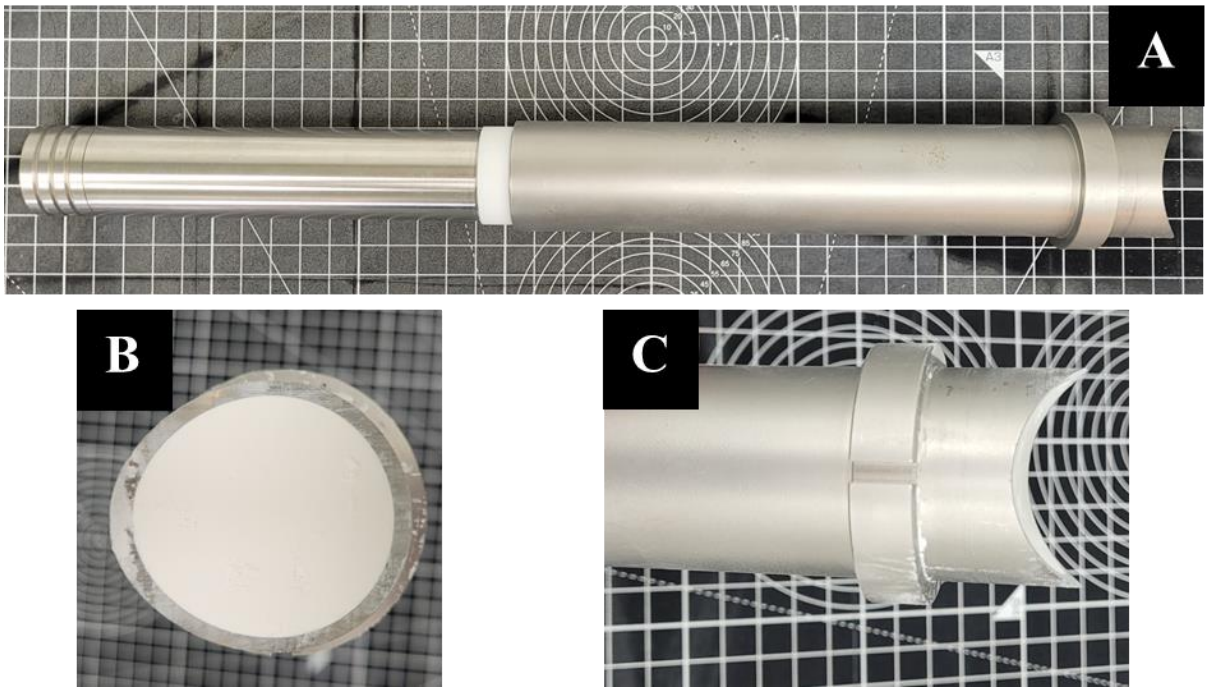

Figure 14: Dust Piston A) at full extension, B) Filled with Test Dust, and C) the collar and Slot for Seating the Piston in the Dust Dispersion Unit

The process of filling the piston is done iteratively to achieve as uniform packing density as possible. The packing density inside the clearance volume is defined by the amount of material placed within a defined volume (ρ_{comp}). This can be calculated using Equation 23, which calculated the difference between the empty and filled piston (Δm) over the piston area (A) multiplied by the filled length (L_{filled}).The maximum length available for filling is 154.2 mm This is the maximum movable distance of the piston, measure from the shallowest point of the curve shown in Figure 14 (C). The calculation of the compact density can then be calculated based on the new final position of the piston, with respect to its filling height and mass.

Iterative partial filling (followed by light compression) in combination with a weighted rod helped achieve a uniform packing density and kept any variation as low as possible. The only variable in Equation 23, is the mass increase, (Δm), caused by the addition of the test dust/powder to the clearance volume. If a higher/lower compaction occurred in a defined volume, then the packing density in that region will also be higher/lower, affecting the concentration delivered to the outlet. The weighted compression rod applied an equal and repetitive compression load which reduced any potential variation. Once a finite volume of powder/dust is loaded, the rod is placed in and allowed to compress under gravity.

$$\rho_{comp} = \frac{M_{piston,full} - M_{piston,empty}}{A_{piston} \cdot H_{piston}}$$

Equation 23: Packing Density of the Clearance Volume Determination

Whilst it would be possible to perform larger, quicker, fills to result in less iterations of filling/compressing, the resultant packing density (ρ_{comp}) would be significantly lower and potentially less uniform. This would result in a concentration variation at the nozzle during dispersion, which would consequently impact the accuracy of a test. In contrast, whilst the time taken to perform the recommended iterative filling would be noticeably higher it would lead to a more accurate and uniform dispersion.

Dust Piston Speed and Concentration

The maximum piston height/length that is achievable is 154.2mm. Upon completion, the test is halted/stopped. This allowed the piston to be removed and refilled. The piston diameter is 33mm. The concave nature shown in Figure 14 (C) allowed for the piston housing and bottom of the rotatory brush to sit flush together. As the piston is pushed into the aerosol generator, the test dust encounters the nylon brush and is dispersed through and towards the test filter by the compressed air. The mass concentration of the dust out of dust dispersion unit is calculated by Equation 24, using Equation 23 which determined the compact density of the test dust.

The resultant mass concentration can be calculated by Equation 24. The dust concentration delivered to the nozzle $(C_{m,filtrate})$ is a function of the piston velocity (v_{piston}) and assumed constant packing density(ρ_{comp}) previously defined in Equation 23.

$$C_{m,filtrate} = \mathrm{v}_{piston} \cdot A_{piston} \cdot \rho_{comp}$$

$$\therefore \mathrm{v}_{piston} = \frac{C_{m,filtrate}}{A_{piston} \cdot \rho_{comp}}$$

Equation 24: Mass Concentration of Test Dust/Powder as a Function of Packing Density and Piston Speed

As the packing density decreased, the piston velocity needed to achieve a constant mass concentration was higher, shown in Figure 15. In addition, as the packing density increased, a similar concentration can be achieved through a reduced piston velocity. Given the finite clearance volume and stroke length available, it was initially suggested that the packing density should be as high as possible; this would allow for longer studies to be performed with fewer stoppages to change the piston.

However, as the packing density increases, the resultant friction between the material and walls of the piston housing increase, which exert an increased pressure on the motor to deliver the required feed. Furthermore, manual tamping exhibits a degree of variation due to user strength and fatigue. By using gravimetric forces from the compression rod and iterative filling, each fill of the piston will be more accurate. Whilst this would require refilling the piston more frequently, it would aid in prolonging the lifespan of the equipment. In addition, a lighter packed material will be more readily dispersed from the nylon brush and less likely to get entrained in the bristles or damage them. As a result, the piston should only be filled using the compression rod and gravity.

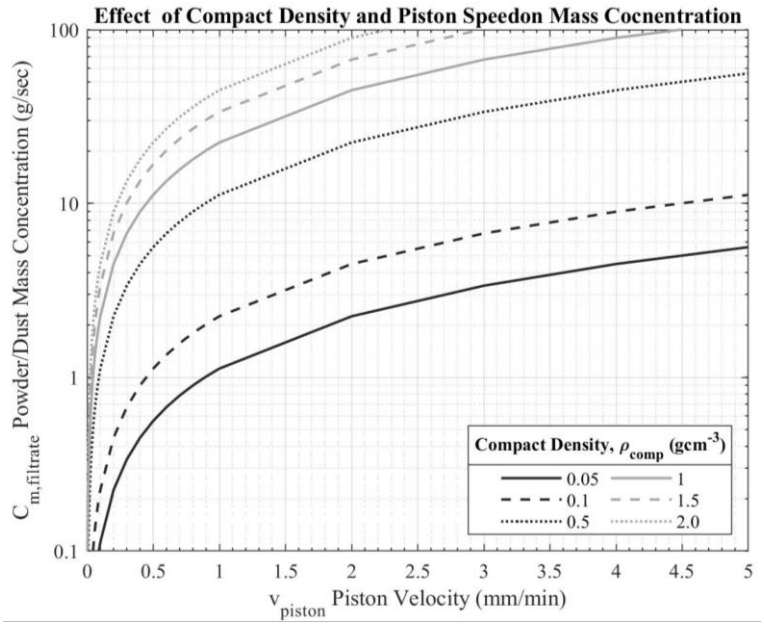

Figure 15: Concentration Calibration Graph

This mass concentration in Equation 24 denoted the concentration leaving the dust dispersion unit and not the concentration at the face of the filter.

Given the expansion between the generator and test filter, coupled with the filtration velocity, the mass concentration at the test filter would be lower. Therefore, a material balance accounted for the difference and allowed for the calculation of the concentration needed to be emitted by the dust generator to equal the desired dust concentration at the test filter.

Effect of Particle Size on Operation

Previous studies such as Li et al., [137],Steffens et al., [171], and Kumar et al., [260] have shown the correlation between particle size and effect on differential pressure. These studies illustrated the impact that small filtrate had on pressure drop evolution across the filter and downstream emissions. As the particle size decreased, particle adhesion to the filter increased [260], which resulted in the baseline differential pressure across the filter to also increase [137]. Furthermore, small particle sizes more readily made it through the filter which increased emissions [137]. In contrast, as the size increased, the rate pressure drop decreased. Larger particles tend to allow for lower packing density due to their reduced volume coverage per area. If the particles are incompressible, this leaves channels which more readily allow for air to pass through, in comparison to smaller particulates where the opposite occurred.

Whilst both the talc and PuralNF test dust exhibited a normal distribution in Figure 16, the observed volume density was more noticeable for PuralNF. PuralNF exhibited a relatively larger particle size volume density about 0.1µm-9µm in comparison to the talc powder. In contrast, the talc powder presented a narrower distribution about its mean of ≈25µm. The larger volume of particles in the <10µm range suggested that the PuralNF test dust may exhibit a higher rate of differential pressure increase at the test filter. The notably concentrated volume of the talc powder at ≈25µm, coupled with the narrowness of the distribution, may suggest a lower rate of differential pressure increase than the PuralNF test dust.

A summary of the particle size distribution of the two test dusts shown in Figure 16 and Table 8.

Table 8: Particle Size Distribution Summary of Two Test Dusts

Test Dust	$d_p(10)$ $[\mu m]$	$d_p(50)$ $[\mu m]$	$d_p(90)$ $[\mu m]$
PuralNF	0.965	7.130	32.000
Talc	6.100	24.600	66.000

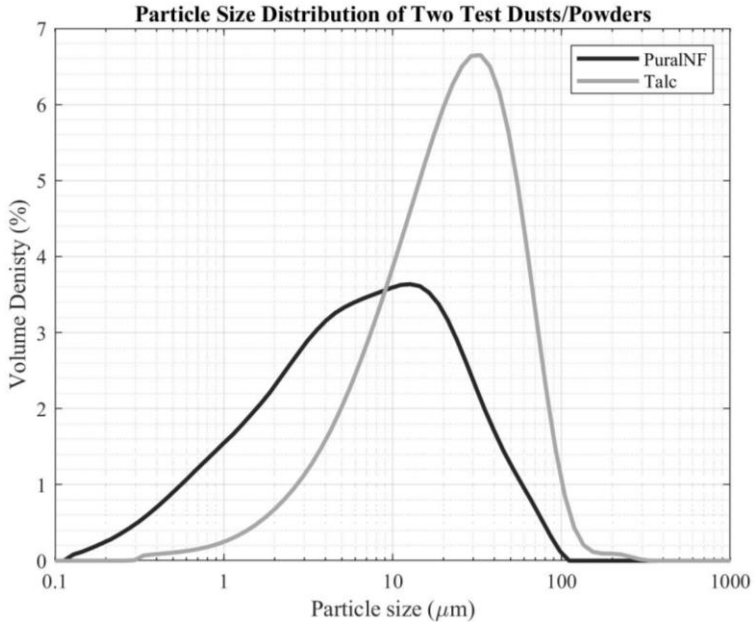

Figure 16: Particle Size Distribution Difference of Talc Powder and PuralNF Test Dust

Multimodal particle size distributions were observed for both the energy from waste (EfW) site and Biomass Site are shown in Figure 17. Both sites utilized lime as a flue gas treatment, with the biomass site also using powdered activated carbon (PAC). One of the difficulties in replicating a fly ash sample is information pertaining to the particle size distribution across the spatial directions of the bag house. Studies that generate their own particle size from atomization or use a standard test dust restricted the output in favour of repeatability. This reduced their potential output towards industry. At an industrial scale, the bag house may contain various cells/compartments which each exhibit a set of unique characteristics affecting the particle size at any given three-dimensional location within the cell/compartment. Consequentially, without multiple experimental and computational studies, a certain limitation existed on the definition of a representative test dust substitute for fly ash. Locational variation of particle size may show a distinct size distribution, which would affect the results if the study aim were to simulate conditions of the site.

For a representative fly ash particle size distribution from a given site, acquisition of multiple samples from various locations would subsequently allow for a suggested, overall size distribution. From this, it may be possible to blend test dusts in order to replicate the test dust in terms of particle size. Although accountability for density is omitted in this method, it would provide academically controlled research to be a step closer towards the replication of industrial operations and therefore more attractive for future funding and improvements.

Site variation would also need to be accounted for when considering a site not previously studied for its respective fly ash particle size distribution.

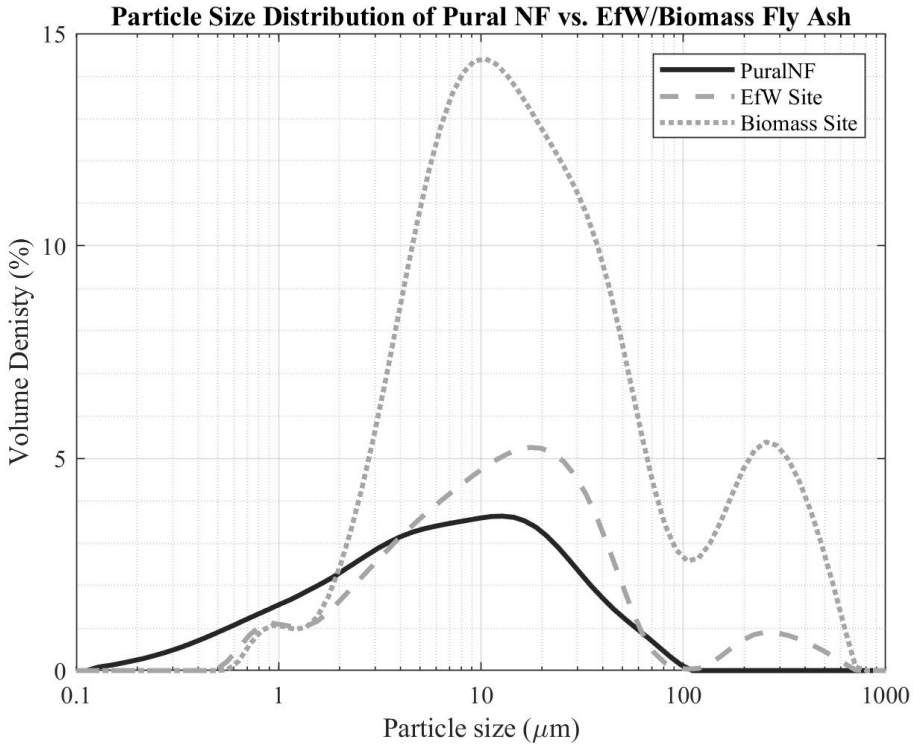

Figure 17: Particle Size Distribution of PuralNF vs. Energy from Waste (EfW) Fly ash and Biomass Fly Ash Samples Retrieved from the Surface of Used Filtration Media

Filtration Velocity

Filtration velocity is defined by the distance at which the gas is travelling at the air entry point of the test filter per unit of time. As presented in Figure 12, the surface area exposed to the gas is circular. Due to the clamping mechanism, which fixed the sample securely, the exposed surface area of the filter (A_{filter}) is kept constant at 2.243x10^{-3}m^2, with a diameter (d)of 0.169m. The total volumetric flow of air (Q_{air}) through the filter is characterised by vacuum pump, which is downstream of the test filter. This pump functioned as an induced

draft fan, which pulled air through the test filter. At the interface between the main body of the FAR and Dust dispersion unit, a permeable fabric provided airflow through to the test filter, but omitted any test dust loss outside the FAR. The face velocity at the test filter (v_f) is determined, by the volumetric flowrate through the vacuum pump, over the surface area of the filter which calculated the velocity through the filter in units of length per unit time.

Throughout testing, air leakage/ingress into the FAR was assumed zero. To allow for this assumption, a leakage test on all fittings/sealants occurred to indicate any unwanted air movement. The standard SOP on leak detection provided from the manufacturer, afforded a methodology to conduct said test. This test yielded no evidence to support or suggest air leakage/ingress to the rig. Each fixture and fitting were subsequently checked for correct seating and tightness. Each jubilee clip's tension was adjustable using a screwdriver and checked for tautness prior to test commencement to ensure achievement of a tight seal. This validated the assumption, providing the aforementioned checks where conducted and periodic leak testing occurred as per the operational manual.

A massflow controller at the vaccum pump controlled the user specified flowrate through the test filter, and kept it relativly constant throughout experiments. Seven tests where conducted at defined setpoints as shown in Table 9 to determine what effect the dust dispersion air had on the mass flow recorded. Comparative results between the anticipated and actual flowrates are detailed in Table 9.

Tests A, B, and C used only the vacuum pump to define the volumetric flowrate. At the set volumetric flowrate, the resultant means only marginally deviated from the set value. Test D used only the compressed air supply from the RGB/dust dispersion unit, without the vacuum pump in operation. Due to the vacuum pump not being on, the resultant airflow recorded by the mass flow controller was zero. However, as there was an anticipated flowrate of compressed air at 60 $Lmin^{-1}$, the anticipation was that there should have been a flow detected. The mass flow controller is one directional, meaning the recorded data is the noise within the sensor. However, expectation during the test was that even though the vacuum pump was not operating, the sheer volume introduced would naturally flow through and out downstream of the pump causing a positive detection of a flowrate regardless of inoperability.

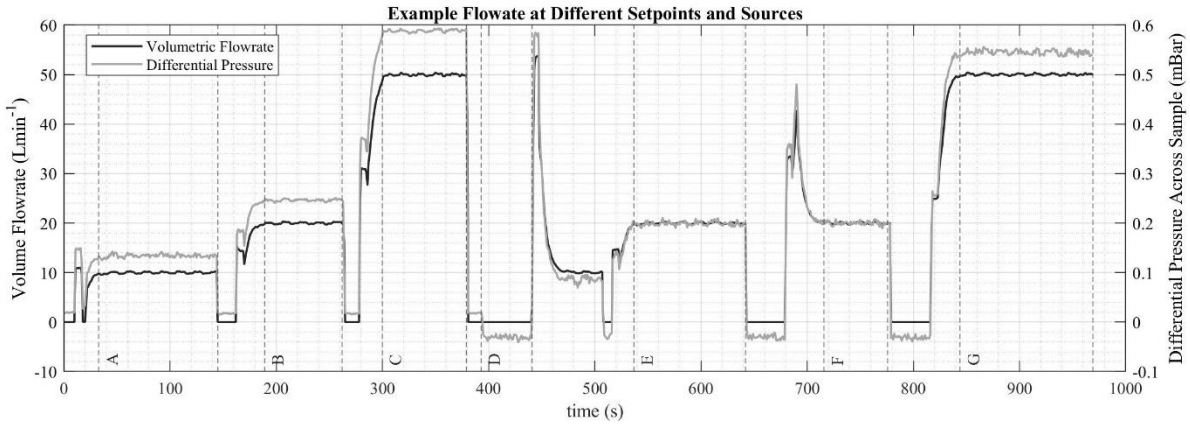

Figure 18: Example Volumetric Flowrate Data (Only) from the FAR. Note: See Table 9 for Detailed Explination of the Letters

Table 9: Set and Actual Volumetric Flowrates

Letter	Vacuum Pump Set Flowrate ($Lmin^{-1}$)	RGB2000 Set Flowrate ($Lmin^{-1}$)	Total Anticipated Flowrate ($Lmin^{-1}$)	Recorded Flowrate ($Lmin^{-1}$)
A	10	-	10	9.99±0.03
B	20	-	20	19.95±0.05
C	50	-	50	49.97±0.04
D	-	60	60	0
E	20	60	80	19.98±0.04
F	20	60	80	20.07±0.04
G	50	60	110	50.04±0.03

Differential pressure across the filter sample indicated a negative value. In normal operation, the differential pressure is determined by the subtraction of the downstream pressure probe from the upstream pressure probe. This would yield a positive value. Occurrence of a negative value suggested that the downstream pressure was higher that the upstream, which would lead to a negative differential pressure. This negativity is therefore indicative of the flow direction. In all subsequent tests, the negative differential pressure value afforded to the data occurred when the compressed air flowrate continued operating after the vacuum pump had ceased operation. This suggested the air was leaving the FAR upstream of the test filter. This led to the theory that the 60 $Lmin^{-1}$ left the FAR at the upstream permeable barrier due to the pressure gradient. This barrier is permeable enough to allow for a large airflow through in either direction. Flow of the air through the barrier, instead of travelling through the downstream accounted for the omission of any recorded flowrate, due to the restricted flow

direction of the mass flow controller and the negative differential pressure observed at the test filter.

Tests E, F, G used both the flowrate of the vacuum pump, and the flowrate of compressed air from the RGB unit, which better simulated actual operational conditions. Whilst the noted variation was similar to tests A, B, and C, the inclusion of the compressed air stream resulted in a slightly raised recorded flowrate in comparison to the set vacuum flowrate. This implied that a small proportion of the compressed air supplied by the RGB fed to the vacuum pump which resulted in the slightly higher value recorded. The mass flow controller worked in combination with the vacuum pump to ensure that the desired volumetric airflow through the test filter was achieved; any excess would be forced out through the permeable barrier upstream of the test filter until an equilibrium is reached.

Settling velocity is defined as the critical velocity at which a particle must be travelling in order to remain suspended in the fluid/flow path. For the filtration assessment rig, the filtration velocity, (v_f), denoted the criteria, whereby if $v_{St}(d_p) < v_f$ then the particle of size d_p will remain suspended in the stream. At $v_{St}(d_p) > v_f$ particles will exhibit separation due to the gravimetric force which would result in a different particle size distribution at the surface of the test filter. The settling velocity can be calculated using Equation 25 [117], correlated the particle density (ρ_p) and size (d_p) against the gas characteristics and gravimetric force (g) to calculate the settling velocity (Ω_{St}). Application of Equation 25 [117] during the experimental design phase provided an insight into the likely particle size distribution at the surface of the test filter.

$$\Omega_{St} = \left(\frac{\mu_g}{\rho_g d_p}\right) \exp\left[-3.07 + 0.9935 \cdot \ln\left(\frac{4\rho_p \rho_g d_p^3 g}{3\mu_g^2}\right) - 0.0178 \cdot \ln\left(\frac{4\rho_p \rho_g d_p^3 g}{3\mu_g^2}\right)^2\right]$$

Equation 25: Gravitational Settling Velocity [117].

Application of Equation 25 [117] using the properties for PuralNF yielded Table 10. Results reported that a settling velocity of 1.01ms^{-1} is the minimum filtration velocity required to keep all particles in suspension. This value of 1.01ms^{-1} at a particle size of 120µm in Table 10 considered the particle to be perfectly spherical. For example, BS11057:2011 "Air Quality – Test method for filtration characterization of cleanable filter media" [202] required a face velocity of 2mmin^{-1} which equated to 3.33x10^{-2}ms^{-1}. At this velocity, separation would begin to occur at a $d_p > 15.85\mu m$. Deposition would therefore occur towards the vertical bottom

of the test chamber, depending upon the particles original position and trajectory. Consequently, given the likelihood of separation, particularly at smaller filtration velocities, factor must be considered during the experimental design phase, before the conduction of a test occurred.

Table 10: Settling Velocity of Various Particle Sizes of PuralNF Test Dust Using the Settling Velocity (Equation 25)

Particle Size $[(d_p)$ in µm]	Settling Velocity $[(\Omega_{St})$ in m/s]	Particle Size $[(d_p)$ in µm]	Settling Velocity $[(\Omega_{St})$ in m/s]
0.1	$2.08x10^{-8}$	10	0.01
0.5	$4.76x10^{-6}$	50	0.27
1	$2.81x10^{-5}$	100	0.79
5	$2.66x10^{-3}$	120	1.01

Separation of the particulate is likely to affect the overall concentration exhibited at the filtration surface. Therefore, a study on the separation is needed to ascertain the effect on the resultant test. Alternatively, the initial concentration at which the test dust/powder is delivered has to be increased to account for the losses due to separation forces. The decision is based on the test requirements. Consideration of the particle size distribution and settling velocity, prior to the commencement of any tests, should be examined ensure a clearer understanding towards the particle size distribution at the surface of the test filter.

Pulse Jet Cleaning Pressure

Pulse jet cleaning occurred by setting three variables in the software: cleaning type (time or differential pressure), header tank pressure, and the duration of the cleaning pulse in ms.

For the cleaning on time, the user specified the total time duration of the filtration cycle in the software. The test filters differential pressure increased until the allotted time had elapsed. For cleaning on differential pressure, the set maximum differential pressure across the test filter controlled the occurrence of a cleaning pulse. Once this value occurred, a pulse of compressed air cleaned the filter. The software allowed the selection of both cleaning types. In this instance, whichever value occurred fist would trigger the cleaning cycle.

Secondly, the header tank pressure has an operational range of 0-8bar(g). Pressure was regulated through a valve and pressure gauge (visual). There is also a sensor within the header tank, connected to the internal computer and software, which allowed for a more

accurate wind header tank pressure to be set. The latter value is visible on the computer's interface. During testing, the external compressor was set at a higher outlet pressure than required at the header tank. Doing so allowed for the header tank to remain at the desired pressure throughout the test.

Lastly, the pulse duration can be set in the range of 50-500msec. Duration of the cleaning pulse happened through the solenoid and diaphragm valve, whereby the opening and closing time (pulse duration) is set prior to testing. The signal to the solenoid valve controls the opening and closing of a diaphragm valve, which allowed the compressed air to pass into the cleaning nozzle. This nozzle is currently a pipe which is located at the central midpoint of the test filter and conforms to BS11057:2011 "Air Quality – Test method for filtration characterization of cleanable filter media" [202].

Commission test data revealed the potential implication of the time resolution. During commission testing, the differential pressure reading observed in the commissioning data occurred below the baseline differential pressure of the media at ≈0.81±0.02 mBar in five instances. In these five instances, a record of negative differential pressure across the test filter was recorded. Graphically shown, Figure 19 presented an example of the aforementioned occurrence using a sample retrieved in the data. Upon activation of the pulse, the test filter expands upstream due to the pressure difference. This flex facilitated the release of the test dust from the surface. Upon the completion of the pulse clean, the resultant pressure caused the filter to return back to the cage support wires. Compression and expansion against/away from the cage support wires will occur throughout any test. Figure 19 therefore suggested that this compression/expansion could be arbitrary recorded during testing.

Given the negative differential pressure recording, this could suggest that the direction of fluid flow changed from downstream to upstream, resulting in a negative differential pressure reading. The precision at which data recording is unknown. However, the occurrence of negative differential pressure spikes in Figure 19 would suggests that there is a chance for data to be recorded somewhere along the pulse duration as shown by Li et al., [222] particularly when considering larger pulse durations. This will impact the data, particularly during the isolation of local minimums (the start of a new filtration cycle). Future development of the data recording may examine the possibility to install a higher resolution

recorder, to identify the exact point of the cleaning pulse and exact starting point of the next filtration cycle.

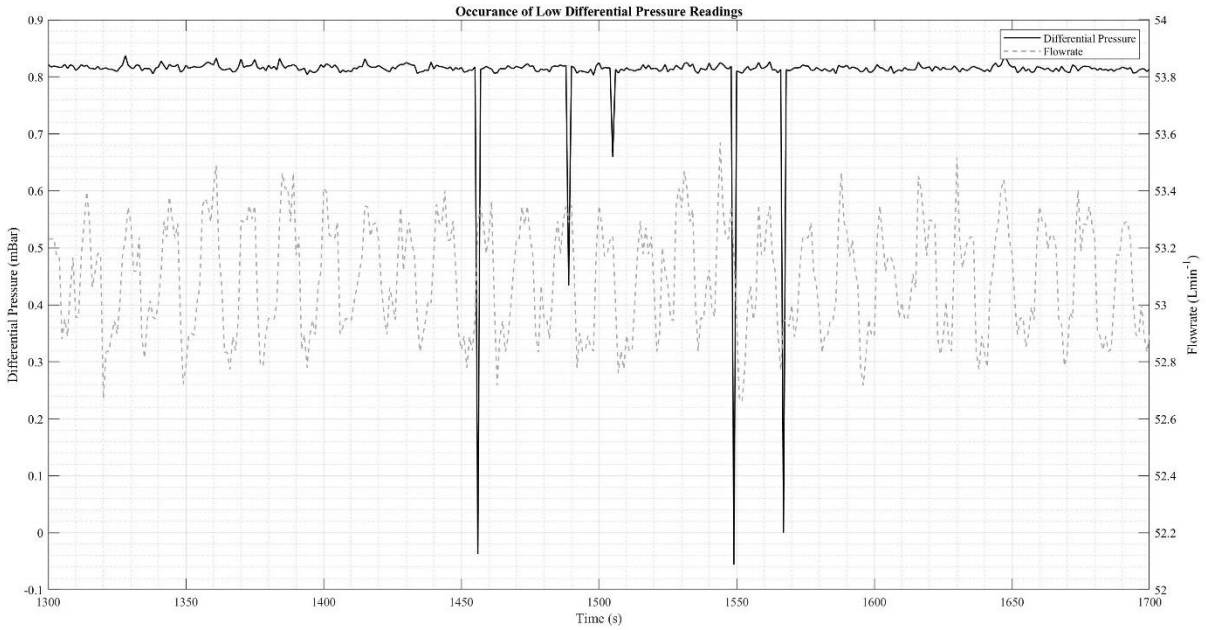

Figure 19: Differential Pressure Variation During Aging Phase of BS11057:2021[202], Particular Attention Should be Drawn to the Negative Readings of Differential Pressure and Low Flowrate Spikes

Data Recording

Current data probes record: differential pressure across the test and backup filter, downstream temperature, and mass flowrate, at a resolution of one datapoint per second. The software internally presented the data graphically but provided the option to export the data in a .xlsx format. Upon exportation, a unique identification tag prescribed to the data allowed for traceability back to its representative test conditions and information. A separate .xlsx file stored this data and tabulated the relevant files reference names. From this, previous prehistoric data is readily available for future researchers if needed.

Future advancements of the FAR would see the resolution of the data recording become sub 1s intervals. In addition, separation of the differential pressure to two unique pressure points would allow for quantification of the variation between the upstream and downstream of the test filter. Lastly, insertion of additional probes would further enhance the data retrieved from any conducted test. Sections 3.2.3 discussed this in further detail.

Data Processing

Data processing occurred semi-automatically using a pre-determined MATLAB code, which stored and sectioned the data into its constituent variables. Upon completion of a test, the combination of all data files from testing transpired (if necessary) prior to processing. From this, the bespoke code returned the data in more manageable forms. The analyst can then save these variables for later, and/or progress to look at the data as desired. Currently, two different codes exist: one for the standard testing a reporting as described in BS11057:2021 "Air Quality – Test method for filtration characterization of cleanable filter media" [202], and the second pertaining to longevity testing. Independent of this, an analyst can recall the saved variables for their own use. This developed interface is continually undergoing development to increase ease of use, but to also automate the process of report generation.

Other Aspects of Rig Operation

Dust Dispersion Cover Maintenance

Part of the daily operational and maintenance procedure is to remove the dust dispersion lid for daily cleaning. Depending on the test dust/powder used, adhesion on the metal surface of the powder/dust can occur. Once adhesion has taken place, the flow characteristics through the aerosol generator become variable, which may lead to potential problems occurring such as a variable dust delivered to the FAR or backpressure. After two and a half pistons worth of PuralNF, a significant air leakage at the bolts of the dispersion head resulted in the FAR having to be shutdown. Upon removal, a significant amount of PuralNF had adhered to the metalwork, as seen in Figure 20. Figure 20 (left) showed the rotatory brush, prior to the dust cover and air inlet being removed. Figure 20 (middle) showed that large agglomerates had formed between the bristles of the brush and the flow channel (from the bristles to the bottom of the image). Furthermore, adhesion extended throughout the flow channel, particularly at the walls, which indicated that this build-up had occurred until failure. Inspection inside the nozzle also showed evidence of this. Figure 20 (right) showed the same occurrence for the flow channel on the bottom face of the dispersion cover, which further demonstrated the adhesive build-up over time.

Moisture content may have aided in the facilitation of adhesion. Free moisture determination showed that the moisture content of PuralNF was ≈3%. At low moisture content, it is impossible to use completely dried powder, without having to commit to massive economical

investments to reduce the atmospheric moisture. Upon drying, reabsorption began instantaneously, which demonstrated that even if dried, by the time its incision into the piston and compacted, moisture uptake would have occurred. The talc powder also displayed a similar moisture content. Evaluation of the set-up ensued, to evaluate if the compressor drier was operational, and that no fixtures or seals where damaged which would allow for air ingress and therefore additional moisture into the aerosol generator. The dryer was working, and no apparent air ingress points where noted.

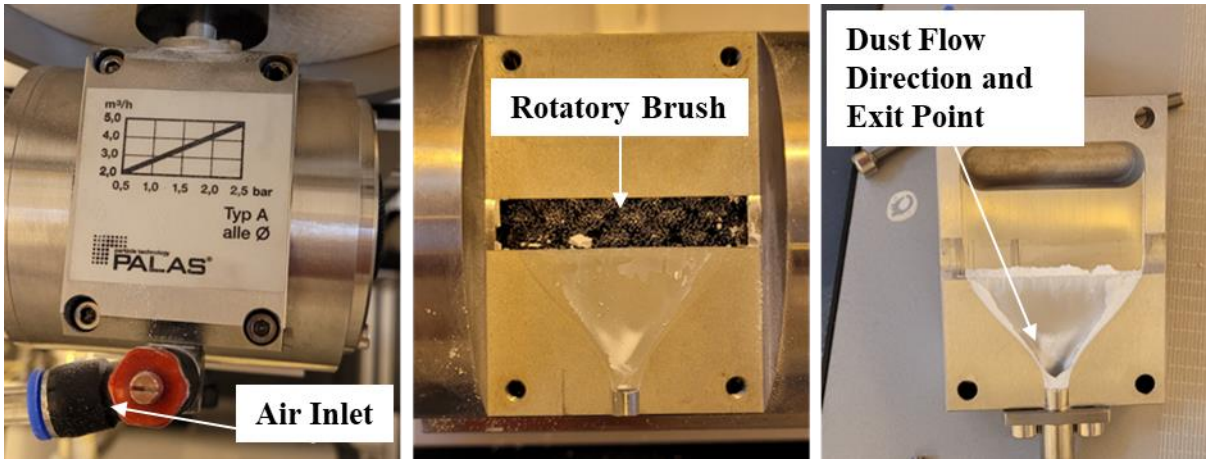

Figure 20: Dust Dispersion Location (left), Aerosol Dispersion Face (middle), and Bottom Face of the Dust Dispersion Plate (Right). Photos Taken After 3 Pistons of PuralNF Had Passed Through the Interface Between the Left and Right Images

This leak did not occur during any of the tests with talc. Use of PuralNF during experimental testing identified this problem. The original operational and maintenance manual specified this test dust but did warn of its adhesive nature. Adhesion only happened on the metal work and not on the glass. To determine the best method to clean the PuralNF off the metalwork, Palas was contacted where they suggested using an ultrasonic bath and cleaning detergent to remove the contaminants. Following cleaning, the FAR was clean and operational again.

To aid in the prevention of adhesion of the PuralNF in future tests, both the piston and dispersion cover where designated as daily cleaning items using the ultrasonic bath. After each full piston use, cleansing and drying of the piston and dispersion cover commenced in an attempt to prevent the occurrence of both adhesion and accidental leakage. For the surface of Figure 8 (middle and right), after the removal of the nylon brush, a small amount of cleaning fluid on a cloth over the affected area allowed for the removal of the material from the surface. Light wiping removed the adhered material without damaging the machined surfaces.

3.2.3 Potential Advances for the MMTC2000

Advances in the operation of the FAR would yield far more data from a particular test and would provide a deeper understanding as to what is happening during the test. As such, during the commissioning and preliminary testing, any potential improvements that would be advantageous to future studies were recorded. Three key improvements towards the FAR, as discussed below.

1. Implementation of a dust hopper unit

During longevity testing, there is a notable accumulation of powder upstream of the test filter. Depending on this volume, it can cause a negative impact on the testing data. Preliminary tests which used a talc powder, showed that accumulation tended to occur at the vertical bottom at the face of the test filter. Over time, this led to a significant build-up of talc powder which resulted in an artificially higher baseline differential pressure within the data. Once manually removed, the baseline differential pressure recovered considerably. This accumulation decreased the accuracy of the results. This negative impact on testing needed to be addressed imminently, particularly when conducting longevity tests which would require near continuous operation and minimal downtime.

Implementation of a collection hopper reduced the negative impacts to the data. This allowed for the filtered test dust to fall into the hopper and not collect at the bottom of the test filter. Procurement of a hopper system, from Palas, provided the solution and allowed for quick implementation to the existing FAR. This hopper fitted inline and directly upstream to the test filter as shown in Figure 21. Upon completion of a cleaning cycle, the bulk of the talc powder (or other testing powder) would be collected in the hopper. This allowed the test filter to remain unobstructed from the previously filtered test dust. The consolidated powder within the hopper could either be reintroduced to the piston cylinder or disposed of following standard laboratory protocol.

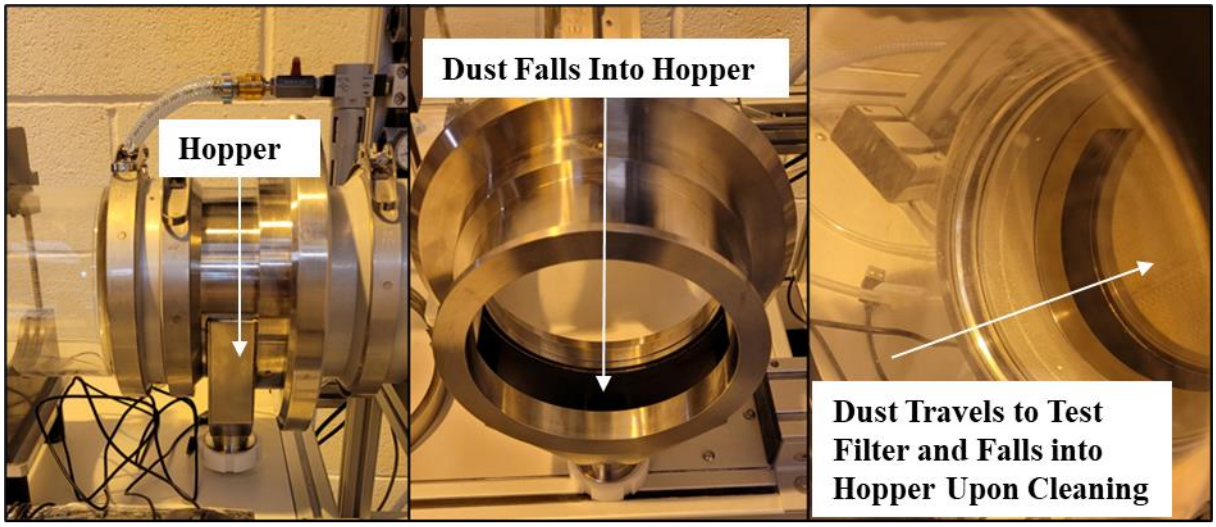

Figure 21: The Dust Hopper In-situ (Left), Angled Overview Showing Hopper (Middle) and In Situ Photo Showing Filter Sample and Hopper (Right)

2. Deployment of an in-line particle analyser downstream of the test filter

In terms of future development of the FAR, instillation of a Palas Promo® and Welas® aerosol sensor system from Palas, Germany would facilitate studies about the downstream particle size and concentration experienced during testing. Studies have previously used different models of this equipment such as Kurtz et al., [196], and Kurtz et al., [213] to study the occurrence of downstream emissions from a test filter. Whilst other types of optical particle counters (OPC) equipment exist (which use light scattering to detect and determine particle sizes in-line, such as Li et al., [137], and Lo et al., [193]), the Promo® and Welas® OPC sensor is designed to be used in conjunction with the MMTC200 and relevant software. This would allow for quick and effective commissioning of the sensor within the current set up. Consequently, any data processing would happen outside of the software upon collection of the raw data.

In relation to academic output, the OPC would demonstrate the evolution of particle penetration size and concertation, over service time. Given ultimate failure may be at a given emission point, the OPC would provide an additional data stream which would further improve longevity modelling. The OPC is also capable of identifying when a cleaning pulse has occurred through the spike in emissions as shown by Li et al., [137]. Collection of this data could provide another datapoint towards the determine of ultimate failure.

3. Additional pistons

During longer testing periods, a piston change was required once the piston was empty to all the test to continue until either conclusion or required another piston change. As such, this may require 2-3 pistons per day over multiple days, especially during longer testing/studies. Reduction in the downtime would therefore allow for quicker completion of longer studies. Whilst the test rig is in operation, a secondary piston could be prepared with the same test dust, which would reduce downtime by a single switch of the used position for a new/filled one. This would significantly drop the downtime to ≈5 minutes. The remaining ≈5 minutes downtime is due to the requirement to move the piston down to its minimum position. This movement allowed for the removal of the primary piston and insertion of the secondary piston. Therefore, a secondary piston is an economically viable way to improve efficient operation through a significant reduction of projected downtime.

3.3 Chapters 4,5,6, and 7's Methodology Statements

The following method statements introduced the analytical techniques which were used in chapters 4, 5, 6, and 7. Each chapter used a specific set of analytical techniques, which resulted in the method varying between the chapters. All samples used in these chapters originated from various industrial combustion sites across the U.K. Each chapter performed academic studies on industrially relevant filtration media.

Section 1.5 summarised the aims and objectives of each of the chapters/studies.

3.3.1 Chapter 4: Methods to Clean the Filter Media

BS22031:2021 "Sampling and test method for cleanable filter media taken from filters of systems in operation" [16], section 5.4 suggested various methods to clean the filtration media into a post cleaned state. A total of four techniques where suggested, but no information on a preferred cleaning method or methodology was given within the standard. To determine the most appropriate technique, the use of industrially used filtration media allowed for the results to be more relevant to industry. Results from the study would aid to guide and develop the standard.

The filtration media used was a P84/PTFE needle felt, with a PTFE scrim. The origin site was an Energy from Waste Site within the U.K. The original material data sheet can be found in Appendix A for Site B The time in service was unknown and not provided from the site. Table 11 demonstrated the stages that occurred to obtain the data, which helped to aid the suggestion of an appropriate cleaning technique.

Table 11: Chapter 4 Methodology to Evaluate Different Cleaning Methods

Stage	Description
1) Sample Preparation of Used Media	Acquisition of a 30cm (vertical height) sample from the remaining media. Incision at the stitch allowed the media to become flat. A further 5cm x 5cm sample, removed from the 30cm sample, allowed for mass and thickness evaluation. A total of five samples allowed for the evaluation of each method stated in Stage 3.
2) Evaluation in the As Received (AR) State	Evaluation of the Air Permeability, Mass, and Thickness according to laboratory standards. Air permeability evaluation occurred three times in random positions at 200Pa and a surface area of 20cm^2. The 5cm x 5cm sample underwent thickness evaluation using a digital thickness gauge to two decimal places (mm). The mass of the same sample used a weighing scale gave the mass to three decimal places (grams).
3) Cleaning Method Under Assessment	Compressed air, scraping, brushing, washing, and dust vacuuming where conducted on the surface of the filter sample. Conduction of air permeability, Mass, and thickness evaluations stated in Stage 2.
4) Dust vacuum of Sample	Each sample then underwent dust vacuuming, based on previous laboratory experiences. Performance of the evaluation method in Stage 2.
5) Data Review	Each of the five samples had three distinct groups of data, which allowed for comparison of the methods.

3.3.2 Chapter 5: Mass and Thickness Variation on a Given Sample

Like section 3.3.1, a sample of used, industrially derived, nonwoven filtration media gave more industrially relevant results, which allowed for better methodology development of technique(s). Though BS22031:2021 "Sampling and test method for cleanable filter media taken from filters of systems in operation" [16] mentioned both mass and thickness, it omitted a clear methodology to determine the mass and thickness values. An initial starting point was the British standards 29073 part 1 "Determination of mass per unit area" [230] and part 2 "Determination of thickness"[231], which prescribed a methodology for the determination of mass and thickness of clean nonwoven media respectively. These standards, in combination with current laboratory practices where combined which led to a high-resolution study on a single sample being conducted.

Chapter 5 discussed the differences between both mass and thickness methods. Ultimately, the study aimed to determine an appropriate sampling method for mass and thickness of a given sample size, which could be adopted into BS22031:2021 "Sampling and test method for cleanable filter media taken from filters of systems in operation" [16]. Adoption into the standard would require a statistical assessment of the number of repeats needed to obtain a representative result of the global sample. Furthermore, consideration towards any additional information obtainable from the sample was considered.

3.3.3 Chapter 6: High Resolution Air Permeability

A used nonwoven flue gas filtration bag, derived from an energy from waste combustion facility in the U.K., allowed for the air permeability to be mapped across its surface area. Like Section 3.3.1, the site did not provide any further information about the bag. In addition to the used bag, the site provided a new/virgin bag for comparison. The site did however provide a material datasheet for the new bag, which allowed for the conduction of further analysis (see appendix A Site B). Air permeability was performed in accordance to the parameters laid out in BS 9073-15 "Determination of air permeability" [232]. Each evaluation point on the media was at a fixed sample differential pressure of 200Pa and surface area of 20cm^2.

New/virgin media was evaluated in accordance with BS 9073-15 "Determination of air permeability" [232]. The total surface area available for evaluation of this sample was >1200cm^2. The only deviation from the standard was that ten random sample locations where assessed, which was more than the minimum of three required by the standard. Discussed further within Chapter 6 is the sample preparation, error representation, and calibration of the air permeability machine.

The air permeability mapping used a matrix structure to store the locational information and data of each result from the air permeability test. This transpired through the media being prepared in such a way that allowed it to become flat, as opposed to its original cylindrical form. Both the new and used filtration bag underwent the same preparation steps.

The data retrieved allowed for wide scale statistical testing, to understand the variation. Random sampling, and fixed position sampling provided an insight into the effects on the resultant mean, in relation to the global mean. Furthermore, fixed positioning demonstrated what could happen if an analyst did not apply a random position sampling method. This provided a wide range of results, which could further support the developed methodology for air permeability assessment of a used, nonwoven filtration media bag.

3.3.4 Chapter 7: Critical Evaluation: Preliminary Longevity Data

Chapter 7 explored various analytical techniques which may be used to complement a longevity model. This chapter used two samples: industrially used filtration media and virgin/new media – both from site C. The datasheet of virgin/new media is located within Appendix A site C.

Longevity modelling aimed at predicting the remaining life of used filtration media. A preliminary test performed using the FAR saw two samples ran to failure. The operational parameters of the FAR were selected based on the Site C's operational parameters, which better represented industrial practice. Test yielded two distinct data categories for each sample: the pre-op and post-op characteristics of the media. The data received for these two categories required the physical sample to be tested. Air permeability, mass, thickness, SEM, µCT, and analysis of the online data from testing were used to evaluate the filtration media.

µCT is an emerging analytical technology, potentially capable of evaluating the sample. Based on the limited literature, Chapter 7 presented an exploratory study of this technique. This exploration raised further questions and concepts which future researchers may find useful. Overall, preliminary µCT results showed, in combination with the X-ray profile views, illustrated the porosity variation through the sample, suggesting regions of higher/lower deposition.

To complement the data obtained from analytical techniques, the data retrieved from the FAR was evaluated. Evaluation of the data focused on how a longevity model may be developed. As CoD was used for the tests, the datapoint immediately after pulse cleaning was isolated and its subsequent data noted. Analysis of these datapoints for both samples suggested similar patterns within the data. These results where limited due to only two samples being completed. As such, the results only suggested how the model may be developed as opposed to suggesting a definitive model.

The critical analysis of all results, in both isolation and comparison, suggested a pathway in which future research on the subject may lead.

Chapter 4: Determination of an Appropriate Cleaning Method

4.1 Introduction

A variety of filter cleaning methods can be employed, as stated in BS22031:2021 "Sampling and test method for cleanable filter media taken from filters of systems in operation" [16], to convert the filter from the as received (AR) state, to a post cleaned (PC) state. The definition of cleaning is to remove filtrate from the surface of the sample. Filtrate encounters the air entry surface of the filter, whereby collection can occur on the surface, or depths, of the filter (depending on design and condition). Completion of cleaning allowed for the evaluation of the sample in the PC state. The aim of this analysis was to determine how the filter media has changed from its original condition. Various cleaning methods, such as: shaking, brushing, scraping, and dust vacuuming, exist to perform the cleaning of the filter. Methods presented within BS22031:2021 "Sampling and test method for cleanable filter media taken from filters of systems in operation" [16] where assessed, alongside a new method: washing. Washing was evaluated based on laboratory observations were some filtrate appeared to dissolve into solution when agitated in water. Whilst the standard does not specify a definitive cleaning method, there would exist an unquantified variability between the different methods. Output from this work has been shared and considered by the British Standard Institute (BSI) subcommittee group with a view to reviewing and improving the published standard methods.

The importance of this study was to better understand the effect that different cleaning methods have on the results/data obtained from performing analysis in the PC state. Evaluation of washing as a cleaning method also occurred, given the standard's allowance for the use of any additional cleaning method. Theoretically, a 100% effective clean would remove all the filtrate from the sample. During cleaning, removal of any internal deposits to the filter may be impractical, without subjecting the filter to intense cleaning and treatment processes. Given this, the cleaning method may fail to perform a fully effective clean, which would leave an unknown quantity of filtrate remaining within the filter. Avoidance of internal deposits is impossible and is a natural phenomenon in filtration where filtrate smaller than the pore size can deposit inside the media which is difficult to remove through cleaning. However, if an effective removal of surface/cake filtrate was possible, assessment of filter media variation is still a viable objective.

One alternative cleaning method is to clean the media to its specific operational cleaning specification(s). For pulse jet filtration, this would require vertical suspension of the filter against a cage. Following this, cleaning would occur using a pulse of dry and oil free compressed air at a given pressure, nozzle design, and pulse duration, which is representative of the original cleaning parameters. BS11057:2011 "Air Quality – Test method for filtration characterization of cleanable filter media" [202] suggested a schematic for this cleaning method. One potential benefit is the results from the evaluated PC state would provide a greater understanding into how the remaining filtrate on the surface of the sample affected operation. However, one difficulty with this method is the reliance on knowing the exact peak pressure from the sample's original location spatially.

Experimental studies, such as Andersen et al., [201], Sievert and Loffler [217], and Li et al., [220], have shown that the peak pressure of the cleaning pulse varied along both the vertical height of the full filtration bag and pulse line. Replication of this in the laboratory, would require a deep understanding of the entire bag house, including the associated pulse variation. This led to the assumption that, regardless of the filtration bags position along the pulse line, and the samples respective vertical height, constant cleaning parameters occur at every spatial position of the filtration bag. Extension of this assumption, across the entire bag house would occur, unless specific operational data or cleaning parameter data is available. Consequently, the assumption would negatively impact the results due to over or under cleaning of the filter. The assumption therefore implied that that the removal of filtrate is equal to the exact conditions experienced during normal operation, which given the previously mentioned variation, is questionable. Due to the potential for significant variation, and omission of site-specific operational data/variation, lead to the rejection of pulse cleaning as a cleaning method.

4.1.1 Methodology

This study utilized a used nonwoven filtration media filter bag, from an energy from waste (EfW) combustion site within the U.K. By using industrially relevant media, the results provided more representative data at an industrial level. Analysis required isolation of five samples at 30cm in vertical height/length intervals from the used filtration media. An incision at the stitch allowed each sample to be laid flat, as opposed to cylindrical. Next, removal of a 5cm-by-5cm sample, from each of the six samples, allowed for the conduction (and determination) of mass and thickness across all test methods assessed. The remaining surface

area of the sample underwent air permeability determination, which consisted of an assessment of three random locations at a differential pressure across the sample of 200Pa.

Once evaluated in the AR state, analysis was again reconducted following cleaning. Each sample underwent a specific cleaning method as described in Table 12. Following this, each sample was vacuum cleaned and evaluated again. This led to each sample having three categories of data: AR, Test Method, Vacuum (PC). Performance of vacuuming, post-test method, transpired due to the visual observations prior to this study across various samples from different combustion sites. This allowed for comparison between all the assessed test methods and vacuuming.

Table 12: Description of Cleaning Methods Assessed

Test Method	Description
Dust Vacuum (only)	Across the full surface of the sample
Shaken	Vigorous shaken occurred until no visual removal noted
Brush	Using a clean, soft brush, brushing the filtrate deposit to the side towards the edge of the sample.
Scraped	Scraping of the filtrate towards the edge of the sample
Compressed air	Exposure of compressed air to the surface
Washed	Subjection of the whole filter to a washing cycle at ambient temperature. This cycle consisted of agitation of the sample, rinsing, and spinning. Drying occurred in a drying over at 105°C, until fully dry before testing.

4.2 Results and Discussion

4.2.1 Visual Assessment

Images of the test method clean (1st row) and vacuum clean (2nd row) are shown in Figure 22.

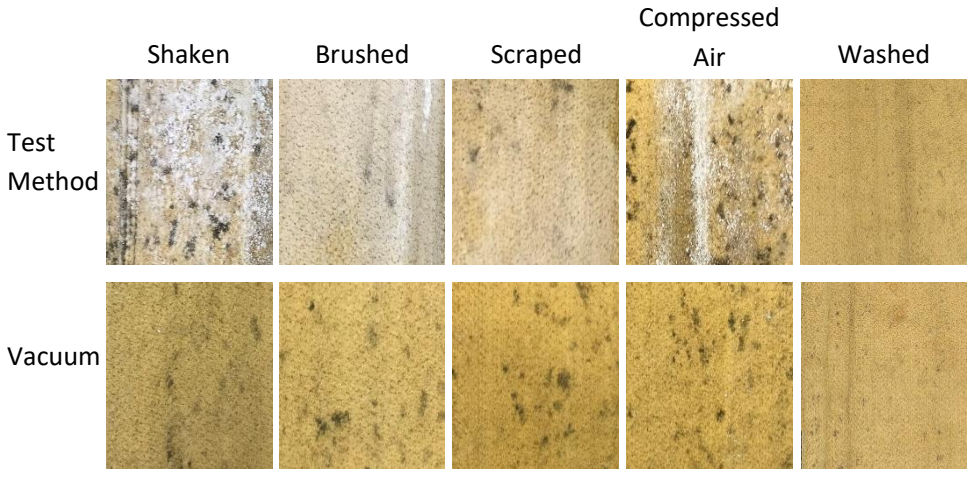

Figure 22: Visualisation of the Air Entry Side of the Sample Post Test Method Clean (Row 1) and Vacuum Clean (Row 2)

Visual observations of the air entry surface displayed different levels of filtrate retention after test method cleaning as shown in Figure 22 Both the shaken and compressed air methods

appeared to have retained a proportion of filtrate on the surface. In contrast, an apparent larger proportion of filtrate remained on the shaken sample. Filtrate removal occurred due to the applied separation force being greater than the adhesion forces of the filtrate to the sample [99], [261]. Therefore, the effectiveness of removal is proportional to the separation force applied but is then also dependent on the ability to collect/remove it from the surface.

For both the brushing and scraping methods, a residual layer of filtrate remained on the surface. For these methods, the separation of filtrate from the filtration media occurred through the motion of the instrument against the surface. Removal of the filtrate took place once the brush/scraper reached the edge of the sample. Due to surface heterogeneity, the movement of the instrument caused accidental redeposition in the pores immediately at the surface of the filter media. Once this accidental deposition had taken place, the filtrate remained, even if repetition of the cleaning method occurred. This resulted in the appearance shown in Figure 22. This motion effectively redistributed the filtrate into the uppermost pores of the filter media, which led to a more homogeneous surface in comparison to the original surface.

Both dust vacuuming, and washing, yielded visually comparable results. As shown in Figure 22, visually little/no filtrate remained on the surface of the media. For dust vacuuming, suction of air, away from the filter, removed the filtrate from the surface. In contrast, the washing process removed the filtrate through a mixture of agitation and dissolution within a solution. Given the visual similarity between the test methods washing and vacuuming, it could be preliminary concluded that they are similar in removal efficiencies based on the ability to see little to no filtrate left on the surface of the media.

However, unlike the other test methods, washing may yield a higher filtrate removal efficiency. Increased removal efficiency would occur if a proportion of the filtrate dissolved into the water, used to clean the sample during washing. Observations made during cleaning saw the colour of the water change from colourless to a grey translucent colour. An unquantified volume of the filtrate therefore could have dissolved into solution, which suggested the possibility for filtrate in the depths of the filter to also precipitate into solution. This may facilitate removal of a proportion of the depth filtered filtrate, during the agitation and drying phases. This observation may suggest that washing may be more effective at removing deposits below the surface of the filter. This ideology needed further investigation and studies to determine if this theory is valid and if so, to what extent.

4.2.2 Sample Mass

The results determined from analysis of sample mass for each AR, test method, and vacuum in grams were presented in Figure 23.

In comparison to the other test methods, washing suggested the best recovery when compared with the subsequent vacuum clean of the sample. Both the washing and subsequent vacuum clean yielded similar mass values post analysis, which resulted in a 100% recovery, as shown in Table 13. Shaking test method performed the worst out of the dataset, which yielded a 34.27% recovery. All other test methods performed better, with recoveries between 60-72%, but still failed to reach a recovery similar to 100%. Definition of the recovery percentile is the percentage of recovery between the testing method data (air permeability, mass, or thickness) over the recovery data (of the same analytical method) when the dust vacuum clean was applied after the test method (discussed further in section 4.2.5).

Discounting the test method washing, all test methods left a visible amount of filtrate on the surface of the sample. This retention of filtrate affected the mass results. Given the aim of cleaning is to determine how the filtration media had changed during service life, filtrate retention on the surface increased the mass, which artificially suggested that a greater proportion of depth filtration had occurred. Given the further recovery upon vacuuming each test method, it showed that the test method still retained a varying degree of filtrate on the sample.

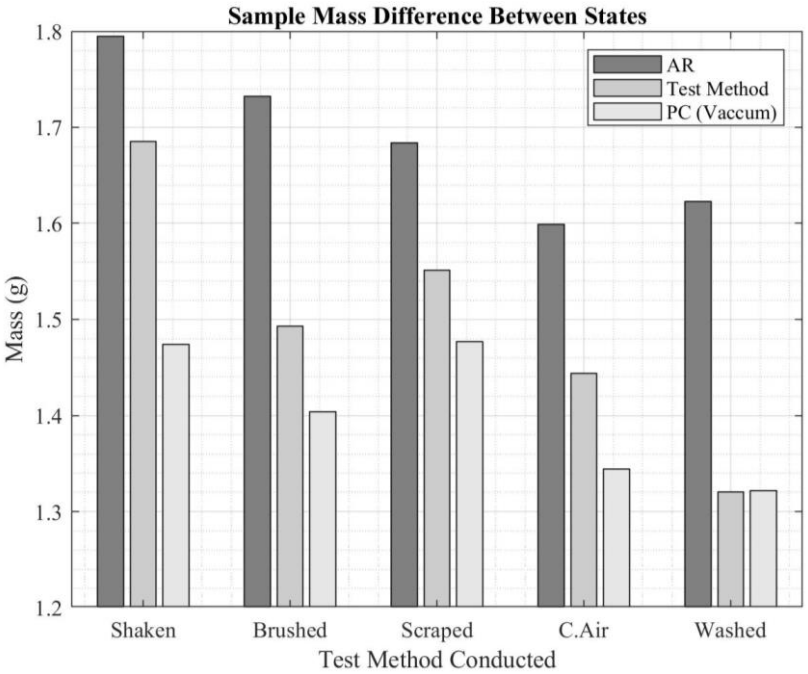

Figure 23: Sample Mass Data

4.2.3 Sample Thickness

The results determined from sample thickness analysis for each AR, test method, and Vacuum in millimetres are presented in Figure 24.

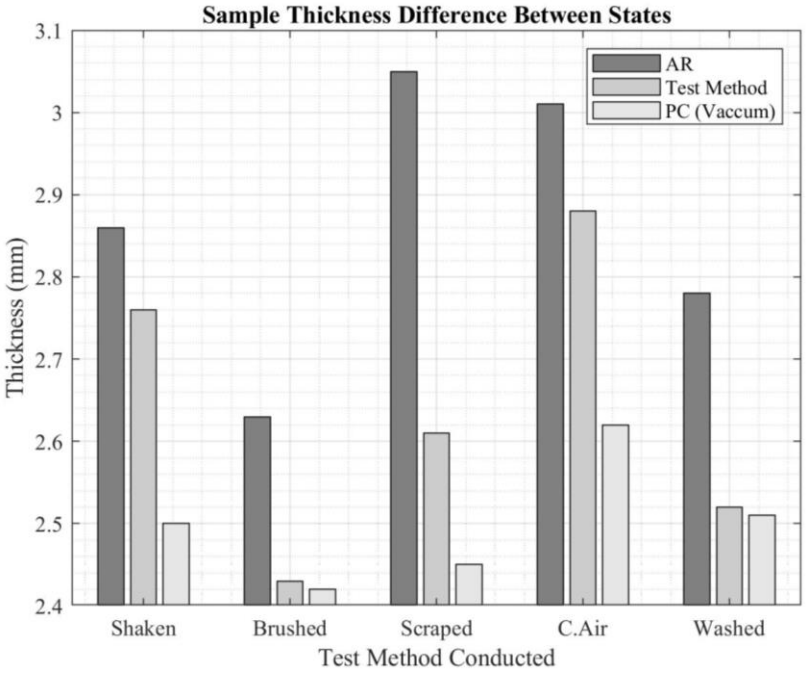

Figure 24: Sample Thickness Data

Likewise for sample mass results, test method washing yielded the best thickness recovery. Similarity between the washing and subsequent post clean (vacuum) results of the same sample led to a 96.30% recovery as shown in Table 13. Again, the shaking test method yielded a poor recovery at 27.78%. In contrast to the low recovery of the shaking test method, brushing yielded a higher recovery at 95.24%, followed by scraping at 73.33%. This recovery is due to the motion of an instrument across the surface, which removed a considerable proportion of the filtrate. However, this method changed the heterogeneous surface of the sample into a more homogeneous surface through deposition of filtrate within the surface pores. This deposition accounted for lower recovery of the sample mass, but showed that once the instrument had passed, it yielded a near comparable thickness to that of the vacuum clean that subsequently followed.

4.2.4 Sample Air Permeability

The results determined from sample air permeability analysis for each AR, test method, and Vacuum (in $Ldm^{-2}min^{-1}$) are presented in Figure 25. For comparative analysis, inclusion of each samples mean air permeability in the vacuumed state (in Figure 25) allowed for direct comparison between the test method and vacuumed results. This is represented in Figure 25

by a cross plot for each representative test method. In addition, the upper and lower confidence interval at 95% for each respective test method is also included.

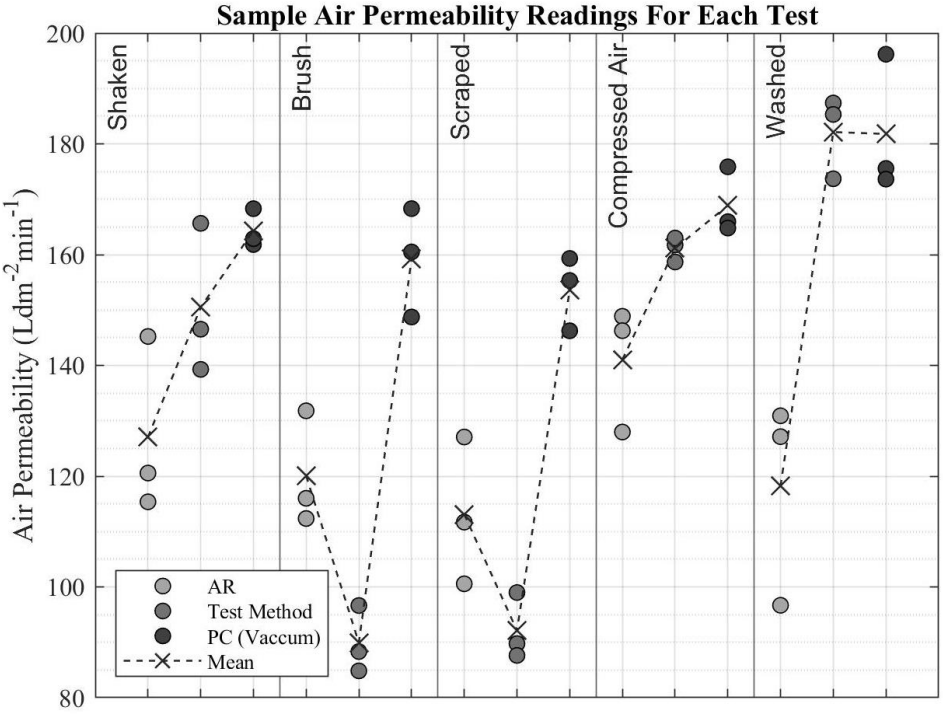

Figure 25: Sample Test Method Air Permeability Mean Data vs. Sample Vacuum Mean

Both the brushed and scraped test methods presented with a significantly lower air permeability than their respective AR states. This observation was likely due to the blockage of the surface pores, which restricted airflow through the media (as visualised in Figure 22). This observation led to a significant difference between the vacuum state and the test methods stated air permeability. As a result, both these methods presented significant issues to evaluate the sample for air permeability.

Recovery variance for the shaken test method was 62.88%. Discounting the brushed and scraped method, this test methods low recovery suggested that the shaking of the sample was ineffective at separating the filtrate from the filter. Whilst some filtrate was removed, a large proportion still remained which contributed to the low recovery. In compliance with BS9073-15:2008 “Determination of air permeability” [232] and BS22031:2021 “Sampling and test method for cleanable filter media taken from filters of systems in operation” [16] the mean of three random sample points is assumed representative of the overall sample surface area examined. Whilst this may be a suitable assumption for new/unused media, given the variation of filtrate retention (as shown in Figure 22) this could lead to a degree of variation in the obtained results from analysis, which cast doubt upon this assumption; particularly

where varying degrees of filtrate retention existed on the air entry surface of the sample. Chapter 6 discussed this observation of potential variation within a given sample surface area further.

Test method compressed air exhibited the lowest 95% confidence interval at ±1.6 $Ldm^{-2}min^{-1}$ of any test method. This could have originated from the assumption that three random sampling positions are representative, given a degree of filtrate attention as shown in Figure 22. If the random locations chosen where similar in terms of surface filtrate retention, then this would result in a similar mean and low confidence interval. Conversely, if the surface of the sample changed between sampling positions, the resultant confidence interval would increase due to the varying anisotropy of the selected sampling positions. For the shaken test method, random sampling may have interfered with the perceived mean and resulted in a noticeably higher confidence interval. Unlike the shaken method, the remaining filtrate on the surface of the compressed air sample appeared to be present a more visually uniform surface, which could have accounted for the lower confidence interval value.

A certain randomness existed within the resultant confidence interval, based on the location of sampling and number of repeats (3). Consequently, this randomness attributed towards the noted variation. However, it must also be noted that variation in the base media itself will also likely contribute to this variation. For example, the compressed air and subsequent vacuum mean difference was 7.8 $Ldm^{-2}min^{-1}$, showing some retention still occurred which was seen visually between the two states.

Comparison between the sample test method mean and vacuum mean gave an indication of the efficiency of air permeability recovery efficiency. Preliminary visual testing (conducted prior to the study) suggested that the vacuum method yielded the greatest recovery of the filtrate from the surface of the media. This facilitated the assumption that the vacuum method was the most effective. For test methods shaken, brushed, scraped, and compressed air, the air permeability results suggested that the assumption held true, given the removal of the remaining filtrate on the surface post-test method, but also given the increased air permeability post vacuum. Given the difference between the test and vacuum means for these samples, the vacuum method provided a more effective filtrate removal and thus air permeability recovery for these methods.

Intriguingly, for the washed test method and vacuum mean, an apparent asymptote existed. Given the closeness of the resultant means, further removal of filtrate was minimal/not observable during the vacuuming stage of the sample. This suggested that both the washing and vacuuming methods are equally efficient at filtrate removal. Furthermore, given the overlap of the confidence intervals, it suggested that both the test method and vacuum datasets where similar in terms of resultant values. Another alternative from this data could be the suggestion that the washing method could be more efficient at recovering the air permeability, owing to an unknown amount of dissolution within the depths of the filter during washing, which the dust vacuum would have failed to remove. This would require further testing with various filters/filtrates to either prove or disprove accordingly.

An additional sample was removed from the bulk AR media which underwent vacuuming as the test method, followed by a wash to better understand the impact of vacuuming on the sample. Identical analysis to this study allowed for comparison of both groups of results. The calculated means for the vacuum and washed states returned a similar difference as to the washed and vacuum state sample. If filtrate dissolution had taken place within the pore structure of the sample, it was negligible and therefore would not impact the resultant data. For different media/filtrate, repetition of this study will allow for the determination of the most effective cleaning method for the given media and filtrate.

4.2.5 Percentile Recovery

The recovery percentile is defined as the percentage difference between the testing method mean over the PC (vacuum) mean. This fraction yielded a percentile of how close the test method came to the vacuum clean, under the assumption that the vacuum clean was the most effective to facilitate filtrate removal. These results are presented in Table 13.

Table 13: Percentile Recoveries of Various Test Methods

	Test Method Percentile Recoveries				
	Shaken	Brush	Scraped	Compressed air	Washed
Mass	34.27%	72.87%	64.25%	60.78%	100.66%
Thickness	27.78%	95.24%	73.33%	33.33%	96.30%
Air Permeability	62.88%	-76.95%	-51.78%	72.23%	100.53%

Most notable in Table 13 is the recovery percentiles of the washing test method. This test method performed the best overall, presenting the highest recovery percentage for each

analytical test conducted. For sample mass and air permeability, a percentile over 100% occurred. For sample mass, the recovery percentage above 100% occurred due to the accidental deposition from vacuuming the sample. A small amount of residual filtrate accidently remained on the vacuum nozzle and was subsequently re-entrained on the surface which increased its mass by ≈0.01g. This accidental deposition occurred only once. Direct comparison of the mass and thickness results was achievable due to the repetitive nature of the analysis about the same sample.

For air permeability, the occurrence of a +0.66% above the vacuum air permeability in the washed test method data likely originated due to random sampling location. As discussed, random sampling resulted in a degree of anisotropy due to separate locations on the surface area of the sample exhibiting different structures. Given that both the Vacuum and Washed surfaces where visually identical, coupled with the resultant air permeability difference of $|0.34\ Ldm^{-2}min^{-1}|$, this difference was likely due to the media structural difference from random sample positioning and not the filtrate.

Recovery of air permeability for the test methods brushed and scraped saw a negative recovery percentage. As shown visually in Figure 22, a near smooth layer of filtrate remained on the surface. Retainment of filtrate at the surface blocked otherwise open pores which restricted the air flow through and therefore lead to a lower air permeability. This led to a lower air permeability than the as received state of the sample, which gave rise to the negative recovery. Given this negative recovery, their suitability in cleaning the filter for analysis in the PC state is questionable. Another factor in the resultant percentile recovery is the random sampling position during air permeability testing. Consideration of the anisotropy of the fibres per surface area, coupled with the random sample positions when conducting testing, could increase the likelihood of yielding a less representative percentile recovery. Further work, presented in chapter's 5 and 6 looked at this variation in greater detail for mass, thickness, and air permeability.

Collectively, for mass and thickness, the recovery was minimal for the shaking test method due to a significantly higher retention of filtrate than the other methods within the same category. In comparison, whilst the compressed air method removed twice the filtrate mass as the shaken method, the thickness recovery was comparable to the shaken method. This is due to a higher retention of filtrate on the surface, caused by insufficient separation forces,

redeposition, and general failure to remove the filtrate from the air entry surface, which lead to the thickness being similar.

Further analysis between the compressed air and shaken test methods for air permeability only showed a ≈15% recovery difference in favour of the compressed air, despite the near 100% difference in recover of the sample mass. This suggested that whilst a greater amount of filtrate removal occurred, the remaining filtrate on the surface still restricted the air permeability recovery.

Regardless of the test method used, the laboratory employs an extraction system with additional HEPA filters to collect the filtrate to prevent it going to the atmosphere. Bulk ash is collected and stored in multiple layers of containment to mitigate against accidental release to the atmosphere. The collected ash is then disposed of following local requirements for safe disposal. The vacuuming test method mitigates against aerosolization given the suction force drives the filtrate and air into the bagged unit. Any ash that is not entrapped by the vacuum either falls into a hopper on the extraction system or is deposited on the HEPA filters. Other methods, such as shaking, increase the risk of deposition outside the confinement of the extraction system and could lead to breaches in the workplace exposure limit in the laboratory, as well as ash deposition on other surfaces which increase the risk of cross contamination. Consequently, vacuuming appeared to be the safest way to perform the cleaning step, with the collected ash easily contained for disposal.

4.2.6 Statistical Testing

As the sample testing for mass and thickness followed standard operating practices for the laboratory, no repeats where conducted. This practice limited the statistical analysis of this study to the air permeability data. The difference between the test method and subsequent PC (vacuum) was calculated and shown in Table 14. Chapter's 5 and 6 discussed the potential variation across a given surface area, for mass, thickness, and for air permeability, including any noteworthy statistical significance. This limited analysis to the air permeability results, where three random sample positions were assessed per sample, per state.

Initial comparison of the air permeability results suggested that the washing method was the most effective at removing the filtrate from the sample. Whilst the compressed air method was close to the vacuumed air permeability, all other test methods had a distinguishable difference in terms of air permeability recovery. Both the washed and compressed air test methods yielded a comparatively low difference, in comparison to the other test methods. All

differences noted in Table 14 are visualised in Figure 25, which aid in showing the difference between the test method and PC (vacuum) states.

Table 14: Statistical Summery

	Test Method				
Air Permeability	Shaken	Brush	Scraped	Compressed air	Washed
Mean Difference Between Vacuum and Test Method ($Ldm^{-2}min^{-1}$)	13.85	69.24	61.50	7.73	-0.34
t-score	-5.6337	-9.9453	-12.9937	-1.7968	0.0385
p-value	0.0150	0.0049	0.0029	0.1071	0.5136

For the brushed and scraped test methods, their reduction in air permeability led to a significantly larger difference and percentile recovery. Whist minimal recovery took place for the shaken method, a 13.85 $Ldm^{-2}min^{-1}$ difference suggested, in combination with other data and visual observations, that the recovery was neither uniform nor potentially comparable to the samples vacuumed state. Compressed air (test method) performed better, which yielded a lower difference. A negative difference for the washed sample occurred due to the mean air permeability of the washed state being greater than the vacuumed state. This occurred due to the randomness of the air permeability sampling positions which evaluated different surface areas of the media and thus a degree of anisotropy existed within the results as shown by the confidence interval.

Utilisation of a t-test on the air permeability data determined if the proposed test method was statistically significant in relation to the vacuum method. Criteria selection to establish evidence for the alternative hypothesis was determined prior to analysis to protect against data bias. Criteria for the test was set at 5% significance level and two degrees of freedom, resulting in a two tailed t-distribution score of |4.303|. A two tailed test assessed the potential resultant mean of the test method falling either side of the vacuumed mean. Table 14 summarised the results from testing, showing the respective t-score and p-value from the analysis.

Resulting evidence supported the alternative hypothesis, $H_1: \mu_{vaccum} \neq \mu_{test\ method}$ for all test methods except for the test methods compressed air and washed. Apart from the two aforementioned test methods, these methods showed a statistically significant difference between the means. This also translated in the resultant p-value which corroborated this

finding given P<0.05, which supported the evidence to support the alternative hypothesis. In contrast, the compressed air and washed test methods supported the null hypotheses, $H_o: \mu_{vaccum} = \mu_{test\ method}$. Compressed air was less supportive of the hypothesis, given an absolute larger t-score/smaller p-value in comparison to the washed method. Whilst the compressed air method revealed evidence for the null hypothesis, the visual observations between itself and the washed were different due to the visual retention of filtrate on the compressed air sample. Consequently, consideration of the visual filtrate retention is just as important in the determination of an applicable cleaning method as the statistical evaluation. As a result, Table 14 largely corroborated both the visual results of Figure 22, as well as the findings from Figure 25, but only the washed sample showed neither statistical significance or any visual retention of filtrate on the air entry surface.

4.3 Practicality Implication of Test Methods

During large scale testing, the time required to prepare the filtration bag for analysis is therefore dependent on the cleaning methodology employed. Subdivision of the filtration bag saw it divided into three distinct samples as described in BS22031:2021 “Sampling and test method for cleanable filter media taken from filters of systems in operation” [16]. Following analysis in the AR state, performance of the cleaning method converted the sample into the PC state. As a result, the selected cleaning method needed to be both effective at removing the filtrate and minimise preparation time. Under current laboratory standard operating practices, the cleaning method employed is dust vacuuming. This decision is largely due to the visual assessment, which gives a good visual indication to effective cleaning. As a result, any alterations to the cleaning method need to consider the time impact to prepare the sample for post cleaned analysis.

Whilst the washing test method provided a similar clean to the vacuum cleaning method, due to its submersion in a liquid, it required additional preparation time to dry the sample before the commencement of analytics. Drying saw the sample placed in a drying oven for a minimum of two hours to remove the residual moisture from washing. This caused the time required to complete analysis of the sample to increase significantly, in turn, affected the sample turnaround time. Furthermore, given the limitation of space within the drying oven, a backlog of samples could occur when multiple filtration bags required analysis, which could lead to sample misplacement. This would further delay the overall sample turnaround time. Therefore, the washing test method may not be practical for a large number of sample required for analysis given the significant increase in preparation time.

Apart from washing, sample analysis occurred immediately after sample cleaning. Evaluating one filtration bag at a time allowed for easier sample management given the reduced preparation needed, such as drying, before assessment and saw sample turnaround time remain within largely similar turnaround times. However, if washing occurred, utilisation of the drying time would see more samples prepared, which increases the chances of sample misplacement due to the backlog caused by the maximum allowable number of samples within the oven at any given time. Consequently, the increased preparation time for washing as a cleaning method led to it being less favourable given the potential for lower sample throughput and increased preparation times.

For brushing, scraped, shaking, and compressed air, varying degrees of aerosolization of the filtrate can occur. All sample preparation occurred on an extraction bench to mitigate the associated effect of aerosolization. Compressed air cleaning used a pressurised air supply to blow the filtrate off the surface. This caused a significant dispersant of the filtrate into the surrounding air, despite operation of the extraction bench. This also occurred for the shaking test method. Discouragement of these methods, to clean the filter, will reduce the potential to exceed the workplace exposure limit, as per the associated COSHH forms for safe laboratory practice. In comparison to compressed air and shaking, a noticeably reduced amount aerosolization occurred due to the brushing, scraping, and shaking test method preparation, however the same recommendation applied to both the compressed air and shaking cleaning methods, which would help to ensure that the workplace exposure limit is as low as reasonably practicable.

As a result, the vacuum test method appears most suitable from a practicality view given: the reduced preparation time, ease of use, reduced workplace exposure, and the ability to safely collect the filtrate for further analysis. Vacuuming collected the filtrate into a storage bin, which allowed for further testing of the filtrate as required. In addition, it led to a comparatively reduced amount of aerosolization, whereby the filtrate removed was safely collected into the vacuum system.

4.4 Conclusion, Further Work, and Novelty

4.4.1 Conclusion

BS22031:2021 “Sampling and test method for cleanable filter media taken from filters of systems in operation” [16] required the assessment of used filtration media in two states: as received (AR) and post cleaned (PC). Whilst the standard gave analysts a choice of cleaning

method to employ, it also allowed for an entirely new cleaning method to be employed. The underlying assumption is that, regardless of the selected cleaning method, the resultant clean would produce a similar result. Consequently, analysis across various cleaning methods (including the addition of a new method: washing) ascertained the variation exhibited from each different method through mass, thickness, and air permeability assessment. The use of industrially relevant samples allowed for a better understanding of the implications of the results/recommendations if they were adapted into the standard.

Overall, this study used five samples from a used filtration bag from an EfW combustion facility in the U.K. Assessment occurred in three defined states: as received, test method, and vacuum cleaned. Following the test method, vacuum cleaning allowed for the assessment of the remaining filtrate post-test method.

Overall, the test methods brushed and scraped performed poorly at recovering the air permeability due to the method of spreading the filtrate over the surface of the media. This led to a lower air permeability than their as received states, which is not possible under normal operation. Filtrate retention also increased the sample mass, which affected the interpretation of the results which suggested a greater internal deposition occurred. Subsequent vacuum cleaning removed the residual filtrate from the surface and resulted in a higher air permeability.

Both shaking and compressed air test methods had less retention of filtrate on the surface of the sample, in comparison to the brushed and scraped methods. However, compressed air provided statistical evidence to support the null hypothesis that the air permeability results for the test method and vacuum cleaning were similar. In contrast, the shaking, scraped, and brushed test methods yielded evidence for the alternative hypothesis. Once vacuumed, the mass and thickness of the samples reduced further which suggested that there was still a degree of variation in the data, regardless of the statistical analysis observed for air permeability.

Washing the sample yielded the best result in comparison to its respective vacuum cleaned state. Once all samples were analysed in their respective test method states, they were cleaned using the dust vacuum. This resulted in all the surfaces of the samples becoming similar in appearance. No noticeable/distinguishable difference existed between this test method and the vacuum clean within the data, both statistically, and visually. One of the difficulties with washing is the need for clear sample management to reduce the chance of sample

misplacement, but also the drying time required to prepare each sample. In addition, given the increase in time required to complete analysis, this method would significantly increase turnaround time to complete analysis.

Retention of filtrate on the air entry surface negatively impacted the data and thus the interpretation of the results. As shown, various test methods exhibited degrees of filtrate retention, which affected the mass, thickness, and air permeability results. Given that the aim of the cleaning method is to assess how the filtration media had changed over its service time, any retention of filtrate therefore artificially impacts on this assessment. As shown, both the vacuum and washing cleaning methods returns a fabric with no visible filtrate left on the surface. Furthermore, given the data and statistical analysis presented, both the washing and dust vacuuming appeared to be the most effective cleaning method evaluated.

In conclusion, upon consideration of the data and practicality/implementation considerations, dust vacuuming appeared to be the most appropriate method for cleaning the sample. The recovery of all visible surface filtrate using a dust vacuum was comparable to the washing method, without the submersion of the sample in solution. Therefore, although washing reported applicability as a cleaning method, the increased sample preparation time and resultant increased turnaround time led to this method being less suitable than vacuuming.

4.4.2 Further Work

Given that the interaction between the filtrate and media can vary, the dust vacuuming may not be the most appropriate for every sample. Based on this study's findings, requisition of two or more samples for analysis from the bulk/unused media, would allow for this to be determined. This would allow for the completion of a similar study in order to determine the most optimal cleaning method for a given filtrate/media sample. Acquisition from bulk/unused media would not impact the final test results or report for the sample. Initially, assessment of both washing and dust vacuuming, in alternative steps, would provide a timely determination of an appropriate cleaning method. Analysis of the results would determine the variation between the two methods and suggest the optimal method. However, dependent on the number of filtration bags for analysis and analysis turnaround time required, dust vacuuming may still be the most optimal cleaning method regardless.

Other cleaning methods, such as ultrasonic bathing in various solutions, may provide a more efficient clean. However, consideration to the effect on sample preparation and resultant turnaround time would have to form part of the analysis. Future analysis of other viable

cleaning methods may show that dust vacuuming is less efficient. The use of imaging, from µCT or SEM would further support the findings of the study and provide an insight into the effect of washing on the internal deposition. However, at this stage and given the results of this study, dust vacuuming appeared to be the most effective in terms of cleaning and sample turnaround time.

4.4.3 Novelty and Output

In literature, no previous studies were found that considered the effectiveness of the cleaning methods stated in the standard BS22031:2021 "Sampling and test method for cleanable filter media taken from filters of systems in operation" [16]. The standard provided multiple cleaning methods and allowed the analyst to use any other method to clean the filter media, on the understanding that it did not damage the media. Any damage caused by the cleaning process would impact the final results. From the literature review and subsequent searches, no information found suggested an optimal cleaning method, nor support the standard's recommendations. This study provided the basis for a methodology to determine a suitable cleaning method for used nonwoven filtration media within the energy sector.

The results of this study are useful for the British Standard Institute (BSI) subcommittee group that look after the aforementioned standard. Discussions are ongoing, but a review of the standards wording about how to clean the filter is advantageous in order to allow either dust vacuuming or washing to become the recommended post cleaning method. This would standardise the assessment of used filtration media across the industry and allow for relatively comparable data, regardless of the company of origin of said data.

Chapter 5: Understanding Mass and Thickness Variation

5.1 Introduction

5.1.1 Background

Compliance with British standard 22031:2021 "Sampling and test method for cleanable filter media taken from filters of systems in operation" [16] required a reported value of mass and thickness for the vertical top, middle and bottom sections of a used flue gas filtration bag. To report the mass/density, the required units are in either grams or kilograms per meter squared (gm^{-2} or kgm^{-2}). To report the thickness of the media, the required units are in millimetres (mm). Conduction of comparative analysis, between the as received (AR), Post-cleaned (PC), and virgin/new media state (VN), yielded an insight into how the media had changed over service time. As a result, the aim of performing this analysis was to provide an insight into how the filtration media had changed over its service/operational life through mass and thickness readings.

Due to the media used in this study being sectioned into 5cm by 5cm squares, it was not possible to perform additional analytical techniques (such as air permeability) on the media. As such, for air permeability an independent study on this assessment technique, in isolation of other techniques, is discussed further in Chapter 6.

Whilst this was a requirement by the standard, omission of a clearly defined methodology introduced a level of uncertainty in its determination. One argument from the wording of the standard is that analysis of the entire/whole filter sample should take place. Whilst this would give an overall value, it would fail to determine (if any) local variation along the vertical height of the filter. Another alternative could be the utilization of the samples taken along the vertical height for both machine and cross directional analysis for mass determination. This method would provide a greater insight into variation along the vertical height of the bag. However, the standard also showed an example report in the appendix, the former argument appeared more probable given the reporting of both the AR and PC state for the whole filtration bag. However, determination of mass across each representative third would have enabled some accountability for an unquantifiable degree of variation across the vertical height of the filtration bag.

Additionally, one optional extra characteristic within the standard is the potential to take thickness readings of the sample. Similar for mass, there was no provision for a methodology

to determine the thickness parameter. Upon inspection of the standard, appendix C.1 [16] reported five samples assessed for thickness, yet C.2 [16] only used three samples before the evaluation of the mean. Furthermore, the standard omitted a clear definition of the required state (AR or PC) within the report, AR, or PC for the thickness value. Moreover, the inclusion of the thickness results in the report templates suggested that this measurement may not be optional.

Consequently, a degree of confusion could arise when using the standard, which could cause the results of a test to unintentionally, not comply fully to the standard. As a result, the standard therefore provided a degree of freedom towards both the ways in which representation of the final mass and thickness values. There is also a question surrounding whether the optional extra of the thickness measurement is indeed optional given the standards appendix. Most notably is the requirement to state the number of tests conducted for sample thickness. For sample mass, the implied assumption is that the reported value is representative of the whole sample regardless of sample size taken for the analysis.

This uncertainty led to the need for a controlled study to 1) determine the variation of mass and thickness across a used sample, 2) highlight any potential differences between the states AR and PC, and 3) suggest a clear methodology to perform mass and thickness analysis, which provided a representative result with a reduced analytical time. To help achieve these goals, conduction of analysis across a VN media sample provided a baseline for the method development.

5.1.2 Methodology

Acquisition of a new and used nonwoven filtration bag from a 60 MWe EfW combustion facility, located within the United Kingdom, allowed for the conduction of this study. Prior to utilisation of the used filtration media within this study, the sample first underwent analysis according to current laboratory practices. This saw subdivision of the filtration bag into three distinct vertical height regions. Subsequent analysis on each of the sections included: air permeability, microscopy analysis, but also mass and thickness determination. Following this, using an unexamined piece of industrially used filtration media, conduction of the study was possible.

Further subdivision occurred which saw a 30cm length, in the vertical height removed from both the new and used filtration media. The assumption applied for the virgin/new media was that the sample obtained from the new media was representative to that of the overall bag and

media in general. Table 15 provides a summary of these results for the used sample, including a summary of the new media according to the datasheet.

Table 15: Summary of New Media Parameters

Parameter	Value	Parameter	Value
Air Permeability (@200Pa $Ldm^{-2}min^{-1}$)	80	Mass (gm^{-2})	380
		Mass (g per25cm^2)	2.075
Thickness (mm)	1.3	Density (gcm^{-3})	0.64

Following isolation of the sample, a vertical incision along the vertical height allowed the sample to open and become flat against a surface. Following this, the sample was further prepared into multiple squares, each of which were 25cm^2 in surface area. To achieve this, a manufactured template of the same surface area allowed for each subdivide sample to be removed from the overall sample. Manufacture of a secondary rectangular template of 5cm by 40cm further eased the subdivision process through the allowance of subdivision of strips as seen in Figure 26 (left). This reduced the risk of accidental incisions to neighbouring squares which may affect results. After which, each resultant strip division into six equal squares ensued. Examples of which can be visualised in Figure 26 (middle and right). Overall, this yielded a total of fifty-four squares from both the virgin/new media, and the used media sample.

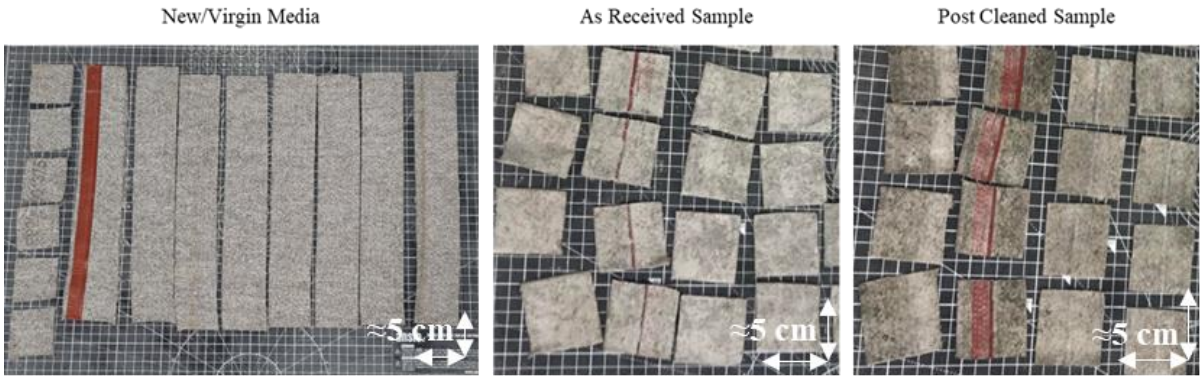

Figure 26: Illustration of Sample Preparation and Example Visual Differences Between the States

Subsequently, conduction of analysis for mass and thickness occurred on each of the fifty-four samples. Use of a weighing balance, which measured to 3d.p. in grams (g) determined the mass of each of the given 25cm^2 sample. A digital thickness gauge which read to 2d.p. in millimetres (mm) determined the thickness of each of the 25cm^2 samples.

Upon completion of the assessment in the AR state had transpired, the square samples where then cleaned using a dust vacuum following the results reported in Chapter 4. Transition of the sample into the PC state allowed for not only an understanding as to how the media had deviated from the virgin/new media state (VN), but also provided an indication as to the interaction of the filtrate at (and above) the surface of the media.

Assessment of the samples in the PC state assessed how the media had deviated from the new/virgin media. Due to the division of the overall sample into identical units, each sample had a unique spatial location which provided a further datapoint for analysis. To aid in the orientation and management of the spatial locations of each sample, positioning of the stitch point at the vertical left provided a checkpoint to further aid in sample management. This resulted in the cross direction being on the horizontal plane. During analysis, each sample's assessment was independent of any other sample and replaced back to its original position before another sample's assessment. This ensured that each samples representative location was consistent throughout the study. Each sample was measured for mass and thickness over the AR and PC state, with the data stored in matrix form to corroborate the locational information with the result. This yielded 54 datapoints per state per analytical method.

5.1.3 Research Aims and Outcomes

Overall, the aim of this study was to determine how the mass and thickness may vary across a sample with a vertical length of 30cm and impact the reported results. Conduction of a methodical and controlled study allowed for assessment of the data, particularly to reveal any relationships within the machine and/or cross direction of the sample which may affect the result.

In addition, given the nature and wording of BS 22031:2021 "Sampling and test method for cleanable filter media taken from filters of systems in operation" [16], omission of a clear methodology allowed for any particular method to be chose to assess mass and thickness. Standard laboratory analysis required three 30cm samples for analysis one from each of the vertical heights (the vertical top, middle, and bottom) of the filtration bag. This is a similar methodology to BS 22031:2021 "Sampling and test method for cleanable filter media taken from filters of systems in operation" [16] but deviated slightly through the acquisition of a larger singular sample as opposed to two samples from the same region. Frequent practice in the laboratory is to requisition a singular 25cm^2 surface area sample for mass and thickness

testing. As a result, this method provided the basis for the development of an appropriate method for the determination of mass and thickness of a sample.

Consideration as to the practicality of any method, during method selection, is advisable. One of the major constraints in large scale testing is the turnover time for samples. If the bag house is offline, with no alternative for flue gas treatment, the entire process may have to become offline. This would cause an overall economic loss to the site, given no generation of electrical power during the offline period. Therefore, the developed/selected methodology should consider the potential impact it may have on the time required to conduct analysis on multiple flue gas filtration bags/samples.

Whilst the methodology in BS22031:2021 "Sampling and test method for cleanable filter media taken from filters of systems in operation"[16] does not explicitly reference additional standards, its mention of the BS 9073 series provided an initial basis for mass and thickness in parts one [230] and two [231] respectively. In addition, the BS 9073 series illustrated various other test methods for nonwovens, such as tensile testing and air permeability testing. Given the omitted methodology in BS22031:2021 "Sampling and test method for cleanable filter media taken from filters of systems in operation" for mass and thickness, these standards where originally used as the premise for the development of a suitable mass and thickness methodology for used nonwoven filtration media.

In summary, the aim of this work is to address the following:

1. Illustrate the potential variation of a given sample, within a clearly defined sample size.

2. Determine the number of samples required to get a clear representative result of the defined sample size, considered against the implications of large-scale testing.

3. Compare and contrast the results with other potential test methods such as BS 9073-1 "Determination of mass per unit area" [230] and BS 9073-2 "Determination of Thickness" [231].

Consequently, the study concluded with a suggestion for a suitable methodology for mass and thickness for used nonwoven filtration media. This methodology contemplated the potential for variation in such a way that the reported value is more likely to represent the larger sample.

The overarching assumption, not assessed, is that the vertical height sample of 30cm in length is representative of its original vertical third; as stated in BS 22031:2021 "Sampling and test method for cleanable filter media taken from filters of systems in operation" [16] through the division of a filtration bag into three vertical regions. Consideration of this assumption as true was due to the inability to perform a high-resolution map of mass and thickness, across the full surface area of a used nonwoven filtration bag. This was due to other parts of the original filtration bag being used for routine analysis prior to this study. Whilst this study did not utilize a full filtration bag, it does provide an insight into how the thickness and mass may vary along the vertical and axial length.

5.2 New Media Variation

For new nonwoven media, the BS9073 series "Textiles. Test methods for nonwovens" (or equivalent), are frequently used to determine the mass/density and thickness of the media. For sample mass, a minimum of three 50,000mm^2 samples were required to determine the mass by area weight. However, following consultation with the end user, adjustment of these values can be set at any value to suit the analyst and consumer, so long as both parties agree. This allowed for an economical reduction of loss, particularly if the manufacture cost of the fabric is high. For thickness, the standard BS9073-2 required a total of ten samples, each with a surface area no less than 25,000mm^2. To determine the mass/density and thickness of the VN media, multiple samples were taken from new media for analysis.

BS 9073 part 1 "Determination of mass per unit area" [230] and 2 "Determination of Thickness" [231] required two different sample sizes, however due to the defined sample size, definition of the size was through the resultant available surface area of the sample as opposed to the standard. As the largest size required in the standards pertained to the mass determination, the use of a smaller sample allowed for a greater understanding of variation within the sample. Direct comparison between the mass and thickness was achievable due to the fixed sample position for each of the 25,000mm^2 samples.

Given the fixed sample size, this resulted in over and under sampling in accordance with the standards BS 9073-1 "Determination of mass per unit area" and 2 "Determination of Thickness"[230],[231]. For sample mass, compliance with the standard required three samples, with a cumulative total surface area of 150,000mm^2. In contrast, the study used forty-eight samples of flat media which had a 120,000mm^2 surface area: lower than the required area for standard compliance. On the other hand, a total of fifty-four samples within

this study outweighed the required number of ten samples of 50mm by 50mm for thickness determination, each with a surface area of 2,500mm^2. If selection of the largest mentioned area/repeat in each of the standards, this was the resultant difference; however as previously stated the number of repeats and/or largest area of analysis could differ, depending on agreement between the analyst and consumer.

Embedded within each standard is the potential for a customised sample size and number of samples, if agreed upon prior to testing. This statement allowed for deviation in both the sample size and number of samples to be variable, yet still comply with the standard. As such, this allowed conduction of a higher resolution study, which allowed for the development of a suitable methodology for each of the vertical thirds.

5.2.1 Discussion on the Data

Differences between flat and stitched media samples are visually shown in Figure 27.

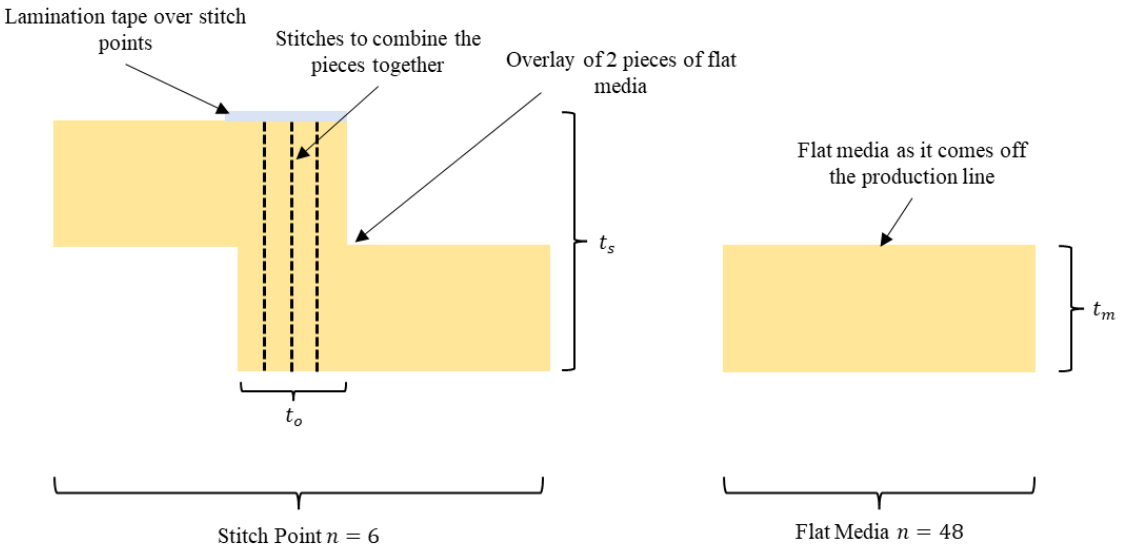

Figure 27: Visualisation of Key Differences Between Flat and Stitched Samples (where n = the number of samples)

Variation is an inherent occurrence within any manufacturing process. Properties such as punch density, needle penetration depth, and stroke frequency [133] coupled with the variation in the fibre mats [132]. This culminates in an unspecified degree of variation within the final product, particularly noticeable when considering the machine and cross direction [254]. This affects the number of fibres present within a given sample size (fibre density), which affects not only the overall mass and thickness, but other properties such as air permeability [132] and material strength [254].

Therefore, there will be an inherent variation between samples. Whilst the datasheet for this media provided a nominal value and complied to standards, it failed to include the confidence interval. This omission, which is valid under the standards, obstructed identification of any significant variance within the flat media. It was noted that in an operational and maintenance manual for a different site/media, that tolerances for the mass and thickness of the VN media as a $\pm$percentile of the absolute mean value. This suggested that there was at least a preliminary agreement between the manufacturer and buyer for an acceptable tolerance within the media. Omission of confidence limits from the manufacture data sheet raised the question as to why it was absent in the first place. Naturally, there will be an inherent tolerance from the manufacturing process. Therefore, multiple samples/repeats allow for a mean and confidence interval to be determined to better describe a given parameter. Compliance with the standards did not require, only recommended, the reporting of the confidence interval. As such, it may be difficult to ascertain if the results for the VN state validate the method and are representative of the originally state values.

Given the observable difference noted in Figure 27 for the stitch point, the tolerance is more complex. To fabricate the media into a cylindrical shape, one side of the flat media must be overlayed to the other. The overlay including the stitch, must be substantial enough to securely attach the top piece to the underlying piece. As a result, the overall thickness of the stitch point (t_s) will exhibit its own representative confidence interval, which would likely be equivalent to two (t_m)'s due to the overlayed nature. Encompassed in this confidence interval, is the variation in the lamination tape (present in this media) which will also have its own respective mean.

If the assumption of perfect alignment is applicable, the increased mass will also be a function of t_o. This would further increase due to the lamination tape, placed over the point where the stitches where made (if applied). Moreover, there will be a slight increase due to the stitches added to the sample to secure both sides together. Expectations from the results were, due to this phenomenon, that the stitch point would be notably higher in mass than the flat media sample.

Presented in Figure 28 are the results for both mass and thickness spatially in a heatmap. As expected, Figure 28 showed notably higher values for mass and thickness at the stitch point (50-100mm in the cross direction). In contrast, the remaining samples, all flat media, presented with an apparent similar value in both cases.

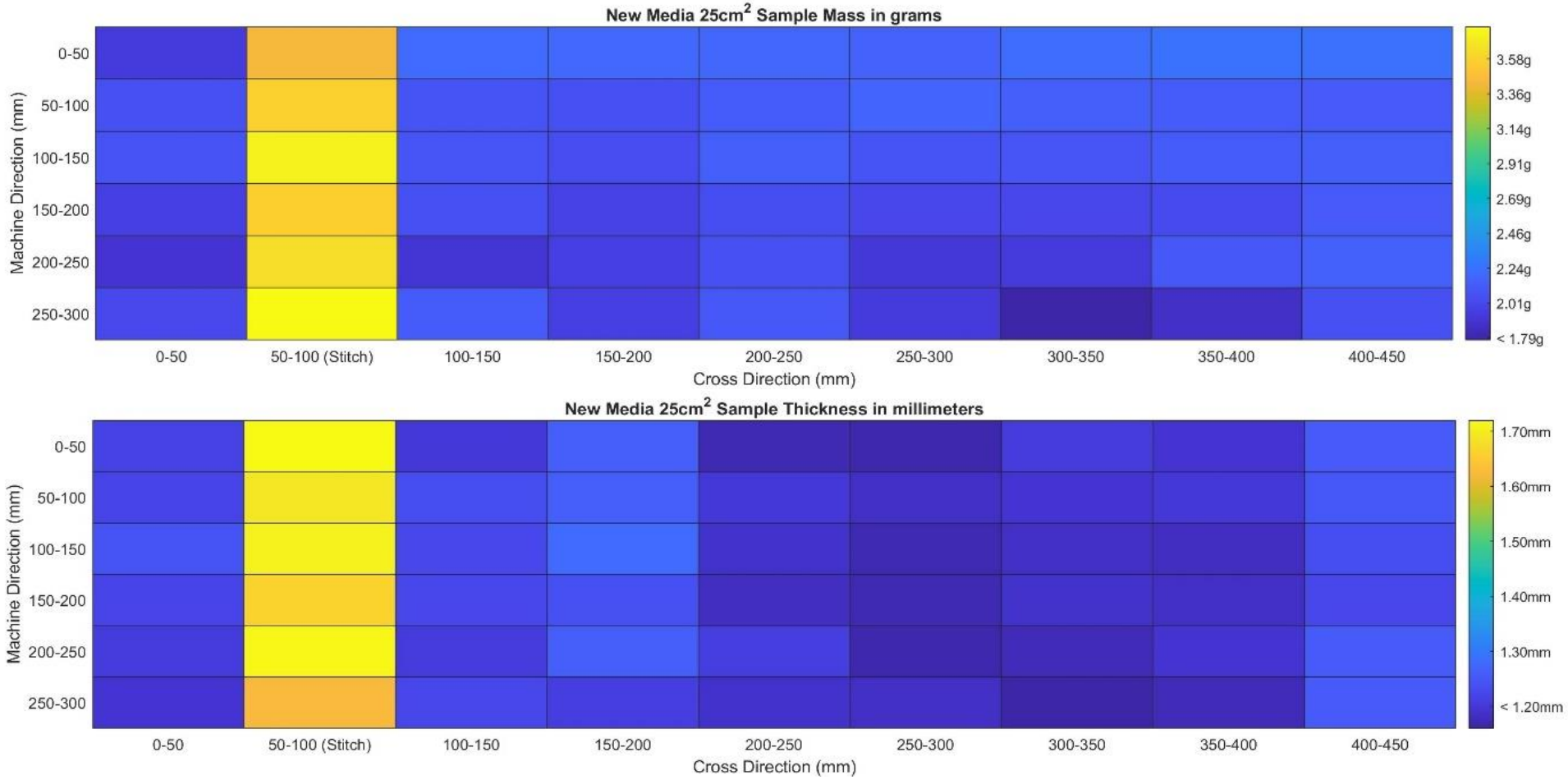

Figure 28: Heat Map Depiction of Mass (top) and Thickenss (bottom) Data

One limitation of the heat maps is the classification of data within bins, which led to the allocation of a particular colour to each bin. Owing to the stitch point data being larger than the flat media, this caused a split the data into two distinctive classifications: one for the flat media and other for the stitch point. This classification of the data caused the representative colours to be similar in each case. Owing to this classification the identification of data variation became difficult, particularly in the flat media data.

As a result, removal of the stitch point data would yield a greater understanding visually of the variation in the flat media. Analysis of the distributions of both mass and thickness results, shown in Figure 29, show a clear distinction between the flat media and stitch point. This corroborated the classification assumed in Figure 28. Furthermore, due to the classification of data, given the similarity between the results for the flat media and the datasheet, the conclusion was that the datasheet evaluated flat media only. Comparing the mass (areal density of $830gm^{-2} \approx$ equates to 2.075g per $25cm^2$ sample) and thickness (1.3 mm) values of the datasheet to the distributions in Figure 29 suggested that the datasheet only considered the flat media. Though not explicitly stated, the assumption was that the evaluation considered only the flat media due to the stitch's origination from postproduction methods and therefore not representative of the overall media as shown in the results through the data separation. Given these discussed factors, removal of the stitch point data occurred from future analysis.

Whilst further analysis on the stitch point ceased, Table 16 illustrated the statistical overview of the data, which presented both the mass and thickness results for both flat media and the stitch point. The presentation of this data may provide useful for future research into the expected deviation between the two structural differences. This was achieved by knowing the positions of each of the fifty-four samples, coupled with the distinct segregation of the data shown in Figure 29. Whilst the stitch point only contributed to a marginal percentile of the surface area, in comparison to the overall filtration bag, further work should focus on its effect during operation, given its omission within literature.

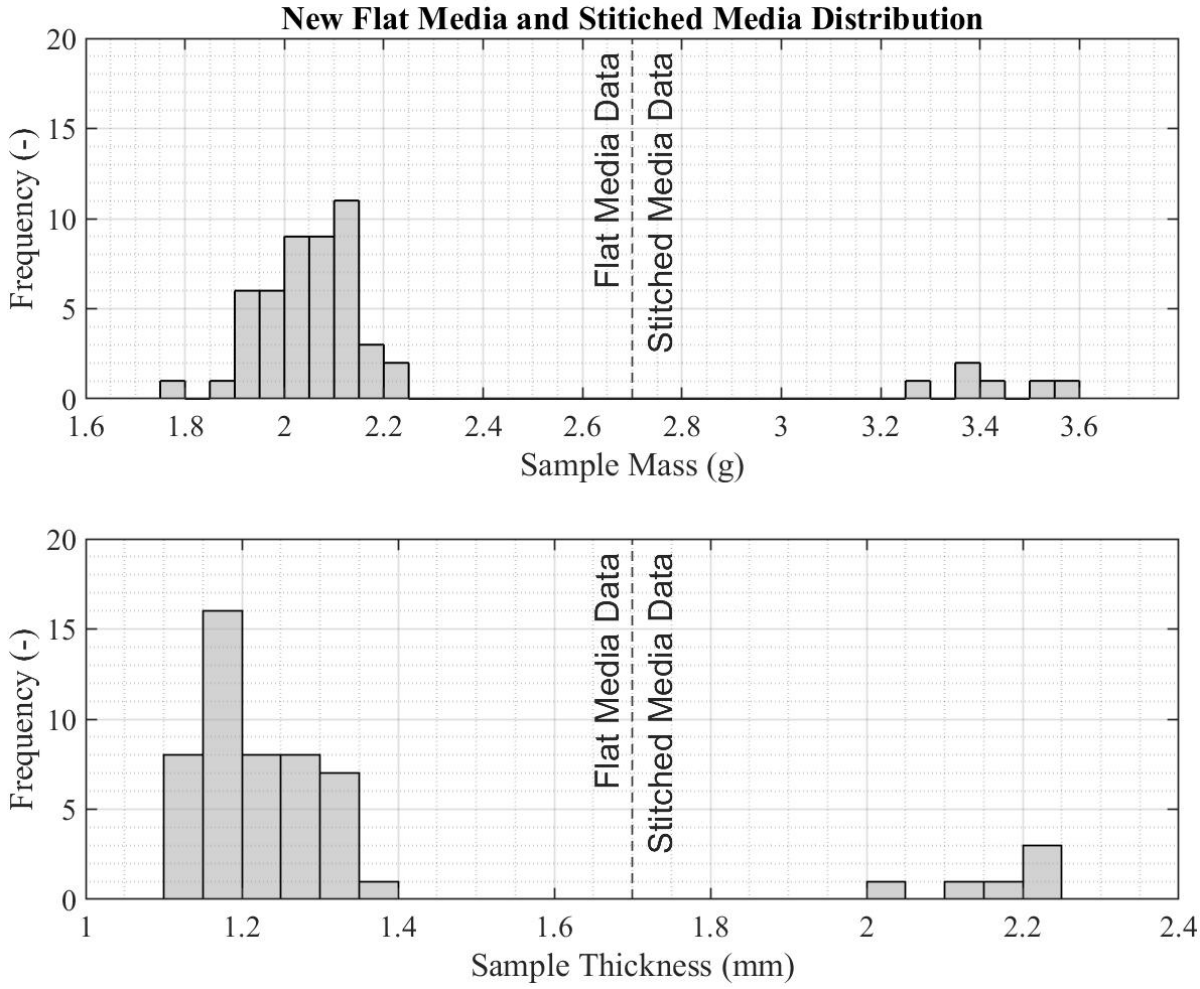

Figure 29: Data Distribution of Flat Media and Stitch Point Data for Mass (top) and Thickenss (bottom)

Table 16: Data Summery of the Flat Media and Stitch Point Data for Mass (top) and Thickness (bottom)

	Mass (g per 25cm^2)							
	n	Minimum	Mean	Maximum	Range	Standard deviation	Confidence interval (95%)	Coefficient of variation
flat media	48	1.79	2.04	2.21	0.42	0.09	0.14	0.86%
Stitch Point	6	3.27	3.43	3.58	0.32	0.11	0.03	1.32%
	Thickness (mm)							
	n	Minimum	Mean	Maximum	Range	Standard deviation	Confidence interval (95%)	Coefficient of variation
flat media	48	1.12	1.22	1.36	0.24	0.06	0.09	0.38%
Stitch Point	6	2.05	2.17	2.24	0.19	0.07	0.02	0.52%

Expectations where that the resultant analysis of mass and thickness of new nonwoven filtration media, would produce comparable results to that of the manufacturer specification, given the compliance to the standards. The datasheet for the new media state a singular value of 2.075 gcm^{-2} and 1.300mm for mass and thickness, respectively. Whilst the standards recommend the reporting of the confidence interval, its omission does not affect compliance. When considering the mean mass and thickness, presented in Table 15, for flat media, both values differed by 0.035 gcm^{-2} and 0.08mm, respectively. However, when considering the reported values of 2.04±0.14 gcm^{-2} and 1.22±0.09mm, the data sheet values fell within the confidence interval. Sampling position could have differed between this study and the manufacture, which lead to the slight difference in values. Whilst this study focused on a specific machine direction, the manufacture may have taken a more representative sample along the machine direction. Given the localised nature of the sample for this study, acquired from part of a new/unused nonwoven filter bag, coupled with the low difference in values from Table 15 and Table 16, are comparatively similar. The similarity, in turn, validated both the method and standard for assessing the mass and thickness of new/unused nonwoven filtration media.

One conclusion, is that the recommendation of confidence interval reporting, should be a requirement. Although for this study, the resultant difference in mass and thickness was marginal, it could easily not have been. Providing this interval would allow for a direct comparison, determination, and understand any deviations between the manufactured value and the analysis value. Consideration between the localised vs. representative sample difference between the laboratory and manufacturing respectively gave the potential process variation across the machine direction. If evaluation of a localised sample occurred to confirm/ validate the datasheet, then reporting the confidence interval would help distinguish between natural variation and any potential abnormality within the results. Ultimately, reporting the confidence interval would allow analysts to understand if their determined mean were within an acceptable range.

A normal distribution was suggested in Figure 29 within the flat media for both mass and thickness. As a result, Figure 29 also included the cumulative and normal distributions for further consideration. The cumulative distribution, plotted with a 95% confidence interval, displayed there each datapoint laid on the curve. In addition, the presentation of the mean and respective $\pm 2\sigma$ in the cumulative frequency distribution graphs achieved a greater

understanding of the distribution about the mean. This further aided the discussion of whether the reported data conformed to a standard distribution.

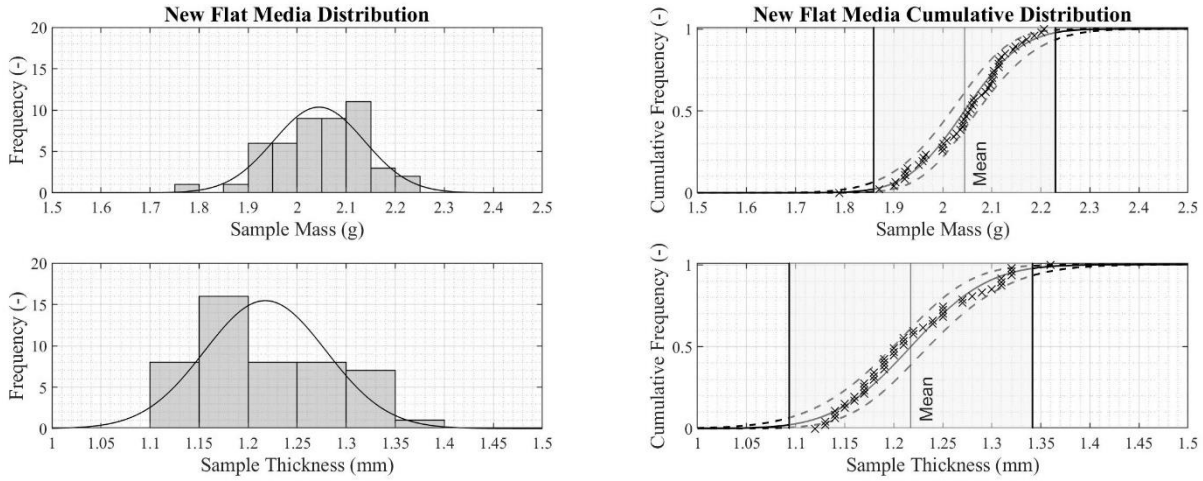

Figure 30: Distributions of Flat Media Mass (top row) and Thickness (bottom row)

Isolation of the flat media, as shown in the first column of figures in Figure 30, suggested a Gaussian distribution existed within the data for both the mass and thickness data. The second column of figures showed the cumulative frequency of the data and highlighted only 1 datapoint fell outside the standard deviation in each instance. Conduction of further mathematical tests on the data, to support the assumption of normal distribution. Table 17 summarised the results from this test. Apart from the Anderson-Darling test for thickness, all tests returned supporting data that a normal distribution exists in both datasets. The Anderson-Darling test for thickness returned no evidence to support this, which lead to a h-value of 1. Interestingly though, the p-value was only 0.0004 points away from yielding evidence of support. Additionally, assessment of the probabilities within each standard deviation showed evidence to support normal distribution. As a result, due to the exhibited evidence, a normal Gaussian distribution existed within the data.

Table 17: Normal Distribution Test's Conducted and Results

		Mass data		Thickness Data	
		h-value	p-value	h-value	p-value
Test	Anderson-Darling	0	0.3253	1	0.0497
	Lilliefors	0	0.4237	0	0.1390
	Jarque-Bera	0	0.2433	0	0.1197
Average		0	0.3308	0.33	0.1028

Given the normal distribution, removal of the stitch point data, and re-arrangement of the data resulted in Figure 31 which showed the flat media datapoints only. Due to the reduction in the data range and resultant lower colour classification range, the resultant bin width reduced which allowed for better visualisation of the data.

An apparent relationship for a fixed machine, variable cross (FMVC) direction for the sample mass was suggested in Figure 31. This suggested a near similar value for each row of data. In contrast, the fixed cross, variable machine (FCVM) direction appeared to notably vary in no discernible pattern. In contradiction, the thickness data suggested the opposite. A fixed cross, variable machine direction suggested a similar value as opposed to the fixed machine, variable cross which yielded no distinguishable pattern in comparison.

In contrast to the heat maps shown in Figure 31, a previous study performed by Fukasawa et al,. [237] did not have a similar finding. This could be due to their study utilizing a larger sample size of 49cm^2 as opposed to this studies samples size of 25cm^2. Furthermore, it is unclear in their study if their nonwoven products were similar in construction, which could affect the observation of this pattern. Moreover, the sample utilized in this study does not represent the full length of the machine direction, which could reach six meters. As a result, postulation about this apparent pattern could be localised and therefore not representative of the entire manufactured nonwoven. As a result, assessment of a larger sample in the machine direction could provide evidence for or against this pattern.

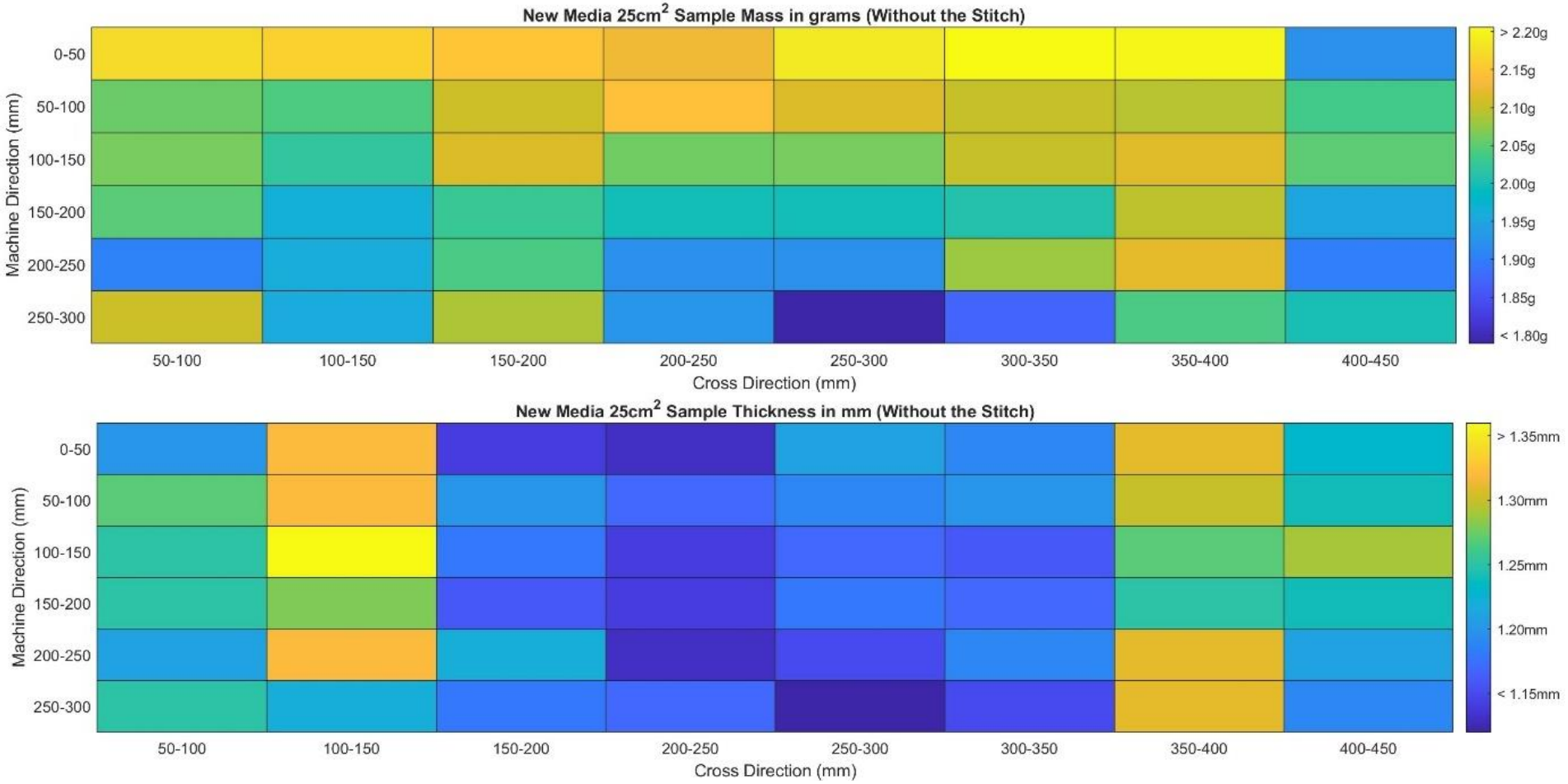

Figure 31: Heat Map of Flat Media Data for Mass(top) and Thickness (bottom)

To ascertain if this could lead to a statistically significant difference in either mass or thickness, application of a statistical t-test in fixed and variable directions would yield evidence to prove/disprove the significance. This used the mean mass at 2.04±0.14g and mean thickness of 1.22±0.09mm of all the flat media data. Application of a two tailed t-test with seven degrees of freedom which resulted in a t-value of 3.499 at a 1% confidence for a fixed machine, variable cross direction. Similarly, a resultant t-value of 4.032 to define the pass/fail criteria at the sample confidence for 5 degrees of freedom for the fixed cross, variable machine direction. Application of a two-tailed test in conjunction with the resultant mean in any given fixed/variable direction being capable of being either higher or lower than the overall mean of the data. Presented in Table 18 are the results of this test for both the fixed cross, variable machine direction (FCVM) and fixed machine, variable cross direction (FMVC) for both mass and thickness.

Table 18: Statistical Significance Testing Results for Mass (top) and Thickness (bottom)

Direction	t-score (flat media sample mass)				
	Minimum	Average	Maximum	Error (±)	Significance (%)
Fixed cross variable machine	-1.535	0.721	3.539	0.534	0.00
Fixed machine variable cross	-13.869	-6.871	-2.002	2.007	66.67
direction	t-score (flat media sample thickness)				
	Minimum	Average	Maximum	Error (±)	Significance (%)
fixed cross variable machine	-0.170	8.377	20.172	2.485	75.00
fixed machine variable cross	2.662	3.750	4.969	0.372	33.33

Statistical testing showed that the resultant means, in a proportion of the fixed/variable directions, yielded a statistically different mean in comparison to the overall flat media mean. For sample mass, significance skewed towards the fixed machine variable cross, which yielded an overall significance of 66.67%. Visually, Figure 31 suggested this may occur due to the row data being similar in comparison to the column. Only two rows yielded a similar mean to the overall. No noticeable significance occurred within the FCVM direction. This is due to the apparent parabolic nature within the data which brings the mean towards an apparent local minimum, which is approximate to the global mean.

In contrast, a proportion of the fixed machine variable cross direction for the sample thickness showed significance. Two rows of data reported a significance, due to significantly higher data point values in contrast to the other data within the row. However, noted in the FCVM direction, significance was 75%, a near 42% increase from the FMVC direction. Whilst the global thickness mean was 1.22±0.09mm, the resultant column mean was significantly higher across six of the eight columns as visually shown in Figure 31. Though the inclusion of significance in the FMVC direction resulted due to the occurrence of two distinct higher values in the fixed cross directions of 100-150mm and 350-400mm.

In both cases, the resultant mean was higher than the global which resulted in a t-score greater than the pre-described limit. As shown in Table 18, this resulted in t-score in the double digits suggesting that the localised mean was particularly more significant in comparison. Significance occurred due to the standard deviation being significantly low enough to yield a higher t-score. This occurred due to the standard deviation being low for a given fixed/variable direction. For each row/column of data, evaluation of a finite number of data points occurred. This occurrence can therefore be mathematically summarised through $\sqrt{n}=\text{constant} \therefore \text{as } \sigma \rightarrow 0$, t-score$\rightarrow\infty$, assuming the difference in the original and new mean differed slightly, but not significantly.

One of the limitations of this test is the assumption that the performance of analysis is on a specified fixed and variable direction. This yielded conditions in which resulted in a notable statistically significant result. Due to this observation, it may not be advisable to take a mean at a fixed/variable direction as it may yield an artificially higher value which could negatively impact further/future analysis. Instead, undertaking random sampling as opposed to a Fixed/Variable directional approach could protect against directional bias and yield a better mean from testing that is representative of the actual, global mean of the larger sample.

5.2.2 Impact on Standard Testing

Given the bias towards testing in each fixed direction on the sample, random sampling arose to determine if a more agreeable mean could be determined. Given that the number of potential combinations for the 48 datapoints tended towards the millions, a small selection of the potential random combinations transpired. This would appear counterintuitive, however it provided a sufficiently large confidence interval about the resultant mean and t-score (see Figure 32) which would better represent a singular random test conducted. In addition, as the number of samples and repeats analysed increased, the range of the confidence interval

decreased. Therefore, utilization of ten random non-repeated sequences of the forty-eight datapoints where utilised to aid in determining the recommended number of samples to determine a representative sample mass and thickness of the sample.

The random sample taken from all 48 datapoints point and increasing sample size determine (represented by d.f), is shown in Figure 32 (left), with the resultant t-score values in Figure 32(right). For the t-score (right hand side of Figure 32), the upper and lower dashed line represents the criteria for evidence of significance to be determined. In addition, the zeroth line represented the global mean of all datapoints. The illustration in Figure 32 provided a graphical representation of the potential outcome of random sampling testing utilizing an incremental increase in step of sample numbers (d.f.).

Results shown in Figure 32 suggested a hill like function exists when determining the mean. For both sample mass and thickness, at one random sample location, resulted in an exhibited difference/range of ≈0.03g and ≈0.03mm from the overall mean to only taking a random single datapoint. From this, as the number of samples increased, the trend tended towards the global mean. This suggested that the minimum number of samples required to yield a representative mass and thickness was low.

In contrast, the resultant t-score yielded a contradictory result. For both mass and thickness, datapoints outside the upper/lower limit were observed, which suggested the possibility of obtaining a statistically different mean when compared to the global. However, evaluation of the mean t-scores for both mass and thickness, only one datapoint fell (just) outside the limit. However, given that the mean presented in Figure 32 (left) for both mass and thickness tended towards the global, with the variation noted throughout the increasing sample size, the t-test results are questionable given the clearly defined tendency towards the global in contrast to the t-test results shown in Figure 32 (right).

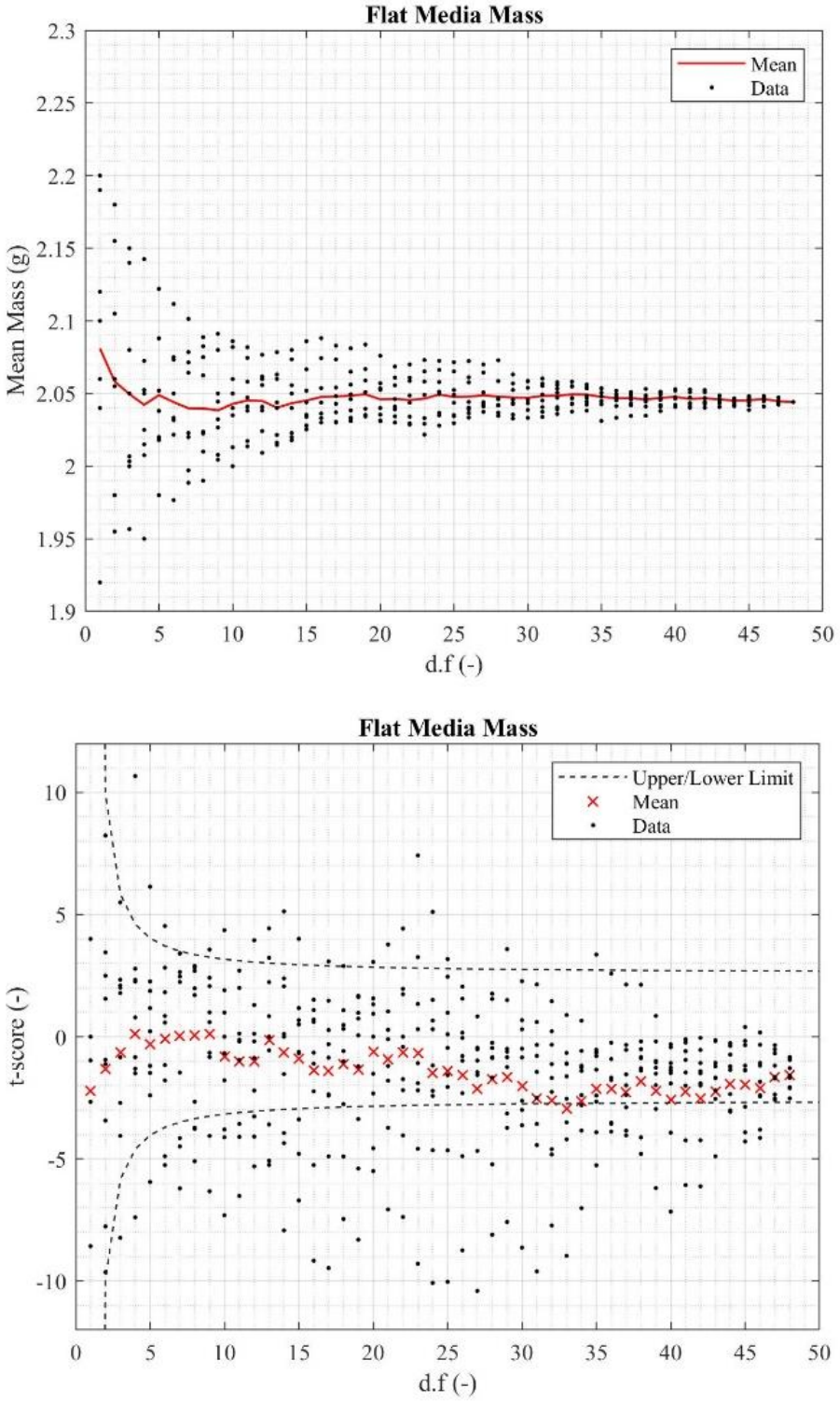

Figure 32 Part 1: Depiction of the Mass Data for Random Sample Position Testing (Top) and the Applied T-test results (Right)

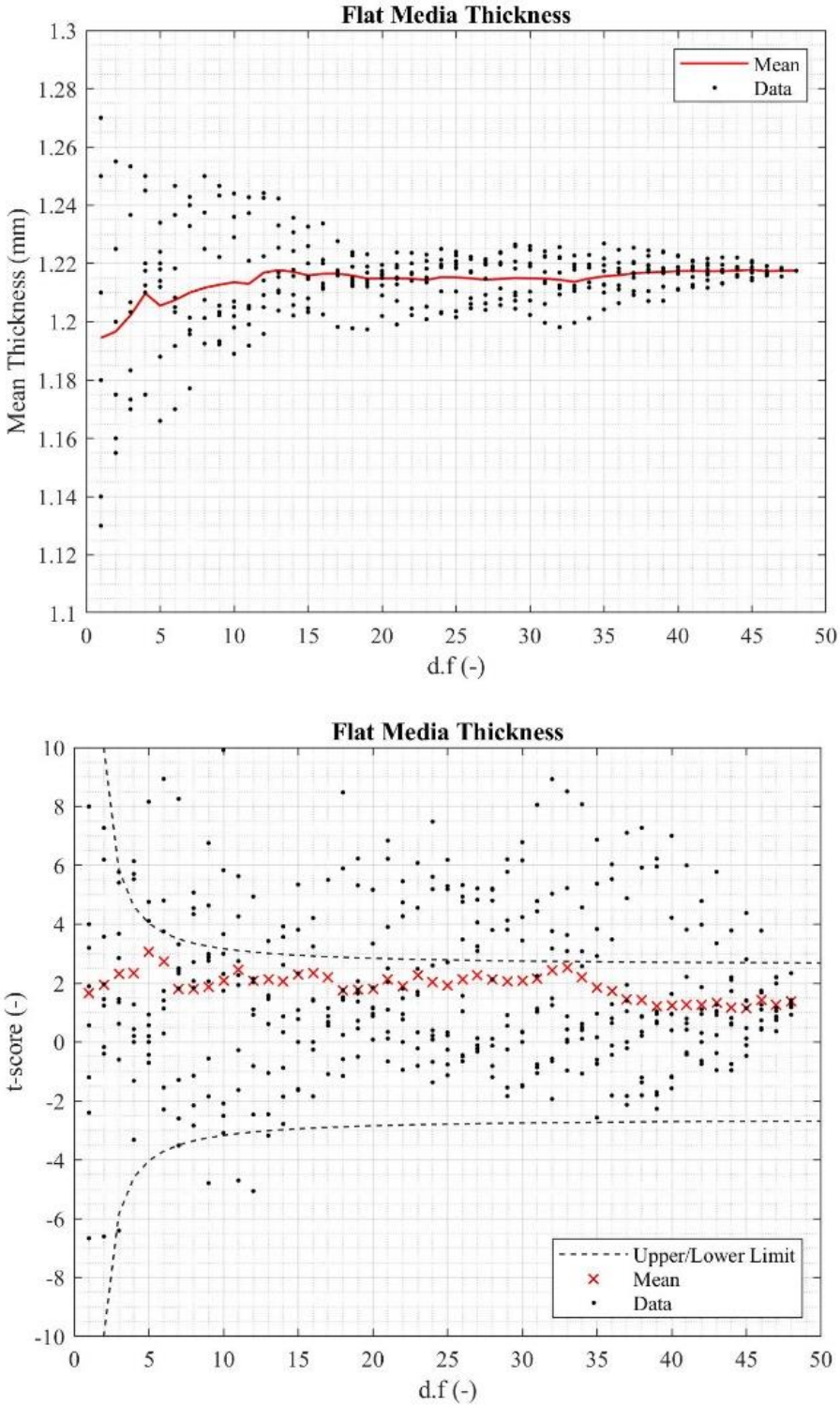

Figure 32 Part 2: Depiction of the Thickness Data for Random Sample Position Testing (Top) and the Applied T-test results (Right)

Figure 32: Random Sample Position and Number Testing

As shown in Figure 32 the likelihood to yield a representative mean from minimal, randomly located, samples are high. Whilst the number of repeats conducted is low, this allowed for a more significant confidence interval which would aid in the determination of a minimum number of samples to yield a representative value of the sample.

Consideration to the standard's BS 9073-1 "Determination of mass per unit area" [230] and BS 9073-2 "Determination Thickness" [231], stipulated that the actual size of the sample analysed can be lower, if agreed by the end user/customer. Whilst the total surface area was lower than originally stipulated for sample mass, Figure 32 (right) showed that the use of a significantly lower surface area to determine mass and/or thickness still obtained a representative mean of the overall sample size taken for analysis. The same conclusion showed for sample thickness, which differed from the standard due to a significantly larger surface area analysed than required.

One of the key drawbacks is the omission of the confidence interval from the material datasheet shown in Appendix A. Comparison between the datasheet and this study yielded an ultimate disparity of 0.035g and 0.08mm. Given that the datasheet provided for the media omitted both the number of samples, and the confidence interval, it is difficult to ascertain the possibility that the data from this study is similar in comparison. It further showed that there is the potential to yield significantly different values from the datasheet. Particularly if performed in a fixed position, instead of random sampling. For both a mass and thickness of 2.04±0.14g and 1.22±0.09mm respectively, this would place the stated mass and thickness of 2.075g and 1.30mm within the confidence interval and therefore validated both the test method and datasheet.

To illustrate the results in Figure 32 further, Table 19 tabulated the obtained results in terms of number of samples evaluated randomly. Calculation of the magnitude percentile difference was based on the mean value of all eighty-four samples. Table 19 illustrated that a low sample number, yielded a similar value to the mean, based off random samples, repeated a total of ten times. As expected, when the number of samples increased, the resultant mean approached the global mean, which facilitated the percentile difference to tend towards zero.

One of the results from the data shown in Table 19 is that a single sample would yield a representative sample, within a couple percentile difference. However, considering the maximum, minimum, and potential range that could occur (as shown in Table 16), this percentile difference could be as high as 12.3% for mass and 11.5% for thickness. As the

number of samples increased, this percentile will reduce exponentially, given both the normal distribution and evidence within Table 19. The number of repeats done would have to be pre-defined prior to analysis but could be between 2-10 to yield a near representative sample. Therefore, utilisation of a single value should not take place to ensure a better representative mean of the overall samples surface area.

Table 19: Effect on the Resultant Mean Using Random Sampling

	Number of Samples				
	1	2	3	5	10
Mean Mass (g)	2.073±0.052	2.051±0.051	2.045±0.039	2.044±0.039	2.044±0.017
Mean Thickness	1.193±0.032	1.198±0.020	1.202±0.016	1.205±0.014	1.212±0.012
Mass Difference (|%|)	1.62	0.51	0.25	0.22	0.19
Thickness Difference (|%|)	2.21	1.84	1.48	1.21	0.7

This, coupled with the applicability of the minimum number of samples to achieve a representative mean, showed that the methodology can give a representative result, if use of two or more individual samples from the surface area of the sample. Avoidance of sampling from the same direction (i.e., fixed machine or fixed cross direction) decreased the likelihood of returning a more statistically significant value. Recommendations from this analysis would see the datasheet and the standard updated to include the confidence interval, which would allow for easier determination of a significant variation in the result. This would allow for not only better product management but allow for the end user to better verify that the product is within the applicable tolerance.

5.2.3 Section Review

5.2.3.1 Conclusions

- Demonstrated the difference in the stitch point and flat media both structurally and numerically in terms of mass and thickness. Whilst the stitch was discounted, it is a point of interest for further studies.
- Exhibition of a pattern in the colour plots for the mass and thickness data. It was assumed that this occurred due to the manufacturing process, yet as the sample was not representative of the full size, a repeat is needed to confirm/deny this theory.

- Assessment of mass and thickness in fixed directions yielded a statistically significant mean.
- Random sample locations for mass and thickness determination yielded a more representative mean.
- Whilst the methodology used for this study deviated slightly from the recommended method within the standards, it was still capable of determining a representative sample mass and thickness for new nonwoven filtration media.

5.2.3.2 Recommendations

- Random sampling should take place, instead of multiple samples from the same direction. This yields a better representative mean.
- The datasheet should insist on showing the confidence interval and number of samples testing for reproducibility purposes.
- The reporting of the confidence interval should be mandatory instead of recommended in the standard.

5.2.3.3 Further work

- Further work and analysis on the stitch point in recommended, based on the limited information presented in literature.
- A full machine direction sample from the manufacturing process should be acquired to confirm/deny the pattern exhibited and discussed in Figure 31.
- Discussions and conversations with both the standards committees and manufacturers to promote the reporting of the number of repeats, and confidence intervals as part of their standard compliance to allow for better quality checks by the end user

5.3 Used Media Variation

Sample preparation of the used filtration media was identical in terms of methodology to that of the VN state. Similarly, evaluation of the stitch point occurred, omission from any analysis occurred again similarly to that of the VN state. The stitch point samples still underwent the transition from AR to PC state, with their respective datapoints recorded.

In addition, the difference between the PC and AR states can yield an indication as to how the filtrate or filtration cake impacted the mass and thickness results. Lastly, as the new media is the same as the used filtration media, the difference between the PC and new states provides an indication as to how the felt has changed over usage time. This resulted in four unique data categories from the sample: AR, PC, cake/filtrate, and the difference between new and PC.

For the latter, the resultant mean value from the VN test represented the absolute value. This caused a negative uniform shift in the PC data.

5.3.1 Discussion on the Data and Methodology Consideration

The data was presented as colour maps in Figure 33 from the mass data. Similarly, Figure 34 displayed the colour maps from thickness analysis. Both figures presented the four data categories: AR (top left), PC (top right), Filtrate/Cake (bottom left), and PC-new (bottom right). Table 20 summarised the data.

Visualisation of the mass results, shown in Figure 33, indicated the apparent variance in mass between each sample. Whilst a mean of 3.50±0.09g was found for the AR state, however the AR colour plot in Figure 33 (top left) demonstrates a considerable number of higher/lower values which questions the reliability of this measurement. Indeed, for all data categories, this observation continued. Furthermore, the data appears more sporadic in nature which resulted in the inability to observe a pattern visually like noticed in the VN heat map. Additional analysis of the data would be required in order to ascertain the extent of this perceived variation given the visual results of Figure 33.

Similarly, Figure 34 suggested the same findings as discussed for Figure 33. Whilst the PC stated mean was 1.44±0.03mm, consideration to the PC colour map in Figure 34 displayed a clear bias of the mean towards the lower range. This bias is in all data categories, for both the mass and thickness data, and suggested that the mean is not central to the data. It therefore suggested that there are significantly less higher values within Figure 34. This would suggest that the distribution for the thickness data is towards the lower end of the mean. As a result, consultation of the histograms transpired to aid analysis and understanding of this potential bias.

For both the mass and thickness data, the resultant difference between the PC state and the new/virgin media values caused a negative shift in the PC. This assumed that the new media measurement for mass and thickness was representative. A positive value indicated that, overall, a degree of internal deposition had occurred within the sample for mass. For thickness this indicated that the felt had become thicker, either due to deposition, pore/fibre deformation, or a combination of both. A negative value would have indicated felt loss: either by mechanical deformation, chemical deformation, or a combination of both. As such, the difference yielded an indication as to have the felt had changed over its service period.

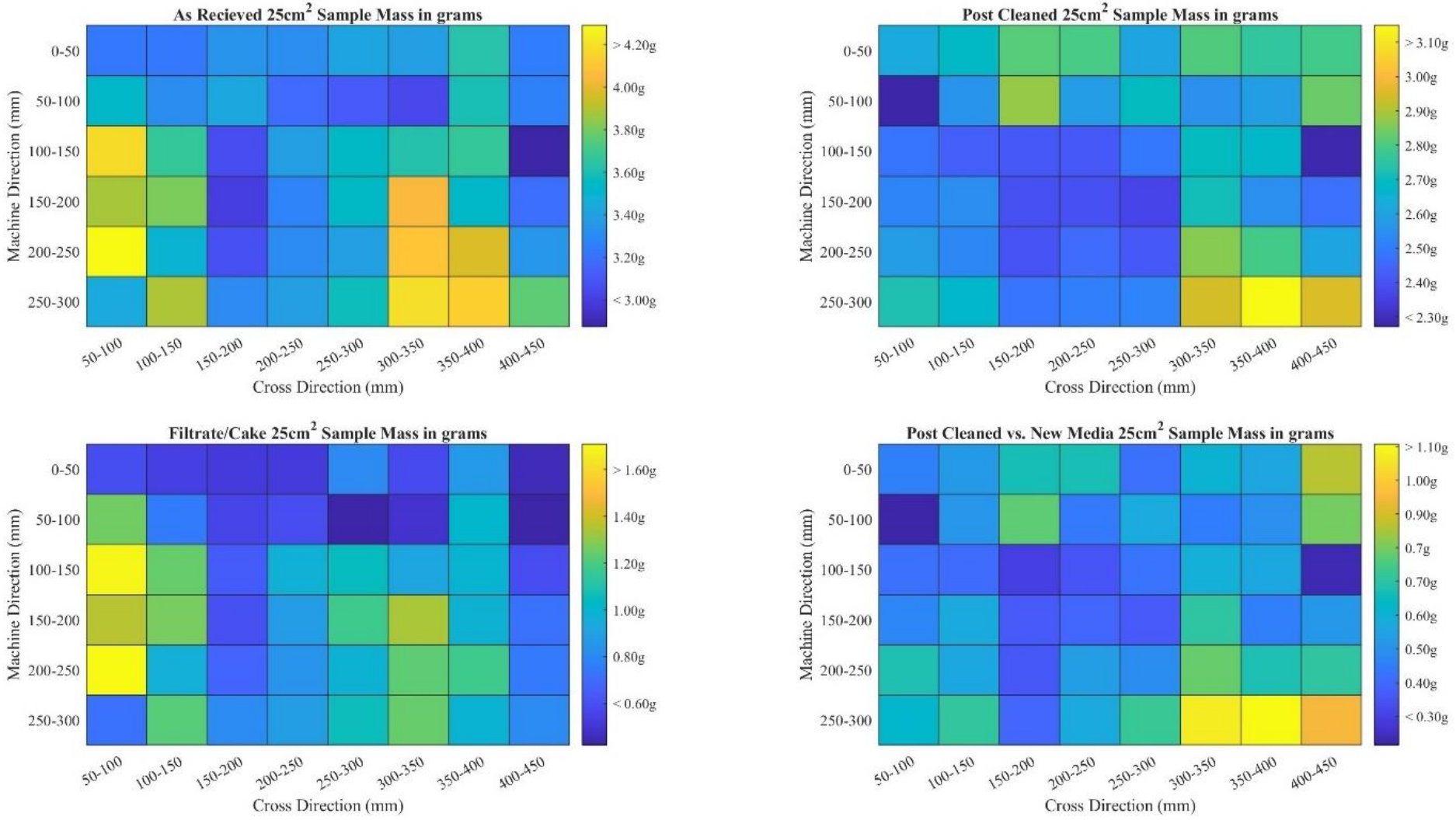

Figure 33: Colour Maps of Each Data Category for Mass: AR (top left), PC (top right), Filtrate/Cake (bottom left), and PC-new (bottom right)

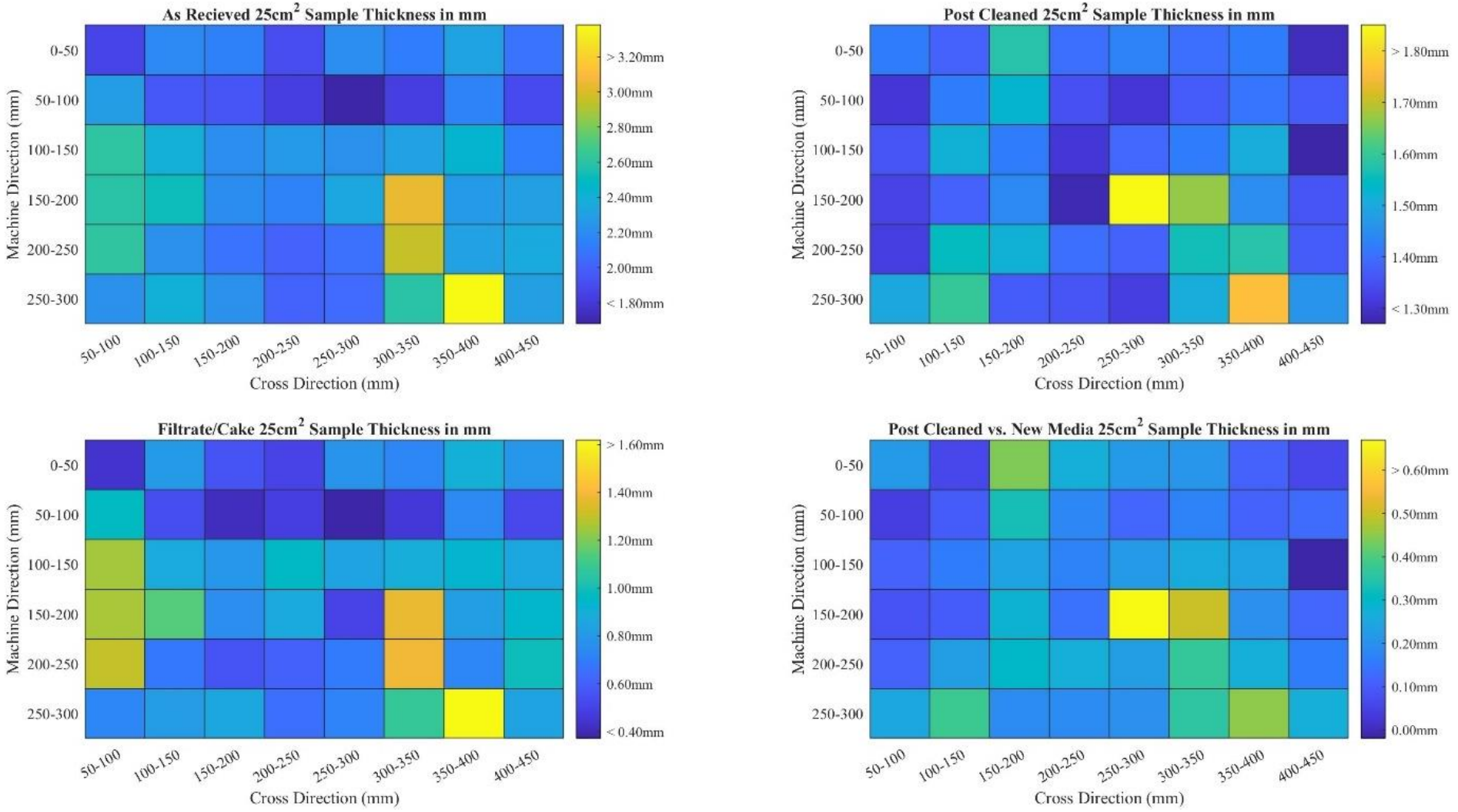

Figure 34: Colour Maps of Each Data Category for Thickness: AR (top left), PC (top right), Filtrate/Cake (bottom left), and PC-new (bottom right)

The data presented in Figure 33 and Figure 34 was numerically summarised in Table 20.

For both mass and thickness, a high dispersion transpired about the mean. In both cases, the coefficient of variation was approximately 1.5 times higher for the as received data than the post cleaned data. Given that the PC variation, in both instances was low in comparison, this suggested that the filtrate deposited on the surface contributed to the results which lead to this higher variation. The data for the filtrate/cake, supported this which showed that when considering the filtrate only, the variation was high. This preliminary analysis suggested that the distribution of the data for the AR state may differ to the PC state.

Most notably is the variation for the difference between the PC and new state, which had a variation of 33% and 56% for mass and thickness, respectively. The perceived variation originated from the lower population mean of the data, which resulted in a higher coefficient. However, as shown in Table 20 for both the mass and thickness, the range, deviation, and confidence interval remained equal to the PC state. Consequently, this led to the inflation of the values for the variation.

Table 20: Data Summary of Mass (top) and Thickness (bottom) Results

	Flat Media Mass (g)							
	n	Minimum	Mean	Maximum	Range	Standard deviation	Confidence Interval (95%).	Coefficient of variation
AR	48	2.87	3.50	4.29	1.42	0.34	0.09	13.99%
PC	48	2.27	2.61	3.15	0.88	0.19	0.05	7.22%
Filtrate/Cake	48	0.42	0.89	1.71	1.29	0.32	0.08	35.52%
PC-New	48	0.23	0.57	1.11	0.88	0.19	0.05	33.09%
	Flat Media Thickness (mm)							
	n	Minimum	Mean	Maximum	Range	Standard deviation	Confidence Interval (95%).	Coefficient of variation
AR	48	1.68	2.25	3.38	1.70	0.32	0.09	13.99%
PC	48	1.27	1.44	1.85	0.58	0.12	0.03	8.41%
Filtrate/Cake	48	0.37	0.92	1.62	1.25	0.28	0.08	29.92%
PC-New	48	0.05	0.22	0.63	0.58	0.12	0.03	56.00%

Performance of further assessments determined any skewness within each data category, which would cause a non-equal distribution. Figure 35 illustrated these distributions if normal distributions occurred.

For both the sample mass and thickness, the distribution for the PC vs. New data was identical to the PC state with a uniform shift in the data caused by the subtraction of the mean mass/thickness from the PC data. Due to the classification of the data in bins of 0.2 width for mass and 0.1 width for thickness, respectively, a slight deviation in the distribution arose. Whilst this occurred, the data distribution still remained visually similar, even when the bin width was reduced.

In contrast, both the as received and cake data yielded a less precise/ wider distribution. Table 20 showed that the mass and thickness data range for AR was noticeably higher than the PC data. This, coupled with the lower variation coefficient, showed that the cake/filtrate had an impact on the results. Furthermore, it suggested that the cake/filtrate on the surface varied across the sample, suggesting that it caused the sample to be comparatively heterogeneous between different samples. This resulted in the distribution becoming shallower and wider in comparison to the PC data.

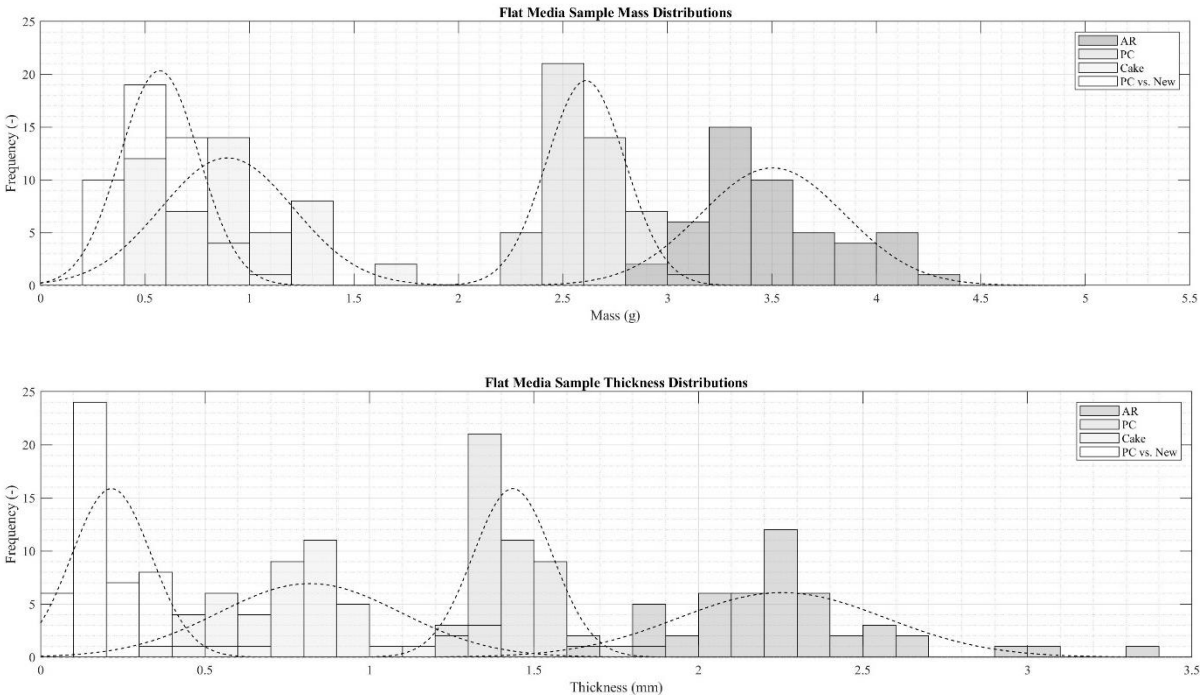

Figure 35: Data Distribution of Sample Mass (top) and Thickness (bottom)

Distributions shown in Figure 35 assumed normality, to validate this assumption, each data category as shown in Table 21, underwent additional assessment.

The empirical test for normal distribution was applied across all data categories, with results shown in Table 21. This method provided an alternative insight into the data's potential distribution. The mass data passed empirical testing yet failed a larger percent in the thickness data across the categories. This showed that there was some, unquantified skew in the data, particularly about the >95.4% region. At the 99.6% pass criteria for thickness, all samples needed to be within the third standard deviation. However, for AR, PC and PC vs. New, one less than this was outside this. This could suggest that this datapoint was an outlier, which would then suggest that the empirical test would return a normal distribution upon its removal. As such, further analysis of the skewness and Kurtosis parameters were needed, before forming a definitive response for the thickness data.

Table 21: Empirical Testing for Normality Distribution of Mass (top) and Thickness (bottom)

Empirical Test for Mass Data					
	Pass Criteria	AR	PC	Filtrate/Cake	PC vs. New
Pass/Fail	68.2%	68.8%	97.7%	62.5%	64.6%
	95.4%	97.9%	97.7%	95.8%	97.9%
	99.6%	100.0%	100.0%	100.0%	100.0%
Empirical Test for Thickness Data					
	Pass Criteria	AR	PC	Filtrate/Cake	PC vs. New
Pass/Fail	68.2%	93.8%	95.8%	66.7%	72.9%
	95.4%	93.8%	95.8%	95.8%	95.8%
	99.6%	97.9%	97.9%	100.0%	97.9%

Analysis of the skewness and Kurtosis parameters for the thickness data and presented in Table 22 aided in the decision to define the distribution. Given the convincing evidence to support normal distribution in the mass data, across all categories, the analysis focused only on the thickness data given the near failure noted in Table 21. The criteria to pass this test to support a normal distribution varies in literature as discussed by Orcan [262] which discussed numerous studies with different criterion ranges. For this test, evidence for the alternative hypothesis (non-normal distribution) transpired if the values obtained where outside ±2 for skewness and ±7 for Kurtosis, as suggested by Curran et al,.[263]. Whilst the selection almost became a estimation due to the varying criteria as suggested in Simon [264], the selected

values from Curran et al., [263] presented a near average of those values previously seen in literature and resultantly formed the basis for this analysis. Although there are some discrepancies with the use of these values, with some authors suggesting that kurtosis provided little indication of the exhibited peak [265], though these arguments, in literature, did not occur often. Consultation of all tests conducted, prior to the declaration for/against a Gaussian distribution presented within the data, aided in the decision to confirm, or disprove, Gaussian distribution of the data. Resultantly, consideration of the criteria against the thickness data in Table 22 across all data categories returned evidence to support the null hypothesis/ a normal distribution.

From the analysis, it was determined that a normal distribution existed across the thickness data in all categories of the data. This is based around the empirical testing for the mass and thickness data shown in Table 21 coupled with the supporting evidence presented in Table 22 for the thickness data.

Table 22: Skewness and Kurtosis Parameters for All Data Categories of the Thickness Data

Thickness Data				
Parameter	AR	PC	Filtrate/Cake	PC vs. New
Skewness	1.2560	1.3404	0.7550	1.3404
Kurtosis	5.5985	5.0225	3.4198	5.0225

As previously shown for new media, two to three 25cm^2 samples provided a representative mean of the overall sample. Therefore, the method presented for new, virgin media provided an initial starting point to develop a suitable method for industrially used nonwoven filtration media.

The 48 datapoints for mass and thickness where randomly rearranged a total of ten times for the flat media. Whilst the potential unique combinations of this rearrangement were in the thousands, ten samples intentionally provided a larger interval. Doing so, allowed for a better representation of random sampling, without having to perform analysis on all forty-eight unique samples for this defined sample size.

The results determined that the 30cm length sample had a mass of 3.503±0.10g per 25cm^2 and a thickness of 2.25±0.09mm respectively in the as received category. Exclusion of

analysis in all other categories arose due to each specific datapoint being representative of a unique location from the original sample.

The mean variation as the number of samples increased for the AR state is shown in Figure 36. During random sampling, each AR state datapoint corresponded to a particular PC state. For both the mass and thickness, the lower and maximum dashed line of the figure represented a 10% difference in the respective global mean. This aids to visually inspect the number of samples, such that a selection of a suitable sample number which is both minimal and representative of the overall mean.

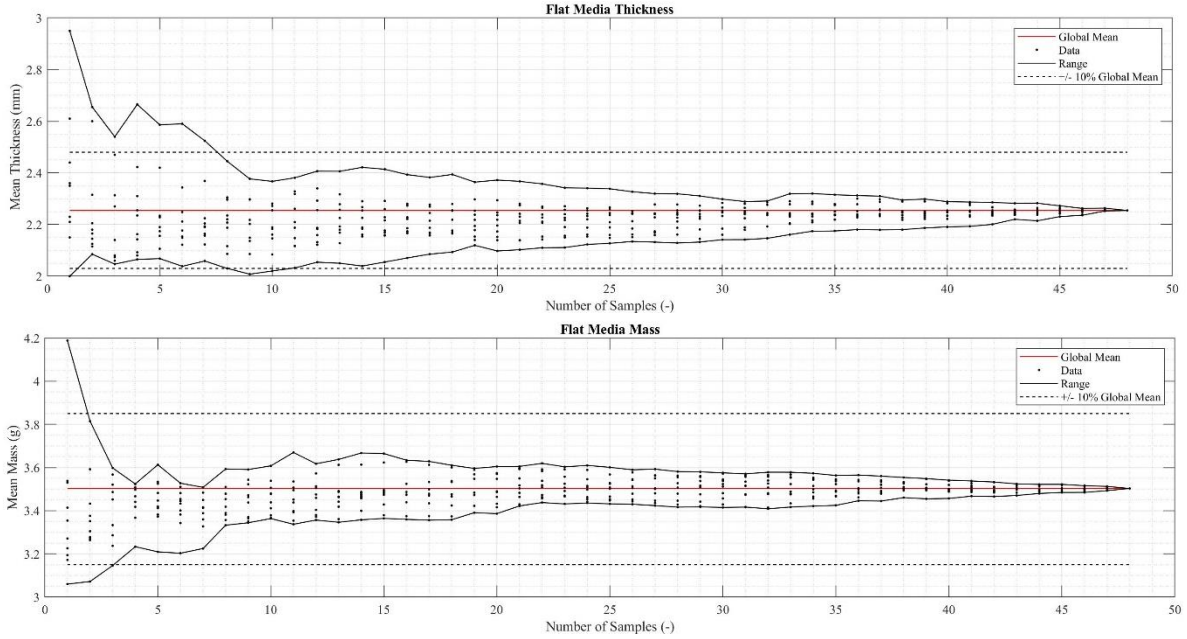

Figure 36: Number of Samples Mean Variation for Sample Mass (top) and Thickness (bottom)

As shown in Figure 36 (irrespective of mass or thickness) as the number of samples increased, the mean tended towards the overall global mean of the sample. Furthermore, the range between each number of samples appeared to decrease as the number of samples increased. This decrease is caused by the inclusion of more focused data about the resultant mean. After a sample size of 10 and 3 for mass and thickness respectively, the sample mean, is confined to within ±10% of the global sample mean. Whilst there is still a slight deviation between the global mean and sample mean, given that the sample mean and respective confidence falls within the global, the number of samples required to obtain a representative mean can be defined at a minimum of 10 samples at an area of 25cm^2.

However, consideration should be given to the practicality aspect of this analysis. For large scale sample testing, isolation of eleven samples equated to a 22.92% reduction in the sample size used in this study. If random sample testing occurred, this would potentially negatively impact other testing methods such as air permeability testing, which required a minimum of three random 20cm^2 sample areas as described in BS9073-15 "Determination of air permeability" [232]. As a result, further analysis is required to either reduce the number of samples required or increase the sample size such that the interference caused by random sampling for mass and thickness assessment is mitigated.

A selection of a reduced sample number, including the absolute difference between the sample mean and global mean respectively for mass and thickness is summarised in Table 23.

Table 23: Number of Samples Summary for Mass and Thickness, Including the Difference between the Mean and Overall Mean

	Number of Samples				
	1	2	3	5	10
Mean Mass (g)	3.39±0.20	3.38±0.13	3.42±0.10	3.44±0.07	3.46±0.05
Mean Thickness	2.33±0.18	2.26±0.13	2.23±0.11	2.24±0.10	2.20±0.06
Mass Difference (|%|)	3.23	3.51	2.37	1.80	1.23
Thickness Difference (|%|)	3.55	0.44	0.88	0.44	2.22

Due to the random nature, coupled with the small repeat number of 10 repeats, some fluctuation was expected in the resultant difference between the sample and global mean. This fluctuation is due to the variance in the data being more sporadic in nature, as opposed to the new media which was focused and narrow about the resultant mean. Though both Table 19 and Table 23 showed that as the sample size increased, the mass/mean difference generally decreased also. As a result, the identification of a definitive sample number is based on the user defined tolerances for analysis.

In reference back to Figure 36 which showed how the sample size affected the potential mean, whilst ten samples appeared best suited, five samples could be suggested, given the apparent absolute difference between the two sample sizes being similarly low. Consideration should be given towards the accepted tolerance for analysis. If a potential 2.37% difference is acceptable to all parties (the analyst and recipient of the data), then the sample size could be

reduced. These results are limited to the sample used in this study and results may differ due to sample location and operational time difference.

Regardless, consideration should be given to the total number of flue gas filtration bags needed to be assessed. Following BS22031:2021 “Sampling and test method for cleanable filter media taken from filters of systems in operation” [16] each filtration bag would require three sections analysed, which would equate to a total of nine unique samples for mass and thickness, assuming that the mean of three is taken for each vertical section of the bag. The total number of unique samples is therefore a multiple of three. As such, this has the potential to have an impact on the turnaround time of each bag. Isolation of a single sample in each of the vertical region yielded a highly variable result. However, through an increase in the sample size, the potential for variance between its respective mean and the global mean of the entire sample decreased, this showed that the sample size that should be assessed is between five and ten. Although, as low as three samples may suffice in yielding a representative mean, so long as the absolute difference is acceptable as a tolerance to the test. Lastly, consideration should be given between the number of bags, required turnaround time as this will dictate the maximum possible number of unique samples per vertical section. Agreeance between parties should be sought as to the number of samples per verticals section, before analysis is conducted.

Whilst BS22031:2021 “Sampling and test method for cleanable filter media taken from filters of systems in operation” [16] does not stipulate a definitive methodology, the adapted methodology presented in BS9073-1 “Determination of mass per unit area” and 2 “Determination of Thickness” [230],[231] used within this study can still conform to both standards, without compromising on compliance. Current phrasing in the BS9073-1 “Determination of mass per unit area” and part 2 “Determination of Thickness” [230],[231] standards required agreement between the customer and analyst on any deviation from the required surface area. Additionally, the optional reporting of the confidence interval would be overturned and made mandatory for compliance. This would further aid in analysis of future samples. As a result of this study, coupled with the recommendations to the standards and impact on sample turn around, a minimum of three to five random samples should be taken for mass and thickness testing. From this, the mean and confidence interval should be reported across both the as received and post cleaned state.

Given BS22031:2021 “Sampling and test method for cleanable filter media taken from filters of systems in operation” [16] does not require the assessment of the cake and PC vs. New state, this data category/analysis requires further investigation before incorporation into the standard. However, it does provide a useful insight into not only how the filtrate/cake has interacted during operation, but also how the felt has changed over time.

5.3.2 Axial Variation

Due to the machine direction length not being representative of a full bag, further analysis is restricted to the cross direction. The cross-direction length is representative of the circumference of the filtration bag. Division of the sample into 25cm^2 of known location upon the sectioned sample therefore allowed for inspection of any potential variation in the cross direction. Each sample is represented by the centre point along their respective 5cm intervals.

Fixed cross direction results for mass and thickness, with the inclusion of the stitch point are shown in Figure 37. The mean of each fixed cross direction was calculated and presented as a circular datapoint also to aid visual assessment.

In the as received state for both mass and thickness, the data suggested an approximate similarity between the stitch point and 75cm sample. In comparison to the new stitch point, only a slight difference was observed. The lamination tape would have reduced the open pores within the stitch point, thus limiting the amount of filtrate/cake deposition on the sample. Given the structural variation, coupled with the previous discrepancies discussed in the stitch point data, the stitch data was omitted from further analysis.

Further studies are required about the stitch to explore the effect on mass and thickness results. Whilst this study sectioned the media and evaluated the stitch point, its structural difference would have had an unknown effect on the deformation processes during operation. Additional test methods such as µCT and SEM imaging would begin to provide a qualitative and quantitative assessment of the filtrate and felt interaction at the stitch point of the media.

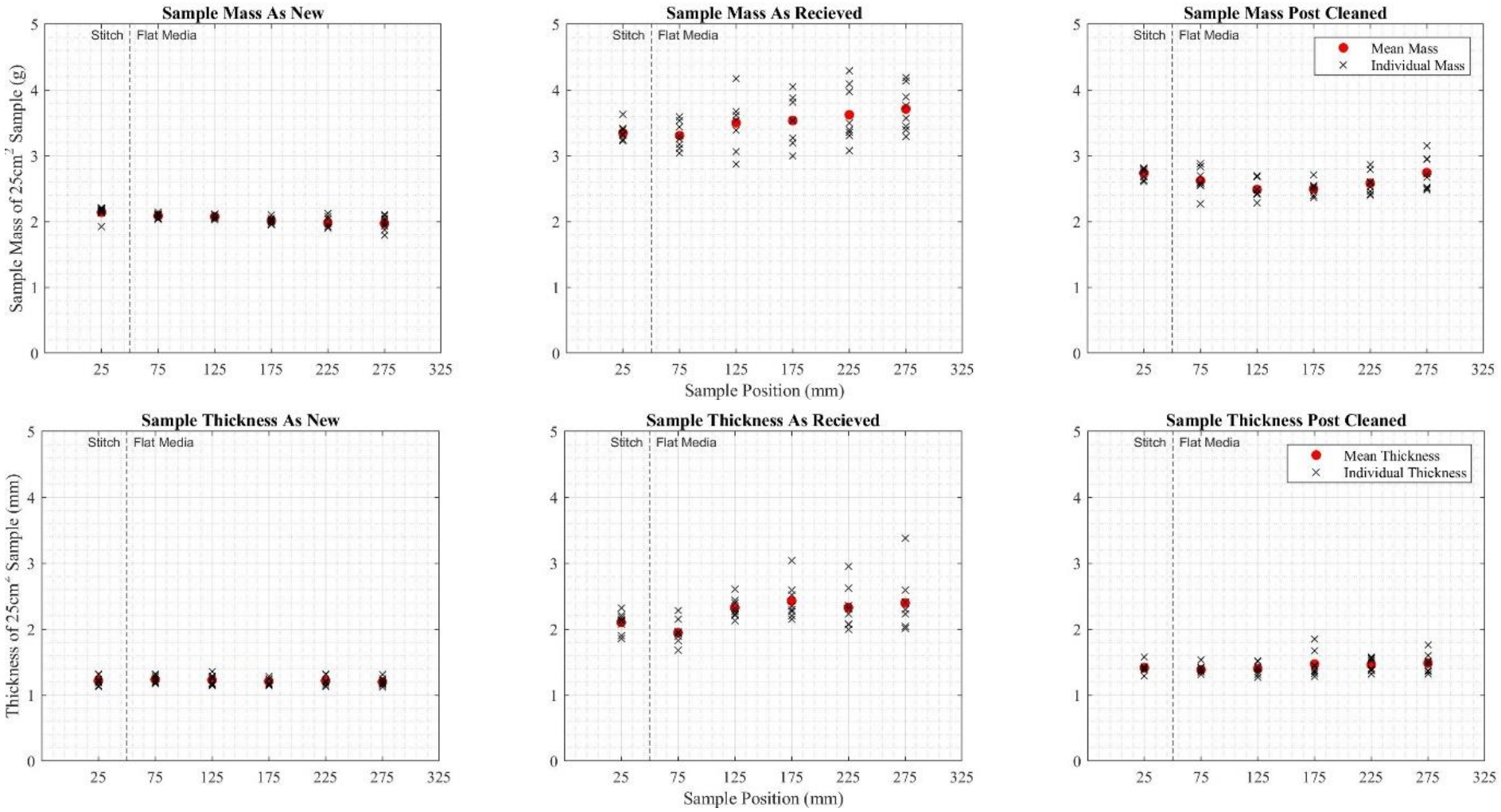

Figure 37: Sample Data Visualisation in A Fixed Cross Direction for Mass (top) and Thickness (bottom)

An apparent wave like function exhibited throughout the data categories, including the new media. For the new media, Figure 31 shows an apparent data pattern for a given fixed direction. Most notably was the variation about the fixed cross, variable machine direction for sample mass. As shown in Figure 37 this observation was also noticed slightly for the new media. For the new thickness data, this is less discernible in Figure 37, due to the apparent pattern in Figure 31 being largely focused on a fixed machine variable cross direction. Which resulted in a more prominent wave like function for sample mass as opposed to sample thickness in the new media data.

Unlike new media, used media (across all data categories) did not visually present a similar pattern as shown in Figure 31. However, an apparent wave like function was exhibited, regardless, as shown in Figure 37. Appearance of a wave like function through all data categories suggested the potential for a relationship between the datapoint and location. Given this, a regression analysis was conducted about the mean of each data category to determine the best mathematical relationship to describe the suggested curve/function.

Table 24 depicts various mathematical relationships which were evaluated to determine the best suited function to describe the data. The data is reported in terms of the range across all data categories, showing the minimum and maximum R^2 value respectively.

Table 24: Regression Fitting Against Mass and Thickness Data

Sample (Minimum and Maximum)	Quadratic (R^2)	Cubic (R^2)	Fourier (R^2)
Thickness	0.1289-0.5576	0.1956-0.6529	0.6392-0.8768
Mass	0.05422-0.6809	0.2353-0.8769	0.6210-0.9237

Assessment of various mathematical functions revealed that a Fourier regression best represented the data. As shown in Table 24, for quadratic and cubic functions, the representative coefficient of determination, R^2, was comparatively lower than Fourier. One of the negative impacts of quadratic and cubic relationships is that the regression identifies a singular local minimum/maximum, before tending to infinity. Given that the cross direction is representative of the full circumference, it was theorised that the pattern should repeat continuously about the circumference indefinitely, dependent only on the degree at which the results are examined. This theory further supported the Fourier regression, given that the determined pattern was representative of the full circumference of the sample.

Therefore, a Fourier regression was selected, defined using the mathematical expression denoted in Equation 26. In this study the term (y_λ) denoted the mass or thickness and used constants (a_o, a_1, b_1) and (w) in conjunction with the cross sectional length (x).

$$y_\lambda = a_o + a_1 sine(x * w) + b_1 \cos(x * w)$$

Equation 26: Fourier Expression

The Fourier regression for each individual data category for both the sample mass and thickness is demonstrated in Figure 38. The addition of the confidence interval demonstrated that there is a good agreement between the data and the regression, which is supported by the large coefficient of determinations denoted previously in Table 24. One of the limitations with this analysis is that at the 0^{th} or 9^{th} reference point, the stitch would theoretically occur. This omission led to the regression plot not combining at the extreme points. As a result, this affected the determination of the local minimum and maximum points in the cross direction.

It can be visually seen from Figure 38, that the apparent local minimums and maximums for all data categories tend to agree regardless of the data category. This further supports the positive relationship between mass and thickness, but also the visual observations made in Figure 37. Isolation of these local maximum and minimum points, and conversion to a representative degree, can was tabulated and presented for both mass and thickness in Table 25.

From the analysis of the regression, two distinctive local minimums and two local maximums were found as shown in Table 25. Given that each apparent minimum/maximum where similar values across the data categories, the table showed the difference between each point as an average percentage. The conversion from reference point to degrees assumed that the stitch was the start/finish point at the 0^{th} position. In addition, the eighth point extended fully to the ninth position, which was also defined similarly as the 0^{th} position to allow for a complete circle. From this, each local minimum and maximum could be represented by a specific degree.

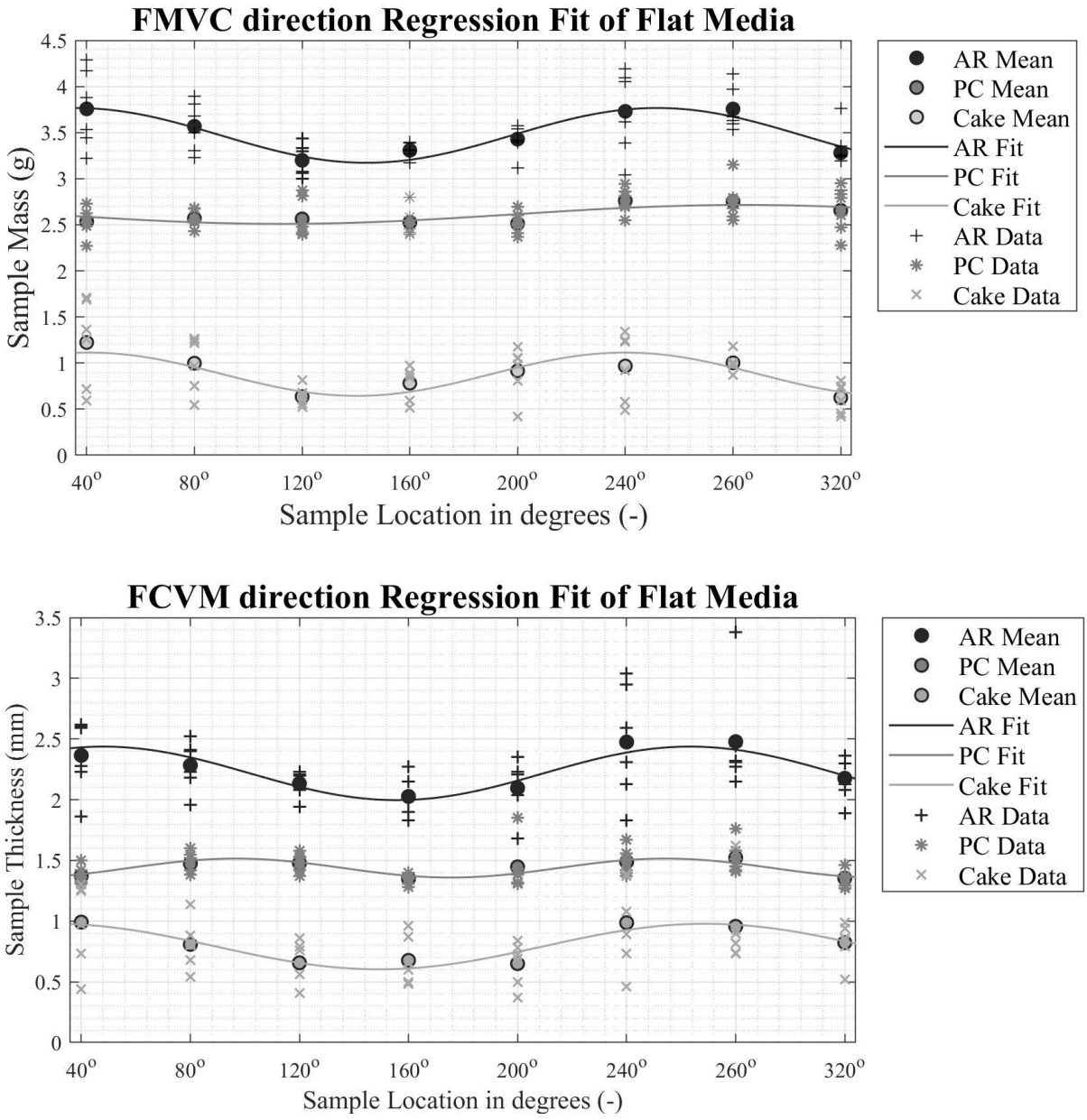

Figure 38: Fourier Regression Plots Against All Categories for Mass and Thickness

Table 25: Regression Analysis of Local Minimum and Maximum Points for Mass and Thickness

Measurement	Stitch (Assumption)	Regression Point			
		$L_{min,1}$	$L_{max,1}$	$L_{min,2}$	$L_{max,2}$
Thickness (°)	0/360	72	144	252	324
Mass (°)		36	119	234	313
$\Delta\lvert T-M\rvert$ (°)	0	36	25	18	11
$\%\Delta$ (%)	0	100	21	8	4

Given the data is representative of a cylindrical filtration bag, Table 25 showed that the as the difference between the mass and thickness for each local minimum/maximum decreased as the angle increased. This phenomenon is due to the definition of the 0^{th} position, which was done to re-introduce the omitted stitch point from the data. Further analysis is needed to examine this and determine the exact cause of the phenomenon.

Division of the cylindrical bag into four quadrants was done in a bid to further understand the data. These quadrants were defined utilizing the stitch point as the start/finish, like previous descriptions for analysis. As such, each local minimum and maximum corresponded to a particular quadrant. More interestingly was that each the pattern of local minimum to maximum was followed.

Occurrence of a minimum to maximum to minimum pattern suggested preferential deposition patterns. Given the positive relationship between mass and thickness, coupled with the Fourier regression, it is likely that for this sample, an increased amount of deposition occurred at the local maximum points.

Given the results demonstrated in Figure 39 and Table 25, a preferential deposition can be suggested the local maximum points. This increased rate of deposition led to a higher degree of deposition internally to the felt (referred to as blinding). This is supported by the increased mass in the PC state at these points, compared to the local minimum points. Comparison of the filtrate/cake category showed that the filtrate on the surface was prominent at these local maximum points, which further supported this. Post cleaned showed only a slight variation, however the increase in thickness corresponded to both the AR and filtrate/clean peaks, which again suggested a greater interaction of the filtrate with the felt causing an increased thickness.

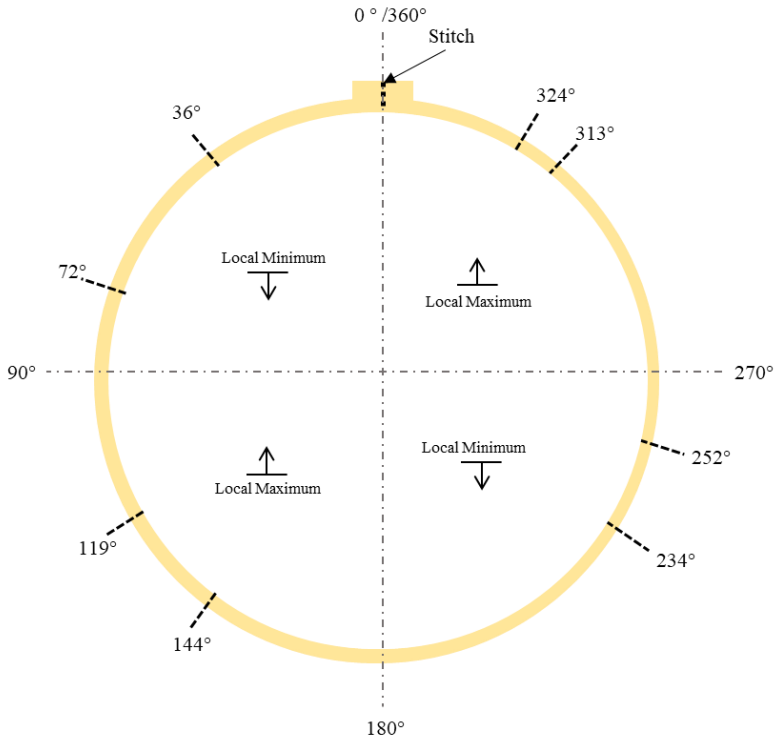

Figure 39: Visual Depiction of the Local Minimum and Maximum Found from the Regression Analysis

Once in-situ, filtration bags are not rotated or moved until they are withdrawn from service. This, coupled with the findings of the used media, suggested that some degree of preferential flow occurred about the cross direction of the bag. Given the assumption of the stitch, it is difficult to quantify the exact position of the bag during operation which lead to this assumption. However, if preferential flow did occur, it would be expected that each bag would differ by some undefined value across the tube sheet. Therefore, a clear understanding of the flow through the cell or bag house is preferential, before definitively stating that this is the root cause.

5.4 Conclusions and Recommendations

This study provided the first initial steps in fully understanding mass and thickness variation on new and used filtration media.

For new filtration media, a pattern for mass and thickness values emerged during the consideration of flat media only. This pattern suggested that taking multiple samples in a fixed direction would yield a biased result, which would not be representative of the global mean. As such, sampling in a different, random, location was advisable. Analysis of this showed that taking three to five samples of new media was sufficient to yield a statistically similar mean in comparison to the global mean. However, it should be noted that deviation between the results and datasheet occurred. Given the confidence interval was not stated, it is

difficult to ascertain if these studies determined mass and thickness where within the range determined for the data sheet. Consequently, the British Standards should require that the confidence interval of the mean be stated for compliance.

Analysis of used nonwoven filtration media, of the same material and make as the new media evaluated, was conducted to determine a methodology for mass and thickness assessment. Currently BS22031:2021 "Sampling and test method for cleanable filter media taken from filters of systems in operation" [16] doesn't stipulate a method for assessing these parameters. Therefore, the methodology used for the new media was used, which used the exact size required by the standard: a 30cm section from the machine direction.

Results showed that the data varied, showing no discernible pattern when consulting a heat map of the data. Further analysis showed that this variation was normally distributed. From this, randomisation of the data occurred multiple times. Doing so allowed for a better representation of an actual test, which would not be repeated continuously. From this, results showed that a three to five samples pool of the overall sample was sufficient to obtain a representative mean. This test was not repeated for the post cleaned state, given that each sample taken would be cleaned, which allowed for an understanding of the cake/filtrate on the surface. Therefore, it is assumed that the three to five samples taken for assessment would also provide a representative mean in the post cleaned state.

One impact of increasing the number of samples taken for analysis is the impact it has on the time to remove, analyse, and report/interpret the data. Therefore, during the determination of the required number of samples to determine mass/thickness, consideration was given to the time impact. If multiple filtration bags are presented for analysis, the number of samples taken increases dramatically. This regard led to the optimised number of samples to achieve a representative mean, without a detrimental impact on sample turnover time.

It was mathematically shown that two local maximum and two local minimums existed within the data. Utilisation of a Fourier plot, in combination with the respective mean and confidence intervals, demonstrated good agreement. The location of these local points complemented each other for both the mass and thickness data. These locations where surmised and plotted visual, using the stitch point as the $0^{th}/360^{th}$ degree, due to the bag being cylindrical. A repeating pattern between a local minimum and maximum was noted in each respective quadrant of the bag. Consequently, it could be surmised that a preferential flow

was exhibited to the filtration bag, which caused this observation, however further studies are needed to confirm/deny this root cause.

5.4.1 Further Work

The following points summarise the recommended steps to be taken, following this study.

- Analysis of the full machine direction should be performed on new media, in the same manner as this study. Doing so would highlight if the patterns observed I this study are localised, or if they are representative of the process.
- A more detailed, controlled study of the mass and thickness variation across the cross direction is needed. If possible, a representative sample of the cell should be taken, noting the position at which the bag originated. Furthermore, the position of the stitch, to a predefined arbitrary point (for example the bag orientated towards the centre of the inlet), should also be recorded. Following the proposed methodology, samples in the vertical middle, top, and bottom should also be assessed for mass and thickness. Following this analysis, the basis of this study can be used to potentially corroborate and support the findings.
- Additional analysis should be conducted along different vertical heights of the used media to ensure that the number of samples is still representative. If not, then a detailed understanding and mapping may be needed to ascertain why and optimize the methodology.
- An academically controlled study to assess the effect of rotating bag filters during operation. This study would use a pilot scale combustion chamber attached to a baghouse. After a certain period of operational time, the bags would be removed and evaluated. From this, new filtration bags would be inserted, and periodically rotated approximately 90 degrees. Following this, the comparison between the results from the non-rotated and rotated filtration bags would indicate any differences. Furthermore, if a noticeable difference in favour of rotation is noted, then a new baghouse design can be suggested, in which the bags rotate either continuously or periodically automatically. This design would, in effect, be a rotisserie bag house.

Chapter 6: Understanding Air Permeability Variation on A Full Filtration Bag

6.1 Introduction

Air permeability is one of the most common techniques used to characterise post operational nonwoven filtration media. This technique determines the volume of air that passed through the sample, at a given surface area and differential pressure per unit time. Evaluation required a flat piece of media to perform this test. In accordance with BS 22031:2021 "Sampling and test method for cleanable filter media taken from filters of systems in operation" [16], assessment is performed in three different locations on the filtration bag: the vertical top, middle and bottom. Therefore, the analysis aimed to suggest the variation in each given test region of the filtration bag, irrespective of the available surface area of the bag. Performance of additional test methods, such as mass and thickness determination are often used in conjunction with air permeability to yield further information about the filtration bag. Characterization of the post operational sample therefore yielded a degree of understanding of how operational conditions had affected the filter bag since installation.

This study aimed at identifying any variation across a full, used, filtration bag from an EfW combustion facility. The EfW combustion site supplied a new/virgin/unused filtration bag and a used filtration bag for this study. Apart from the manufacturer data sheet of the filtration bag shown in Appendix A, the site provided no further information.

Resultant air permeability values are dependent on a sample's relative density, thickness, and porosity [266]. For used nonwoven filtration media, pore blockage (a decrease in porosity) restricted the volume of airflow through a given surface area, which at a fixed differential pressure across the same surface area, would result in a lower air permeability. In contrast, pore deformation causes the average pore size to increase due to mechanical and chemical deformation [8], [187]. This deformation process led to an increased air permeability at a fixed differential pressure. Filtrate deposition on the surface caused the thickness of the sample to increase, which could negatively impact the air permeability by requiring a higher differential pressure to achieve the same air permeability. Though the effect of filtrate deposition is governed also by its intrinsic particle size, if sufficiently large the effect can be negligible. This is because larger particles for a less dense structure which allowed for greater volumes of airflow through at a given pressure. During operation, the filtration bag will

exhibit a plethora of these conditions, which will ultimately affect the end air permeability. The aim therefore of performing the air permeability test is to determine how the operational conditions have impacted the suitability of the filtration media, making it less suitable for further use.

As previously shown in Chapter 5, local variation at a resolution surface area of 25cm^2 occurred within both new and used nonwoven filtration media. This study further supported and suggested that there is a degree of air permeability variation both locally and globally. If the overall mass of the PC state increased from the VN state, this suggested a degree of internal filtrate deposition. This internal deposition (referred to as blinding) would reduce the air permeability, owing to filtrate blocking. Conversely, if this value is minimal, but the change in thickness increased, the air permeability at that region was likely to have been higher. Consequently, understanding how the air permeability changes gives an indication towards how it is performing during operation.

Common practice is to employ the methodology stated in BS 9073-15:2008 "Determination of air permeability" [232] (or similar standard) to determine the air permeability within each third of the filter bag by using a subsequent sub samples surface area. The air permeability is a measurement of the volume of air passing perpendicularly through a sample, at a defined differential pressure across the sample and timeframe. Compliance required that the assessment area be 20cm^2, 38.3cm^2, or 50cm^2 within a tolerance of 0.5%. Furthermore, the differential pressure across the sample can be either 100Pa, 125Pa, or 200Pa within an accuracy of 2%. Whilst the standard required a minimum of five tests, BS 22031:2021 "Sampling and test method for cleanable filter media taken from filters of systems in operation" [16] required three. From these tests, calculation of the average is possible and reported. Discrepancy between the standards increased the chance for misunderstanding which standard to comply with.

Similarly, for mass and thickness determination, the omission of the resultant confidence interval occurred. Whilst technically this does not affect compliance, it reduces the information obtained about the variation, particularly as the number of samples reduces. Whilst, BS 9073-15:2008 "Determination of air permeability" [232] did stipulate that the coefficient of variation should be reported, BS 22031:2021 "Sampling and test method for cleanable filter media taken from filters of systems in operation" [16] doesn't which meant it's inclusion was only recommended and not required. Resultantly, reported analytical

results may omit this information and yet still comply with a standard. The inclusion of the confidence interval may provide useful, especially when comparing historical test results.

This study utilized the operational parameters required for BS 9073-15:2008 "Determination of air permeability" [232] compliance. Given that the minimum number of repeats stated in BS 9073-15:2008 "Determination of air permeability" [232] is five for a given sample size, the study exceeded this minimum due to the whole sample bag being examined. For subsequent sub samples of each vertical third, a total of twenty-five datapoints were used. The sample size difference between five and three sample points was also evaluated to determine the difference between them.

6.1.1 Methodology

Parameters stated in BS 9073-15:2008 "Determination of air permeability" [232] were used to determine the air permeability. A brief overview of the apparatus requirements for testing is shown in Table 26. To ensure consistency throughout the study, these parameters were not changed. A slight deviation was conducted in regard to the methodology prescribed for compliance with BS 22031:2021 "Sampling and test method for cleanable filter media taken from filters of systems in operation" [16]. As this study focused on the analysis of the full bag, omission of the requirement to isolate subsamples arose which allowed for air permeability maps to be drawn. Upon completion, the data can be prepared in such a way by defining where the original sections would have been, without the need to physically remove them from the filtration bag.

Table 26: Operational Parameters to Determine Air Permeability

Description	Parameter (tolerance)	Additional Comments
Test head	$20cm^2$ ±0.5%	Fixed throughout test.
Vacuum pump to generate the differential pressure across the sample	100/125/200Pa ±2%	Fixed at 200Pa±2% throughout test.
Flowmeter / Orifice number	Experiment Dependent ±2%	Numbered 1 to 9 which incrementally increase with size. Used to enable a stable flow at a given differential pressure. Fixed throughout test.
Sample Size	100mm by 100mm	Due to the nature of the study, the sample size was greater than this value.

Following laboratory protocol, calibration happened at the start of every working day. Two different calibration plates with nominal diameters of 7.8mm and 21.6mm, respectively were used for calibration, along with a test head of 20cm^2.Following the manufacturers guidelines, the differential pressure across the calibration plate was set at 125Pa. The calibration sequence required the completion of four tests and is summarised in Table 27. Following analysis, the reported air permeability difference between the reference value and obtained value must be $\leq 2\%$. This is determined through Equation 27, which utilised the reference values (Q_{ref}) in Table 27 against the observed air permeability (Q). If the percentile error (Δ_e) value remained $< \pm 2\%$, calibration was complete.

$$\Delta_e = \frac{Q - Q_{ref}}{Q_{ref}} \cdot 100$$

Equation 27: Air Permeability Calibration Test

If $\Delta_e > \pm 2\%$ (failed), there could be an unidentified error in the experimental set-up, such as the air connections not sealed, or the calibration plate not seated correctly. Additionally, given the orifice plate was screwed into position, the tightness of this can affect the error. However, during testing, the absolute error generated fell within the specified limits. The resultant percentile error, Δ_e was |0.73%-1.28%| across the data.

Table 27: Air Permeability Calibration Data

Orifice Number (-)	Calibration Plate (Ø mm)	Pressure (Pa)	Test Head (cm^2)	Q_{ref} (mms^{-1})
3	7.8	125	20	114.5
4	7.8			114.5
5	21.6			855
6	21.6			855

	Day 1	Day 2	Day 3	Day 4
$\lvert\Delta_e\rvert$	1.28	0.97	1.25	0.73

Analysis of air permeability required flat samples, with no discernible folds or creases. The occurrence of these within a sample would negatively impact the obtained results from testing. To ensure that the sample is taut, a compression ring was used which allowed the sample to remain taut and flat throughout the test. From this, movement of the test head into

position and was pressurised. Completion of this saw the sample ready for analysis, provided no visible creases, folds, or defects were observable.

Compliance with BS 22031:2021 "Sampling and test method for cleanable filter media taken from filters of systems in operation" [16] required two samples be removed from each section. These samples where to measure 25mm x 200mm and 200mm x 25mm in the machine and cross direction, respectively. This methodology allowed for analysis in the latitudinal and longitudinal direction to illustrate the potential variation in the machine and cross direction, respectively. For comparison between this study to the standard's methodology, a single sample which measured 30cm in vertical length simplified this requirement, given both the sub samples would have occurred within this larger sample size. This would still allow for completion of a latitudinal and longitudinal assessment but simplified the determination of the position of each respective sample.

Flue gas filtration media assessed in this study was a PTFE/P84 needlefelt, which also had a PTFE scrim.

Sample preparation required the filtration bag to be converted from its original cylindrical shape to being flat. Removal of the top and bottom cuff from the filtration bag used a sharp knife. Once removed, an incision at ≈5cm's parallel to the stitch along the vertical height transpired, which allowed for the evaluation of the stitch. This incision made allowance for the removal of the cylindrical nature and allowed for the bag to become flat, whereby the filtrate was facing vertically upwards. Minimalization of any agitation, towards the filtration bag happened throughout the study to avoid any loss of filtrate, which would affect the analysis.

A matrix structure stored the evaluated air permeability data, whereby each element of the matrix represented a unique location. Subsequent locational information also followed this ideology based on the first datapoint position. The vertical height/length of the sample equated to the machine direction. In contrast, the width/circumference equated to the cross direction. These descriptions originated from the manufacture process of flat media, which commonly referred to the length of the machine as the machine direction. Cross direction is dependent on the width of flat media required. This resulted in the machine and cross direction becoming the axial positions of x and y respectively unless otherwise specified. Overall, the study produced a matrix of 6 by 83, equivalent to 498 unique datapoints per state.

Demonstrated in Figure 40 [2] is the matrix structure, including a brief outline of the three states assessed in this study: AR, PC, and Filtration cake permeability. The latter state is the difference between the PC state and AR state. This is possible due to the fixed locational position of each sample point. Characterisation of how the felt changed since instillation required a shift in the data negatively on the used PC data, by the new/virgin media's mean air permeability.

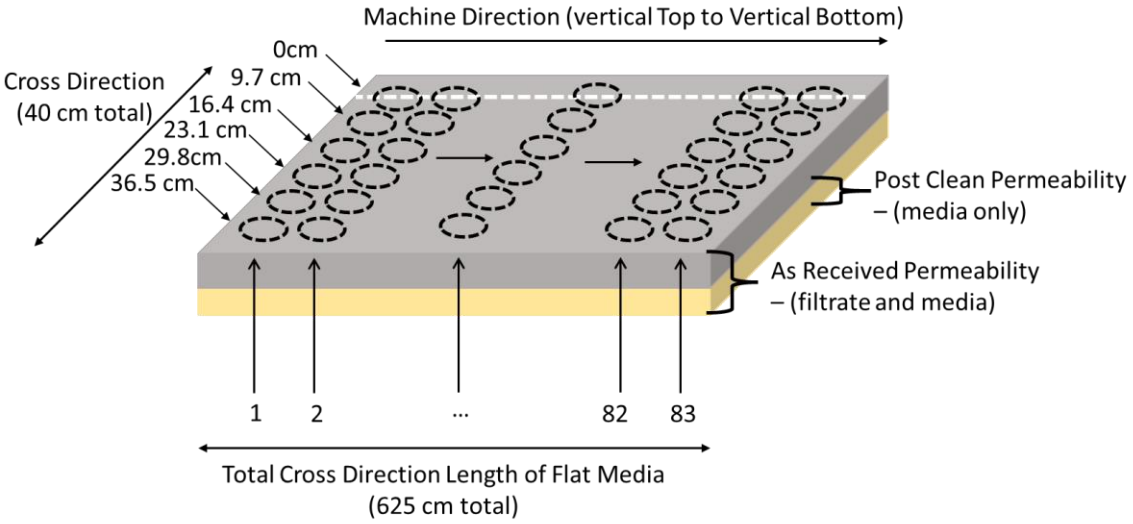

Figure 40: Pictorial Representation of the Various States Analysed [2]

Evaluation of air permeability was possible on the sample in two states: the as received state (AR) and post cleaned state (PC). Definition of the AR state is the original state of the sample, as presented for analysis. PC state used the results of Chapter 4 to determine the most appropriate cleaning method. Given that this study used the same post operational media as Chapter 4, the method selected was dust vacuuming. Testing in the PC state yielded an insight into how the felt has changed during operation. Once cleaned, air permeability evaluation occurred again in the same unique sampling positions as the AR state, allowing for direct comparison between the data sets. Subsequent calculation of the filtrate/cake layer and felt change required completion of the AR and PC states.

A pictorial representation of the difference between the AR and PC state is shown in Figure 41.

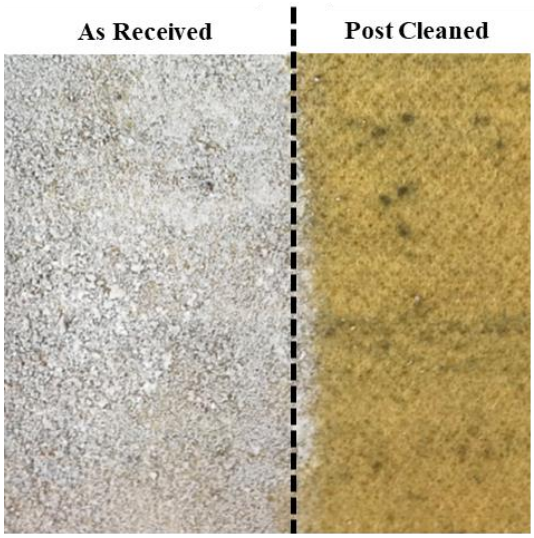

Figure 41: Visual Difference Between the As Received (AR) State and the Post Cleaned (PC) State

Prior to the examination of the used sample, air permeability evaluation of a different used sample, from the same site and operational time, occurred, a total of fifty times. This provided the baseline air permeability variation of the AR and PC states. One of the downsides to the study is the considerable amount of time taken to perform the analysis. This perceived variation described the expected variation in the data, given repetition of the sample multiple times was not possible and determined to be ±0.48 $Ldm^{-2}min^{-1}$ for AR and ±0.73 $Ldm^{-2}min^{-1}$ for AR and PC states, respectively.

The filter media manufactures datasheet defined the new air permeability at 175$Ldm^{-2}min^{-1}$ at 200Pa. To confirm, isolation of a swath from the new/virgin bag allowed for independent laboratory analysis. Assessment of ten random sample locations yielded an air permeability result of 256.06±16.66 $Ldm^{-2}min^{-1}$. The resultant difference between the stated and determined air permeabilities was 81.06 $Ldm^{-2}min^{-1}$. Ratification of this datasheet was in 2015. Over the past seven years, withdrawal from operation of multiple filtration bags has required the instillation of new/virgin bags. If the assumption that the site has not changed suppliers or bag types is true or the manufacturer has not changed their manufacturing process somehow, then the datasheet value(s) should also be true. Whilst an unknown degree of variation could have influenced the air permeability, the datasheet could be outdated given its age. This uncertainty led to the utilization of the laboratory-based air permeability for comparative analysis given the site provided a new bag of the same material as the used one.

6.1.2 Research aims, Novelty, and Potential Outcomes

No previous literature has conducted such a large-scale air permeability study on used, industrially relevant, nonwoven filtration media. This novelty is further extended by the consideration, impact, and review of the testing methodology stated in BS 22031:2021 "Sampling and test method for cleanable filter media taken from filters of systems in operation" [16] for air permeability. This is achieved using the methodology stated in BS 9073-15:2008 "Determination of air permeability" [232], which is also referenced in BS 22031:2021 "Sampling and test method for cleanable filter media taken from filters of systems in operation" [16].

Overall, the aim of this study was to determine any potential variation across a full, used, nonwoven filtration bag. By conducting a methodical and structured experimental procedure, identification of any potential variation across the latitudinal and/or longitudinal direction of the bag allowed for reliable observations and quantifications to be made. To achieve this aim, the following points where addressed:

- What does the air permeability look like across the machine direction and cross direction of the full sample?
- Is there any statistical significance or difference between these directions in a sub-sample? Is the variation significant to the local or global region?
- Given the fixed sample position in the as received (AR) state and post cleaned (PC) state, can the difference between them provide more information on the effect that the filtrate has/had on the air permeability?
- The current assumption is that three air permeability readings of a 30cm sample is representative of the vertical third it came from. Is this true or false? What is the potential variation in the mean and is it relevant?

6.2 Data Visualisation and Preliminary Review

In compliance with BS 22031:2021 "Sampling and test method for cleanable filter media taken from filters of systems in operation" [16], a visual inspection of the sample determined any areas where failure may have occurred. The visual inspection looked for any holes or tears in the filtration bag which could have impacted results as this would have indicated failure. Upon inspection, no defects or obvious cuts/holes were noted on the sample, across the entire surface area. Images shown in Figure 42 depict examples of the sample in the AR

and PC state, detailing the stitch in the first column (example 1) and flat media in the second (example 2).

Initial visual inspections of the air entry surface of the sample suggested that the deposition of filtrate on the surface of the media was heterogeneous, whereby the filtrate appeared to be uniformly distributed across the surface area. Whilst most of the sample surface area exhibited a deposition like AR example 2 (in Figure 42), it was noted that some small regions exhibited a deposition more like AR example 1 on the AR surface of the media. Acquisition of the sample required manual extraction from the bag house and its cage. It was therefore likely that during this extraction, an unquantifiable, unavoidable, degree of agitation occurred which resulted in filtrate loss. Furthermore, manual handling of the bag could have resulted in filtrate loss as operators grabbed the bag to stop it falling into the baghouse.

Transportation of the filtration bag in a spiral occurred which attempted to restrict movement. Subsequently, insertion of the filter bag into a clear bag reduced any exposure to the filtrate and further limited accidental filtrate loss during transportation. Spiralling occurred from the top cuff down the vertical height leaving the bottom cuff accessible and mitigated against accidental internal deposition: though a small amount did occur. Whilst great care to minimise filtrate movement/loss occurred during the preparation stage, a minimal amount of filtrate loss did naturally occur. Consequently, there exists an unquantified degree of variation between the in-situ filtration bag surface and the surface prepared at the laboratory for analysis. Given this, the assumption that the degree of variation between the in-situ bag and prepared bag was deemed negligible.

Post cleaning used a dust vacuum, in accordance with the study conducted for Chapter 4. Both studies used the same media, which originated from the same site. As such, the AR and PC states are shown in Figure 42. Due to the results presented in Chapter 4, dust vacuuming was an optimal cleaning method to determine the characteristics of the felt post operation.

Removal of two 5cm by 2cm samples from each vertical third allowed for further analysis using scanning electron microscopy (SEM). Each sample originated from a point whereby the removal would not interfere with the air permeability test. One sample, from each vertical third, underwent cleaning, which allowed for SEM imaging in the PC state. The samples where then mounted in epoxy resin, cured, grinded, and then polished. Subsequent SEM imaging provided an insight into the differences between the AR and PC state.

Visually depicted in Figure 43 are the results of the SEM imaging.

At the microscopic level, a heterogeneous filtrate layer occurred across all samples in the AR state. Whilst a small proportion of the filtrate loss would have occurred during acquisition and sample preparation, the remaining filtrate is sufficiently bound such that it would take a greater force than general sample movement to remove said filtrate. As such, the SEM images for the AR state in Figure 43 were deemed representative. At the same scale, the thickness of the filtrate is noticeably varied across the sample. Various AR regions exhibit a discernible amount of filtrate, which would have had a corresponding impact on the air permeability [266]. Consequently, the SEM images provide an indication of the potential variation in the AR state, whereby if the filtrate was heterogeneous, the air permeability data distribution may be narrower and more precise.

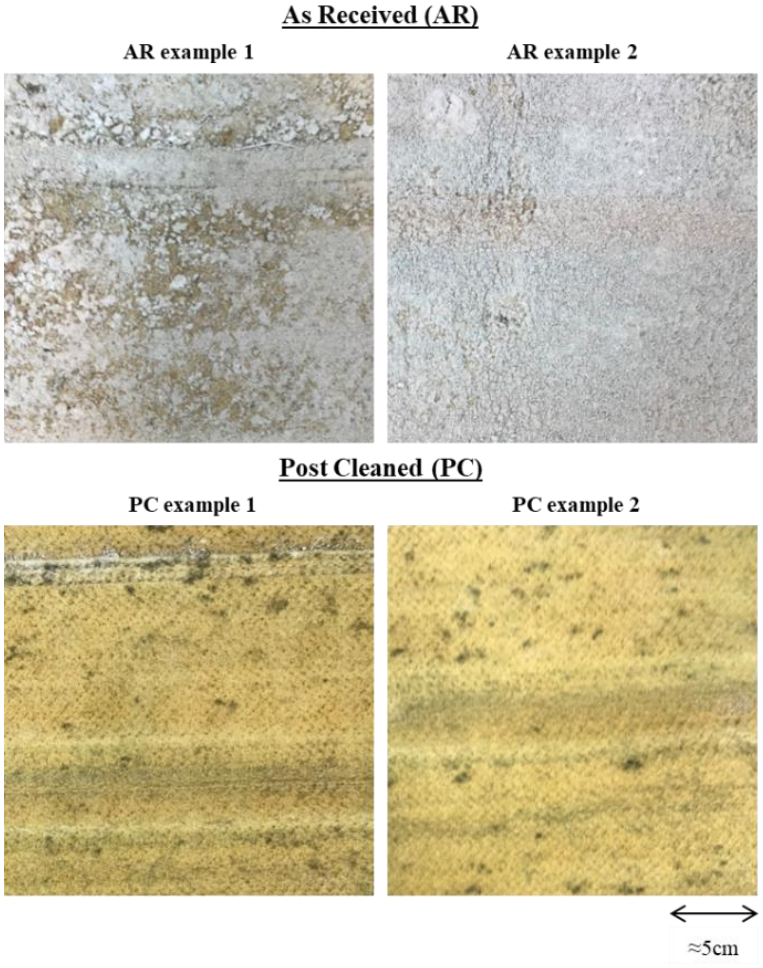

Figure 42: Visual Representation of the Stitch (example 1) and Flat Media (example 2) in the AR and PC state

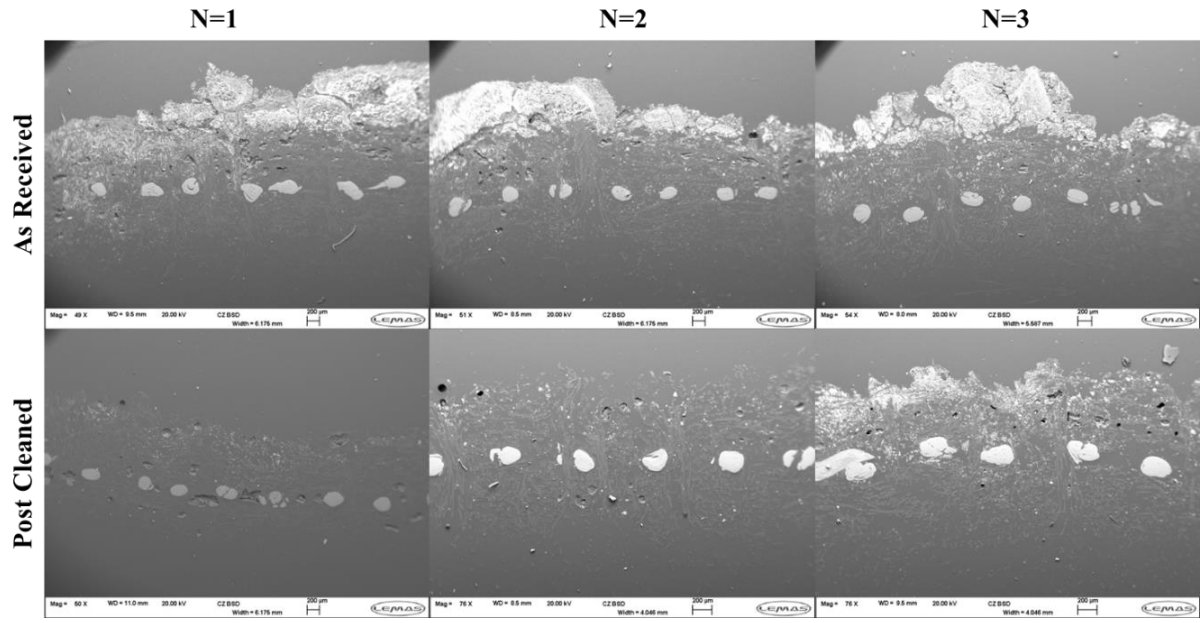

Figure 43: SEM Images of the Vertical Top (N=1), Middle (N=2), and Bottom(N=3) in the AR state {row 1} and the PC state {row 2}

Further analysis of the AR SEM images revealed a degree of blinding within the fabric. Over time, internal deposition of the filtrate will occur, due to filtrate entering the pores. Once this occurred, the effectiveness of filtrate removal dropped towards zero. As discussed by Schuberth et al,. [205], the rate at which this occurs is dependent on a large number of parameters such as: filtration velocity, cleaning time, cleaning pressure and duration, particle size, pore size [205]. Whilst the service time was not known for the sample, blinding (to an unknown extent) occurred within the media as visible in Figure 43. Interestingly, a substantial proportion of the blinding to the felt appeared to be within the needlepoints. Due to the needlepoints, orientation of the fibres changed from horizontal to vertical through the sample thickness. This appeared to have created a channel like stricture in the felt, which had allowed a greater rate of internal deposition to occur. Deposition also arose in regions where the needlepoint had not occurred, which could be incidental, or caused by a greater proportion of air movement through these channels which diffused into the surrounding fibres. Lastly as the SEM image is of a singular plane, it could be that the filtrate deposition happened outside the needlepoint due to the pore network behind the slice which is unobservable within these images. There is therefore a requirement for further work to ascertain the causation and definitive impact of this observation. Regardless, the occurrence of blinding will proportionally reduce the air permeability through a sample area.

Post cleaning further showed the extent of blinding. However, the blinding appeared to be reduced in comparison to the AR state. This could be due to an unquantifiable amount of the filtrate removal via the suction of the dust vacuum close to the surface of filtrate side of the sample, which removed a considerable proportion of the apparent blinding in this region. Whilst the PC state samples for the vertical middle (N=2) and top (N=1) showed minimal blinding, the sample for the vertical bottom (N=3) had a more prominent retention of filtrate. The retention appeared focused about the surface, particularly towards the left hand of the image, with the right-hand side appearing like the other images in the PC state. Therefore, it was assumed that this occurrence was a localised incident, given that the surface of the sample appeared clean and like that of the PC examples in Figure 42.

Overarching analysis of the SEM images is the assumption that three images are representative of the overall filtration bag. Given the vertical height of the whole filtration bag was ≈6 meters, there is a degree of variation between the samples taken due to the resultant distance between the acquired samples from the felt. Given the experimental cost associated with SEM usage, a large-scale SEM imaging study was ill-advised given limited funding. However, it may be appropriate to conduct a partial analysis to quantify the variation about the cross direction in a fixed machine direction. Doing so would further support and provide evidence to support the results obtained in Chapter 5. In addition, it would provide evidence to support the apparent variation within the cross direction. Overall, the SEM images shown in Figure 43 provide an indication as to how the permeability may vary, until a more structured study is performed to quantify both the air permeability results and the obtained SEM images.

6.2.1 Distribution Analysis

The distribution of the whole air permeability data in the AR and PC state are shown in Figure 44. Initial impressions for the AR and PC state revealed an apparent right/positive skew in the data. Upon subtraction of the AR against the PC, the filtrate data appeared more normally distributed, which suggested that the degree of skew was similar for both AR and PC states. This subtraction yielded the air permeability distribution of the recovery/difference between the AR and PC state on the surface of the sample. A skewness value, determined by difference between the mean and minimum values, over the standard distribution of the data showed a skewness value of 1.99 and 1.71 for AR and PC, respectively. Visual analysis of the AR and PC distributions shown in Figure 45 did present with a slight skewness, but by calculating the skewness value, it is possible to quantify if the they just appeared skewed or if

they are indeed skewed and if so, to what extent. The PC distribution suggested a more prominent skew in contrast to the AR state. In contrast, the recovery/difference between the AR and PC state distribution had a reported skewness of 2.96 which did not meet the threshold to suggest skewness.

Origination of the skewness could be from structural variation in the sample. Given that Figure 44 included the data for the stitch, which attributed to a sixth of the overall data, this could account for the skewness. The main structural difference in this study, like Chapter 5, is that included examination of the stitch point. The stitch point and flat media became two independent/isolated slices of the data.

Demonstrated in Figure 45 is the distribution differences between the stitch point (in column 1) and flat media (in column 2). Complementary to this, a summary of the data is provided in Table 28 for the flat media only, with Table 29 summarising the data for the stitch point data only. Both tables depict the data across the three states: As received (AR), post cleaned (PC) and recovery/difference between the AR and PC state. Separation of the structural differences, coupled with the data overview yielded a better insight into the distribution behaviour of the raw data. Assessment of each structure and state lead to a normal distribution following empirical testing.

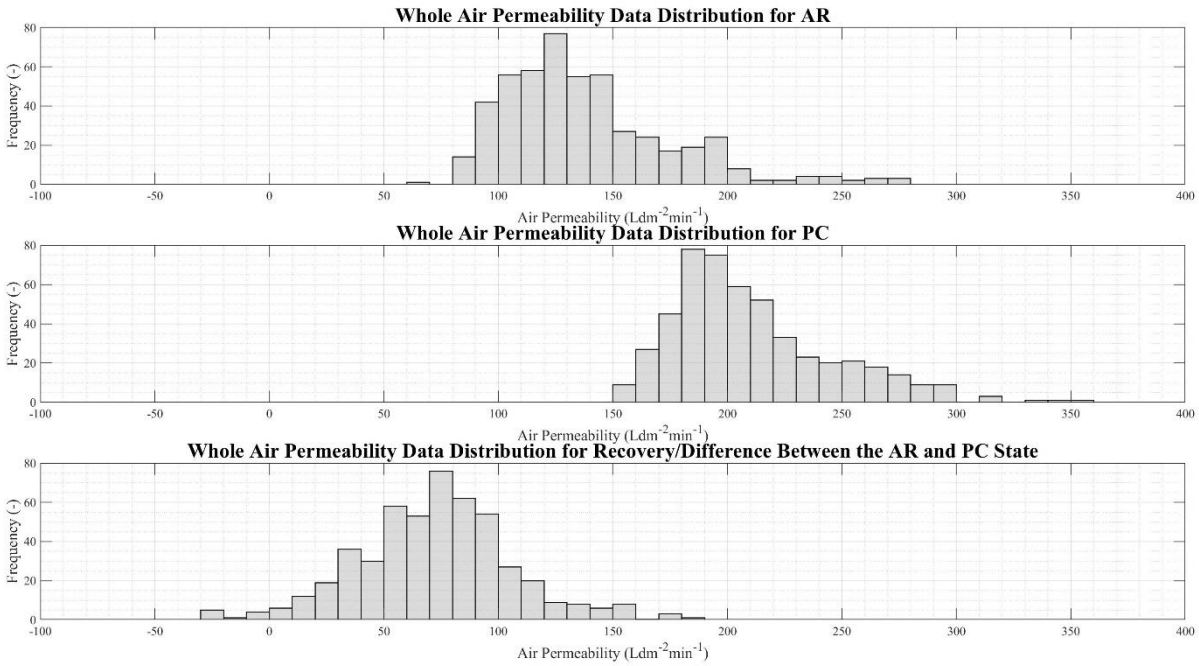

Figure 44: Distribution of the Whole Data for AR (top), PC (middle), and Filtrate (bottom)

Initial observations determined that the variation coefficient was comparatively higher for all states of the stitch data in comparison to the flat media. Inflation of this value was likely (partially) due to the number of sample points for the stitch equating to eighty-three, in comparison to the 415 of the flat media, which resulted in the higher value. Furthermore, the analysis of the stitch point could have introduced a greater error, given the clamping ring may have inadvertently created an open channel for airflow. However, for the PC state, the values where almost half when compared in isolation (Table *29* only). Both the standard deviation, confidence interval, and variation coefficient were notably lower for the stitch data, which occurred due to the lower data range of 143.13$Ldm^{-2}min^{-1}$. This resulted in the standard deviation of 27.91 $Ldm^{-2}min^{-1}$, which is comparable to the values obtained in Table *28*.

Furthermore, for both the AR state and the filtrate state stitch data, the large standard deviations in relative comparison to the PC state further exasperated the increased variation coefficients noted in Table 29. For the flat media, Table 28 demonstrated that standard deviation range remained similar within ≈ 3 $Ldm^{-2}min^{-1}$. Compared to the stitch point, whereby this range increased to ≈ 24 $Ldm^{-2}min^{-1}$; an increase of 700%. Both standard distribution ranges for AR and filtrate states are higher than the PC state, which resulted in a wider distribution as shown in Figure 45, which caused the deviation value to increase and therefore the variation coefficient also.

Given the removal of the stitch point data lead to a normal distribution when considering the structural differences, the skewness originally noted in Figure 44 can be described as the product of the combination of these two structural differences. The resultant skewness occurred due to both the frequency of the data and respective values, which caused a slight shift and therefore the suggestion of skewness. Cross analysis of Figure 44 and Figure 45 yielded further insight into the origin of the tails. Whilst the recovery/difference between the AR and PC state suggested a normal distribution in Figure 44, which can be prescribed to the difference between the PC and AR state which yielded this, large right-hand tails were noted for AR and PC which contributed to the skewness. This could have originated from an insufficient clamp, causing an increased airflow through the sample, due to the step increase of the sample thickness. For AR, the right tail occurred in Figure 44 due to the stitch point, which had noticeably higher air permeability values as shown in Figure 45. For PC state the tail originated due to a combination of the apparent outlier value of 353.84 $Ldm^{-2}min^{-1}$, coupled with the positioning of the data for the stitch. The stitch point data for PC had values between ≈201$Ldm^{-2}min^{-1}$ and ≈344$Ldm^{-2}min^{-1}$, which was higher than the flat media at ≈151

$Ldm^{-2}min^{-1}$ and ≈353 $Ldm^{-2}min^{-1}$. This, coupled with the frequency at which the data occurred, lead to a proportion of the right-hand tail noted in Figure 44.Consequently, further analysis should only be conducted on one specific, isolated, structure.

The study presented in Chapter 5 removed the stitch data from analysis due to: 1) the structural difference between the flat media and stitch, 2) the resultant effect the data had on interpretation and analysis, and 3) no previous work found quantified the difference between the stitch point and the flat media. Analysis of this data will provide an initial starting point in the determination of how the stitch point varies from the flat media. This study is complementary to the work conducted in this and Chapter 5's work. Consequently, omission of the stitch data occurred from any further analysis, until a decisive assessment strategy exists.

Air permeability values for the cake/filtrate are calculated by subtracting the PC state from the AR state at the same location. This theoretically yields a positive air permeability due to the PC state having less material at the surface blocking the pores within the media. Conversely, if the PC state is saturated (blocked) with filtrate, then the difference between the values will be close to zero. A negative value may occur if the AR state is higher than the PC state. The distributions showed that the cake/filtrate state did exhibit some negative values, particularly for the stitch point. Whilst it is unclear as to why this occurred, one potential is that some unknown degree of sample misalignment could have contributed to this, resulting in a negative result. Accidental deposition during cleaning could have occurred in the upper layer which was pulled into the media during air permeability testing. The use of the cake/filtrate state is therefore unreliable currently as an evaluation method until further explorations about this idea are conducted. However, theoretically, if the method is viable, it suggested how the cake/filtrate interacted with the media and effected the air permeability.

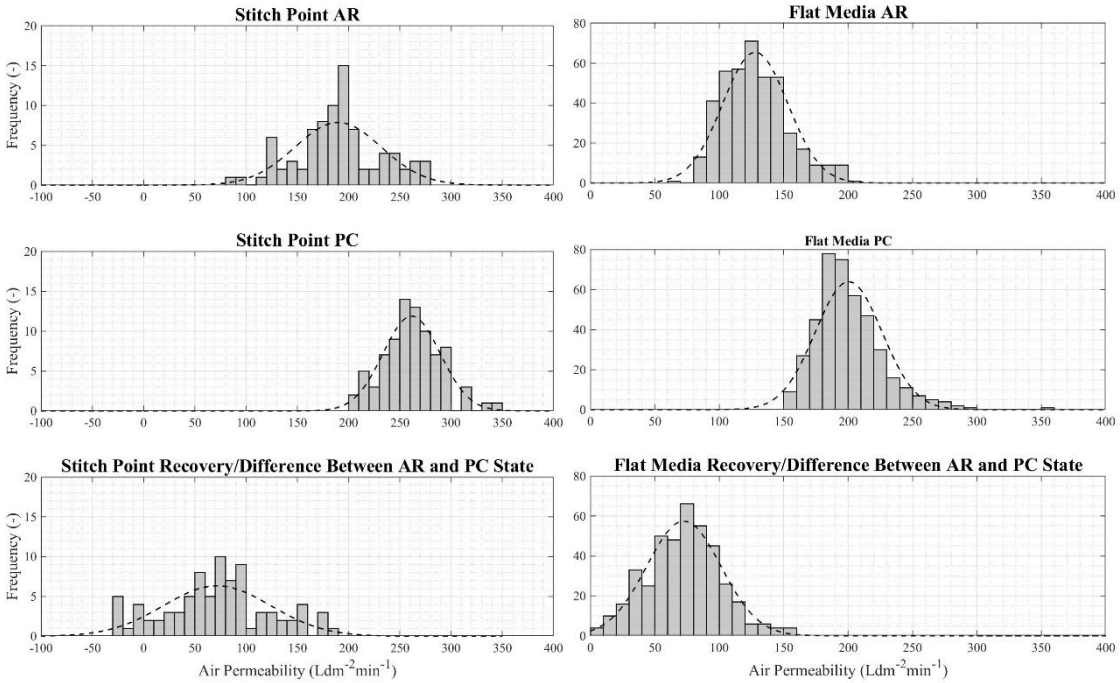

Figure 45: Distribution of the Stitch Data (left column) and Flat Media Data (right column) for the AR, PC, and Filtrate States

Table 28: Statistic Summary for Flat Media Data

State	Minimum	Average	Maximum	Range	Standard Deviation	Confidence Interval	Coefficient of Variation
AR	64.60	127.96	200.12	135.52	25.31	2.44	6.10
PC	151.26	200.48	353.84	200.58	25.91	2.49	6.24
Recovery/Difference	5.15	72.52	159.03	153.88	28.84	2.78	6.95

Table 29: Statistic Summary for Stitch Point Data

State	Minimum	Average	Maximum	Range	Standard Deviation	Confidence Interval	Coefficient of Variation
AR	86.45	189.84	270.85	184.40	42.09	9.05	50.71
PC	201.83	261.58	344.96	143.13	27.91	6.00	33.63
Recovery/Difference	-27.89	71.74	186.44	214.33	52.31	11.25	63.02

6.2.2 Data Visualisation

Representation of each datapoint against its representative locational information allowed for Figure 46, Figure 47, and Figure 48 to be produced. Representation by a colour scale allowed for a more prominent visualisation of the variation in the spatial direction. This used the minimum and maximum values presented in Table 29, which allowed each subsequent graph to be within its own data range. The maximum and minimum data range selected ensured encompassment of all data within the stipulated range. For clarity, the stitch equated to the zeroth locational point on the cross direction and the zeroth for the vertical top in the machine direction.

Presentation of the stitch data in air permeability maps shown in Figure 46 and Figure 48(A) acted as a reference point towards future studies about this structurally different point. Whilst this study focused predominantly on the flat media, the results shown suggest an overall higher air permeability as visually shown in Figure 46 and Figure 48(A). Consequently, as with Chapter 5, no further analysis was performed on the stitch point data until the conduction of academically controlled studies.

Suggested across both the AR, PC, and recovery/difference categories overall in the FMVC direction are apparent parabolic relationships. This parabolic relationship is characterised by a local minimum about the 23.1cm cross directional point, whereby the air permeability rises towards the two local maximums at 9.7cm and 36.5cm's in the cross direction. For the 9.7cm cross direction, the air permeability appeared to be the highest when compared to the 36.5cm Interestingly, the subtraction of the AR from the PC values (which yielded the cake/filtrate category) further suggested this but was less suggestive. This suggested that whilst the overall visual may suggest the local minimum at approximately 23.1cm in the cross direction, it may not be factually correct in both cases. If the local minimum was equal between the AR and PC state, then the recovery/difference's minimum would also appear to be equal. This suggested that there is variation about the minimum in the variable machine direction, which influence the local minimums actual position.

Suggested in Chapter 5 was that the mass and thickness of a different used nonwoven filtration bag exhibited a similar relationship. Unlike the parabolic nature, it suggested a Fourier relationship with two local minimum and maximums. This difference stemmed from the significant reduction in sample size when compared to this chapter, which allowed for a more detailed study across the media. The limitation of this chapter is the inadvertent

compression of the surface filtrate at the clamp point, which limited the number of examinable regions. This resulted in a more holistic view in comparison, but still methodically examined a comparatively larger surface area coverage of a filtration bag. However, given the apparent omission in literature of a similar study, comparison of the results with Chapter 5 it still suggests a local minimum, but with a different mathematical representation than that of Chapter 5. This suggested whilst the results are different (including the media and filtrate) there could be a prevalence of this apparent phenomenon within a wide range of nonwoven filtration bags in the sector. The prevalence of either a cyclic or parabolic relationship across the cross direction of circular filtration media may prove diagnostically useful for an analyst.

In the FCVM direction, the visualisation of the data suggested that the air permeability of each data point only slightly increased or decreased with each iteration/step change across the machine direction. In combination with the FMVC data, the data variation appeared marginal in comparison against the apparent parabolic nature. Assessment of the air permeability in this fixed direction would suggest that any resultant confidence interval would be drastically low, suggesting that the region of examination is more uniform. Conversely, under examination of the FMVC direction, the resultant confidence interval would be drastically higher due to the variation in the data in this direction. In both cases, the resultant mean may be similar (to within a couple of datapoints), yet the confidence interval would provide more useful to represent the variation, given the prevalence at which the data varies in the FMVC direction as opposed to the FCVM direction.

Previous analysis of the data, published in 2022 [1] suggested that a region of significant air permeability difference existed on the sample. For the AR state, a region visually appeared to exist between positions 16-48 (120cm-360cm), however this was not visualised in Figure 46 (A). Their paper introduced an unintentional bias in the analysis through the data visualization step. Using a contour plot with interpolation between the fixed data points, the visualisation of the data became skewed, which in turn created the unintentional bias during visual assessment. A bleed like pattern in the FMVC direction, demonstrated by Curry et al,. [1], suggested that regions of low to high air permeabilities existed in a wave like function down the vertical height. The use of heat maps (for Figure 46, Figure 47, and Figure 48), allowed for a more critical and clearly defined review of the data visually, without the assumption that the distance between each datapoint can be appropriately described through interpolation.

In both Figure 47 (A and B), an apparent parabolic like nature existed in the FMVC direction. This suggested that there is a local maximum of air permeability at a focused cross direction. Section 4.3.2 discussed this observation further.

Figure 47 (C) demonstrated the effect that the recovery/difference had on the media. A trapezoidal like shape existed between the bases of (26-33, at 36.5cm) and (15-45, at 9.7cm). This region exhibited a lower air permeability than its surrounding regions, suggesting that the formation of cake here differed. In Figure 47 (A), the same trapezoidal shape materialised, which suggested a higher air permeability. For the AR state (in Figure 47(A)), this higher air permeability would suggest that the combination of media and filtrate resulted in more channels for air to flow through, which resulted in the notation of an increased air permeability. The surrounding regions had a lower overall air permeability which suggested that a larger proportion of the flue gas may be flowing through the media within this region. Subtraction of this region with its respective region in Figure 47 (B) resulted in a lower value, which suggested that the values were similar in air permeability in the AR and PC state. This could suggest one of two events: either an unquantified amount of blinding had occurred, which led to lower recovery, or that regardless of the filtrate presence, the size of the particulate led to minimal blockage of new and existing pores, such that the airflow through remained similar. For the former to hold true, the air permeability would have tended to zero, given blockage and a requirement for the sample to experience a significantly higher differential pressure across it to yield a higher air permeability value. Consequently, the latter suggestion holds more weight, given that the air permeability appeared similar/higher than the surrounding regions. This observation was not possible from the initial study [1] owing to their choice of data visualisation.

Studies such as Fukasawa et al., [4], Kanoka [138],and Fukasawa et al., [237] are the only other examples found that depicted the air permeability of a nonwoven in a similar fashion to this chapter. In Fukasawa et al., [237], the study utilised a total of 189 datapoints, 21 in the machine direction and 9 in the cross direction. Their conducted air permeability study used a NV sample surface area size of 38.5cm^2 at differential pressure across the sample of 125Pa. Their study used new media and correlated the air permeability with fibre mass and thickness. Unlike this study which used a 20cm^2 test surface area and differential pressure of 200Pa, their study sectioned the media into 7 x 7cm squares. This could have given rise to accidental airflow through, depending on their clamping system and alignment of each sample. In contrast this study reduced the change of accidental cuts to the media by keeping

the sample as whole as possible, instead of subdivision of the total surface area for examination. Whist they showed the possibility of mapping, their division of the sample and size could have led to data obscurity; either in the form of artificial raises in the data due to accidental cuts or misalignment in the clamping/securing system, or data loss due to the larger surface area. However, their study was applicable for the new media they examined and showed that consistency between the reported manufacturing guidelines and their own results, suggesting that the method of large-scale testing is an applicable method.

An additional paper by the same authors, Fukasawa et al,. [4], repeated the methodology, but instead increased the number of datapoints from 189 to 250. Again, mass, thickness, and air permeability were evaluated and reported for new media. Their application of the samples to assess collection efficiency using a particle counter provided a basis for subsequent academic studies. For this study, which focused on air permeability only, a smaller sample surface area was advisable, which led to the difference between the studies. However, Figure 46, Figure 47, and Figure 48 showed that there is potential for future studies, which present the air permeability as a heat map, which yielded more information about the media to aid in the assessment of used filtration media: which didn't occur in studies such as Fukasawa et al,. [4], and Fukasawa et al,. [237] due to their assessment of new/virgin media.

An earlier study Kanaoka [138] presented a heat map of the air permeability, which indicated the air permeability variation through colour and not value. This study omitted defining the surface area examined for air permeability and the differential pressure assessed. However, it did identify regions of interest, so long as the total surface area is large enough. Regardless, these studies used new/virgin media, and is only comparable in terms of data presentation style. As shown, the visualisation method of showing the air permeability maps in Curry et al., [1] was sub optimal, and should have followed that of Fukasawa et al,. [4], Kanaoka [138], and Fukasawa et al,. [237], which led to the decision to use heat maps for this study, as shown in Figure 46, Figure 47, and Figure 48.

Lastly, it must be noted that Figure 48 is identical visually to that of Figure 46 (B) and Figure 47 (B). This stemmed from the equal subtraction between the PC state and the absolute NV state's air permeability, which saw ever datapoint shifted equally. This resulted in the visual assessment of the PC state becoming equal to that of the PC vs. NV states.

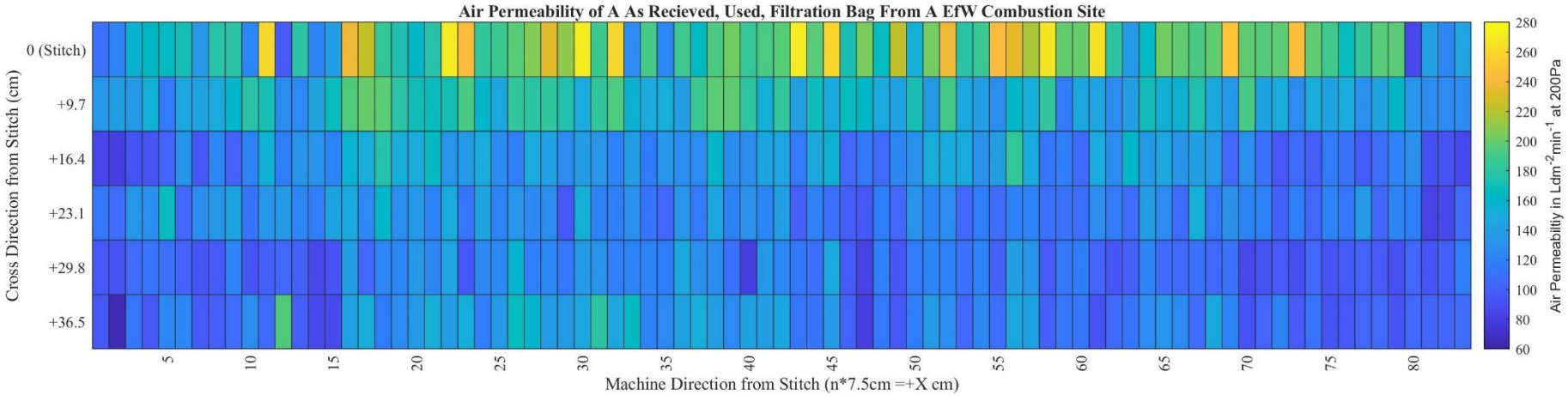

Figure 46A: Heatmap Depiction of the Air Permeability Variation of the As Received State

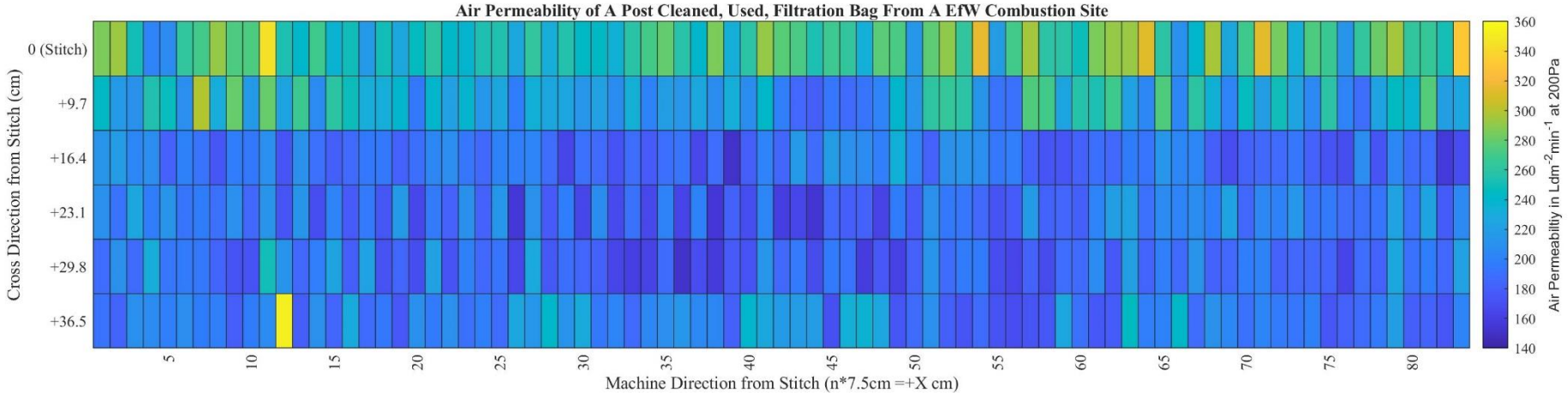

Figure 46B: Heatmap Depiction of the Air Permeability Variation of the Post Cleaned State

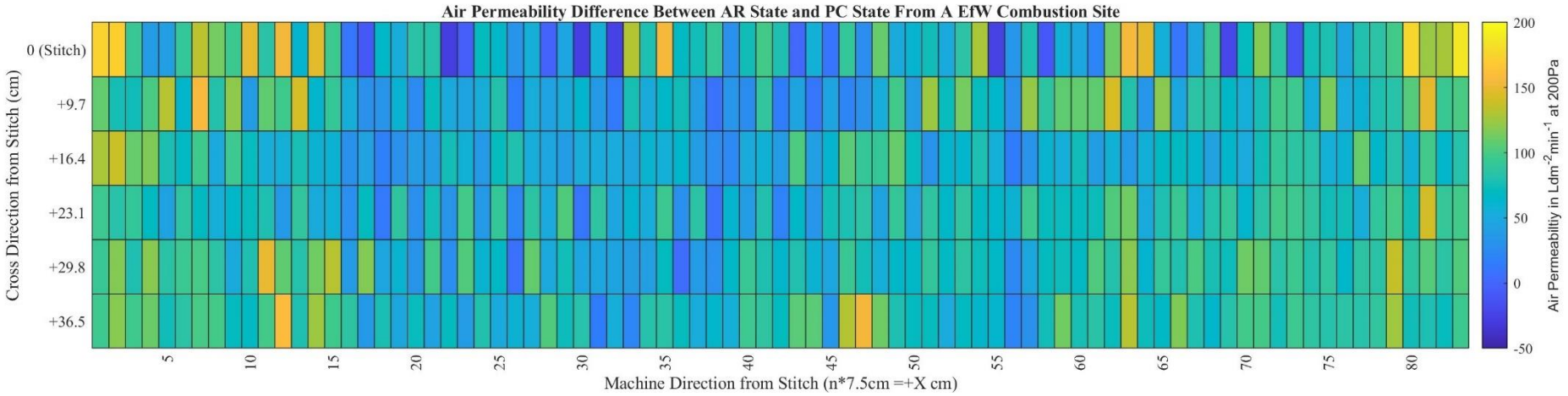

Figure 46C: Heatmap Depiction of the Air Permeability Variation of the Recovery/Difference

Figure 46: Three Heatmaps Depicting the Air Permeability Variation Across the Full Sample, Including the Stitchpoint, Across Various States

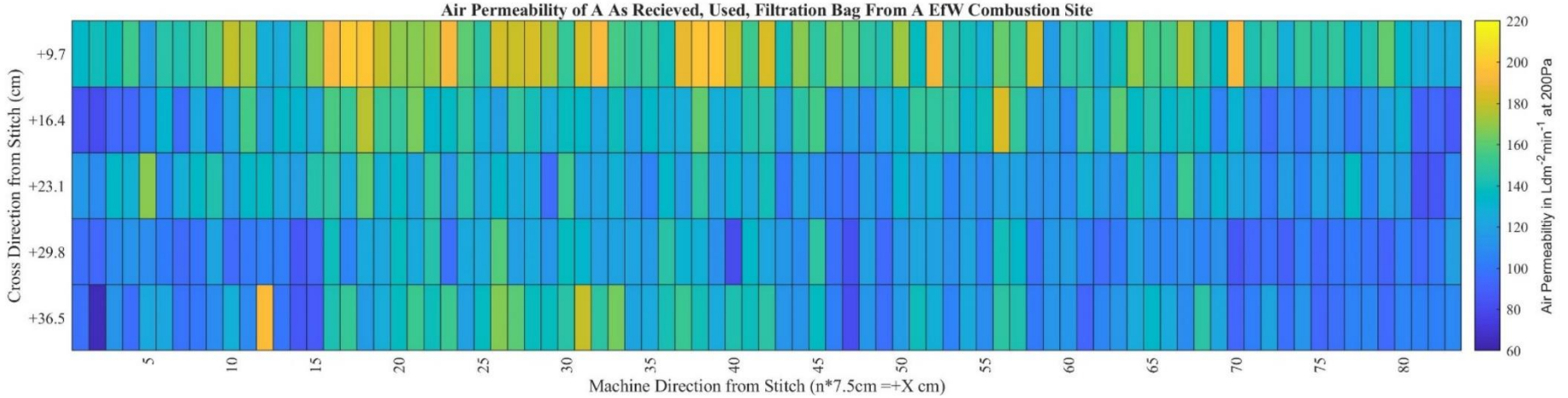

Figure 47A: Heatmap Depiction of the Air Permeability Variation of the As Received State Discounting the Stitch Point

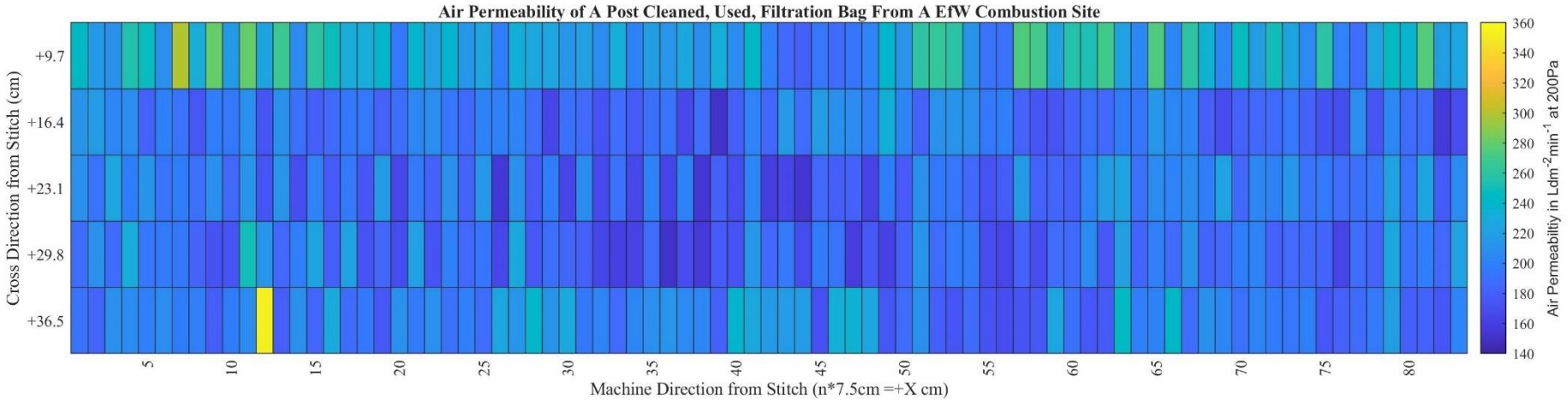

Figure 47B: Heatmap Depiction of the Air Permeability Variation of the Post Cleaned State Discounting the Stitch Point

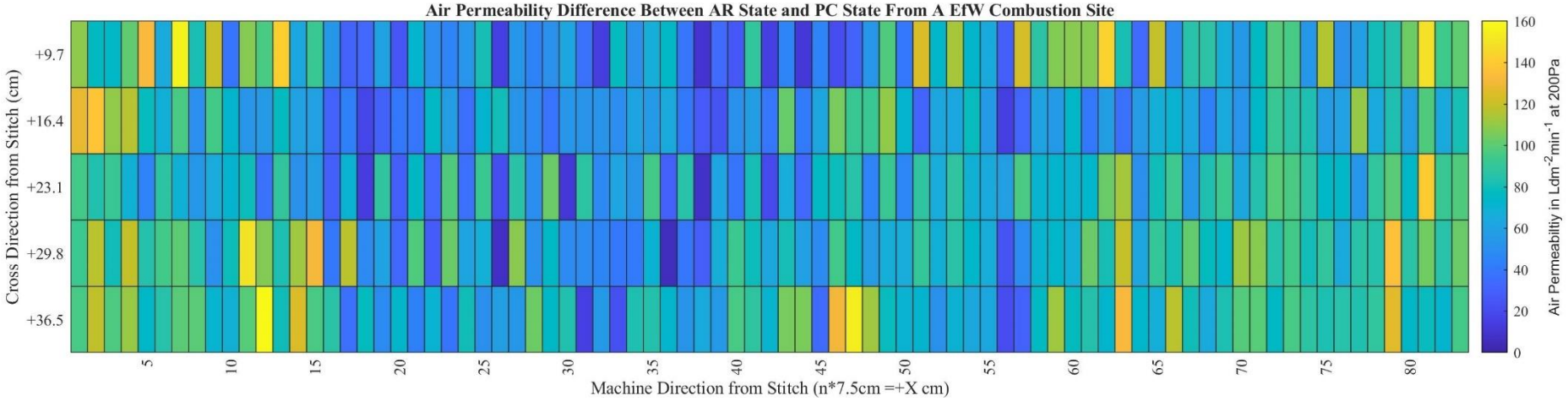

Figure 47C: Heatmap Depiction of the Air Permeability Variation of the Recovery/Difference Discounting the Stitch Point

Figure 47:Three Heatmaps Depicting the Air Permeability Variation Across the Full Sample, Discounting the Stitch Point, Across Various States

Depicted in Figure 48 is the variation over service time in the media and was determined through the subtraction of the mean air permeability value of 256.06 $Ldm^{-2}min^{-1}$ from the post cleaned values. The mean was determined based off ten random sample positions on a swath of new media. Whilst the true mean air permeability is 256.06±16.66 $Ldm^{-2}min^{-1}$, the absolute mean value, used for the subtraction, was due to it being statistically representative on the most frequent value of the test. Consequently, Figure 48 was determined by difference between PC data and the mean air permeability value of new media of 256.06 $Ldm^{-2}min^{-1}$.

Subtraction of the new media mean from the PC state provided both a numeric and visual representation of how the media had evolved since installation. This resulted in the classification of the data into two distinct categories for positive and negative air permeability, respectively. Figure 48 showed visually the negative values obtained when subtracting the PC state with the mean air permeability value of the new media, which accounted for a total of 96.14% of the data. In contrast, only 3.86% (16 out of 415 of the data points) were positive. Separation of the two, lead to the average for positive and negative air permeabilities being 18.82±23.45 $Ldm^{-2}min^{-1}$ and -59.19±21.04 $Ldm^{-2}min^{-1}$ for each category, respectively. Whilst the range of data appeared similar (at ≈95 $Ldm^{-2}min^{-1}$ and ≈105 $Ldm^{-2}min^{-1}$ for positive and negative respectively), positive skewedness occurred towards the zeroth value for the positive side, as opposed to the negative values which were more gaussian in distribution. All positive datapoints where localised to the +9.7cm cross direction (sporadic in nature across the machine direction), which clouded any judgment made about any trend or correlation about their occurrence.

Resultant negative air permeabilities, obtained from Figure 48, provided evidence that a degree of blinding had occurred, quantified by the resultant negative difference in air permeability. At the fixed differential pressure across the region of examination (200Pa) the value obtained for the PC state fell below the NV absolute mean, resulting in a negative difference. The scale of which suggested the extent at which blinding had occurred. The evolution and local variation of the blinding phenomenon, whilst mentioned holistically in literature, studies have not examined this in detail. The results presented in Figure 48 attempt to address the latter part but showing the variation of this throughout the sample. Due to pore blockage, the sample would have to experience a higher differential pressure to achieve the same permeation/flowrate through said sample. Given the fixation of the sample pressure, the resultant air permeability difference noted above correlated to the loss of airflow through the sample due to blinding.

In contrast, positive values represented an overall increase in air permeability from the original starting point. An increased air permeability can be associated to an increased (empty) pore volume, which facilitated a greater airflow through the sample at a given differential pressure across the sample. As shown in Chapter 5, the thickness of the material increased through usage. Under the assumption that there is either no/minimal fibre loss during operation, which allowed for the determination of the amount of filtrate present within the media and cake respectively in the chapter, the media could have expanded. This expansion resulted in the pore network/volume within the given sample size increasing which resulted in the increased air permeability. During normal testing on used nonwoven filtration media, there is a distinct increase in the thickness of the PC state when compared to the VN state.

However, for both the increased and decreased air permeability readings, neither occurrence is solely isolated and in fact, both an increase in the pore network/volume and internal deposition will occur simultaneously. This duality, within general operation, blurred the analysis to the point where attribution can only be towards the prominence of one point or the other. Consideration of the absolute upper and lower limits (to account for the variation in the air permeability Table 30 provided a summary of these limits, which showed the apparent difference between the results. Comparatively, whilst the highest potential positive values increased by 3.61% in the lower absolute limit, this still only represented thirty-one datapoints, which occurred due to the negative skewness presented within the positive datapoints. Conversely, the decrease of 2.17% in the higher absolute limit saw a proportion of the skew transition into the negative values. The overall tendency, regardless of the lower/higher absolute limit, showed that the media tended towards an increased blinding, sampled in Figure 48. Therefore, the data suggested that the filtration bag had experienced a degree of blinding throughout usage, as shown illustratively and expected theoretically.

Table 30: Upper and Lower Absolute Limits to Consider the Difference Between the PC state and New Air Permeability Results When Determining the Prevalence of Blinding/Pore Volume Change

Air Permeability ($Ldm^{-2}min^{-1}$)	Positive Percentile	Negative Percentile
Absolute (266.66)	3.86	96.14
Lower Absolute Limit (240.00)	7.47	92.53
Higher Absolute Limit (273.32)	1.69	98.53

Any other visual analytics is limited to that of the PC state, given that the data maps illustrated in Figure 48 are the result of shifting the data at a uniform value. Unlike the used filtration bag, the mapping of the air permeability of a new bag would have led to an increased inaccuracy, given the potential for variation between two states. To implement the NV state, the air permeability of the NV required mapping first, before fabrication and installation of the bag into operation. Doing so would allow for a direct understanding of the localised variation as opposed to a global value. Consequently, this limited the analysis of the variation between the PC and NV states.

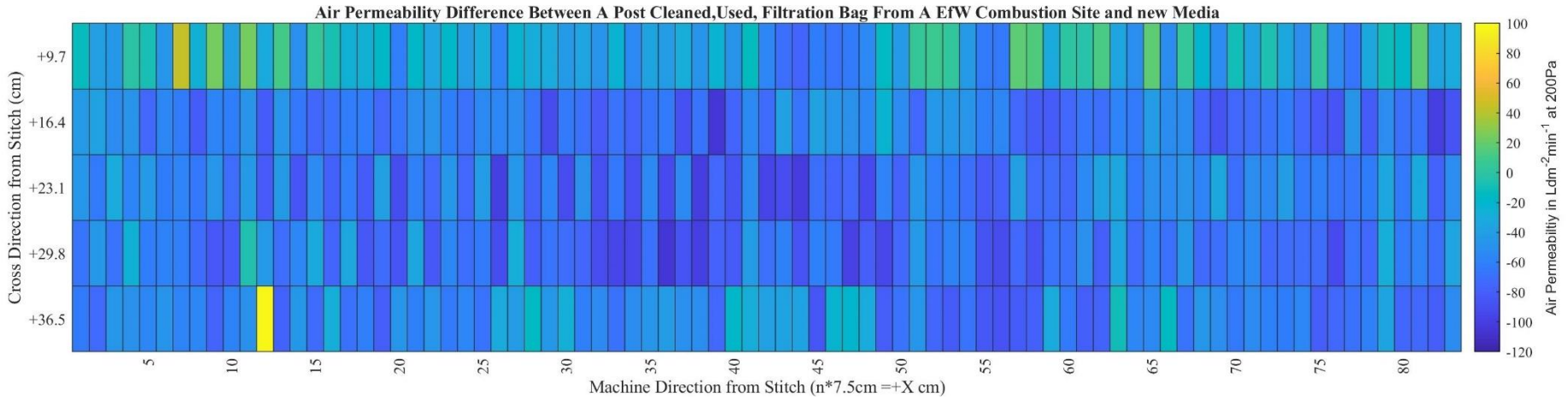

Figure 48A: Air Permeability Difference Between the PC State and New Media Value, Discounting the Stitch

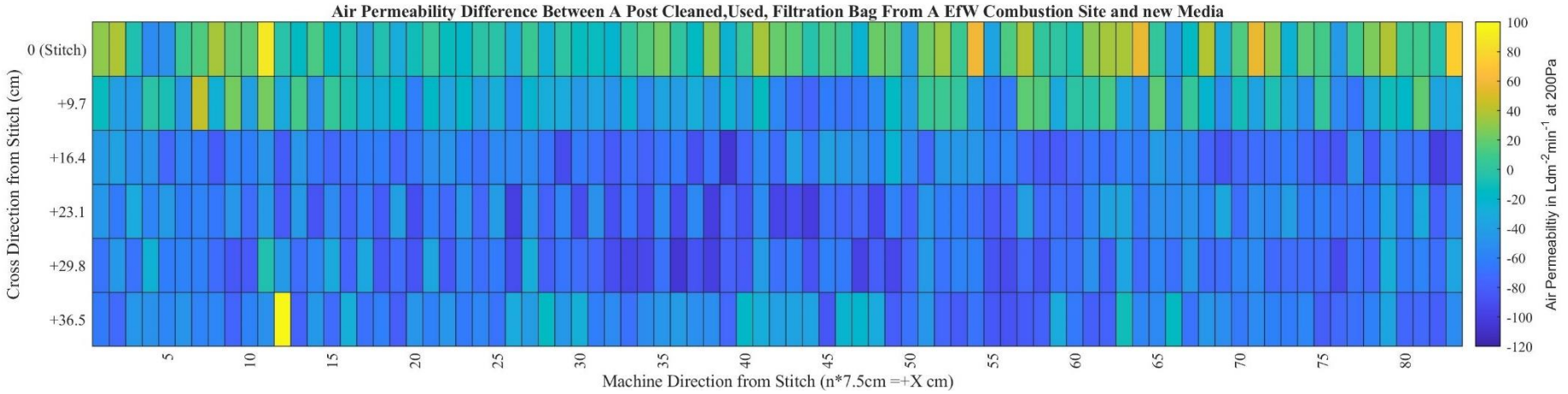

Figure 48B: Air Permeability Difference Between the PC State and New Media Value, Discounting the Stitch

Figure 48: Two Heatmaps Depicting the Air Permeability Variation Difference Between the PC state and New Media (Using the Assumed mean value of 256.06 $Ldm^{-2}min^{-1}$)

6.3 Air Permeability Assessment Method Review

Compliance with BS 22031:2021 "Sampling and test method for cleanable filter media taken from filters of systems in operation" [16] required two samples of 25mm by 200mm in surface area be taken in the latitudinal and longitudinal direction of the filtration bag respectively. This method of sampling happened in all three vertical sections of the filtration bag, denoted in the standard as top, middle, and bottom. This sample size is in contradiction to the standard BS9073-15:2008 "Determination of air permeability" [232] which states a sample size should be 100mm by 100mm if the analytical device used to determine the air permeability is incapable of handling large sample sizes. For analysis, the minimum size the sample can be is 50mm by 50mm, plus approximately 10-15mm on each length to prevent accidental air leakage which would impede results and ensure adequate sealing. Initial testing utilised the 25mm by 200mm sample, but it was found that air leakage occurred due to the size of the 25mm length being below the minimum of 50mm, which prevented adequate clamping/sealing. Due to the nature of the study, sectioning of the sample was ill advised given the potential for sample misrepresentation, therefore the decision was taken to keep the sample whole whilst analysis was performed, which was acceptable under BS9073-15:2008 "Determination of air permeability" [232].

Laboratory practice saw the isolation of three 30cm long samples in the vertical length at the vertical top, middle and bottom, respectively. Once removed, an incision at the stitch point allowed the media to transition from cylindrical to flat. At this stage, removal of a latitudinal and horizontal sample for tensile testing and/or elongation ratio determination as per the standard could occur. This approach resulted in enough surface area for the air permeability assessment in both directions and provided enough surface area for all additional testing required. The defined sample size in this study of 30cm in the vertical height which represented the vertical top, middle, and bottom contradicted the standard, but was allowable if agreed prior to the standard.

Naturally, no withdrawal of extra samples occurred for analysis, given the study focused on the air permeability variation only. In addition, the removal of the representative sub samples in the vertical top, middle and bottom occurred at the vertical centre of each respective third. These defined locational points where kept constant between the AR and PC states, which allowed for further analysis of the filtrate/cake and deviation from new media. Though not required by the standard, they provided a greater insight into the sample. Lastly, the stitch point data was removed which is not required by analysis in BS 22031:2021 "Sampling and

test method for cleanable filter media taken from filters of systems in operation" [16] and is common practice within the laboratory. Resultantly, this led to a 5 by 5 matrix of 25 datapoints which represented the air permeability of each section.

6.3.1 Definition of Sample Size

In accordance with BS9073-15:2008 "Determination of air permeability" [232], a minimum of five readings were taken, with the mean, and confidence interval reported. For the given sample size of twenty-five, this resulted in 53130 potential combinations. The assumption made was that regardless of the normal distribution, the probability of picking a location for analysis was equal. This allowed for the determination of each combination. From this, Table 31 reported the obtained mean and resultant confidence.

However, the determination of air permeability through five samples is only a guideline and is amendable upon agreement prior to the start of any analysis. BS 22031:2021 "Sampling and test method for cleanable filter media taken from filters of systems in operation" [16] required only three samples be taken from each sample. This reduction in sample number inadvertently suggested that the difference between five samples and three may be negligible. This reduced the number of potential combinations from 53130 to 2300, assuming no repetition for both cases. This data was summarised in Table 32. One of the major advantages of a lower sampling size is the reduction in sample processing time. This argument could explain why BS 22031:2021 "Sampling and test method for cleanable filter media taken from filters of systems in operation" [16] deviated from BS9073-15:2008 "Determination of air permeability" [232]. This reduction would almost double the evaluation speed of the air permeability testing. Furthermore, it would allow for a quicker turnaround time of the analysis and allow the operator(s) of the bag house to react more quickly than with a five-point sample. Preliminary analysis of 3 vs. 5 sample points (including the 95% confidence interval to understand the potential spread of the air permeability value) would suggest that the former is more appropriate, however comparative analysis of Table 31 and Table 32 should be conducted before this decision is implemented throughout the analysis.

Overall, the absolute average difference between Table 31 and Table 32 falls to 3.19% which suggested that the difference in sampling number had little effect on the defined samples. Isolation of the most notable variation was in the PC vs. the New state, which saw a 1.69%, 6.98%, and a 11.67% for the vertical top, middle and bottom, respectively. In comparison to the other states, the percentile range was comparatively lower at ≈3%, where the global

average was 2.12%, 1.83%, and 2.02% for AR, PC, and cake/filtrate, respectively. In terms of quantification, the 11.67% difference equated to an air permeability of 6.16 $Ldm^{-2}min^{-1}$ which is well within the confidence interval of both tables. This consideration, applied across all other states, revealed that the variation was approximate to 2.60±1.36 $Ldm^{-2}min^{-1}$. This resulted in, unless otherwise stated, that the determination of a sample's air permeability being represented by three random sample points as stated in BS 22031:2021 "Sampling and test method for cleanable filter media taken from filters of systems in operation" [16].

Table 31: Resultant Value of Air Permeability at 200Pa from a 5-sample Mean

	Data Category			
Section	AR	PC	Recovery/Difference	PC vs. New
N=1 (Vertical Top)	128.80±33.51	209.48±45.72	80.53±39.76	-46.59±45.56
N=2 (Vertical Middle)	131.15±26.22	191.84±31.81	60.64±28.18	-64.19±31.77
N=3 (Vertical Bottom)	129.01±33.69	209.50±45.61	80.45±39.83	-46.62±45.59

Table 32: Resultant Value of Air Permeability at 200Pa from a 3-sample Mean

	Data Category			
Section	AR	PC	Recovery/Difference	PC vs. New
N=1 (Vertical Top)	127.54±32.89	209.16±46.15	80.51±39.92	-47.39±44.16
N=2 (Vertical Middle)	133.76±26.92	196.12±27.46	62.27±33.02	-60.00±27.47
N=3 (Vertical Bottom)	124.76±24.68	203.10±24.81	77.80±20.22	-52.78±24.14

Results stipulated in Table 31 and Table 32 are the product of the following assumptions:

1. The probability of picking any datapoint is equal, regardless of its location.
2. There is a negligible amount of ordered sampling. Ordered sampling is were the next datapoint is immediately adjacent from the previous (not random)..
3. The central position of the sub-sample (25 datapoints / 5 by 5 matrix sample), of each vertical third, is representative of the overall original third, regardless of the surface area size available for analysis in said third.

Linked together, assumptions 1 and 2 are down to the sampling behaviour of the analyst. The definition of ordered sampling is the structured analysis of a sample, which saw the sample only changed in one fixed direction, which results in a solely latitudinal/longitudinal mean. If true random sampling followed, the first assumption holds true. However, external subconscious bias could enter the analysis, whereby the analyst continually repeats the determination in a specific pattern. Exacerbation of this could occur by the analyst intentionally/unintentionally performing ordered examination of the sample for example. Consequently, the assumptions would fail due to the exhibited bias. If biasness occurred within the analysis, then the first assumption becomes untrue, given an unconscious preferential sampling structure (focused about a particular area and/or ordered sampling).

Lastly, the third assumption was implemented not only for the construction of the above two tables, but also for compliance in BS 22031:2021 "Sampling and test method for cleanable filter media taken from filters of systems in operation" [16]. This assumption originated from the necessity to perform analysis quickly, without excessive repeating. The total time taken to complete the analysis of air permeability mapping in both the AR and PC states amounted to five days, which is not feasible if multiple bags required analysis. Consequently, the high-resolution mapping of air permeability, across a full, used, filtration bag afforded an insight into the potential variability. If this assumption is incorrect, then there is the requirement for an alternative approach, following careful analysis of the subsequent data.

6.3.2 Fixed Sample Positions

The definition of a "fixed sample position" in this study is an assumed representative sample taken centrally from the vertical top (N=1), middle, (N=2), and bottom (N=3), analysed in a specific pattern. Subsequently, definition of this pattern is being either in the fixed cross variable machine direction or fixed machine variable cross direction. This resulted in two distinct results from the each of the N=X section(s). Whilst the recommendation is random sampling (no pattern), there is no guarantee that this will occur; particularly when mass testing within a limited timeframe occurs.

Isolation of three samples, each 30cm length in the vertical height, at the centre of each vertical third from the data each represented their original vertical sections and described the N = X sections. These samples yielded a five-by-five matrix as shown in Figure 49. The mean ± confidence interval was previously reported in Table 31 (five sample mean) and Table 32 (three sample mean). As shown in Figure 49, a range of air permeability values

where observed. This resulted in average ranges of 99.38±14.67 $Ldm^{-2}min^{-1}$ and 117.40±63.30 $Ldm^{-2}min^{-1}$ for as received and post cleaned, respectively. Due to the occurrence of a significantly high datapoint in PC N=1, the resultant range and confidence interval where artificially higher.

Visualisation of the data in Figure 49 suggested a degree of variation in the results. Throughout all the dataset's, the minimum range of the data was 80 $Ldm^{-2}min^{-1}$ which suggested the extent of the variation. Application of a colour scale helped to reveal areas of specific higher/lower air permeability. However, given the classification of the data into a particular colour was dependent on the resultant data range (±2s.f.), the resultant colour profile indicated the range in terms of the data's maximum and minimum. Visually, there appeared an equal distribution of the data within the range. No apparent trends where observable, except for a fixed cross, variable machine direction (FCVM) in N=3 across both AR and PC. Additionally, for both AR N=1 and N=2, the fixed machine variable cross (FMVC) direction at sample point 5 appeared to exhibit a somewhat parabolic pattern. Other regions supported this, but quantitative assessment is required to determine the validity of this observation.

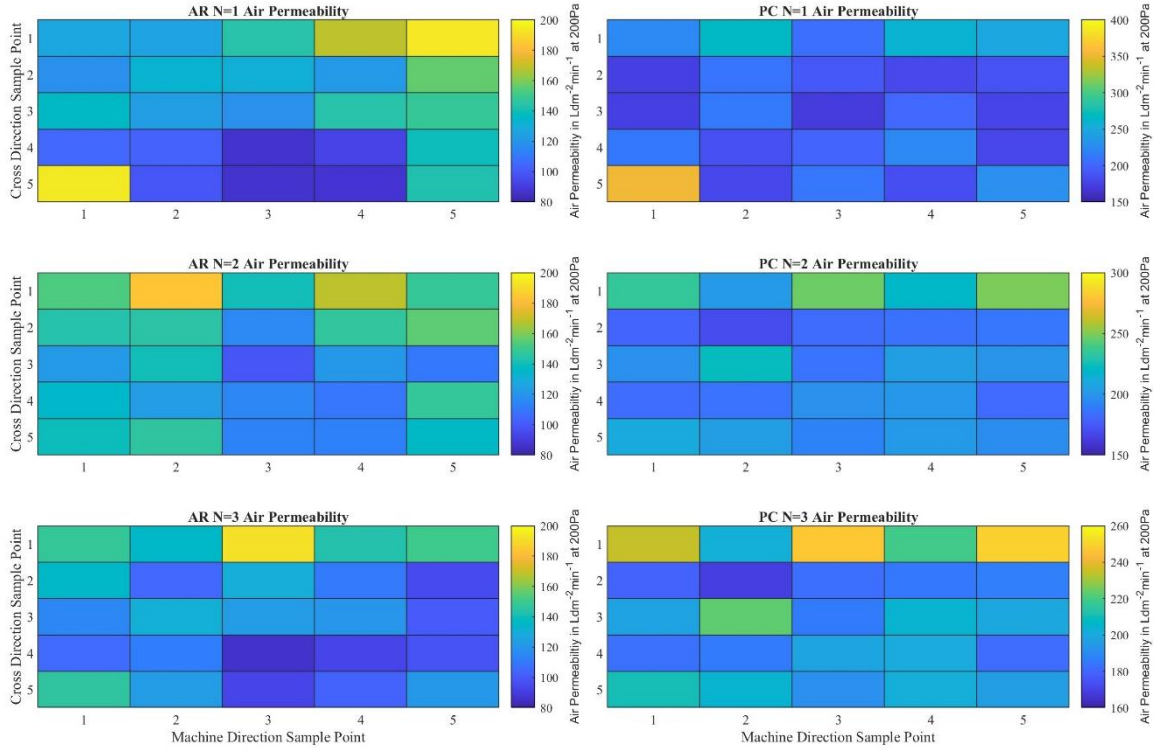

Figure 49: Air Permeability Maps of Each Middle Section of N=1, 2, and 3 in the AR (left column) and PC (right column) States

Data from each section in Figure 49 allowed for quantitative assessment through statistical testing. Due to the Gaussian distribution, a t-test used the global mean as the original mean to determine statistical significance. The new mean and respective standard deviation were determined following a fixed cross/machine direction with respect to a variable machine/cross direction, respectively. Subsequently, each state and vertical position revealed ten unique t-scores. Calculation of the respective t-scores is shown in Table 33 for the as received state, and Table 34 for the post cleaned state. Determination of a statistically significant mean (the new mean is not equal to the original) was set at 5% and 1% of getting a more extreme result, respectively. The results are reported as a percentile at the bottom of Table *33* and Table *34*. For the post cleaned state, evidence suggested no statistical significance existed across any of fixed/variable directions. Given the narrowness of the distribution exhibited in each of the post cleaned dataset, the occurrence of no statistically relevant means was not a surprise. Figure 49 showed that the data appeared to cluster about a set value, where only a couple of each of the datapoints, per set, appeared to be greater/lower than this apparent pivotal point. When a higher/lower datapoint existed in the section, the resultant score only changed slightly. This showed that although the apparent range was large, due to the narrow distribution and minimal occurrence of larger/lower datapoints, the resultant new mean was statistically like the global mean.

AR state showed that a quarter of the data was statistically significant in the FMVC direction which visually suggested a parabolic nature in Figure 49. Significance occurred due to the increased difference between the global and new mean. If a parabolic relationship existed in the data, then the resultant new mean would likely show significance dependent on the severity of the curve. At a 5% confidence, 16% (4 positions) of the FMVC direction demonstrated significance, which suggested that the visual observation may hold some validity. Whilst this reduced from 16% to 12% of the total FMVC directions, it provided more evidence that support this decision. Whilst some of the FMVC direction may be statistically significant, this test wouldn't be able to conclude if any of the results as being parabolic or otherwise. Therefore, the statistical test only showed that there is a difference in this direction, and based on previous observations, this could be due to an apparent parabolic region within the FMVC direction.

Table 33: As Received State Results from t-testing Against the Overall Mean and Fixed Sampling Position Mean

	Fixed Cross Direction (cm) Variable Machine Direction				
	9.7	16.4	23.1	29.8	36.5
N=1	0.115	-0.369	-0.529	-0.131	0.263
N=2	0.128	-0.099	0.835	1.340	-2.695
N=3	0.924	0.529	-0.814	-0.048	-1.390
	Fixed Machine Direction (cm) Variable Cross Direction				
	0	+8	+16	+24	+32
N=1	0.097	-0.367	-0.261	-0.079	0.550
N=2	3.448	-0.435	-1.765	-2.373	-0.140
N=3	3.094	-0.193	0.373	-4.873	-1.178
Percentile Occurrence where $P(\lvert t\rvert \geq \lvert t_{\alpha,v}\rvert)$					
		$t_{0.025,24} = 2.064$		$t_{0.005,24} = 2.797$	
FCVM		4.00%		0%	
FMVC		16.00%		12.00%	

Table 34:Post Cleaned State Results from t-testing Against the Overall Mean and Fixed Sampling Position Mean

	Fixed Cross Direction (cm) Variable Machine Direction				
	9.7	16.4	23.1	29.8	36.5
N=1	0.5663	-0.6917	-0.5177	-0.2260	0.1376
N=2	0.3203	-0.1780	-0.5434	-0.1998	0.4142
N=3	0.5882	-0.6843	0.0241	-0.2751	-0.1702
	Fixed Machine Direction (cm) Variable Cross Direction				
	0	+8	+16	+24	+32
N=1	0.1102	0.0192	-0.3784	0.0109	-0.0718
N=2	-0.1803	-0.0408	0.5428	-0.1531	-0.0041
N=3	0.1859	-0.0362	-0.1312	-0.0351	-0.0255
Percentile Occurrence where $P(\lvert t\rvert \geq \lvert t_{\alpha,v}\rvert)$					
		$t_{0.025,24} = 2.064$		$t_{0.005,24} = 2.797$	
FCVM		0%		0%	
FMVC		0%		0%	

Visually perceived in Figure 46 and Figure 47's AR and PC state was an apparent parabolic nature in the cross direction, which was visible due to the classification of the data into a heat map based on the global minimum and maximum of the dataset. To ascertain this mathematically, a box and whisker plot of the data, against its respective cross directional

point was drawn and shown in Figure 50, which aided to demonstrate any potential relationship within the data. To complement this figure, inclusion of each datapoint against its respective cross direction, regardless of its original machine direction location, showed whether it could be an outlier or was within the confidence of the cure fitting. The resultant cure fit of the data in Figure 50 across both AR and PC states, revealed a strong correlation towards the data being parabolic in nature. Equation 28 described the resultant parabolic fit and determination coefficient for both he AR and PC states.

The stitch data was included in the analysis of Figure 50 and subsequent determination of the parabolic nature, due to it completing the cylindrical nature of the original sample. However, the accuracy of the data for the stitch point data has previously been questioned, owing to the possibility of secondary air ingress due to insufficient clamping of the sample during examination. Regardless, omission of this data still suggested a parabolic like nature existed in the data visually.

The observed local minimum for both the AR and PC state occurred between the 23.1cm and 29.8cm cross direction position, at positions 28.8cm and 26.2cm, respectively. This resulted in a difference of 9%, or 2.6cm. This difference likely stemmed for the combined errors within the sampling method, whereby slight deviations in the examined positions between the AR and PC state saw a slight shift in the location of the local minimum. Regardless of this shift, the local minimums in both cases still occurred between the 23.1cm and 29.8cm region, which suggested that the actual local minimum could originate somewhere within this region. Consequently, the local minimum for both cases appeared to originate roughly at the 27.50cm length of the cross direction. The parabolic cure fit and coefficient for both the AR (φ_{AR}) and PC (φ_{PC}) state, in relation to the cross directional length (L_{cross}) are shown in Equation 28.

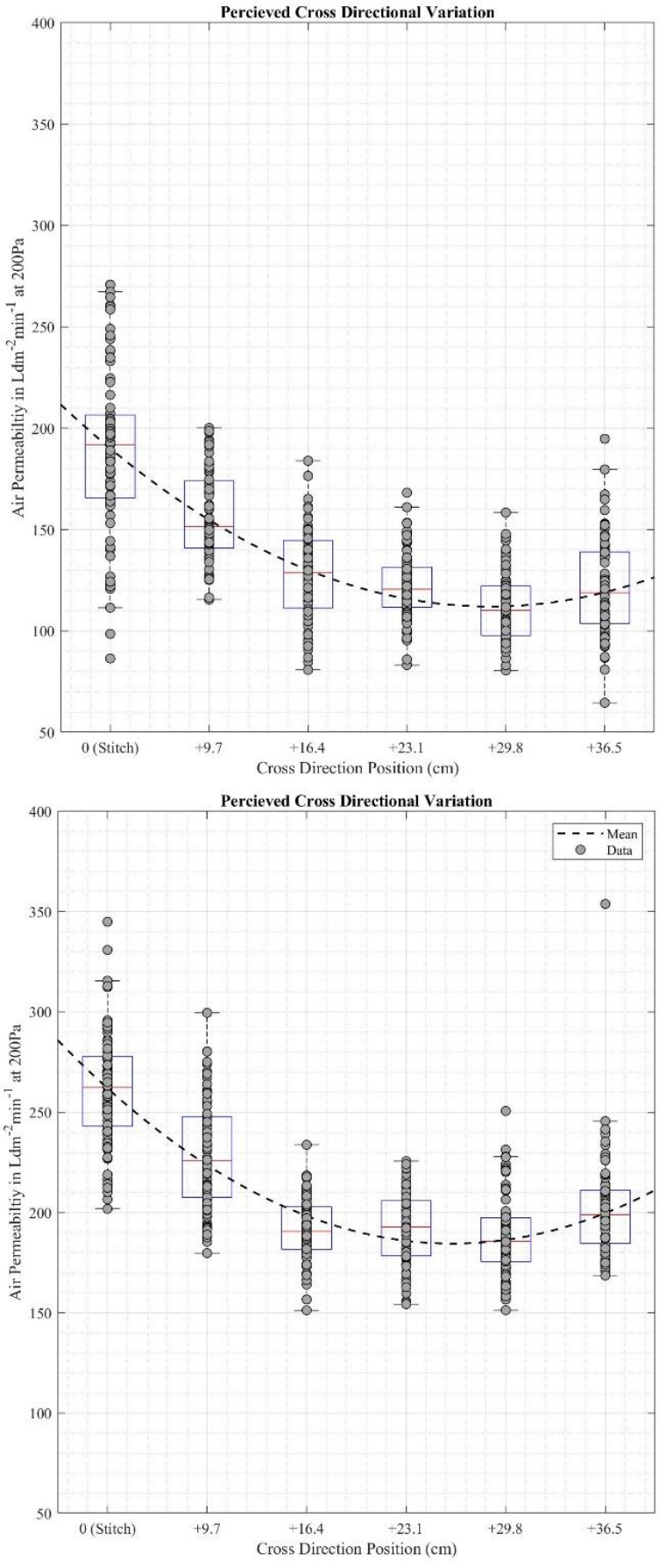

Figure 50: Fixed Cross Variable Machine Direction Analysis of Air Permeability Variation in the AR State(top) and the PC State (bottom)

$$y = ax^2 + bx + c$$
$$\varphi_{AR} = 5.27L_{cross}^2 + (-51.10L_{cross}) + 235.90\ (R^2 = 0.99)$$
$$\varphi_{PC} = 6.45L_{cross}^2 + (-57.59L_{cross}) + 313.10\ (R^2 = 0.96)$$

Equation 28: Mathematical Description of Curvature Through Quadratic Regression

Suggestion of a local minimum implied, to an unquantifiable extent, that preferential flow could have occurred. In the AR state, a lower air permeability represented pore blocking at the surface which reduced the amount of airflow through at the given pressure. In addition, it could also be indicative of filtrate building on the surface, irrespective of porosity, which resulted in a lower air permeability. Upon cleaning into the PC state whilst recovery had taken place (as shown by Figure 50), there still existed some blocking of the pores which again reduced the airflow through the sample area. Figure 43 showed SEM images of both states and demonstrated that the amount of internal penetration of the filtrate varies. During sample acquisition for these images, the parabolic nature was unknown and therefore can only suggest the local minimum existing due to this penetration. Although, given that both the experimental and theoretical results coincided with the parabolic results (if blinding is prevalent, then the AR state will also exhibit this air permeability reduction regardless of cake formation), no literature found supported this observation as no studies have assessed the effect of flow variation around filtration bags and its resultant effect on the media during operation.

Drawing on relevant studies for flow profile and single fibre particle deposition modelling suggested evidence to support the occurrence of a local minimum at the large scale. Recent advancements in CFD have allowed for the assessment of fibrous structures, to determine the structure at which deposits form on fibres. Hosseini et al,. [267] illustrated the formation of these deposits on a singular fibre, which suggested how each capture mechanism may perform under different flow conditions. The limitation with this, is that it is visually unclear as to what particles pass by, and in the context of filtration, if these particles are subsequently collected. Whilst the mathematical determination of the particle sizes can be used to suggest capture or evasion, it doesn't definitively define if it will or will not be captured/evaded. Other studies exhibited a similar conclusion such as Wang and Otani [155], Wang et al., [268], and Przekop et al., [269]. With the addition of multiple fibres, such as the work done by Wang et al., in [178], this obstacle can be overcome. One study by Wang et al., [178] showed that the difference between a structured and staggered array of fibres when collecting particulates under different collection mechanisms. Whilst their simulation gave an insight

into how the depth filtrate deposition occurs, the location of the formed deposition is noteworthy. Both interception and impaction deposition appeared to deposit at the inlet side, whereas diffusion deposition occurred all around the fibres.

Directional flow will therefore dictate the prevalence of a particular capture mechanism. If extrapolation of the deposition mechanism results to a flue gas bag are true, this would have suggested that due to the preferential flow through one side of the bag, a large amount (in comparison to other sides of the same bag) of the deposition will occur towards the location of this flow. The study by Wang et al., [178] could suggest that the fibre structure is representative of large scale bag houses in terms of how the filtration bags are positioned. This, coupled with the likelihood of preferential flow patterns as shown in CFD and experimental simulations by authors such as Chen [149], and Yang et al., [181], it could be suggested that the depositions noted in Wang et al., [178], mimic the overall prevalence of deposition (subject to actual operational parameters and conditions). Over time, the cleaning pulse will then likely transition the filtrate from the surface, where a proportion of the filtrate will fall into the hopper, but an unquantifiable proportion may be redeposited depending on the force of the cleaning pulse and the proximity to which it encounters another filtration bag. Kim et al,. [144] suggested that the distance the filtrate removed from the surface may be substantial enough for an unquantified proportion to redeposit onto a neighbouring bag. Whilst this could cause the Fourier like wave exhibited in Chapter 5 Figure 38, it would suggest that this effect on air permeability is negligible owing to only one local minimum occurring within Figure 50. Resultantly, there is a requirement for further tests about this theoretical reason to ascertain not only if this occurs, but also the prevalence (if it does occur) and any resultant effect that would occur both along the vertical height, but also across the baghouse spatially.

Only one, larger scale numerical study found combined their results with experimental data, which yielded promising results in favour of not only this chapter, but also Chapter 5. Liu et al., [241] illustrated that the mass and thickness of a candle filter exhibited a somewhat similar deposition model using CFD over a 1.5m vertical height, to that of Chapter 5. Whilst this data did not provide any evidence for the air permeability, it suggested, and supported the findings, given that the media used across both studies originated from similar industrial circumstances. Though this argument is weak, it is the closest study available currently, until the conduction of a methodical, academically controlled study.

The occurrence of blinding, or clogging of the pores within a nonwoven have been extensively researched in various studies such as Niefler et al,. [14], Thomas et al,. [139], Kim et al,. [144], Barros et al,. [156], Boudhan et al,. [162], and Schuberth et al,. [205]. These studies provided evidence that the media transitions between depth, to surface, to cake filtration which results in an increased differential pressure across the filter due to the particulate. Barros et al,. [156] and Niefler et al,. [14] provided example SEM imaging of the initial internal deposition in a filter. Over time, the baseline differential pressure increases due to increased internal deposits [205], until such a point where the blinding is so severe that the rate of differential pressure increase tends to infinity. Cirqueira et al,. [189] detailed the evolution of blinding/clogging as a function of cycles. Other factors, such as available surface area [144], gas humidity [162], filtration velocity [158], dust concentration [148], as well as particle size [213] and settling velocity [117] will also affect this. Due to the spontaneity/uncontrollability of the sample origin (due to the sample originating from an industrial application), these parameters cannot be definitively defined and correlated as to the reason behind the exhibit parabolic nature noted in Figure 50. Future studies, surrounding these parameters will allow for evidence to support or reject the findings of Figure 50.

Alternatively, the variation about the fixed machine direction, provided an indication towards the evolution of air permeability about the vertical height. Figure 51 illustrated this evolution for the sample, detailing the original cross directional position for each datapoint. Previous analysis has removed the stitch point data due to structural variation. However, it has been included in Figure 51 for one singular point of note: when comparing a large proportion of the data points and subsequent global mean value, the air permeability for both the AR and PC states showed that the stitch point exhibited a higher air permeability than the flat media. Further research about this subject will determine the reason, and if this occurrence has a negative impact on overall efficiency and longevity of the media. Barring the stitch media, Figure 51 also presented the global mean of the flat media data in the AR and PC state.

Visually, no distinct pattern transpired in the flat media datapoints across the machine direction. Figure 51 appeared noisy, due to the variation exhibited within the dataset. Figure 47 and Figure 49 examined a significant degree of “noise”, by showing that the air permeability value moved sporadically. They also showed that whilst the global data exhibited a parabolic relationship (Equation 28), the local variation may not resemble this. The latter point is refutable in terms of relationship validity through the way in which the conclusion as made following review of Figure 50. This variation transferred through into

Figure 51, due to the resultant difference between the minimum and maximum air permeability. Rotation of a singular machine direction data row 90° would suggest the variation in the cross direction at a given point, which was discussed previously.

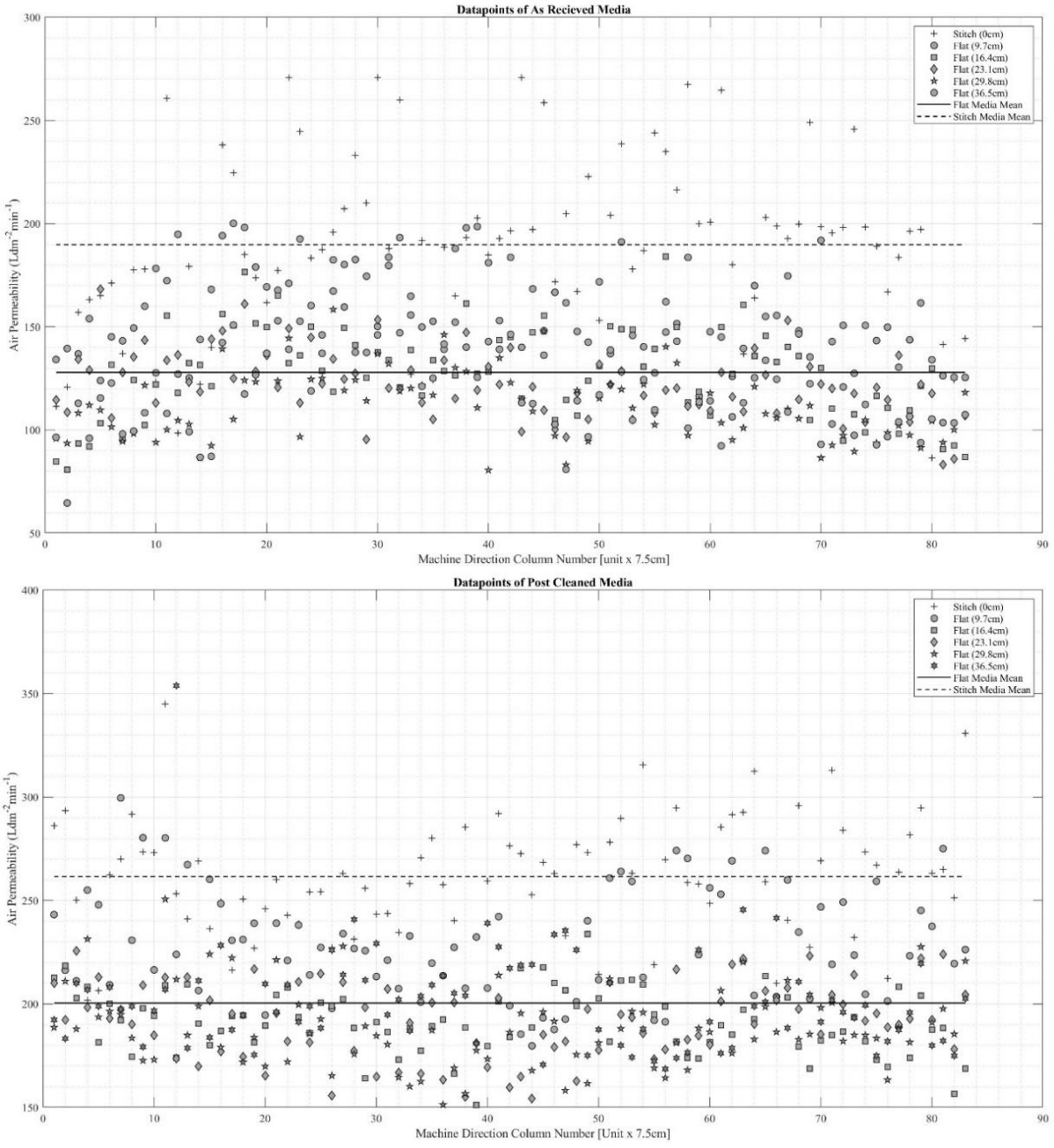

Figure 51:Fixed Machine Variable Cross Direction Analysis of Air Permeability Variation in the AR State(top) and the PC State (bottom)

6.3.3 Variable Positions

If the position on the vertical third is not central, this could impact the result obtained. Deviation from the assumed standard methodology that each sample from a vertical third is from the vertical middle examined this. For this, the sample size of 30cm in vertical height

does not change (which would yield a possible twenty-five datapoints) and that the number of repeats is equal to three. This also assumes that taking an average of three datapoints is representative of the total sample size, which is discussed further in section 6.3.4. For sample positions 1-4 and 81-84, these would have ascending/descending multiples of five respectively, given the evolution of the sample size to represent the original sample size. A sample size of twenty-five, with three combinations yielded 2300 combinations. If all 2300 combinations where calculated, the resultant confidence interval would be significantly low. To obtain a better representation of the potential variation, a limited repeat of ten times occurred. This yielded a high sample range, which would better represent the mean and indicate any potential improvements to the method. This somewhat counterintuitive method allowed for the illustration shown in Figure 52, which showed what could happen if an analyst decided to deviate from the centre of the third and chose to evaluate a different location.

Initial observations led to the suggestion of a somewhat parabolic nature exhibited during the comparison between each vertical third in Figure 52 in the AR and PC state. Indeed, curve fitting would yield parabolic equations for the AR state and PC state ($\varphi_{AR} = -6.27x^2 + 24.75x + 109.6$ and $\varphi_{PC} = 6.13x^2 - 28.35x + 228.10$), but as shown in Figure 52, the evolution of air permeability, through the vertical height, doesn't necessarily conform to the apparent parabolic nature. Firstly, the mean of each datapoint didn't truly suggest a parabolic. Though it did appear to have a shape, it may not be truly classified as parabolic given the potential skewness and variation within the data. Secondly, the resultant curve fit was going to return a compelling argument based on the degrees of freedom which provided a false positive. Any further argument for the apparent parabolic nature is by combining the first and second observations against this apparent parabolic nature within Figure 52 was rejected.

One problem during multiple flue gas filtration bag sample evaluations is the potential for slight deviations from the midpoint. Indeed, the standard BS22031:2021 "Sampling and test method for cleanable filter media taken from filters of systems in operation" [16] failed to specify the specific location, thereby allowing an analyst to take a sample from anywhere within the vertical third, whilst still technically complying to the standard. This assumption is problematic, given that it allowed for two neighbouring samples taken at the third's interface, and assumed representative of their respective third. In Figure 52, For the AR state, this would suggest that the vertical middle is like that of either the vertical top or bottom. Whilst this is also the same for the PC state at the vertical top, there is a larger difference between

the vertical middle and bottom. Consideration should also be given towards the location of these mean points, with respect to the global mean and confidence interval. In both cases, if the sample taken at the boundary of the vertical third, there is a high probability of yielding a resultant mean outside the bounds of the global value, which would obscure the accuracy of analysis. This illustrated that if the analysis performed deviated from the centre point of the vertical middle, there is a probability that the resultant mean received would not in fact be truly representative of the global mean, providing further illustration that the apparent parabolic nature is false.

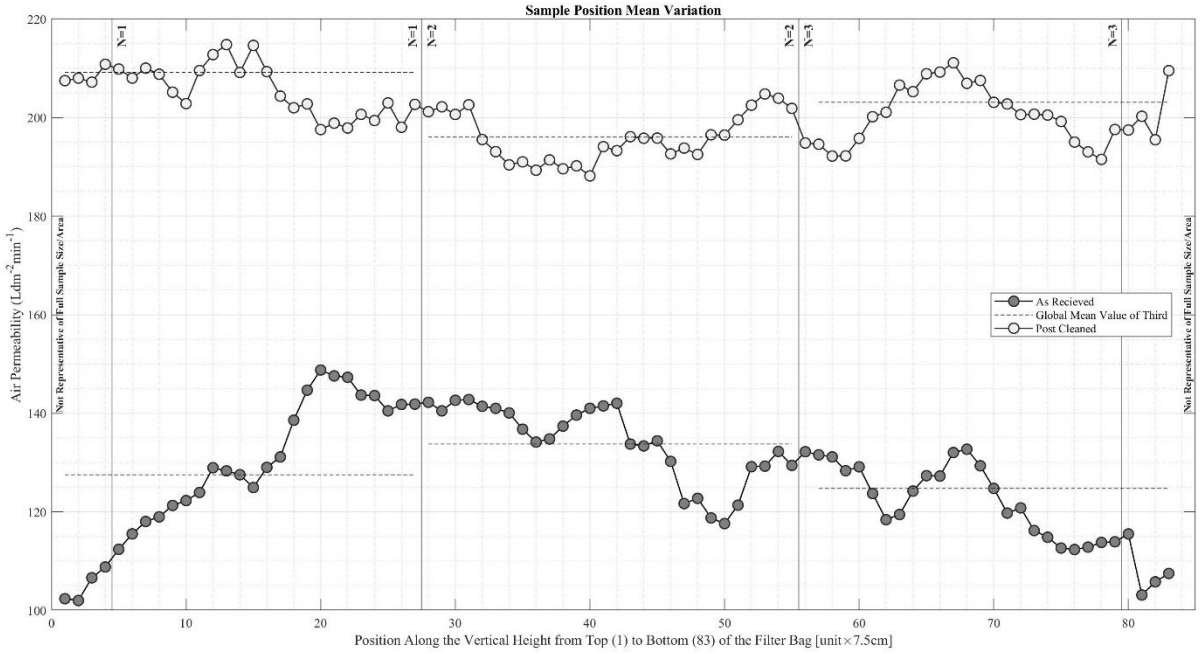

Figure 52:Variable Sample Position Along the Vertical Height of the Full Non-woven Filtration Bag Whereby the Potential Mean is 10 Random Arrangements of Three Random Datapoints Taken from a Maximum of a group of 25 Consecutive Datapoints

Given the variation between the sampling position, another sampling position may warrant examination. Whilst the midway point gave a representative mean of the overall global mean of the respective vertical third, there is an unquantifiable likelihood that other positions may not give the results. As such, assessment of either the centre position, or a minimum of two separate locations would increase the chance to yield a representative global value. The issue with the latter point is that the turnaround time of performing the sample preparation and examination doubles. This would raise the question: Although performing examination in two known locations yields a better understanding into how the air permeability changed over the vertical height. This further questioned whether doing multiple samples of each vertical third added extra value for increased sample turnaround time. It may therefore be more beneficial to perform a larger number of repeats on a single sample, which would give a better

estimation to the range, but reduce the time required in comparison to performing the analysis again in a different location. This ideology could include a fixed cross directional study on the singular sample as previously mentioned. Overall, given the standards requirements, it is not a requirement as the standard assumed that, regardless of the chosen position, the resultant mean is representative.

Inclusion of the confidence interval should also be a requirement, given it could show how the assumed representative region sample is evolving over time. Currently, the standard does not require (only recommends) the reporting of the confidence interval. However, it can potentially provide useful during the evaluation of historical data. If the mean stayed the same, but the confidence grew, this would provide an indication that other regions could be experiencing a larger range of air permeations. The time required to calculate and include the confidence interval in the final report is minimal, given it can be calculated automatically.

6.3.4 Large Scale Sampling and Analysis

Industrial bag house filtration units vary in size and structure, which weakened the assumption that a single sample is representative of the entire unit. The sample withdrawn from service for this study originated from a one of six compartments in a bag house, which had approximately one hundred bags per compartment. Due to previous periodical tests, the age of the filtration bag received could have been 2-3 years of service (including downtime/offline). The combustion site did not supply any other information about the sample. As stated in BS22031:2021 “Sampling and test method for cleanable filter media taken from filters of systems in operation” [16], acquisition of a representative sample is difficult due to the size and structure of the bag house. Extension of this is to the bag house cell, due to the resultant flow and filtrate characteristic variation into each cell. Whilst this has been studied and optimisation performed by authors such as Shin et al., [142],Chen [149],Chen and Cheng et al., [181],Nielsen et al., [186], and Pereira et al., [259], an inherent degree of variation will remain, particularly due to the fuel characteristic variation. To compensate this, BS22031:2021 “Sampling and test method for cleanable filter media taken from filters of systems in operation” [16] recommended a minimum of one sample per cell is taken at the point where the flue gas concentrated. However, they stated that the resultant degradation of the sample varies element by element. This variation across the cell resulted in an unquantifiable degree of difficulty to ascertain a representative sample from a singular point. Consequently, multiple samples require analysis from a cell for a better understanding of the approximate degradation as a function of the spatial dimensions of the cell or bag

house. Each cell can be divided into nine sections to aid in the determination of variation at the cell level [16].

Isolation of multiple bags, per cell, can quickly escalate the time required to perform analysis. Factors which affect the turnaround time, such as removal, transportation, preparation, analysis, and data interpretation contribute to this time requirement. Except for transportation, an increase in samples will have a correlated increase on the overall downtime of the baghouse. During analysis, the baghouse remained offline, which allowed for any implementation of the results/findings from the analysis. Downtime negatively affected the profitability of the commercial plant, given the requirement for the full site to be offline to allow full access to the bag house. Isolation of a single (or multiple) cell is achievable, but this will increase the load onto the other filtration bags/cells. Therefore, the turnaround time should be as low as possible, to ensure that an increased rate of degradation is minimised and/or the site remains offline for as short a time as possible.

Therefore, the sample size of 30cm in the vertical height from the filter bag, per sample, should be minimised without compromising on the result and required timeframe to complete the evaluation. As previously mentioned, BS 22031:2021 "Sampling and test method for cleanable filter media taken from filters of systems in operation" [16] required six samples to be taken, which were undersized for adequate air permeability testing. Resultantly, this study used a sample size of 30cm in the vertical height across the full circumference (cross direction) of the filter bag. Figure 53 provided an illustration of the differences between both methods. Both methods required the division of the filtration bag into three vertical sections: top, middle, and bottom. After which withdrawal of a sample(s) occurred for analysis. The main difference between the methods shown in Figure 53, is this study removed one sample per section, as opposed to the standard which required two. Initial indications reduced the sample preparation time by half owing to three sub samples as opposed to six. Section 6.2 and 6.3 discussed the data implication of this in greater detail. Although Section 6.2.1 showed that this studies method can achieve a representative mean of both the sample and vertical section, there is still the possibility for further optimisation to reduce the time required to perform analysis.

Discussion around the minimisation of repeats was conducted about each vertical sample as shown in Table 31 and Table 32. These tables used random dispersal across three to five evaluation points. This, repeated ten times, allowed for a larger confidence interval, which

showed a suggested variability which might occur when repeating this method under a fixed sample size. Whilst a slight difference occurred, it was not statistically different. This raised the question as to what would happen if the sample size increased, or more importantly decreased. Decreasing the sample size would result in time saving, however, this would cause a more statistically different mean and therefore would not be representative of the overall sample.

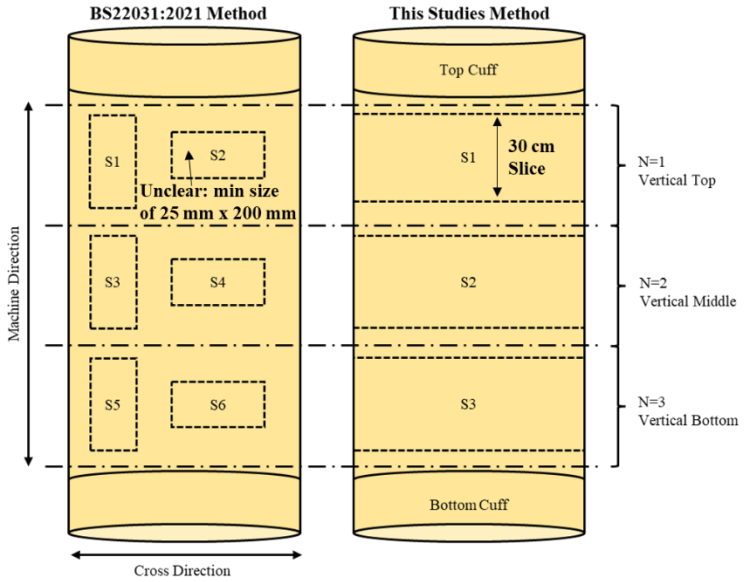

Figure 53: Illustration of Sub-Samples Taken from A Filtration Bag Using BS22031:2021 [16] (left) and this Studies Method (right)

Figure 54 graphically demonstrated the effect of increasing the sample size from one to twenty-five, including a horizontal line showing ±10% of the global mean (GM). Calculation of the mean was determined from the random arrangement of the data across ten times. Ten samples yielded a large range of potential means, which would prove more representative of the potential mean variation during analysis in an industrial setting.

Overall, as the sample size increased, there was an overall decrease in the representative mean moved towards the global mean at sample size 25. This is due to the increase in sample size towards the maximum of 25, the maximum sample size available for the defined sample surface area. Sample size less than 5 exhibited a larger potential range in comparison, due to the variance within the whole of each specific dataset. The extreme case is the first sample point, which could see the resultant "mean" be anywhere within the range of the minimum/maximum of the data. Although Figure 54 suggested that a sample size of ten random samples may display a representative value of the sample, there is a degree of uncertainty given the probability of obtaining the highest or lowest is the same as the mean

value reported. Given this consideration, the sample size should be no lower than 3, which is required for standard compliance.

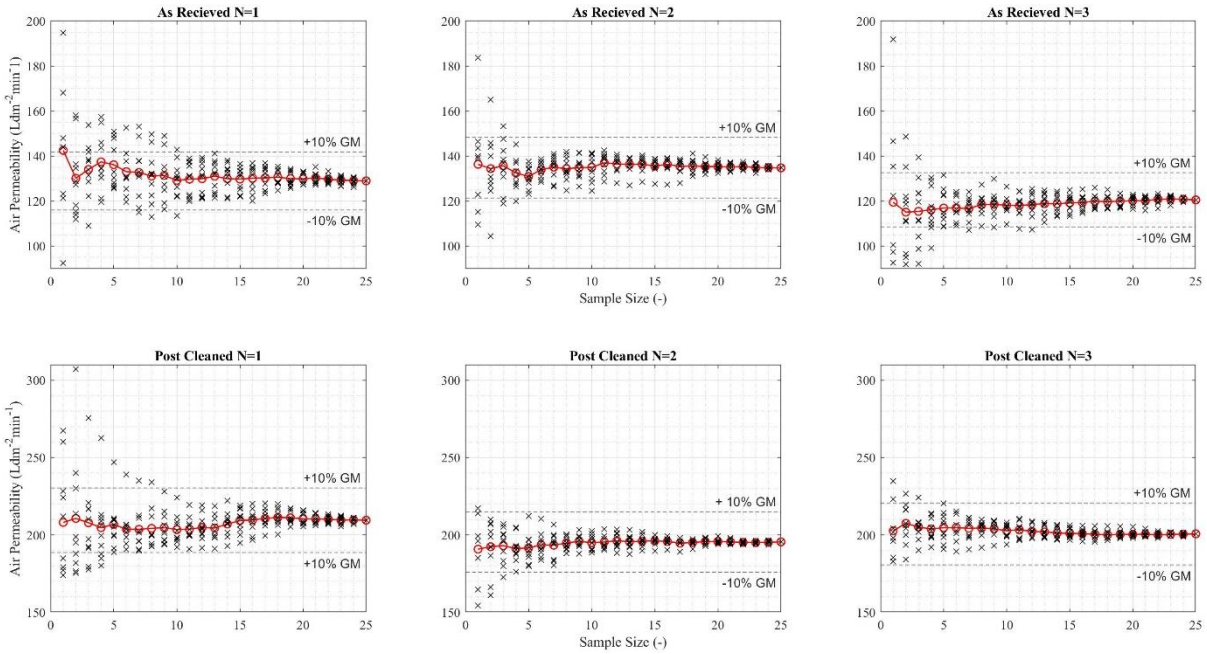

Figure 54: Effect on Mean for Each Vertical Section Under the As Received (top row) and Post Cleaned (bottom row) State, when the Sample Size is Increased from One to Twenty-Five

6.4 Conclusion and Further Work

Conduction of a high-resolution air permeability study, on used nonwoven filtration media within literature, had not occurred until this study. Standard air permeability assessments can require, assuming that the sampling is random, less than 1% of the total surface area to be examined. However, this value is dependent upon the total surface area available for assessment, which is governed by the vertical height and circumference of the filtration bag. Consequently, this methodology assessed a surface area >10% which is a significant increase in the examined surface area. Structured assessment of the surface area allowed for: air permeability mapping, variation assessment, and assessment of the current standard assessment method. This study concluded that:

- Fixed directional assessment can lead to a statistically significant/different mean of the given "N" value sample (the vertical third sub sample) when compared to the global mean of the same sample. Random sample points ensured a better representative mean.
- A parabolic relationship existed in the fixed cross directional when examining the full data. This relationship had a variation coefficient of 0.99 and 0.96 for the AR and

PC state. Whilst recovery occurred, there was a prevalence towards the 27.50cm region for the filtrate to congregate which resulted in a lower air permeability. Due to the PC state's local minimum also being within the 27.50cm region, it is likely that blinding may be a factor which contributed to this.

- For a random 30cm in vertical length sample from the vertical third region, there is a high likelihood of returning a representative air permeability mean of the global third. Figure 52 suggested that whilst the point is true, there is still a degree of variation which may obscure the reported results.
- One limitation is the time required to process multiple samples. The original standard/methodology required three samples, one to represent each of the vertical thirds. Each sample underwent three air permeability tests, at an assumed different location (though not stated within the method). Following evaluation of the number of repeats, Figure 54 showed that the difference between three and five repeats was insignificant, with the main difference being a slight reduction in the confidence interval to which the resultant mean may be located. As such, the number of repeats should remain at a minimum of three. Consideration towards the increased time requirement to perform additional analysis against the fixed cross direction and/or additional samples along the vertical height, to obtain a better understanding of how the media varied across the surface area.

This study provides the basis for further work in a large scale understanding of how air permeability changes during operation. No previous study assessed such a large surface area in the AR or PC state or demonstrated that the difference between these two states revealed information about the resultant cake/filtrate layer on the surface of the filtration media.

Further work

- Development towards the understanding as to how the stitch point would affect the air permeability. Apart from the top and bottom cuff, the stitch point is the largest structural variation exposed to operational conditions. Whilst products, such as lamination tape exists to "reduce particulate penetration," there is minimal literature available to demonstrate how the stitch behaves during operation.
- Conduction of an air permeability study, over service time, would ascertain if the parabolic relationship noticed in the cross direction is coincidental or indicative of nominal operation. This can lead to understanding of where failure can occur in future

samples. Microscopy imaging will prove consequential to this study, as it would indicate if blinding were the reason, but also suggest a rate of blinding under the samples operational conditions.

- An academically controlled pilot scale study to determine how the evolution of air permeability occurred throughout its operational life. This will allow for better modelling towards predicting the longevity of nonwoven filtration media in flue gas combustion filtration systems. This could also be done using industrial samples but would have to account for the spatial variation in the bag house and time between new media installation and when the full bag house media would be changed (approximately 3-4 years).

Impact (Academic and Industrial)

The study provided the basis for future research in air permeability variation in industrially used nonwoven filtration media, controlled studies assessing any parabolic relationships in the cross (and potentially) and machine direction, and air permeability evolution over operational time.

This chapter has furthered understanding of variability during periodical nonwoven filtration media testing from combustion sites. This has enabled analysts to better report how the sample has fared during nominal operation. The results presented at the international conference drew the attention of a member of the BSI, who sat on the committee for the standards used within the chapter. This led to a consultancy-based output on how the standards can better reflect the variability exhibited in a sample. Lastly, the results provided sites and analysts with more information into how they may yield further results from their samples, without having to invest in additional equipment.

Chapter 7: Critical Evaluation of Longevity Study

7.1 Background Theory, Concept, and Coverage

Background Theory

Current practice to evaluate new nonwoven filtration media relies on the methodology laid out by BS11057:20211/VDI 3926(part 1 and 2). Discussed in Chapter 2, the methodology provided a process only for the evaluation of new filtration media. The aging step of thousands of pulse cleaning was an attempt to simulate operation, without the negative impact of operational time, which allowed for completion of the evaluation in hours as opposed to months or years. Previous literature studies such as Yeo et al,. [13], Schuberth et al,. [205], Hoppe et al,. [225], Akduman et al,. [227], and Yeo et al,. [234] provided a platform for the results to be academically comparable, under set parameters including the dust type. Whilst standardisation of the experimental methodology yielded a more academic study, its inadvertent omission to evaluate industrially used filtration media raised the question: “Is there a methodology to evaluate industrially derived used samples?”

In flue gas filtration, both chemical and mechanical degradation occurs on the media. The latter occurred through the oscillation between filtration and cleaning processes. Forward consideration is towards filtration bags which remain open through a metal cage and cleaned through an injection of compressed air: which was the most common approach observed throughout this project. Mechanical degradation occurred through internal deposition of filtrate [189], [205] and expansion and compression caused by cleaning and filtration process directional forces [200]. Oscillation between the expansion and compression against the support cage creates points of wear, whereby the media is constantly rubbing against the metal [200]. In addition, depending on the design and finish, this could create unintentional failure points, particularly if the cage exhibited sharp points which acted may cut the media [198]. Over time, this created indentation marks on the air exit side of the media. Operational temperature, fly ash composition, and flue gas composition (including moisture) will affect the chemical degradation of the fibres [187], [203]. In contrast to the methodology presented in BS11057:20211/VDI 3926 (part 1 and 2), only mechanical degradation is possible, owing the use of compressed and ambient air as the carrier gas through the test facility.

Consequently, a discrepancy between the assumptions made for the methodology led to the uncertainty around the use of the standard towards the evaluation of used filtration media. Unless exact, site specific, operational parameters where known and replicable, any

evaluation method would result in deviation which would potentially impact the results. One of the critics of the BS11057:20211/VDI 3926 (part 1 and 2) methodology, was the four stages presented, particularly the aging step which effectively force cleaned the bag multiple times without dust flow. This would only occur in normal operation if the media was so saturated with filtrate, that the differential pressure post clean was higher than the cleaning differential set-point. In addition, the changed set differential pressure cleaning point and number of cycles performed increased the complexity of analysis. Whilst any suggested new methodology to evaluate industrially used filtration media would match the exact conditions of its original site operational parameters, the simplicity of the methodology would provide a better reflection towards answering the question, using actual, expected, conditions.

Various authors have considered variables such as media choice such as Yeo et al., [234], expansion and contraction of the filter by Saad and El-Newashy [200], humidity variation by Boudhan et al., [162], and effect of pressure drop and efficiency with various particle sizes by Li et al., [137], but their studies often stop before complete failure. Studies which considered longer operational periods, such as 100 cycles by Cirqueira et al., [189],100's of cycles by Schuberth et al., [205], or even 1000's of cycles by Kurtz et al., [213], but failed to stipulate if the media had reached its end of life point or was just a defined stoppage point. BS11057:2011 "Air Quality – Test method for filtration characterization of cleanable filter media" [202] method to evaluate new, virgin, media has been applied in previous studies, but as it has a definitive endpoint and change in variables thought the methodology restricts the date obtained [5]. This led to a gap in literature about longevity prediction of the media. Whilst it is important to understand how the variables affect the performance, if they remained relatively constant, the only variable would be the remaining longevity/number of cycles/operational time of the filter: evaluation of longevity would provide an insight into how long the filter had left before a pre-defined failure point.

The proposed methodology was that once evaluation had begun; the test would continue until such a time that a pre-defined failure point had been reached within the sample. Like BS11057:20211/VDI 3926(part 1 and 2), analysis would require evaluation of a new filtration media sample, prior to the assessment of used filtration media under the new method initially. This provided a baseline result for comparison between new and industrially used samples. However, the proposed method afforded variability which allowed for the implementation of a site's specific parameters into the method as opposed to predefinition. Once defined, these parameters remained constant between the new and used filtration media

sample. Determination of longevity under the methodology of BS11057:20211/VDI 3926(part 1 and 2) is questionable given a clearly established end point, regardless of whether or not the filter has reached it. As such, the new methodology did not specify an endpoint, only that the test concluded upon the failure of the filtration media.

The definition of failure, in this study, was based on of three distinct points within the data:

1. The baseline differential pressure was equal to, or greater than, the cleaning differential pressure. At this point, the cleaning frequency increased to the point where cleaning occurs automatically continuously. This signalled that the cleaning recovery was not sufficient such that the filter had reached its usability.
2. The filtration cycle time dropped to 1-2 second intervals. Similar to the first point, in that the evolution of the differential pressure is so great that the cleaning demand is high. In contrast, the baseline differential pressure may be below the cleaning differential pressure, but the rate of differential pressure increase was so high that within 1-2seconds it exceeded the cleaning differential pressure point.
3. Lastly, failure could be due to the development of a hole or tear within the filtration media. Occurrence of a hole within the filtration media would result in increased emissions [197] as filtrate more readily passes through the void. Collection of emitted any filtrate from the test filter occurred at the absolute filter downstream. Gravimetric analysis of the absolute filter determined the mass of the penetrated filtrate over the course of the assessment period. Visual observation in the data would show the baseline differential pressure reduce and struggle to rise. In addition, the glass wall provided for visual observations of the filter during evaluation which may visually present with a hole depending on the severity of the failure.

Concept

This led to the following aim:

“Whilst performing evaluation at site specific parameters until failure is reached, can the resultant data be used to predict the remaining longevity of industrially relevant filtration media?”

The presented study critically evaluated the new methodology idea, including the subsequent analysis. Doing so provided a basis for future researchers to enhance and develop a potential model to aid in the accurate prediction on the remaining longevity of used filtration media.

Coverage (Limited Data Reason)

Completion of the commissioning phase of the Filtration Assessment Rig (FAR) occurred late July 2022. Initial commissioning used talc powder due to delays in the acquisition of PuralNF test dust. Receipt of the PuralNF test dust allowed for academical studies to be conducted. However, during operation, air leakage and test dust build-up occurred as shown in Chapter 3. This led to the FAR becoming offline. The data within this study originated from the period before the initial inoperability period. Although the data presented is limited, it afforded an opportunity to critically evaluate the current data and method. Thus, it afforded an insight into the anticipated results, but also reflected on them to aid future research.

7.2 Methodology

This section presented an insight into the methodologies used within sample generation, testing methods, and filter media.

7.2.1 FAR Rig Set-up

Table 35 illustrated the pre-defined parameters of the test.

Table 35: Operational Parameters Summary for Preliminary Study

Test Dust Concentration $[gcm^{-3}]$	Filtration Velocity $[ms^{-1}]$	Volumetric Flow $[Lmin^{-1}]$	Cleaning Pulse Pressure $[Bar]$	Cleaning Pulse Duration $[ms]$	Cleaning on Demand Pressure $[Pa]$	Variable $[-]$
5	0.08	110	6	200	1500	Test Media (new vs. Industrially used)

Given the use of industrially used filtration media, the cleaning parameters were set according to the site's operational parameters. As previously discussed, there is an unaccounted variance in the cleaning pulse pressure along the vertical height as discussed in Chapter 2. Due to the inability to determine the exact exhibited peak pressure across the entire bag house, the global set point had to be employed as a constant, regardless of the original position of the filtration media. In actuality, the filtration media from industry will have undergone a different, unknown, peak pressure, which will have impacted the mechanical deformation and cleaning efficacy.

Other parameters, such as the nozzle type, distance between the bag opening and nozzle, nozzle alignment/misalignment, and position along the injection pipe [201], [220], [221] are other unaccountable variables within the current FAR set-up. In addition, the FAR afforded

the pulse clean at a fixed distance, where both the injection point and filter media are in parallel as opposed to perpendicular as it is in industry. Future modifications to the FAR are possible to address these potential issues. Omission of key industrial information pertinent to these variables, coupled with the inability to perform modifications to address them, led to a degree of inaccuracy between the results.

In addition, definition of a constant volumetric flow/filtration velocity, is less representative of true industrial operation. Studies, such as those presented in Table 36, illustrated how the flow variation in a bag house can be evaluated and the subsequent effect defined. It would be possible to generate results of an industrially bag house using a simplistic computational fluid dynamic model which would allow for this parameter to be more representative. However, one of the limitations of doing so would be the limitation about modelling at such a large scale unit with hundreds of porous filtration media. In addition, the deposition of filtrate and subsequent formation of cake on the surface would impact the obtained velocity at a given point. Any CFD model of the operational site would have to be highly accurate, with known operational characteristics for results to have good agreeance with actual conditions.

Table 36: Example Studies Which Evaluated Fluid Flow

Reference	Brief Description	Method
[149][181]	Two studies which explored the distribution of gas into the bag house in terms of its uniformity	Experimental
[183]	Explored improvement of dust distribution and pressure drop	Computational Fluid Dynamics (CFD)
[185]	Fluid inlet positioning into the bag house	Computational Fluid Dynamics (CFD)
[186]	Large scale bag house filtration flow distribution, including velocity profiles.	Computational Fluid Dynamics (CFD)
[259]	Influence that the layout of the filter media has on flow characteristics.	Computational Fluid Dynamics (CFD)

The same arguments can be made for test dust concentration, which affected the formation of the filtration cake [148]. Each specific site's filtrate sample is dependent on the constitutes of the fuel and any additions made such as activated carbon and lime as part of their flue gas treatment process. Furthermore, humidity and temperature will affect the resultant data as examined in Li et al., [7],Li et al., [140],Wang et al., [148], and Boudhan et al., [162]. Chapter 3 discussed the resultant variation between site particle size distribution and the test dust size distribution. As such, to allow for direct comparison between the new and industrially used sample, the test dust was kept constant throughout testing. Given the partial use of ambient air, and the free moisture content of the test dust, the humidity and moisture

present within the test varied with ambient air characteristics. Inability to control nor record the moisture content will have had an impact on the resultant data given the test spanned multiple days.

Overall, the presented data within this study illustrated the potential methods which may evaluate site specific samples. Consideration of the variables Table 35 would give rise to sixty potential combinations if five variables changed three times. The resultant time to complete the study, based on the timeframe of the presented data, would equate to 360 working days, assuming each different combination also underwent a new filter media and industrially used filter media sample. Consequentially, optimisation and reduction of the number variables would aid to facilitate study completion for a given combustion site. For example, given the inability to directly replicate the cleaning parameters, use of commercial sites stated in their operation and maintenance manuals would drastically reduce the time required to complete testing. The assumption would therefore be that whilst there is variation to these parameters operationally, its resultant effect is negligible when evaluating the filter media sample using a standardised methodology.

A small scale, proof of concept, design of experiments would be beneficial towards the validation of this assumption. It would also serve to aid in the addressment of the aforementioned points raised about parameter variation between operational conditions, but also in future evaluations within the FAR.

7.2.2 New/Used Media

Currently used in industry, a nonwoven polyimide (P84) felt, supported by a PTFE woven scrim (Lydall Gutsche GmbH & Co. KG, Fulda, Germany) in an industry biomass combustion site provided the basis for this study. Both new and used filtration media used within this study originated from the same site, which allowed for the assumption that the new media was identical to that of the used when new. Appendix A demonstrated the reported parameters for the media, which originated from Site C. This media also presented with a special membrane at the air entry side of the media. Samples were prepared into cylindrical disks with a surface area of $2.243 \times 10^{-2} m^2$ (diameter of 169mm). Each sample, was fixed in place through manual compression of the outer 1cm disc, supported further by three vertical wires which functioned as a cage, allowed for the sample to remain stationary once vertical. Chapter 3 demonstrated this cage and sample in-situ.

Used filtration media was prepared, cleaned, and dried before starting a test. Following the results of Chapter 4, vacuuming commenced upon the sample, but also underwent washing to ensure an optimal clean. A drying period of 24 hours in an oven set at 105°C dried the sample, before periodical hourly weights provided results to allow for the determination that the sample had become fully dry.

7.2.3 Test Dust

An aluminium oxid-hydroxid test dust (PuralNF, DMT GmbH & Co. KG, Essen, Germany), as required by the BS11057:2011 "Air Quality – Test method for filtration characterization of cleanable filter media" [202] made provision to study loading characteristics of the filtration media. This test dust was widely used in literature, under various conditions to study loading characteristics and in some studies to aid in filter life projection [180], [205], [224], [225], [227]. Chapter 3 afforded an in-depth analysis of the particle size distribution, which is summarised below in Table 37.

Table 37: Particle Size Percentage Volume of PuralNF Test Dust (DMT GmbH & Co. KG, Essen, Germany)

$[d_p]$ at 10% (μm)	$[d_p]$ at (50%) (μm)	$[d_p]$ at (90%) (μm)
0.97	7.13	32.00

7.2.4 Offline Test Methods

Prior to analysis, each sample underwent a broad spectrum of analytical methods, which provided a baseline for future analysis. Sample mass, thickness, air permeability, scanning electron microscopy (SEM) and micro-computed tomography (µCT) allowed for a deeper understanding how the sample changed during the study. As this study focused on the endpoint of the sample longevity, completion occurred upon the occurrence of failure within the sample. Figure 55 illustrated the pre (A+B) and post (C+D) operation samples of brand new/virgin media (A+C) and industrially used media (B+D).

Due to the mechanical clamping mechanism which fixed the filtration media sample in-situ, a 1cm ring on media on the outside of the sample did not experience any filtrate. To account for this band, subtraction of the area from the overall allowed for results to only represent the tested area. The sample was then removed to complete the test. In future samples, which may require removal periodically, care and attention towards the minimisation of fluctuation about the exposed/unexposed regions would allow for repetition of this ideology. However, any overlaps caused would inadvertently create a new region with a potentially lower flow

resistance, and as such negatively impact the results. Consequently, the necessity to periodically remove the sample (not forgetting any disturbances caused to the filtrate in doing so) needs further deliberation prior to its occurrence within a test.

One of the overarching limitations with performing analysis is the resultant disturbances to the filtrate through manual manipulation of the sample. Removal of the test filter from the FAR, clamping during air permeability analysis, manual bending to ensure complete coverage on the balance (inside a glass beaker), and isolation of samples for SEM/µCT analysis will impact the structure and volume present within/upon the sample. Whilst care to minimise this transpired, an inherent amount of accidental damage will result in a degree of variation within subsequent analytics. In addition, the method presented in Chapter 5 was not viable, given removal of a section would render the sample inoperable within the FAR. To counteract this, the whole samples weight allowed for the sample to remain whole. Thickness determination was taken within each quadrant. These steps allowed for each sample to remain whole, with the corresponding results between pre and post op being representative of the same sample. In contrast, SEM/µCT required removal of a section of the surface area for analysis, performance of which could only happen upon completion. Therefore, this technique can only occur upon completion of the set-point of the sample. A new/used sample (Figure 55 samples A and B) allowed for SEM/µCT analysis to occur and provided a further baseline to evaluate the resultant data obtained, between samples A/B and the post cleaned samples C/D respectively.

7.3 Results and Discussion

Shown in Figure 55 and Figure 56, is the difference between the virgin/new and industrially used/cleaned samples (A+B), post operational samples (C and D in Figure 55), and post clean samples (C and D Figure 56). Thus, three distinct data categories over the two samples were examined in this study. In both cases, the samples where ran to failure, regardless of the number of cycles.

Illustrated in Figure 56 is the visual difference between the new/virgin samples, and the post clean sample.

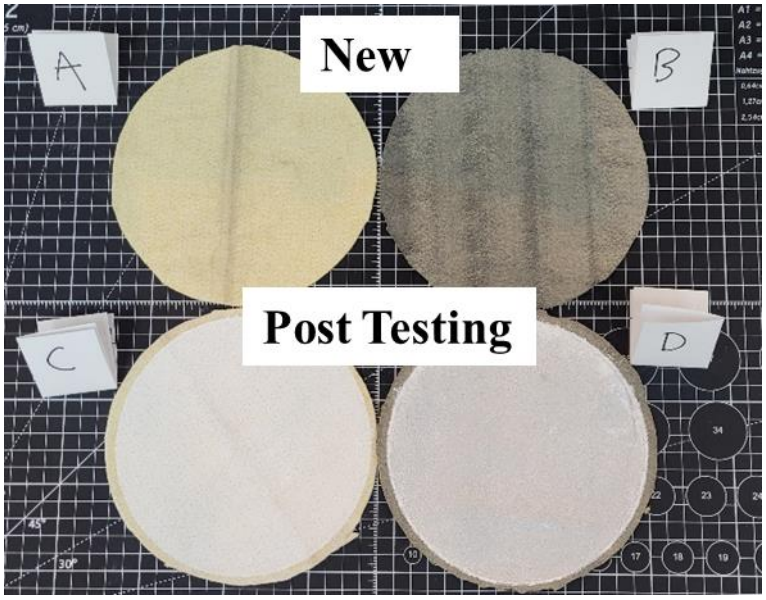

Figure 55: Filtration Media Sample Before (A+B) Evaluation and After (C+D) Evaluation

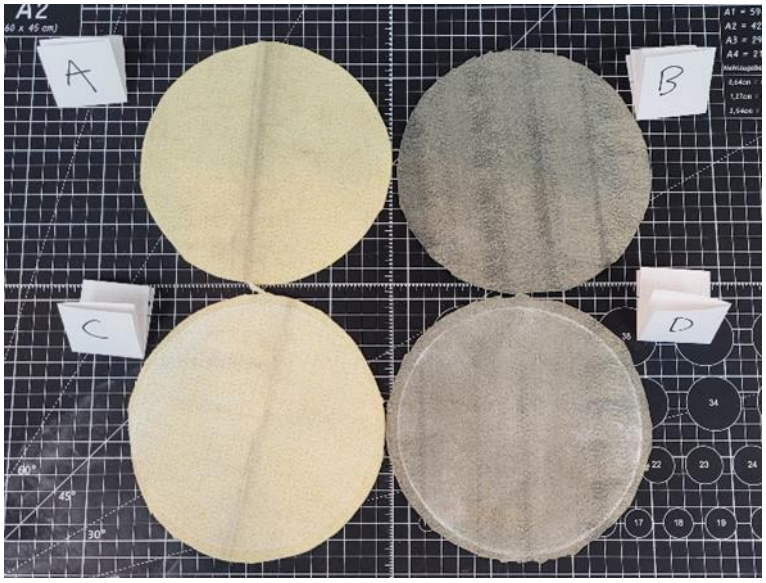

Figure 56: Filtration Media Sample Before (A+B) Evaluation and After (C+D) Post Clean

Sections 7.3.1 and 7.3.2 presented the obtained results from online and offline testing of the data for the aforementioned samples shown in Figure 55 and Figure 56.

In contrast to Figure 55 samples C+D, Figure 56 samples C+D indicated a high removal percentage of the filtrate at the surface of the sample. Employment of the post clean step transpired due to the requirements made within BS22031:2021 “Sampling and test method for cleanable filter media taken from filters of systems in operation” [16] which specified the requirement to perform this step. As stated in Chapter 4, the aim of this step is to evaluate the media. However, given the aim of this study was to evaluate the media performance/longevity, a highly effective clean may artificially skew the results, such that the

resultant post clean data suggested a greater media longevity than actually possible. In addition, given sample evaluation utilized pulse cleaning (unlike that of Chapters 4-6), it would be possible to generate the sample to that of C and D in Figure 55, conduct offline analysis, then perform a pulse clean and repeat offline analysis. This would yield a better representation of the baseline sample characteristics and if desired, a post clean step could be employed after the pulse clean. This would result in the following categories: pre-op, post-op, pulse clean, and vacuum clean.

7.3.1 Online Data

The recorded data obtained from the operation of the FAR with the new/virgin media (top) and the industrially used/cleaned (bottom) sample is shown in Figure 57. The resolution of the data was a reading every second. Discussion of the theoretical impact of this resolution is located in Chapter 3. Data for the differential pressure across the test filter conformed to previous literature. Previous studies such as Li et al., [137],Cirqueira et al., [189], and Kim and Lee [240] have used cleaning on demand, which presented similar graphs to those of Figure 57. The curve similarities showed that the current resolution could deliver relatively representative results of the filtration process. Unlike previous academic studies, the data shown in Figure 57 had points of significantly low differential pressure, particularly towards the end of the test.

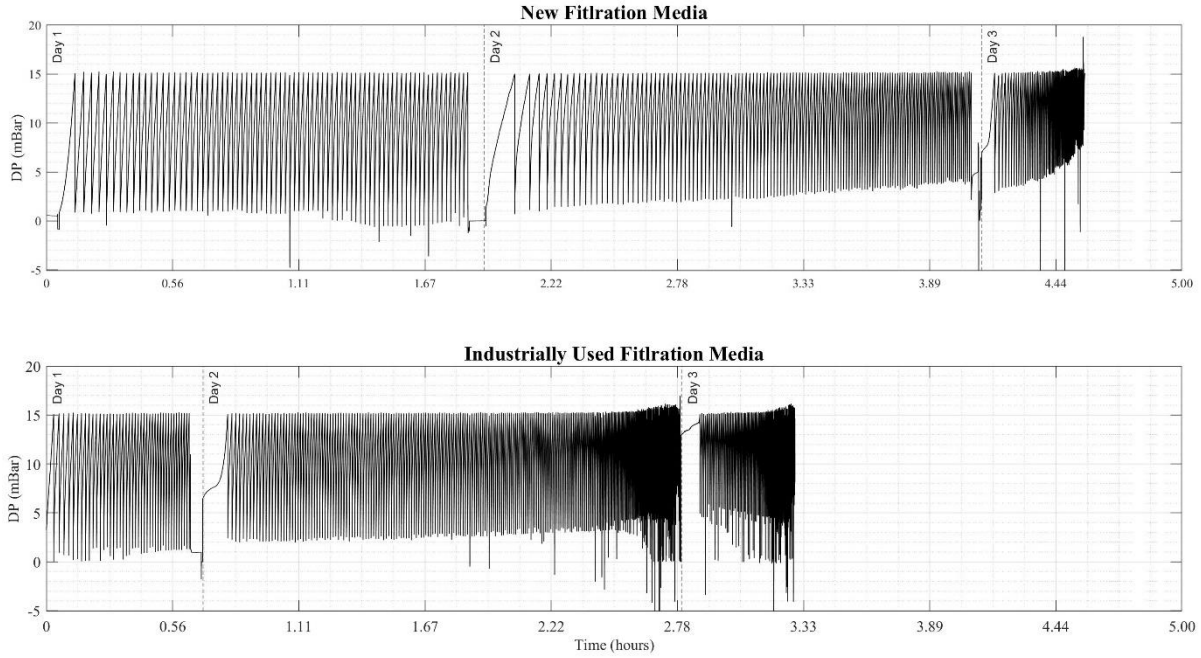

Figure 57: Raw Data Showing Differential Pressure (DP) Evolution of New (top) and Used (bottom) Filtration Media Throughout Evaluation

Data that occurred below the initial baseline differential pressure of the sample suggested operation of the pulse clean during the data recording point. A similar study, conducted by Litchwark et al,. [212], showed a significantly low drop followed by a quick recovering the subsequent datapoint. The study conducted by Litchwark et al,. [212] had a cleaning pulse is parallel and upstream to the test filter, which could have resulted in this being the reason. Time delay and natural variation in the data recording, coupled with the cleaning time and pressure could have resulted in a data recording point during the actuation of the cleaning pulse. High resolution pressure curves studies (such as those found in Andersen et al., [201],Li et al., [210], and Li et al., [222]) demonstrated the evolution of the cleaning pulse. As the data recording is independent, it is logical that recording may take place at any point during the cleaning process, which would result in a negative differential pressure due to the overall change in flow direction at the point where the differential pressure probes are located.

These occurrences increased in frequency towards the end of the test. As the filtration cycle time and difference between the cleaning differential pressure and baseline differential pressure decreased, the probability of inadvertently collecting a data point during cleaning increased, particularly towards the larger cleaning times. Particularly during day three, where the differential pressure in Figure 57 indicated that the cycle duration reduced to near unity. These datapoints negatively impact the subsequent data interpretation, as they do not reflect the actual baseline differential pressure of the sample. Therefore, there is an inherent unspecifiable variation within each baseline differential datapoint, which is dependent on the time position of recording. Instantaneous data recording upon completion of the cleaning cycle would require the resolution to be in milliseconds. Upon completion, a more accurate baseline differential pressure reading would have prevailed. If a datapoint recorded the cleaning pulse such that the datapoint was less than the previous baseline differential pressure, the following datapoint equated to the new baseline. This method assumed that even if the maximum time difference of 800ms occurred, the resultant effect on the pressure evolution was minimal. This assumption needs further clarification, as towards the end of test, it fails given the difference accounted for 27-80% of the total cycle time, where the duration was between 3-1 seconds, respectively.

Cycle differential pressure and cycle duration/time where two isolated parameters obtained from the data using a MATLAB script. This code acted by isolating the peaks and troughs within the data categories and saving them as two columns of data to represent the two

aforementioned parameters. The time between the baseline differential pressure, and the recorded differential pressure defined the cycle duration. Similarly, the difference between these two point's differential pressure resulted in the definition of cycle differential pressure. Table 38 provided a summary of the collected data for each sample assessed.

Table 38: Summary of Data Obtained from Operation of the FAR for Both New and Used Samples

New Filtration Media		Industrially Used Filtration Media	
Baseline Differential Pressure	1.10 (mBar)	Baseline Differential Pressure	3.15 (mBar)
Number of Cycles	240 (-)	Number of Cycles	323 (-)
Test Duration	4.57 (hours)	Test Duration	3.30 (hours)
Average Cycle Time	68.57 (s)	Average Cycle Time	36.73 (s)

The evolution of cycle duration and differential pressure as a function of the cycle number is illustrated in Figure 58.

An apparent multiple reciprocal function (Ae^{-x})developed within cycle duration time. During the literature search, only one paper by Kurtz et al,. [213] presented a curve similar to Figure 58(left), though their experimental set-up was completely different to the FAR. This could have occurred due to the changing of the piston and subsequent non-unformal operation of the FAR. The occurrence of this function appeared whenever the piston change happened, which suggested that the first few datapoints from the main data are not representative of normal operation. Isolation of each days data exhibited a similar graph to those in literature such as Li et al., [137], Cirqueira et al., [189], and Kim and Lee [240]. However, given the continuation of a sample, the expectation was only a singular reciprocal function would occur. This would be whereby the initial cycles would be significantly higher in cycle time due to the transition between depth/surface filtration before a cake had formed promoting cake filtration. Consequently, this suggested that at the end of the test and subsequent restart, this theoretical transition occurred again, even though the sample remained stationary and remained in exactly the sample position before continuation of the test.

However, cycle differential pressure, Figure 58(right) did not exhibit this relationship, instead favoured a continuous Ae^{x} type function. Unlike the multiple (Ae^{-x}) functions exhibited for the cycle duration in Figure 58(left), it was not possible to discern between where each day subsequently finished or started. This therefore suggested that the occurrence of multiple (Ae^{-x}) functions was due to the set-up of the FAR. Given that each time the (Ae^{-x})

function, a newly filled cylinder of test dust occurred, it is likely that the priming of said cylinder was insufficient. This insufficiency led to an unknown remanence of a variable packing density within the concave section. Consequently, this led to a variable dust concentration deliverance to the test filter and therefore resulted in the aforementioned function. Upon equalisation of the packing density, a near linear function occurred. Evaluation of this theory will aid to improve the resultant data and mitigate against unnecessary data treatment steps.

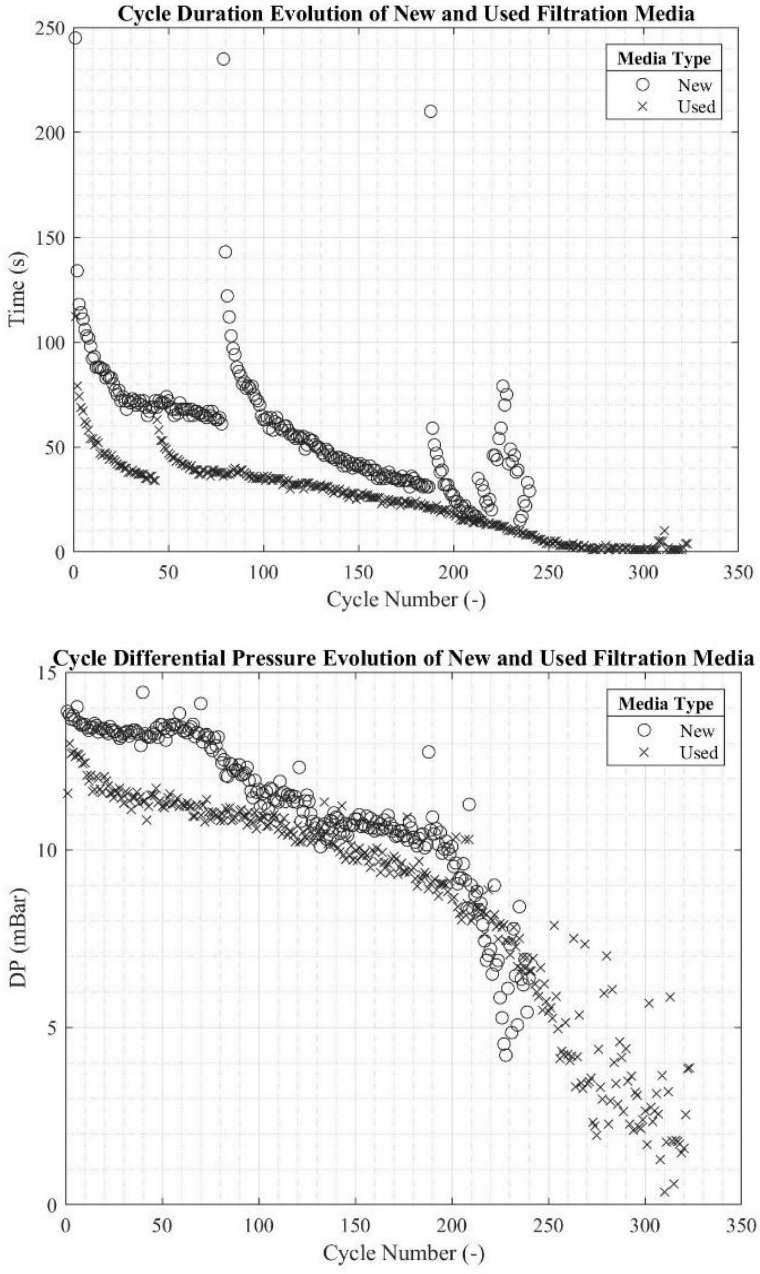

Figure 58: Time (top) and Differential Pressure (bottom) Evolution Until Failure of New and Used Sample

As expected, over the lifespan of both the new and used filter media, a reduction in the obtained parameter occurred. As the baseline differential pressure increased, the resultant difference, in both cycle time and cycle differential pressure, reduced towards unity. In both cases, the aforementioned functions yielded good correlations for cycle duration and cycle differential pressure at (0.76 and 0.94) and (0.90 and 0.96) respectively for new and used filtration media.

In both cases, the definition of failure is the number of cycles where the parameter is equal to zero. The occurrence of this, following curve fitting suggested the actual number of cycles for each sample where those presented in Table 39. The percentile difference noted for cycle time and differential pressure for both samples, could have originated due to the failure of the FAR during testing. Data presented in Figure 58 (and subsequent figures) appeared to fan out, which affected the resultant curve fit and determination coefficient. In addition, a more extensive (Ae^{-x}) function would have contributed to this percentile. As such, repetition of the sample would yield a better representation of this sample, allowing for a more accurate comparison. Consideration therefore fell to the industrially used sample, which exhibited a lower percentile difference, and yielded an average theoretical failure point of 321 cycles from the initial sample.

Table 39: Endpoints Following Curve Fitting

Sample	Cycle Differential Pressure	Cycle Time Duration	Percentile Difference
New/Virgin Media	258.38	341.48	24.33%
Industrially Used Media	343.26	298.31	13.10%
Percentile Difference	24.73%	12.64%	-

Assuming the new/virgin sample's average is an accurate representation at three hundred cycles, only a 6.54% difference occurred between the new and industrially used filter. Given the aim is to determine the remaining longevity of the used media, the direct comparison of averages failed. The filtration media examined had been in operation for up to two years and with an anticipated failure point within the same period. This estimation is based on historical data and plant maintenance, coupled with both the locational information of the used sample and previous analysis from the same combustion site. Subsequently, calculation of the percentile difference of each parameter against the new and used samples gave rise to strikingly comparable results for the cycle differential pressure against the new and used media, to that of the percentile difference of the new/virgin media only.

Given the aforementioned issues surrounding the cycle time duration, the current working thought is that this similarity occurrence is coincidental until proved otherwise through a repeat of the new/virgin sample.

However, given that the aforementioned issues failed to arise in the cycle differential pressure, direct comparison theorised a 24.73% difference. Interestingly, the longevity of the industrial sample was higher than the new/virgin sample in terms of number of cycles. Theoretically, the remaining longevity of industrially used filtration media would be lower, owing to already in operation. Whilst the washing stage could have increased the volume of the pores, the higher baseline differential pressure and shorter duration (as exampled in Table 38) suggested that this was not necessarily true. This contradictory argument between the expected, reduced, duration and increased baseline differential pressure and the increased longevity of the used filtration media needed further exploration. Therefore, the argument suggested that the used filtration media lasts longer than new filtration media, which went against the theory.

Subsequently, until the completion of further analysis, the results suggested that the used filtration media had experienced 24.73% of its lifespan under the specified operational conditions of the site. Though as previously discussed, this absolute value contradicted the theory and therefore may be inaccurate. Until further industrially used samples that have been in service longer can be evaluated, coupled with a repeat of the virgin/new sample, this value is thought to be inaccurate to some unknown degree.

Due to Figure 58's presentation of two different functions, consolidation of the graphs as a scatter plot of the parameters as opposed to the cycle number led to Figure 59, which suggested a singular function. Figure 59 presented both the new and industrially used sample data as cycle differential pressure vs. cycle duration/time, irrespective of cycle number. This suggested a simplified exponential function within both data sets of an exponential nature. Following this observation in Figure 59, employment of curve fitting on the data supported the suspected function within the data and is shown in Figure 60.

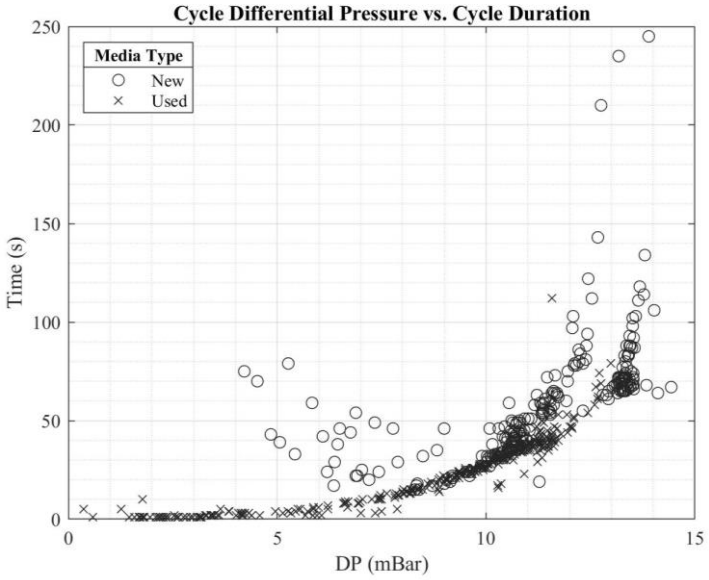

Figure 59: Differential Pressure vs. Cycle Duration/Time of New and Used Filtration Media

Presented in Figure 60 is the resultant curve fitting results, including the representative equation and coefficient of determination. At a differential pressure of zero, the cycle time would also be zero given the baseline and cleaning differential pressure where equal. Consideration of this point during the curve fit allowed for a better representation of the actual operational conditions as opposed to a more mathematically representative curve. This resulted in an exponential function to define the relationship within the data.

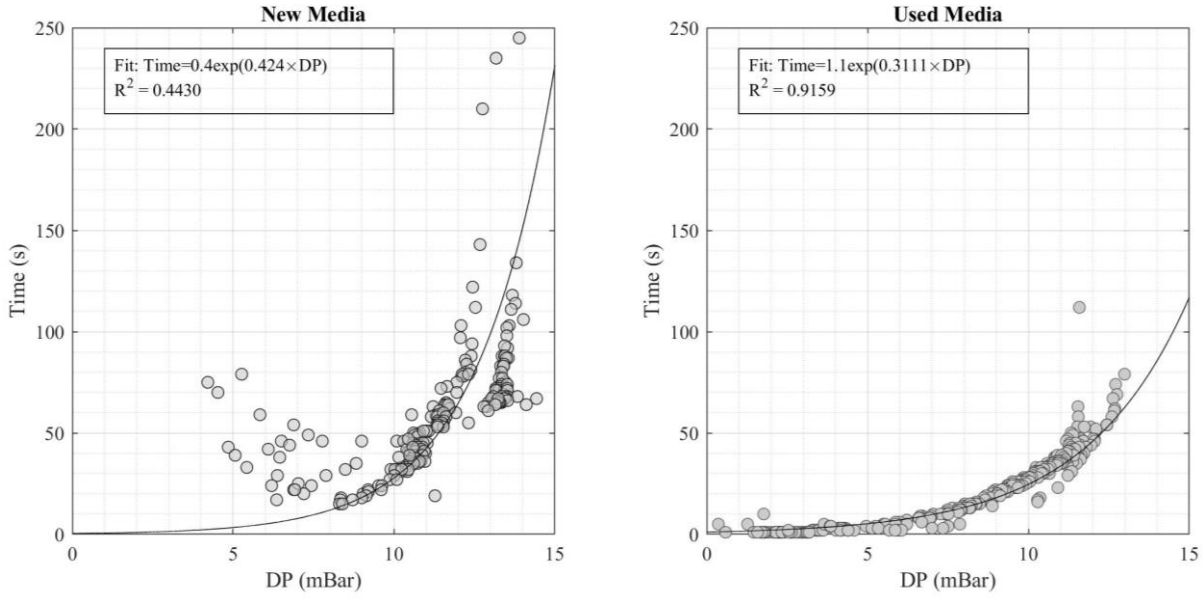

Figure 60: Curve Fit Results Showing Exponential Growth of Differential Pressure vs. Cycle Duration/Time on New (left) and Used (right) Filtration Media

Discrepancies between the new media and used media, in terms of the determination coefficient, yielded an absolute difference of 0.48. As previously stated, failure occurred

upon the cycle time reaching, on average, is one second. Industrially used media reached this point when the aforementioned condition reached. The resultant exponential curve regression presented in Figure 60(right), suggested a good fit to the data. However, a less well fitting curve for the new/virgin media sample, presented in Figure 60(left), transpired for the new filtration media. As stated earlier, the new filtration media was the last test before the FAR became offline. Between the differential pressure of 5-8mBar, an extensive deviation from the curve transpired (a similar transition also occurred for some of the data between ≈13-14mBar). One of the failures noted in the FAR was that of particulate build up on the dispersion cover and air leakage as shown in Chapter 3, Section 3.2.2. As the volume of air and filtrate was lower than the set-point, the time required to reach the cleaning differential pressure increased, resulting in the datapoint's being away from the curve at this point.

Due to the potential discrepancy between the industrially derived sample and the virgin/new sample, repetition of the new media sample would suggest if the variation was caused by the FAR failing during testing or not. This repeat would determine if the data and subsequent coefficient in Figure 60(left) were representative, or if the failure of the FAR contributed to the low determination coefficient. If the repeat data is similar, this would then require further research to ascertain why the new data is better suited to a parabolic rather than an exponential function, given a parabolic function would not support the theory. If the resultant repeat data is similar to the industrially used sample data, then this would suggest that the exponential curve may define the samples, regardless of different media and operational exposures. Following the repeat, further development of the use of Figure 60 could suggest a way in which to deploy it as part of a media performance/ longevity model, if it is similar to that of the used sample which did not experience any noticeable FAR failure during evaluation.

Mathematical comparison of the two curve fit equations demonstrated that although the used media appeared to last for a larger number of cycles (described in Table 38), the change in constants suggested how future industrially used samples (from the same site) may change from the baseline sample. If the new media curve is assumed representative, regardless of the lower determination coefficient, then any change in the coefficients of the curve fit will give some indication as to how the samples differ. Furthermore, it assumed that the next industrial sample continues to exhibit an exponential curve and exhibited higher/lower A and B coefficients respectively.

Production of a site specific chart, comprising of multiple curves from different timepoints across the same site, would enable future samples to be cross compared and suggest remaining longevity. To do so, withdrawal of samples from the site at periodical intervals and distinct locations to obtain a more accurate chart. From this, application of the chart would allow for the prediction of remaining longevity of the media of future samples once a bag change has occurred (so long as the filtration media is the same as previously installed and site operational characteristics remain within tolerances). Subsequent sample evaluation under the same conditions of the chart would not need to be ran to completion. After completing an undefined number of cycles, the subsequent data can then obtain the coefficients A and B. Afterwards, consultation of the chart can predict where the sample laid and its remaining longevity.

This proposed methodology, which requires further samples and analysis before developing a method for industrial use, circumnavigated the omission of the sequential cycle number used in Figure 58. One of the problems with comparison between the new and used samples is that the resultant number of cycles exhibited in the sample was higher for the used sample. At face value, this suggested that the used sample lasted longer than the new media which is illogical. Given the issues surrounding the new sample, the repetition of this test may contradict this and yield a higher number of cycles than the used. Until then, the absolute difference suggested the use of the filter.

Upon completion of the chart, direct comparison between the chart and number of cycles completed is achievable and would aid in the decision of a suitable method to evaluate the remaining longevity of the used filtration media for the site.

7.3.2 Offline Data

Nominal Testing

Air permeability, mass/density, and thickness analysis are common analytical techniques to evaluate filtration media. Provided baseline data is known, performance of the analytical techniques demonstrated the variation caused due to use. To allow for direct comparison, prior to sample instillation, performance of these techniques on both samples afforded said baseline. This baseline was the preoperational values as shown in Figure 61, with post operation defining the sample upon completion of the FAR test. Subsequent cleaning using a dust vacuum, following the results of Chapter 4, converted the test filter from the supposed

"as received" state to a "post-cleaned" state. Figure 61 presented the results for thickness (top), density (middle), and air permeability at 200Pa (bottom).

Unlike Chapter 6, the clamp ring's diameter was larger than the diameter of the sample which meant the only clamping afforded to the sample was by the compression head of the equipment. As such, this left a compressed thickness of filtrate media open, which could have allowed for an increased volume of air ingress through the sample. To minimise this, as concentric an alignment as possible attempted to reduce this possibility. It may prove prudent, in future analysis to perform air permeability on different apparatus, such that as tight a seal as possible occurred to reduce this. Apart from the clamping, no other deviation from the standard transpired.

Given the limitations on the sample size, the sample only underwent sub-sectioning upon conclusion of all tests which allowed the sample to remain whole. This led to a singular value for density in each category. For the thickness analysis, evaluation occurred once in each quadrant, resulting in four datapoints. Unlike Chapter 5, the locational points where not recorded. This led to the assumption that the resultant mean for thickness is representative of the overall sample. Whist this may be true, a record of each quadrant's values could be useful in determining if a preferential flow existed within the sample. If the air permeability evaluation step can be committed and determined based on the experimental data (through Davies equation for example), this would allow for sub-sectioning of the sampling with fixed locational information. Development of this method would therefore allow for retrieval of both global and representative locational information about the samples generated from the FAR.

The post operational category described the sample upon completion of the test. This category retained its filtrate and appeared as shown in samples C and D in Figure 55. Retention of the filtrate therefore led to the expectation of the post operational sample results being higher for thickness and density, and lower for air permeability than other categories. Figure 61 and Table 40 presented the obtained offline data from analysis. The sub sectioning of the bulk sample did not transpire due to the air permeability requiring the sample to remain whole. The density was calculated based on the exposed surface area and converted to a mass per 25cm^2 based on the surface area used to determine the thickness at various positions. Table 41 Illustrated the theoretical porosity results.

Table 40: Results from Offline Tests

	Filtration Media					
	New			Used		
Category	Thickness (mm)	Density (g 25cm^{-2})	Air Permeability (Ldm^{-2}min^{-1})	Thickness (mm)	Density (g 25cm^{-2})	Air Permeability (Ldm^{-2}min^{-1})
Pre-OP	1.330±0.049	1.550	165.063±2.429	1.363±0.015	1.645	271.987±3.321
Post-Op	1.337±0.020	1.732	152.897±1.985	1.442±0.033	1.772	145.777±5.926
Post Clean	1.353±0.031	1.587	418.363±67.402	1.373±0.037	1.633	601.500±62.605

For thickness evolution, Figure 61(top), the new sample did not conform to previous observations, nor to the used sample. Instead of exhibiting a $-x^2$ shape between the three categories, it increased linear, regardless of the removal of the filtrate. This could have originated from the inability to section samples and reliance on approximation during the repeats. This invariably led to a large variation, which suggested that the localised thickness varied, even in the used sample. Removal of the surface filtrate would theoretically return a mean thickness lower than the post op category given removal of the layer, resultantly the data obtained for thickness in the new sample is questionable.

For density, Figure 61(middle), the previously expected $-x^2$ shape exhibited within the data occurred for both the new and used filtration media sample. As discussed in Chapter 5, the difference between the new and post clean category indicated some filtrate remained in the media. For the new and industrially used sample, this value was 0.037 g per 25cm^{-2} and-0.012g per 25cm^{-2} respectfully. The occurrence of a negative value indicated the loss more material than the original density. This could be from fibre deformation, or the removal of an unspecified amount of remaining filtrate from the original media. Determination of the latter would suggest that the clean of the used sample was not full efficient. Microscopy images shed light on this thought. Given the post op sample still retained the surface filtrate, it presented with the highest density. Removal of this and subtraction of the post-op datum suggested the density of the surface at 0.145 g per 25cm^{-2} and 0.139 g per 25cm^{-2} respectfully. The difference between the post-op and pre-op yielded the total filtrate density deposited at 0.182 g per 25cm^{-2} and 0.127 g per 25cm^{-2} respectfully. The used sample exhibited larger densities overall to the new sample due to previous internal deposition, which was not removable.

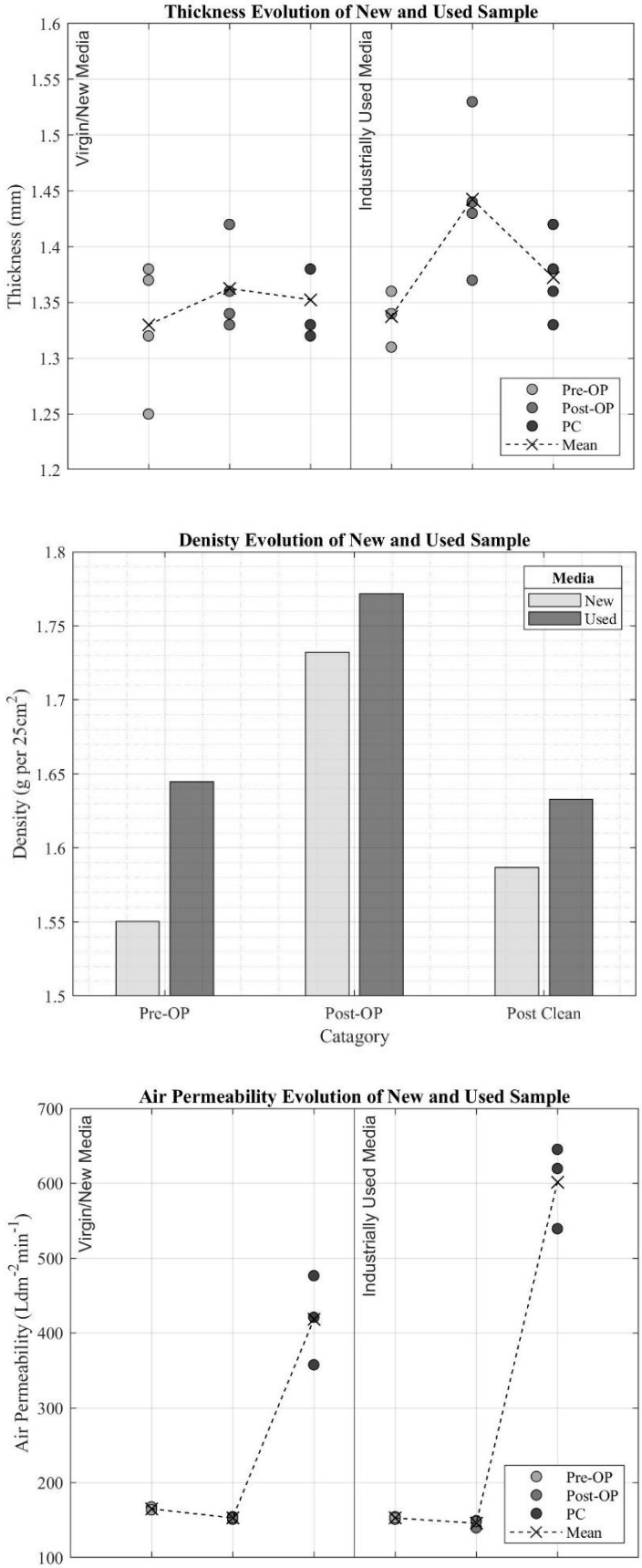

Figure 61: Standard Laboratory Analysis of New and Used Sample, Across Pre and Post Operation of FAR and Post Clean State for Thickness (top), Density (middle) and Air Permeability (bottom)

Given filtrate presence on the surface of both samples in the post-op category, the expected air permeability was lower than the pre-op. This transpired in the data presented in Figure 61 and Table 40 . The difference between both samples in the post op category resulted in 7.12 $Ldm^{-2}min^{-1}$. This reduction is due to the increased material at the surface of the media, which blocked the pores, blocking channels for the airflow. The reduction of the air permeability to near similarity in the post-op state suggested that the media had plateaued to a similar point. Which, given the failure point was where the baseline differential pressure equated to the cleaning pressure for the sample, it is logical that this plateau would transpire in the air permeability irrespective of density and thickness. Upon post cleaning the sample, the anticipated air operability response was a datapoint similar to the pre-op position.

However, as shown in the recovered air permeability extended to over 2.5 and 2.2 times greater than the original air permeability for the new and industrially used samples respectively between the pre-op and post clean categories. Whilst the removal of the filtrate recovered the air permeability, the obtained value would have been similar to that of the pre-op category given no visual holes existed in the sample, nor any other deformation points existed on the sample. Holding both samples up to the light attempted to visualise any areas of severely limited media which could have suggested the reason for such a high permeability. However, this failed to suggest anything. The leading theory therefore surrounded the inability to provide a clamp on the sample which could have led to air ingress which skewed the results. Although the sample was as concentric as possible to the test area, the sides where still accessible which could have allowed for air to ingress in and result in this high air permeability.

Questions towards the effectiveness and accuracy of performing air permeability analysis on test filters resulted, given the data presented in Figure 61 and Table 40. One alternative way to calculate the air permeability is to rely on the use of a combination of online data and mathematical equations such as Equation 29 [240] which calculated the pressure drop across the media and cake (ΔP), which uses the gas and flow characteristics in relation to the deposited mass (D_{cake}),which can yield a value to define permeability (K_{media}, K_{cake}). The deposited mass being a function of the concentration (C), flow velocity (v), and time (t), over the cake density (ρ_{cake}).

$$\Delta P = \Delta P_{media} + \Delta P_{cake} = \frac{\mu v D_{media}}{K_{media}} + \frac{\mu v D_{cake}}{K_{cake}} \text{ where } D_{cake} \approx \frac{Cvt}{\rho_{cake}}$$

Equation 29: Pressure Drop Example Equation from [240]

One difficulty in the calculation of air permeability from the use of Equation 29, even simplified where only the baseline data occurred ($\therefore \Delta P_{cake} = 0$), is the unaccountability for porosity [159], [236], internal deposition [164], variation of parameters such as humidity over time [163], cleaning efficiency [99], or flow characteristics [134], [139] through the media as a result. Previous studies have illustrated the limitations and discrepancies between the experimental data and theoretical studies. Given the complexity of modelling and determining the air permeability, the reliance is heavily on the analytical equipment which provides a value for the given sample based on volumetric flow, without extensive calculations. In terms of this research, the determination through theoretical models of air permeability based on baseline data where forgone given the uncertainty surrounding the theoretical value.

Another potential evaluation method is to determine the porosity of the sample. For fabrics, this can be calculated based on the fabric density over the fibre density as suggested by Gultekin et al., [3] and Hoppe et al., [225] for example. Experimental determination of porosity considering the thickness, density, mass, and surface area data of the sample suggested the overall void of the sample in a defined volume. Equation 30 [135], [136] therefore presented an experimental method to determine the porosity of the results from offline tests for density and thickness for new media.

For Equation 30 [135], [136], the porosity of material x (α_x) required the mass (M_x), thickness (t_x), surface area (A_x), and material density (ρ_x). Given porosity defined the free volume within the given sample, the solidity of the same equated to the subtraction of porosity from unity ($1 - \alpha_x$). The subscript "x" and "y" denoted different phases within the sample.

$$\alpha_x = 1 - \frac{M_x}{t_x \cdot \rho_x \cdot A_x}$$

Equation 30: Experimental Porosity Determination Based on [135], [136]

For nonwoven filtration media samples in the used state (post op and post cleaned), there existed deposits at and above the surface as well as internal deposits to the media. The inclusion of a different material required adaptation of Equation 30. Use of this adaptation

then allowed calculation of specific porosities, of various materials within the sample. Equation 31 demonstrated the adaptation, which derived porosity based on the incurred differences of a sample, for example, this equation calculated the porosity of the filtrate at the surface of the media, using the pre and post operational parameters respectfully.

$$\alpha_{x,y} = 1 - \frac{(M_x - M_y)}{(t_x - t_y) \cdot \rho_{x,y} \cdot A_{x,y}}$$

Equation 31: Adaptation of the Experimental Porosity Variation Presented in[135], [136]

Subsequently, the summation of different solidities $(1 - \alpha_x)$ for the different states determined the overall porosity for a given category. By defining the known materials within the defined sample volume, the solidities can be added together to understand the overall porosity of the sample which has experienced filtration. Table *41* presented the results from the calculations across the new/virgin media and industrially used filtration media.

Comparison between the pre-operational and post operation porosities yielded an insight into how the filtrate had interacted with the media. The post operational sample accounted for all the filtrate, including the surface filtrate. This yielded a global value of the sample, irrespective of layer present. As such, this limited the view of the data, given that the surface filtrate may be densely packed and have a low porosity in comparison to the media such as exhibited in the new/virgin media. Therefore, the resultant value is holistic and cannot definitively define where the region of least porosity is located within the sample. This overview did however show the anticipated porosity reduction, due to the filtrate blocking pores and having a layer of filtrate at the surface.

An overview of porosity is shown in Table 41 and showed that the new/virgin media exhibited a lower porosity (49.36%) than the industrial media (85.38%) in the post operational category. This happened even though the industrial media exhibited a lower porosity (87.62%) compared to the new media (88.05%) in the pre-op state. Furthermore, the difference in the surface filtrate porosity, suggested that the packing density of the filtrate on the new media was higher, which led to a less porous layer. Conversely, the industrial media surface filtrate layer was higher, suggesting either the volume of filtrate present was low and therefore high in porosity, or that nothing formed. The visual presence of filtrate on the surface suggested evidence to discount the former thought. This led to the suggestion that whilst filtrate was present, the resultant thickness and subsequent mass was so low that the

calculation of porosity yielded a high value and consequentially attributed to a higher post-operational porosity.

This occurrence raised a significant issue with the determination of porosity for multi material samples. The occurrence of negative differences will impact the resultant porosity, suggesting really high values as seen in Table 41. The use of a global value assumed homogeneity in the sample, which may not be strictly true. As such, whilst the theoretical calculation of porosity may yield a holistic value, there are instances that can occur where the result is not representative, or contradictory to the theory, such as the internal deposition porosity for the industrially used media in Table 41.

Table 41: Theoretical Porosity of Samples

α_x	New/Virgin media	Industrially used media	Difference
Pre operation	88.047	87.622	0.425
Post operation	49.361	85.379	36.018
Post clean	88.007	87.635	0.372
Surface Filtrate	61.624	97.627	36.003
Internal Deposition	99.960	100.013	0.053

µCT may provide an insight into not only the porosity, but how this varied through the sample. Use of µCT would afford detailed information about the porosity evolution through the sample, regardless of the material present within the sample. As such, application of this technique would provide comparison between both results and suggest if those results in Table 41 are representative. Consequently, application of this technique, alongside SEM imagine determining how porosity varied through the sample, but also how the structure adapted to contract with filtrate.

Imaging

SEM

Scanning electron microscopy (SEM) provided detailed imaging of the air entry surface and air exit surface of the filtration media. The air entry surface is defined as the surface which experienced the filtrate first. The air exit surface is opposite side. The term “air” can represent any gas movement through the filter media. This colloquial term is often applied in industry to aid in the distinction between the two surfaces of the media. Various studies have used SEM imaging to aid in the evaluation of the media and filtrate interactions for many years [14], [136], [146], [189]. To perform the analysis, a five-by-five-centimetre square was removed from each sample using a sharp knife. This size allowed for a small mark to be

placed on the air entry side to ensure correct handling of the samples. This mark did not interfere with the analysis and was excluded from the microscopes field of view. This yielded one subsample from samples A-D and upon completion of analysis yielded images of both surfaces per sample.

The acquisition of a subsample is a destructive process, which removes a section of a sample, leaving the original sample unable to be re-evaluated. This destructive method was performed at the end of the normal testing procedures air permeability, mass, and thickness determination. This involved the used samples being cleaned via a dust vacuum as determined following the results of Chapter 4. As such, a representative sample of the industrially used and virgin/new (not used in the test) media where taken. Non-invasive evaluation techniques allowed for the same sample to be examined at different points. Consequently, upon completion of non-destructive testing, techniques like SEM can suggest further information about the sample at a given point in time.

The aim of the SEM study, over the four samples, was to examine the surface variations between the unused and used states. Figure 62 represented the virgin/new media, before (sample A) and after (Sample C) evaluation in the FAR. Figure 63 represented the industrially used media, before (sample A) and after (Sample C) evaluation in the FAR. Figure 64 and Figure 65 evaluated regions of interest on the new/virgin and industrially used media respectively, at a greater magnification.

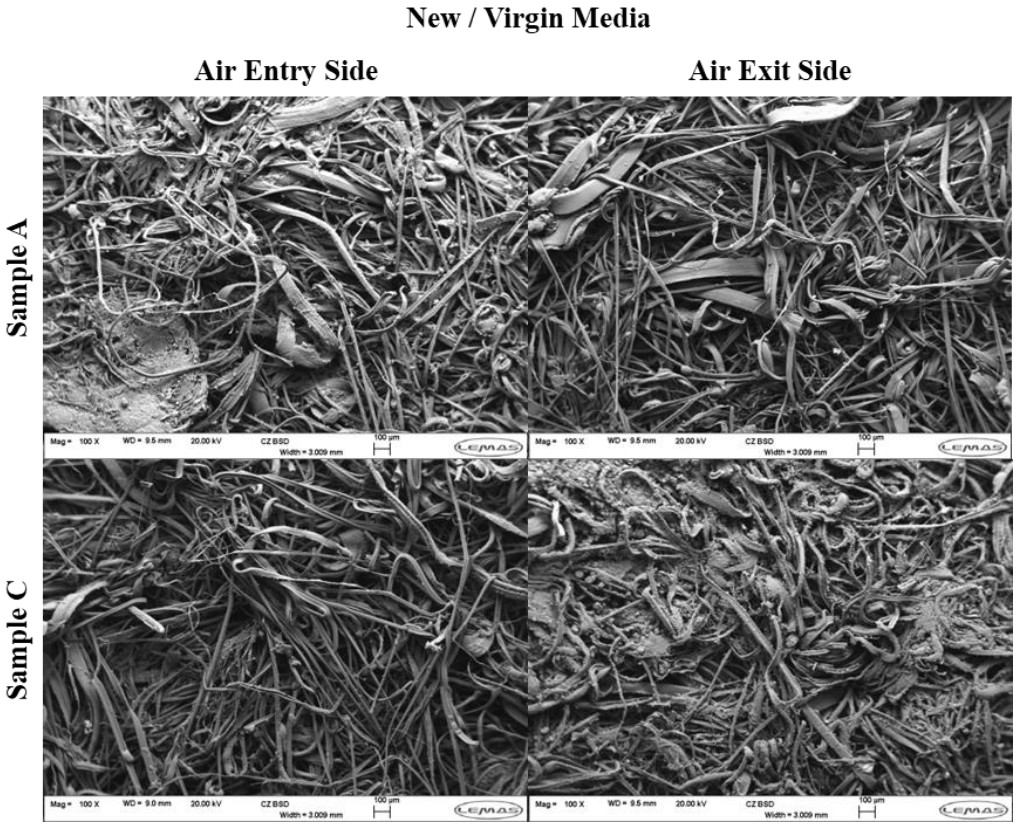

Figure 62: SEM Images of Air Entry and Exit Side of New/Virgin Samples Used in Longevity Study: Sample A = New and Sample C = Used

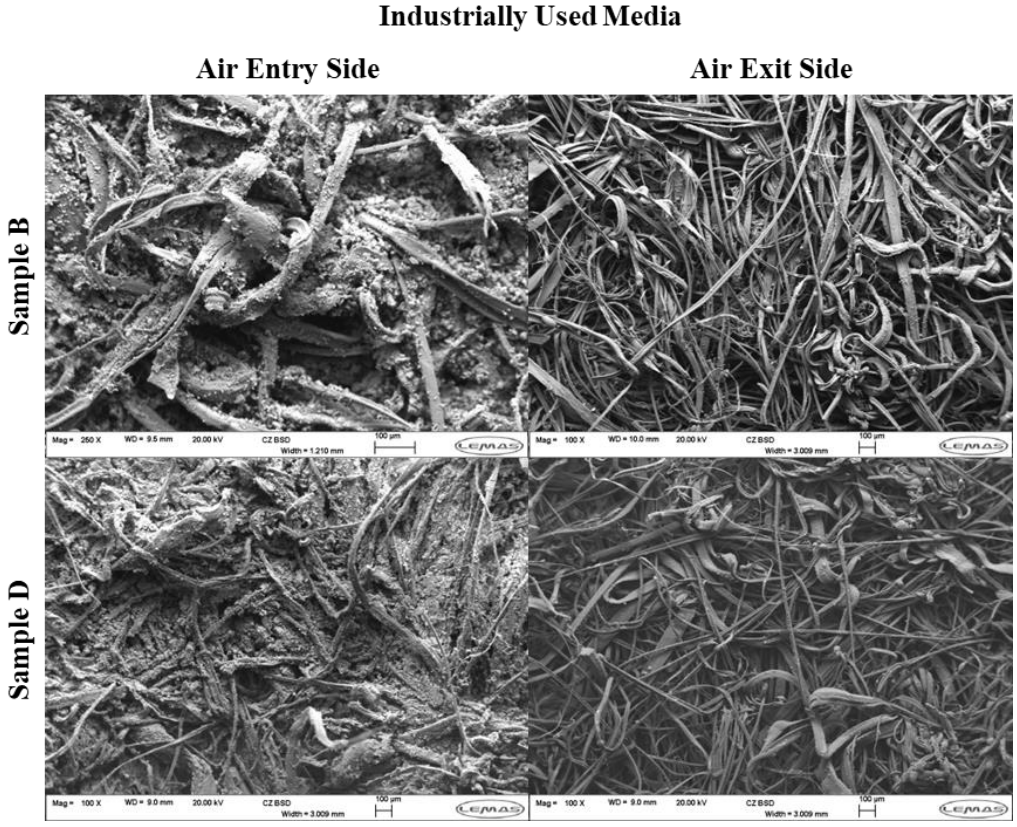

Figure 63: SEM Images of Air Entry and Exit Side of Industrially Used Samples Used in Longevity Study: Sample B = New and Sample D = Used

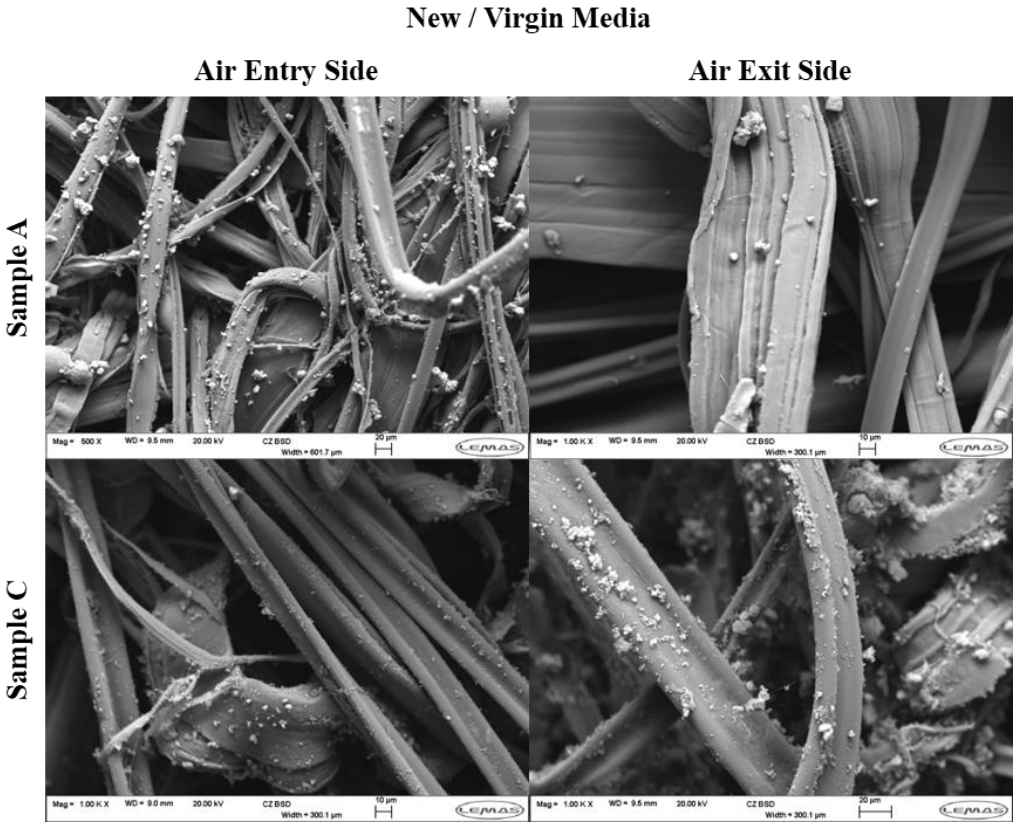

Figure 64: SEM Images of Areas of Interest on Sample A and Sample C

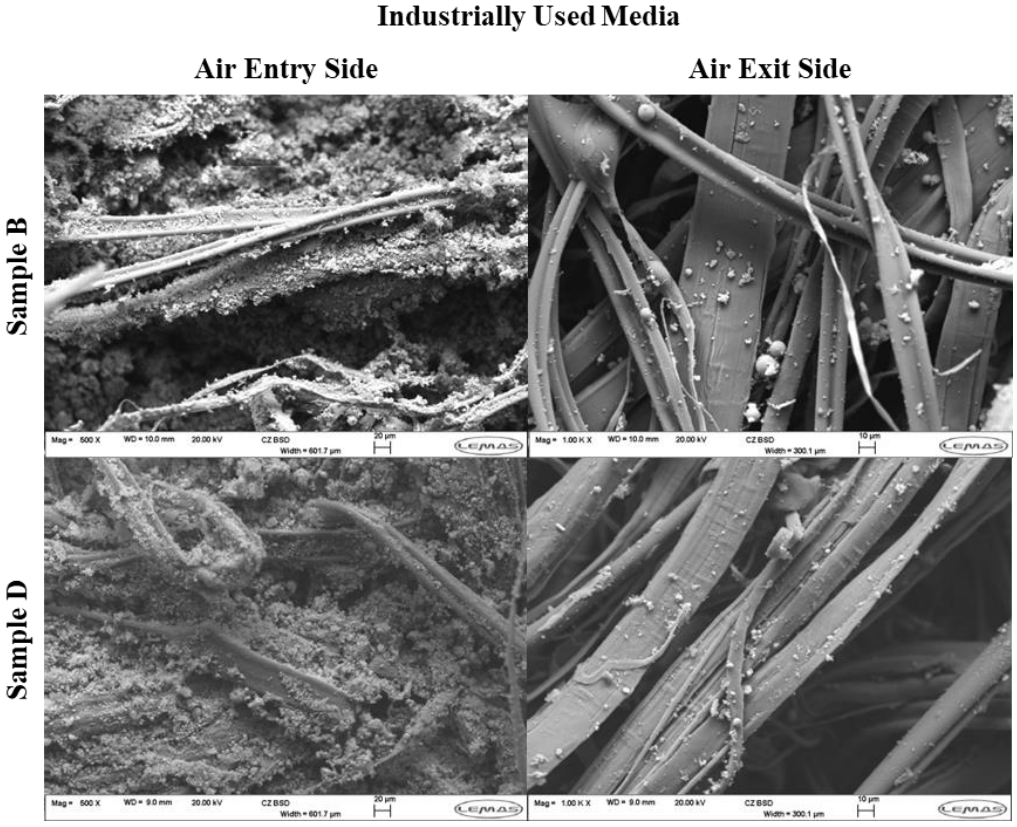

Figure 65: SEM Images of Areas of Interest on Sample B and Sample D

For Figure 62, it suggested that the retained filtrate post clean was minimal/negligible at a magnification of 100. Where sample A was the control (not used), sample C's images comparability suggested that the deposition mainly transpired at the air entry surface. The air exit side in both cases suggested no filtrate present, which was expected for Sample A. Sample C's air exit side did present with agglomerate like structures but given that these were noticed on Sample A's air entry side, it was thought that they originated from the manufacturing process and not due to usage. In addition, both the air entry and exit sides illustrated the heterogeneity of non-woven media, which results in regions where it would appear a channel like structure has formed. This channel could be due to the needle felt process which drives the fibres through the thickness of the media. A study by Cincik et al,. [9] and Chapter 6 illustrated a cross view of the needle point, showing a concave region at the air entry side, which supported this argument. Overall, there visually appeared to be little difference between the new sample (A) and evaluated sample (C) at the current magnification.

For Figure 63, it illustrated the industrially used filtration media, which had previously experienced both chemical and mechanical deformation, unlike the new/virgin media in Figure 62. This difference led to the air entry side of the pre-test media (sample B) exhibiting a degree of filtrate retention on the air entry surface. This retention of filtrate likely caused the baseline differential pressure across the filter. After testing in the FAR, sample D displayed a larger retention of filtrate at the air entry side when compared to sample B even after cleaning. This caused an apparent size reduction in the void spaces noticed in sample B's air entry side, which would promote fluid flow through. The formation of these voids is outside the scope of this work but could originate from the needle felt process. As shown in Chapter 6 Figure 43, the movement of the fibres through the media by the needle punch could have resulted in preferential internal deposition through the creation of channels within the media. For both air exit sides, at the same magnification of X100, there appeared to be minimal/no filtrate deposition. This could suggest that any suggested channels may be simply dispersed fibres which under the SEM image appear as channels. One alternative theory could be that even if there are channels through the media, the filtrate has not traversed through the filter. Regardless of any previous chemical/mechanical deformation, the retention of filtrate prior to analysis led to noticeable differences at the air entry side when compared to Figure 62 sample C.

Whilst both air exit sides of samples C and D suggested minimal filtrate present, their main difference stemmed at the air entry side. For sample A and C, the test used new/virgin media, which had no previous deposition. In contrast, sample B and D had retained some previous filtrate even after intense cleaning. This retention led to an increased baseline differential pressure. After completion, both samples were vacuumed as per the results of chapter 4. However, this led to different results. Significant removal of filtrate occurred for sample C, the virgin. In contrast though, the industrially used sample D appeared to have an increased retention of filtrate. This retention increased the surface area available for deposition to occur, and likely contributed to the apparent further retention noted after completion of the test. Although it underwent a vacuum clean, if the resultant force of the vacuum where not strong enough to overcome the forces acting to secure the filtrate, it would have remained. This observation however is limited by the surface area of the sample placed into the SEM chamber and whilst assumed representative, given the sample only accounted for approximately 11% of the total evaluated area. Whilst there is likely some variation in across the entire surface area of the bulk sample, the assumption of representation allowed for a wider range of samples to be evaluated. It therefore may be beneficial for future studies to evaluate and quantify the variation across the surface of a singular sample, to ensure that the whole surface area of the sample can be represented by a single sub-sample. This would dictate the number of subsamples needed to represent the overall sample, particularly when the considering the potential variation across the air entry side of the filter.

Shown by the particle size distribution graph in Figure 17, and summarized by Table 37, there is the potential that the magnification used in Figure 62 and Figure 63 failed to observe particularly small filtrate. To further examine the apparent minimal filtrate at the air exit side of all samples, the magnification was increased which allowed for the examination of finer details and regions of interest for each sample. Figure 64 and Figure 65 examined the virgin/new and industrially used samples respectively.

For Figure 64, sample A acted as a control sample, given it was not used in operation. Therefore, only fibres should have been visible. However, both the air entry and exit side illustrated flakes of some substance on the fibres. As SEM-EDX was not performed, there was two reasons for this observation. The first being the apparent flake originated from the manufacturing process, this could be part of a pre-treatment process applied to the media for example. Alternatively, is that the flakes could have originated due to accidental deposition from sample miss-handling. Although care was taken to remove the subsample, accidental

cross contamination of instruments within the laboratory could have led to this phenomenon's occurrence. Sample C underwent cleaning, which appeared to have led to some of the removal of these flakes. Understanding the chemical composition of these apparent flakes would help to identify the source of these potential contaminants. Re-analysis of sample A, using a brand-new media which is prepared in a separate, clean, laboratory away from any filtrate would aid to identify the potential source of the supposed contamination to the control.

At the higher magnification, Figure 64 sample C's air exit side suggested a greater amount of contamination to the filter, particularly on fibres below the surface. Given sample C underwent filtration, this could be filtrate that has transitioned through the filter media. Across Figure 64, the heterogeneity of the fibrous structure revealed voids which not only allowed the fluid to flow through but could facilitate deposition internally until surface and cake filtration could transpire. Some contamination is still noticed on sample C's air entry side, however given the potential contamination in the control sample (A), it is difficult to quantify if this is indeed filtrate. As a result, it is therefore difficult to definitively say that the apparent deposition noted at the air exit side of sample C is due to filtrate migration and not because of accidental contamination or from the manufacturing process.

Figure 65 focused on the apparent voids within the air entry side of the samples and again examined the deposits on the air exit side. The findings for the air exit side where like that of Sample C's. Inside the void of sample B, particulate deposition can be observed, which suggested that, to some degree, particulate movement from the surface to the depths of the filter had taken place. One limitation of SEM imaging is the inability to see at greater depths to quantify the extent of deposition with the depths of the filter. As such, this limited the observations to that which is visible in the image. Sample D, post operation and clean, suggested that these apparent voids had closed and reduced in apparent surface area. This would result in restricted fluid flow and a resultantly higher baseline differential pressure at the instance of pulse cleaning. As the sample had completed the test this theory matched the observed the results. Through an increased magnification, the extent of the filtrate retention is better shown, though as it only demonstrates the surface, it is difficult to quantify what happened below the surface as examined.

µCT

One potential technique to evaluate the variation below the surface of the subsample is µ-computed tomography (µCT). This technique has recently emerged to assess nonwoven filtration media. Results from this analysis would examine the porosity variation as a function across a specified direction of the sample. This would result in not only a global value but would describe the porosity evolution across the direction. Therefore, µCT could address the limited viewpoint of SEM and provide quantitative data about the sample as opposed to solely qualitative results from imaging alone.

A review of literature ascertained the current position of this technique in relation to nonwoven filtration media.

Literature Review

Microstructures of nonwoven filtration media consisted of pores within the material. These pores characterise the porosity of the filtration media and impact the baseline differential pressure across the media. Microcomputed tomography (µCT) afforded a way to visualise the microstructure of the sample in 3D, overcoming the 2D limitation place on SEM and other microscopy techniques. Achievement of this is through passing an X-ray beam through the sample at various rotations. A resultant 2D map is mathematically generated based on information afforded to the detector [270]. The sample is then moved vertically at incremental steps and repeated [188]. Thus, hundreds, if not thousands of these 2D maps transpire which are useful to generate a 3D model of the sample. Analysis of these 2D maps /3D models can then be utilised to determine quantitative qualities, such as material density [225], efficiency [14],and porosity [15], but also qualitative results based on the visual inspection of the sample.

This review focused on the applications and limitations of µCT as an evaluation technique. µCT has been used previously in various fields such as medicine [271] and for nuclear [272]. Discussion of the operational settings and general ownership are found in Vasarhelyi et al., [188],Landis et al., [273], and afifi et al., [274] and textbooks such as [275]. However, it is important to note, that the resolution of the image is defined by the voxel pixel size, coupled with the attenuation (μ_a) denoted at the detector [188]. Studies such as Buzug [275] and Li et al., [276] presented the Beer-Lambert (in its differential state), which defined the relationship between the attenuated light from a material of specific properties at a passing distance of (η), based on the Incident light (dI) and transmitted light $\big(I(\eta)\big)$.

$$\frac{dI}{I(\eta)} = -\mu_a d\eta$$

Equation 32: Beer-Lambert Law for Attenuation[275], [276]

An alternative way to consider the attenuation difference of materials is by relating it to the Hounsfield unit (HU) as shown by afifi et al., [274], and Buzug [275]. This scale used pure water (μ_w) as the zeroth point and air (μ_t) at -1000 HU, though the maximum is in excess of 3000 HU [275]. The application of HU is used in medicine to define the attenuation range when looking at particular elements within the subject such as blood [277] or the lungs [278]. One study by Hagita et al., [277] demonstrated the impact of artifacts within a subject, particularly foreign bodies of a metallic compound.

$$HU = CT\ number = 1000 \cdot \left(\frac{\mu_t - \mu_w}{\mu_w}\right)$$

Equation 33: Hounsfield Unit Based on the Beer-Lambert Law [274], [275]

In both medical imaging and examination of filtration material, the identification of foreign bodies determined the difference between normal and abnormal readings. Medical imaging of subjects [279] can be as easy as noticing higher, distinct attenuation patterns in the X-ray such as plastic army person or paper clips [280]. However, if the attenuation of the subject/ region of interest is similar to that of the foreign body, such as the plastic beads or Lego [280], the ability to differentiate becomes more difficult. Therefore, the radiologist (in this case the reader of the images), required a baseline knowledge of a "normal" subject before identification of abnormalities such as a small echogenic lesion [279] can be made. In the context of examining filtration media, it is important to note the original structure, prior to the discernment between original fibres (subject) and filtrate (foreign bodies).

Use of µCT as an analytical tool to evaluate filtration media is currently undergoing research and development to improve techniques and outputs. Software is available to researchers such as the suite of tools available from GeoDict® and Fluent® which take the raw tomographs, allow for 3D models to be built, and subsequent analysis of velocity profiles [235], transverse stress curves [281], particle displacement [282], porosity [283], and air permeability [270]. Use of software increased the accessibility towards performing analysis. Through automated generation of 3D models, computational dynamic simulations further explored the reachability of µCT towards woven and nonwoven textiles. One limitation though, is the expense incurred by the analyst to use software. Whilst free software such as

ImageJ® existed [227], [284], specialist software such as GeoDict® [14], [235] which is proven effective towards evaluating woven/nonwoven media and Fluent® [63] incur a cost to obtain a licence. Use of software streamlines the result acquisition process and reduced the learning curve associated with this technique.

In the past couple of years, studies have emerged evaluation nonwoven filtration media using µCT.

Jackiewicz et al,. [15] studied two distinctly different nonwoven filters under identical operational conditions, evaluation the difference in air blow velocity in the direction across the air entry face. Their work demonstrated that the particulate traversed more readily though the sample at higher blow velocities. The porosity evolutions corroborated this visual result and demonstrated that the initial unblown trough transitioned to a wider, shallower, porosity which revealed the particulate had transitioned more readily through the sample at higher. Their work demonstrated the power of µCT, which suggested the ability to monitor internal deposition through the sample at a given usage. Their limitation stemmed from their employed cleaning method. Experimentally different to pulse jet cleaning, non-removal of filtrate led to an increased collected mass. The orientation allowed the filtrate to remain on the air entry side, regardless of the cleaning flow direction being identical to the filtration flow direction. Therefore, in terms of baghouse filtration, their work provided the basis for analysis, suggesting that the porosity can be in terms of depth across the sample.

Riefler et al., [14] performed a more comprehensive study, using a more representative nonwoven to that of industrial use. Through experimental and CFD techniques, they demonstrated the effect that deposition of filtrate had on the structure. Most noteworthy was their deposition mass against the related penetration depth. At different concentrations, they demonstrated the conversion of particulate deposition to mass, which both isolated and quantified the depositional masses within the filter and their locations. One limitation of their work, stated in their conclusion, is the unaccountability for particle removal through detachment. This limitation s further extrapolated to only evaluating their sample between one cycle. Though at different time intervals between the baseline and maximum differential pressure, their results only simulated a specific cycle. In reality, internal deposition will affect this, due to the internal pores filling and/or expansion of pores. As a result, this not only affect the porosity at any given timeframe within the cycle, but also where the filter was in related to its remaining usable life.

Hoppe et al.,[225] performed a study using two different filters, but advanced previous literature through a more detailed discussion of the single fibre theory (SFT) model. In their work, they divided the sample porosity into slices and considered each individual particle sizes theoretical efficiency. They concluded their work by demonstrating that the deposition mass at a given load, based off the information obtained from the experimental study and the µCT results. Resultant deposition mass graphs illustrated how the filtrate deposited internally, whereby minimal internal deposition occurred if the resultant graph was narrow, and more prominent internal deposition represented by a broader graph. Whilst their work further developed the breadth towards the deployment of µCT to evaluate samples, it did not consider the evolution over service time.

Studies such as Riefler et al,. [14], Jackiewwicz et al,. [15], and Hopper et al,. [225] have illustrated a clear, comprehensive model in which to evaluate CT images. They demonstrated the variation under different exposures, presented the effect of particle size, and attempted to illustrate the impact of cleaning. However, in terms of their translation towards industrial samples, their studies omitted real world parameters such as the fly ash from combustion sites. The chemical composition of fly ash considerably varied [47], dependent on the fuel combusted. Given this, the resultant range of Hounsfield units may be large, which could cause a proportion of the greyscale values of the image becoming near to that of another material. One study, performed by Saps et al,. [280] demonstrated the attenuation differences between objects and background materials. When the bulk and subject densities equated similarly, the subject was not clearly visible in the tomograph. The same could happen for industrial samples, if the Hounsfield unit of the filter media is similar to the background, in comparison to the filtrate. Therefore, the question arose to whether it is possible to examine industrially relevant and used filtration media using this technique. Literature has yet to study these types of samples.

Methodology

Image processing is a step of techniques which convert the raw image into binary. Various authors have provided detailed reviews and software suggestions to accomplish this such as Landis and Keane [273], Cheng and Wang [282], and Huang et al., [283]. Given literature tended to agree with the use of the Otsu method, the Otsu method was chosen to process the resultant tomographs from the µCT scanning. Otsu [285] described the mathematical process which categorized the pixel values based on the image's histogram. This effectively

converted each pixel to one of two values, binarizing the image [285]. Other techniques such as image filtering to remove specs could be carried out before binarization, such as the study by Cheng and Wang [282]. In this study, only binarization transpired. One problem with any image processing technique is the inherent difficulty to validate the computer model based on the physical sample [283]. As processing complexity increases, a degree of material loss can occur, especially where the material observed at the voxel pixel size is below this size. As this study explored the potential application for industrially used filtration media, only binarization through the Otsu method [285] was used.

Table 42 provided an overview of the parameters selected for operation of the µCT machine, based on values observed in literature from Ali et al., [235], Liu et al., [281], and Huang et al., [283].

Table 42: Process Parameters for µCT Scan

	Value
Source Voltage (kV)	40
Source Current (uA)	149
Image Pixel Size (um)	4.18
Object to source Distance (mm)	51.00
Filter	No Filter Applied
Exposure (ms)	295
Rotation Step (deg)	0.70
Frame Averaging	2

A study by Huang et al., [286] utilized the multi-Otsu method by Otsu [285] which converted each pixel into a distinct value based on the threshold and defined number of bins for the data. The mathematical model used for this is presented in [285]. Huang et al., [286] defined this by the number of materials present in the image, which resulted in three distinct peaks when considering the histogram of the images pixels. From this, the idea of using the raw X-rays emerged. No literature was found during the search that used the raw X-rays. This raised the following question: could the raw X-ray be used to quantify the regions of density of the sample, given the heterogeneous nature?

The resultant X-ray exampled in Figure 66 (top left) suggested that there is region of higher and lower densities when looking at the sample. Given the complexity of the sample, particularly in the used state, it is difficult to quantify what is filtrate and what is media. The resultant X-ray image is defining the number of X-rays absorbed by the sample. In the presence of no material, all X-rays are absorbed leading to a near white background. As the

volume and material density changes in the X-rays path, the absorption also varied. This absorption variation resulted in the regions of lighter/darker on the X-ray.

To better understand the number of sections needed to categories the pixel values with for the binarization process, the distribution of the pixel values may indicate regions of significant material. Figure 66 (bottom left) illustrated this for the x-ray in Figure 66 (top left). A wide apparent gaussian distribution was found between approximately 0.1 to 0.8 on the greyscale distribution. In addition, a bimodal distribution was noted with an apparent mean of approximately 0.88 and 0.96 respectively. One of these peaks was more intense, which suggested that this peak may be attributed to the air whilst the other belonged to the sample. The wide distribution suggested that it too belonged to the sample. Its wide distribution meant that if it was assumed at the peak (roughly 0.43), then there may be some loss when thresholding. This led to three distinct peaks of the greyscale distribution of the image.

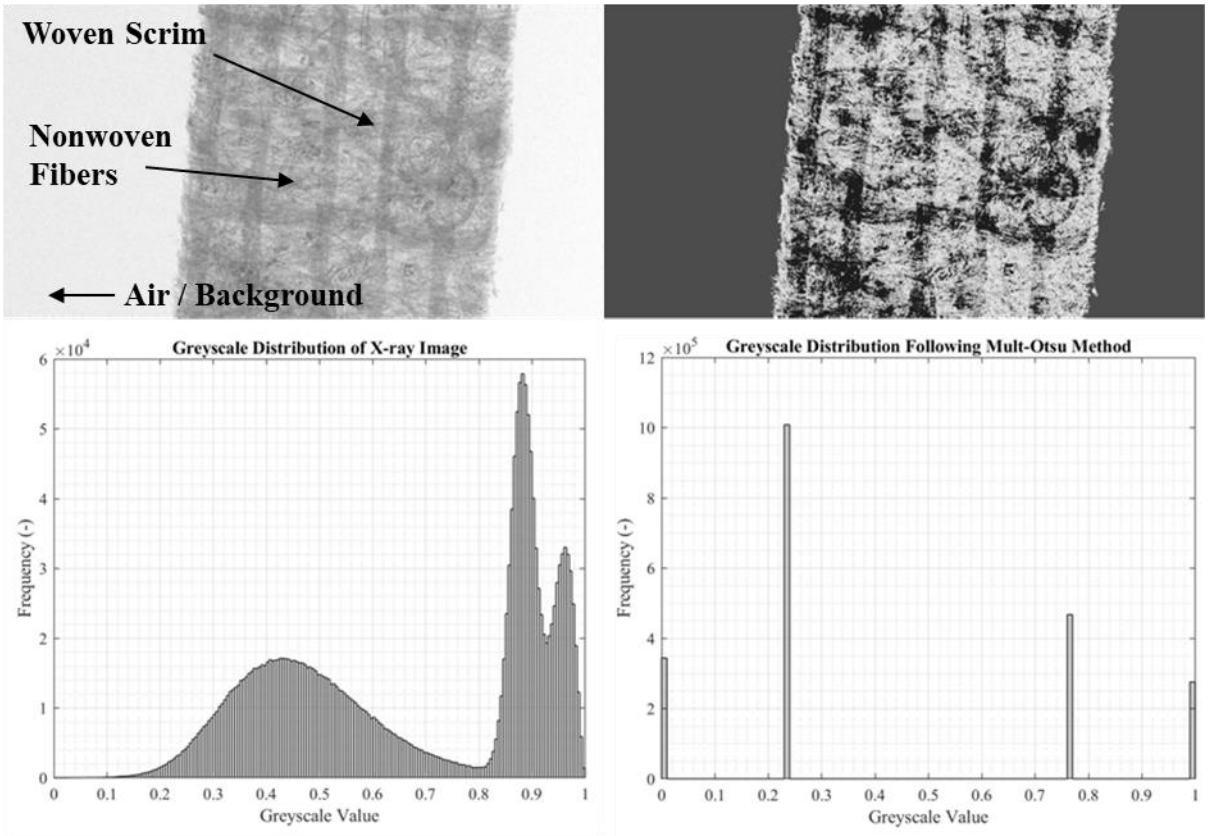

Figure 66: Image Processing to Determine Pixel Density from the Raw X-ray Images

The image threshold was set therefore set at three based on the peaks. This resulted all pixel values being organized into four distinct bins. This classification led to the raw X-ray shown in Figure 66 (top left) transforming into Figure 66 (top right). The resultant pixel values could

then be quantified to represent the density within the raw X-ray as shown in Figure 66 (bottom right).

This process was conducted across all samples face and side profiles.

Future applications of the technology and methodologies are needed to determine a more applicable method for the analysis of the types of samples used within this exploratory study of said technology. Whilst such an exploration of the methods is beyond the scope of this work, it is important to note that there will be a resultant effect on changing any of the operational parameters mentioned in Table 42. As such, the results presented explore some of the potential outcomes of the technology allowing qualitative comparisons and discussions. Consideration should also be given to the cost-benefit analysis of performing such a study, given the associated costs to use and operate the technology. This study therefore provides a basis, whilst still addressing the fact that no literature found has evaluated the raw X-rays, nor used industrially relevant used filtration media, with industrial filtrate.

Results and Discussion

Part 1: Raw X-ray Use

Use of raw X-ray images from µCT has yet to be explored.

Each sample is rotated 0.7° and an X-ray image is obtained. These images are then used to produce the tomographs more commonly associated with CT scanning. 284 X-ray images at different rotations were produced for each sample. This yielded a unique view of the sample at different angles. Profile and side views were removed from the X-rays generated and underwent image processing to ascertain the pixel density variation in each image. Figure 67 illustrated each samples profile and side view respectively.

Profile views of the samples in Figure 67 afforded a view of the scrim, noted as a cross hatch pattern. Appearance of the cross hatch showed that the density through the thickness of the sample, at the given pixel position, was higher than regions without any scrim present. Interestingly, the heterogeneous nature of the nonwoven fibres can be seen on the profile view. There were also some regions of high attenuation noted, particularly for samples B and D which had retained filtrate, although some were noted for samples A and C. Given the potential issue of contamination, it is difficult to attribute this to a particular material. Irrespective of this, the profile views afford a brief overview of the entire sample in terms of

general porosity, where the darker region of the sample is more dense/solid than the lighter regions.

Side views of the samples in Figure 67 suggested a general overview of the porosity over the thickness of the sample. Darker regions suggested more dense/solid regions of the sample. Lighter regions showed regions of lower material present and therefore a lower general porosity. Side views afforded a view of the fibres protruding from the upper and lower surfaces. In all samples, some fibres are visible protruding from the bulk surface. This results in the surface of the sample being heterogeneous. For samples A and C, only the scrim fibres that run parallel between the source and detector are visible. Given that the scrim itself is woven, the other portion will traverse above/below these points leading to a greater density variation and therefore not as visible. Sample B and sample D's scrim appeared more uniform as a singular vertical band, instead of clearly identifiable fibres of the scrim. Both samples originated from industrial use, undergoing chemical and mechanical degradation as opposed to samples A and C which underwent mechanical degradation only. Whilst it is not clear as to why the scrim appeared as a singular dense line, it could be that a degradation caused the scrim to become deformed in such a way to allow for this to occur. As a result, the scrim appeared as a high-density part of the side profile, almost riveling that of the un-removed filtrate deposits at the surface. Overall, the side profile X-ray gave an insight into how the porosity varied across the thickness of the sample.

Observational review relied heavily on the ability to identify patterns. Whilst the X-rays provided a good illustration of the sample at different viewpoints and considered a larger surface area, direct comparison between samples is hampered by sample variation. Thickness, density variations and atoms present will affect the attenuation and therefore the detected. To allow for direct comparison of samples, the assumptions made assume that between each sample group (A+C) and (B+D) the material, densities, thickness, and atoms present are equal.

To allow for comparison of the density variations retrieved from the image processing of each X-ray image, the following assumptions where made:

- The thickness variation between samples (A+C) and (B+D) was low enough to not affect attenuation
- Material densities between samples (A+C) and (B+D) where near identical.

- The presence of any remaining filtrate from testing did not significantly impact the attenuation.

Given the exploratory nature of this study due to the novelty of this approach, the overall method and assumptions need further development using industrial media and filtrate to ascertain the limits at which these assumptions hold true. Without this, whilst each individual sample provided a quantitative result instead of qualitative, direct comparison is difficult to achieve to a satisfactory accuracy. Image processing used the face and side profiles illustrated in Figure 67, the background was removed in each case given the sample size variation which allowed for the results to represent only the sample. Figure 68(top) illustrated the density values for all samples face profiles, with Figure 68(bottom) showing the side profiles.

Figure 68 (top) displayed the contribution of low, medium, and high densities noted for the face profile. The contributions across the samples where similar, with only slight contribution variation noted. The face profile addressed the limitation of SEM to evaluate through the filter. However, it could not differentiate between fibres and/or deposits. It therefore could not say if it was dense due to fibres present at the pixel location (through the sample) or if deposition had taken place. This is particularly true for sample D, which according to the SEM results, underwent more deposition than sample B Theoretically, this should have led to the values for medium/high density being higher than sample B, yet this was not the case. This through doubt on accuracy of the results obtained for the face profile.

Figure 68 (bottom) displayed the contribution of low, medium, and high densities noted for the side profile. Unlike the results for the face profile, there was a distinct difference between samples (A+C) and (B+D). SEM results suggested that samples C and D exhibited a higher retention of filtrate/contamination than their states prior to test completion. Examination of the side profile suggested that the virgin increased by 18%/-10% and industrially used by 12%/-8% for high and medium densities, respectively. The density changes, particularly towards higher densities, suggested that the porosity had decreased in some areas of the filters thickness. The X-ray side profile suggested this increase transpired largely at the scrim and surface of the filter, though it is difficult to ascertain given the inability to differentiate between the materials. Therefore, unlike the face profile, the side profile gave an indication as to the how the sample varied upon completion of the test in both samples.

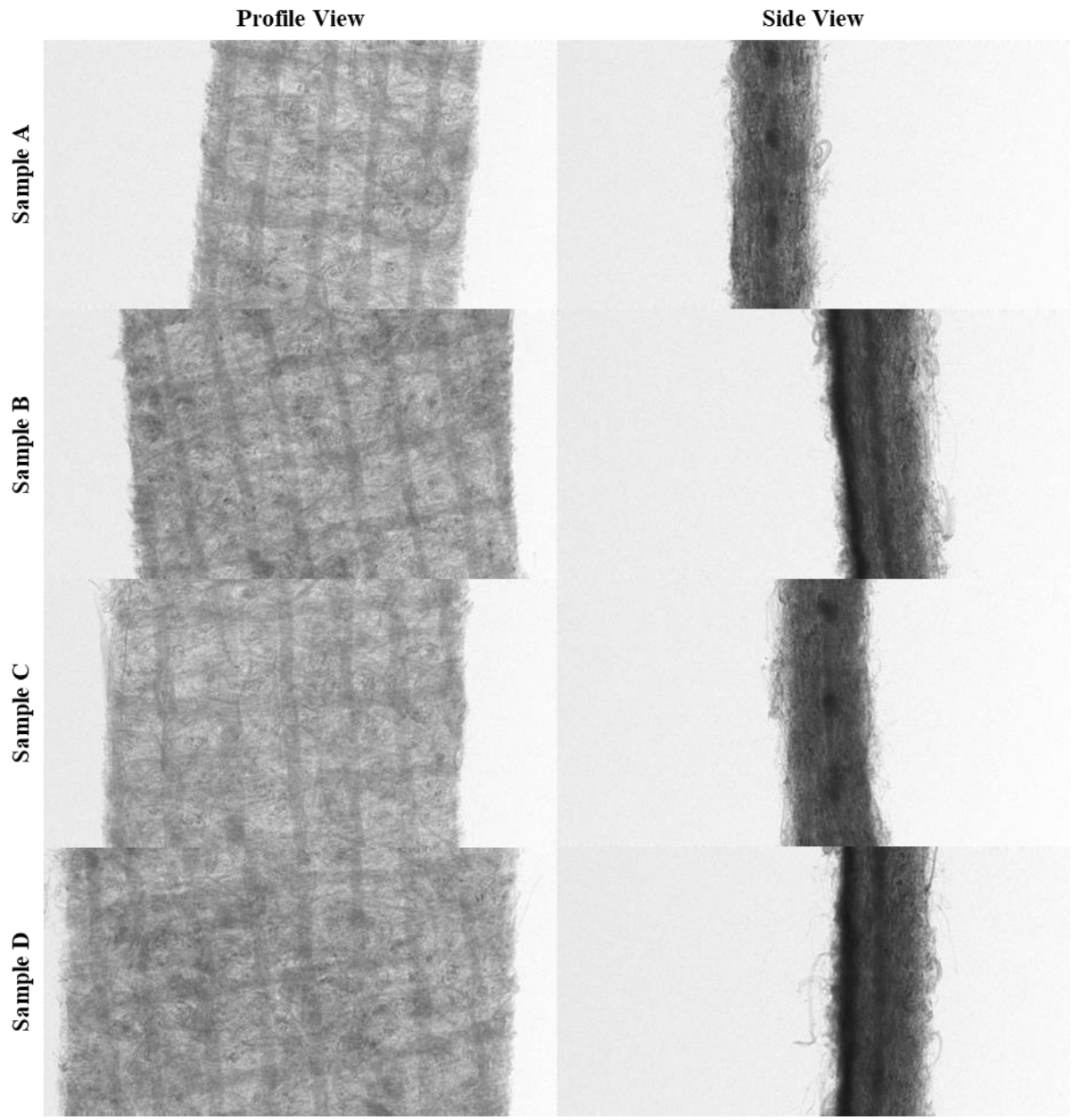

Figure 67: X-ray Face and Side Profiles of Samples A, B, C, and D

Whilst the side profile of the X-ray image suggested the density variation, it couldn't specify an exact value for porosity. The resultant analysis only supported the visual observations made from either the raw or processed X-rays. The benefit of evaluating the X-rays is that it provided a quick and simplistic way to evaluate the sample, without relying on software or additional processing steps to gain a further insight. The porosity variation through the sample can be found by evaluating the tomographs.

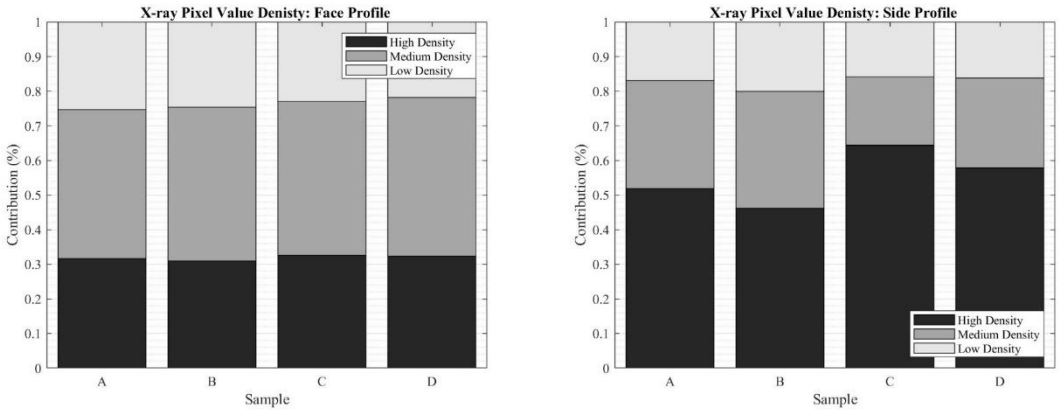

Figure 68: Face and Side Profile Pixel Density Results (Background Removed) for Samples A, B, C, and D

Part 2: Tomograph Use

An example tomograph is shown in Figure 69. Each tomograph represented a 4.18µm slice of the sample and produced a total of 1047 tomographs which equated to a total vertical height 4.47mm. The sample width was defined by the size of the cut and as such varied across each sample as visible in the face profiles of Figure 67. Each tomograph underwent rotation to align the sample parallel to the boundary of the image. From this, a region of interest was removed, comprising of sample and background. Each sample then underwent binarization. An average across the resultant image was taken and this formed the porosity based on the ratio of empty pixels (black) to solid pixels (white). The thickness was evaluated to understand the evolution of porosity through the filter.

To ascertain where the sample started and finished, there was a degree of background left in the image. This was evaluated based on the porosity variation over the thickness. A sample region of known background was removed from the tomograph and its respective porosity calculated. The 95th percentile confidence interval was then used to define the transition point between background and sample. The background was then discounted from the porosity which yielded only the sample. Removal of the background was performed for all samples, which allowed for the determination of the samples thickness.

This process yielded three results: the samples thickness (Table 43), overall porosity, and the porosity evolution through the sample.

Thickness results obtained through µCT varied significantly to that of the thickness gauge as shown in Table 43. The control, sample A, had a thickness like the datasheet shown in Appendix A for Site C. µCT evaluated the thickness of the sample at the point at which the porosity was lower than the background, whereas the thickness gauge was dependent on the

samples ability to resist a constant load. The former led to a slight compression of the sample, whilst the latter considered the start/endpoint as wherever there was a fibre or filtrate, regardless of its protrusion from the main body of the sample. This led to difference noted in Table 43.

Table 43: Sample Thickness from µCT and Thickenss Guage

Sample	Thickness Gauge (mm)	µCT (mm)	Difference (%)
A	1.33	1.72	29.49
B	1.36	2.02	48.45
C	1.35	2.12	56.98
D	1.37	1.99	45.23

The large difference between the thickness gauge and µCT could have originated from a slight misalignment during orientation, which would have caused the filter to protrude slight and result in a higher perceived thickness. Furthermore, the inclusion of loose surface fibres would have influenced the value. The thickness gauge overcomes these problems but could lead to slight compression depending on the heterogeneity of the sample. Given that the thickness gauge method is well established and applied throughout literature, the values obtained through this method for each sample were assumed to have good accuracy for comparison. Therefore, there is a degree of overestimation when evaluating the thickness of samples under µCT if the samples orientation is misaligned or fibre protrusion is sufficient to influence where the background ends and the sample starts.

The global porosity value was the average across the entire samples thickness and is summarized in Table 44. The solidity is also reported in Table 44, which aids in understanding the change between pre and post-test conditions.

Theoretically, the porosity should decrease (solidity increase) through usage due to particulate deposition internally. SEM results for Samples B+D suggested this by the increased presence of filtrate/contamination at the air entry surface. Global porosity results showed that the porosity decreased by 1.7%. This decrease was due to the retention of filtrate. In contrast, the porosity increased by 2.25% for the virgin samples. An increase in porosity could only occur in two ways: when cleaned, more material was removed than the pre-op sample (in this case sample A). Alternatively, the sample underwent a thickness increase which resulted in the pores within the sample increasing in volume and therefore becoming more porous. Whilst the industrially used samples conformed to theory, the virgin/new samples deviated. To examine the deviation further, the porosity evolution through the

sample would indicate where variation occurred, but also offered a further insight into how the filter faired under experimental conditions.

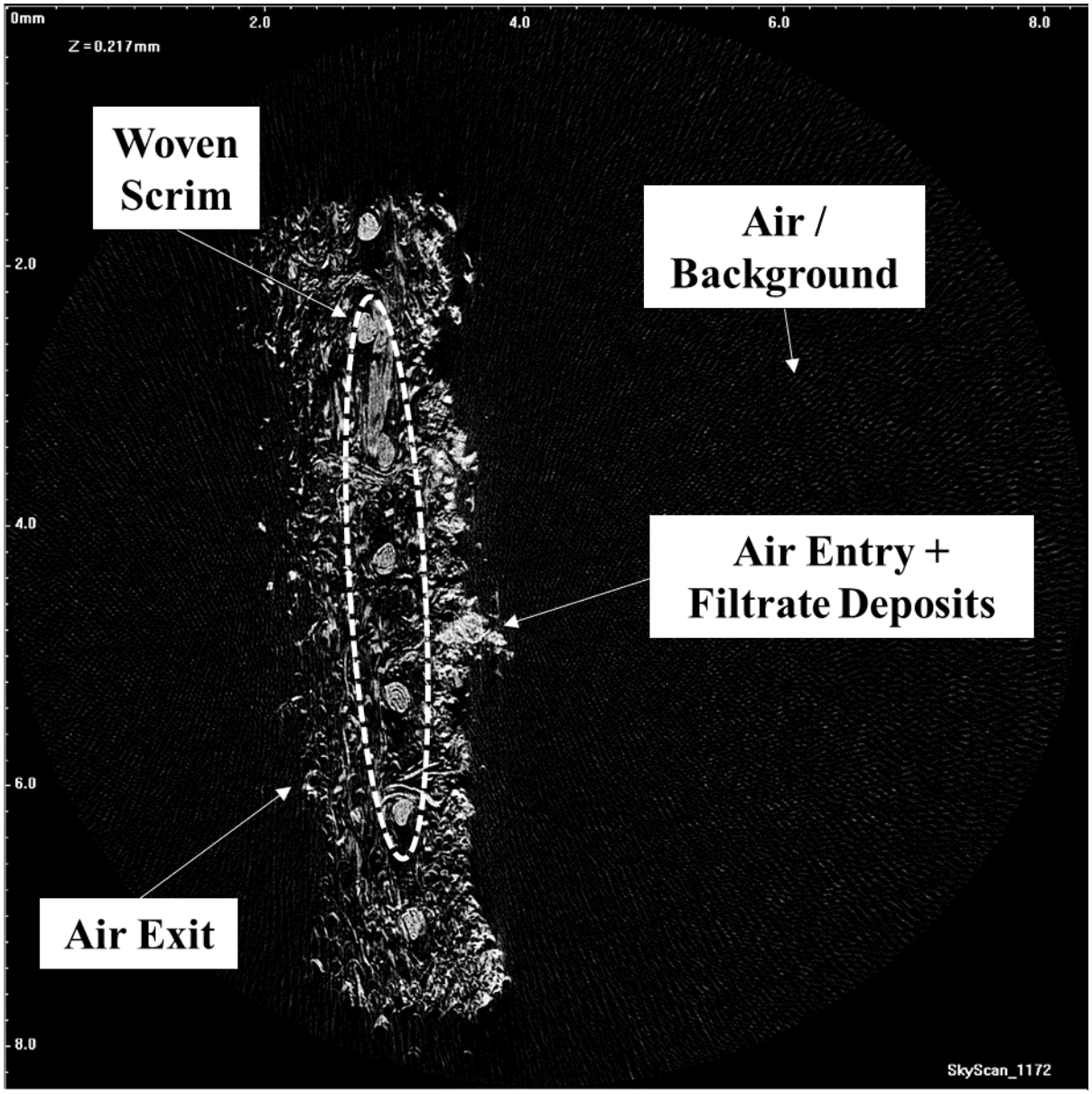

Figure 69: Example Tomograph of Sample B

Table 44: Global Porosity Values for Samples A, B, C, and D

	Sample			
	A	B	C	D
Porosity (%)	78.02	79.19	80.87	77.49
Solidity (%)	21.98	20.81	19.73	22.51

Comparison of the global porosities between Table 41 and Table 44 led to a general discrepancy of 8.94% where the calculated porosities where higher than the μCT results. The calculation relied on the differentiation of filtrate and fibres ad could be subsequently summated. The μCT treated porosity based on the attenuation, regardless of the material present. The observed values in Table 41, though suggesting both had reached the same failure point in terms of porosity, failed to suggest any significant change had transpired between the samples.

Demonstrated in Figure 70, for Sample D, is the porosity variation through all samples. Subsequently, this graph was broken down into two parts: Figure 71 which represented the virgin/new media (sample A+C) and Figure 72 which represented the industrially used media (sample (B+D). These graphs reported the porosity. As the porosity decreases, the solidity increases. The sample was orientated so that the air exit side was at the 0^{th} point of thickness. This meant that the air entry side started at the largest recorded thickness value towards the right-hand side of each graph.

Comparison between the virgin and industrially used media porosity is shown in Figure 70. Initial observations showed that the porosity difference at the air entry side was greater for the virgin as opposed to the industrially. Whilst the industrially sample was washed prior to testing, there was still deposition noticed at the surface as shown in Figure 65. Post filter testing, both the virgin and industrial samples underwent identical cleaning steps before evaluating them under SEM and μCT. Therefore, the main sample difference was the exposure to flue gas and filtrate. This difference contributed to the variation between the samples.

Figure 71 demonstrated that the perceived thickness of the used sample had increased by approximately 0.42mm. This increase, and associated porosity, likely contributed to the perceived porosity increase. The air exit side appeared largely similar up to approximately the 0.46mm mark. At this point, sample A's porosity decreased towards a local minimum at 0.84mm before rising again towards the air entry side. Given the X-ray image, this point is likely to be attributed to the position of the scrim. Sample C's porosity appeared to largely level off at 0.84mm, before rising at approximately the 1.46mm mark.

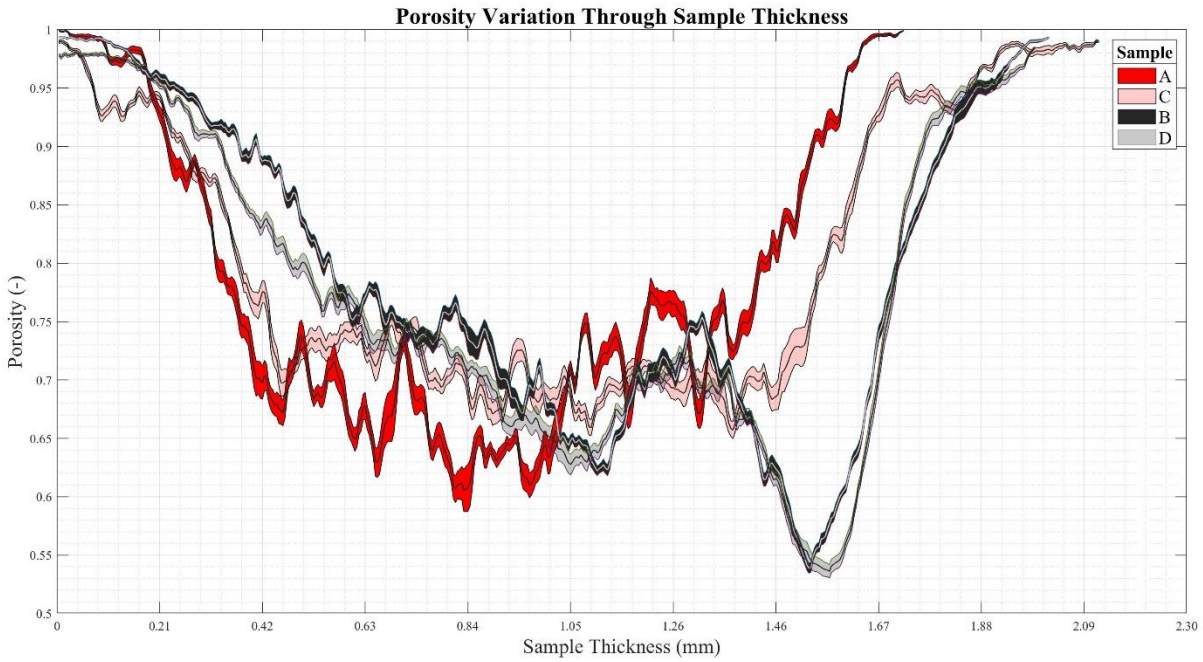

Figure 70: Porosity Variation Through the Samples Thickness for Samples A+B+C+D

At the air entry side of sample A, the porosity of sample C was generally lower between roughly 1.05mm and 1.71mm. This reduction could suggest that some blinding had occurred but was generally 0.42mm below the surface of sample C. This could be due to fine particulate migration through the filter, which was collected internally as opposed to at the surface. Although sample C displayed surface filtrate, the post clean with the dust vacuum appeared to remove most of the deposited filtrate and is supported by Figure 62. If the removal was highly effective, this could explain to some extent why the porosity at the air entry side of sample C is particularly high. Consequently, the removal questioned whether the sample had indeed reached its maximum filtration capacity. Given Chapter 4's findings of the dust vacuum being applicable for nonwoven filtration media, it may not be the correct method for test filters which undergo mechanical degradation only at ambient conditions and use controlled test dusts. However, this failed to account for the apparent expansion of the sample, which led to the global porosity value increasing. If sample C's air entry side matched up, the resultant air permeability would likely have conformed to the theory.

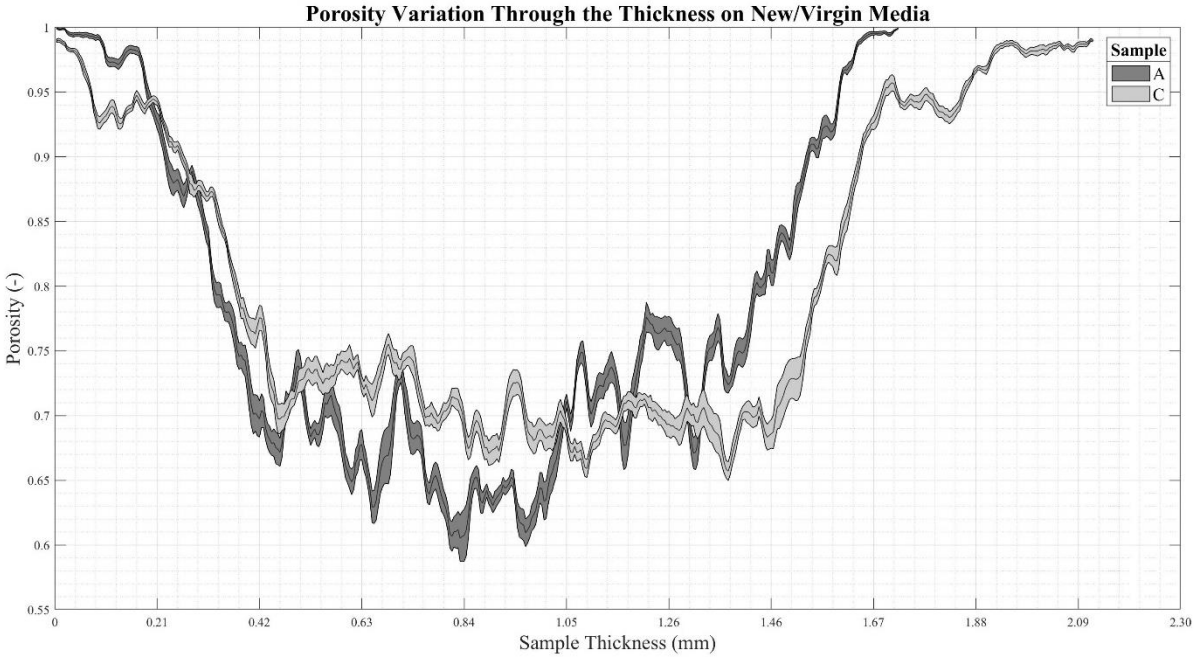

Figure 71: Porosity Variation Through the Samples Thickness for Samples A+C

Figure 72 showed that sample D had areas of lower porosity, particularly towards the air exit side and parts of the air entry side. The air exit side of sample D was predominantly below sample B's porosity between 0mm and 1.05mm. After which, the porosity differences were largely similar until 1.53mm at this point, the porosity was generally lower than the original sample, except between roughly 1.71mm and 1.88mm where the porosity of sample D was higher than sample B. Although there were noted differences, the general shape of the graph remained similar. It appeared that, particularly for the air exit side, more deposition/contamination had taken place which ultimately led to the global porosity decreasing after usage which was expected to happen.

The noted deposition at the surface in Figure 63 transpired in the local minimum porosity at approximately 1.52mm for sample B. This followed theory as the porosity should decrease in the presence of blockage. This feature from sample B translated over to sample D, though with a slight shift towards the air entry side. Given the slightness of the shift, this was attributed to local variation between the sample. The lower porosity at the air entry side also supported the suggestions of Figure 63.

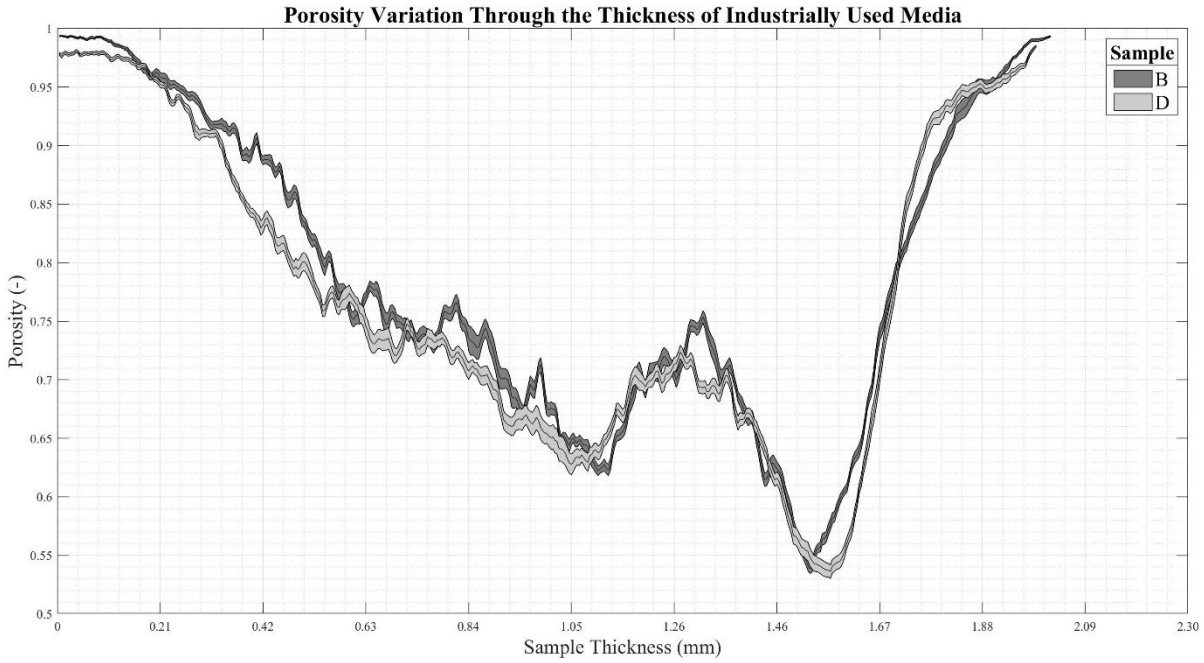

Figure 72: Porosity Variation Through the Samples Thickness for Samples B+D

Conclusion of exploratory study

Whilst the results of Chapter 4 suggested vacuum cleaning as an appropriate cleaning method, it appeared to have removed the bulk of the filtrate from the virgin sample. SEM images and porosity curves for sample C showed minimal filtrate retained in/on the sample and suggested that the thickness had increased. This led to the porosity of the used sample being higher than the original, which went against theory. In contrast, the industrially used sample retained a porosity shape and general thickness. Post-test, the industrial sample reduced in porosity, conforming to the theory that some filtrate would have deposited within/on the sample. This retention could have been facilitated by the retained filtrate from industrial conditions, which increased collection efficiency. This was noted by the shift in the local porosity minimum between samples B and D. This conflict suggested that the cleaning method employed was over efficient and not representative of industrial samples using the current test filtrate and virgin media.

As stated in chapter 4, the aim of the vacuum was to simulate an effective pulse clean. However, as shown, this over cleaned the virgin affecting the results. The testing procedure saw a sample ran to the end of its usable life, deemed to be when the filtration cycle became less that 1-2 second intervals post clean. This saw the baseline differential pressure across the filter being considerably higher than it's original. Given that the test rig operated using a cleaning pulse system, there is scope for the cleaning method to be by pulse instead of

vacuum cleaning. A design study, similar to chapter 4 would evaluate the effectiveness of this. Initial steps would be to stop the test at the deemed failure point, without cleaning, evaluate offline, and then clean via pulse with online conditions (minus filtrate flow). Using a cleaning pulse instead of vacuum cleaning would likely provide a more representative set of results for the virgin sample, showing retained deposits and their impact on porosity.

One potential factor which may have affected the results is the variation between, not only the difference in samples used for µCT and SEM analysis, but also variation from the sample. As only approximately 11% of the surface area was examined for both techniques, and different samples used for each analytical method, there is likely some inherent variation. This required the assumption of idyllic representation between the samples, which as shown for Chapters 5 and 6, may lead to a slight skewness in the interpretation of results depending on the ultimate value obtained. Given the destructive nature of sampling for µCT and SEM, a study using the sample for both techniques, coupled with a methodical study across the sample, would ascertain if single sampling is indeed representative.

µCT has been shown to provide critical information about the porosity through the sample. Whilst some studies have begun to evaluate laboratory controlled samples, this exploratory study used industrially derived media samples, which had undergone chemical and mechanical degradation: the first study of its kind based on the literature review. Whilst method development is still underway, the results appeared promising, particularly for the industrially used samples which conformed to the theory. An example of industrially used sample with respective filtrate remaining on the surface, showing the resultant variation in terms of attenuation on the tomograph can be found in Appendix C. Whilst the exploratory study did not consider the longevity, it demonstrated the obtainable results, which could form part of a study to either model or predict the remaining longevity. Whilst further studies are needed around sample representation and processing, the technique provided an insight into how the sample changed in terms of porosity over the thickness of the sample: something not currently possible using global assessment techniques.

7.4 Conclusions and Recommendations

7.4.1 Overall Critical Analysis

The present study identified a potential evaluation method for industrially used filtration media. Achievement of which transpired through a simplified evaluation method, which defined a theoretical endpoint in which the filter sample had no remaining life. New/virgin media and an industrially used filter media were evaluated using as close to industrial operational conditions as possible. The samples where then removed and tested for mass, thickness, and air permeability. SEM and μCT analysis where also conducted. During analysis of the new/virgin sample, the FAR failed which led to a noticeable difference in the online results when compared to the industrially used sample. Subsequently, repetition of the new/virgin sample (with the possibility to include the emission data if the probe becomes available) would confirm or deny the previously observed data for the industrially relevant media.

Offline data analysis displayed a wide range of techniques to evaluate the sample in isolation of the FAR. However, the cleaning step used to change the sample from the AR to PC state led to some of the results obtained from thickness and air permeability testing to deviate from the anticipated results. One of the reasons for this was the limited sample size for air permeability, which could have allowed for unintentional air ingress, particularly for the PC testing which saw a significantly higher air permeability in both samples. Furthermore, the variability in sample movement during testing for thickness, coupled with the global only value for mass, led to a reduced representation of the sample numerically. Consequently, the practicality of performing air permeability on such a small sample, on the current apparatus, led to the question around omitting it in favour of clearly defined, sub samples for mass, thickens, and porosity. This sequential sub sampling would allow for better control/accountability of samples. Development towards exactly which techniques are essential, and which are optional, will determine the most optimal method of evaluating the sample offline. Furthermore, the option to perform a pulse clean before vacuuming could prove to be more representative of actual conditions, prior to vacuuming.

μCT and SEM imaging afforded both quantitative and qualitative results about the samples. SEM imaging afforded visual clues towards the deposition at the air entry and exit sides. One potential limitation is the presence of potential contamination noted on sample A, the new/ unused sample. Though this could be remnants of the manufacturing process, or some form of pre-treatment, it hampered the ability to differentiate it from filtrate deposited on the

sample after filtration testing. μCT afforded a view through the thickness of the samples and demonstrated the porosity through the sample thickness. These results, in combination with the visuals from SEM imaging, confirmed that the industrial samples B and D underwent deposition, particularly towards the air entry/exit sides. For the virgin media, the SEM results noted no real discernible difference in terms of contamination, yet the porosity results suggested that the sample had increased significantly in terms of thickness. This preliminary study highlighted potential issues with analytical techniques and the current methodology used to evaluate the sample. Furthermore, future SEM and μCT analysis would use the same sample for more accurate qualitative comparisons. In addition, a controlled methodical study across the full surface area would indicate the required number of samples needed to be representative. Lastly, the issue about cleaning using a dust vacuum. For the virgin sample, it seemed to over clean, which led to the suggestion of minimal deposition remaining. Overcleaning would skew the results by suggesting the media is still operational, when in reality, the site would just replace the media to reduce downtime. Including pulse cleaning as an additional analytical data category would likely demonstrate that pulse jet cleaning is in fact more representative of the process. Overall, the exploratory study demonstrated the impact that μCT can have when considering the filtration media performance/longevity.

7.4.2 Novelty and Impact

Though preliminary, this study afforded an insight into evaluating the media performance/longevity of new/virgin filtration media and respective industrially used filtration media samples through a simplified and representative evaluation method. This study evaluated samples up to their endpoint: something not performed within literature. The failure point of this study surpassed the industrial point by going until the differential pressure difference between the cleaning and baseline equated to zero, with subsequent cycle duration/time also equating to near unity. Industrially defined failure relied on emission data and economic costs, which were not considered as these vary depending on site and management specifications. However, the results of this study suggested ways in which this may be determined, such as through the definition of failure at a cycle time or set cycle difference differential pressure.

Critical assessment of the data and subsequent analysis discussed how further analysis/research may obtain the best possible results from each sample. Discussions on the online data led to the suggestion to create a chart for each site, using new media as a baseline. Different operational aged filtration media would allow for the completion of said chart and

would guide future samples in determining the age of subsequent samples, without having to complete the full study.

Offline data demonstrated multiple of evaluation techniques. The post clean method needs further investigation. Removal of air permeability evaluation would allow for focused sub sampling of the sample, which would yield a more accurate global value with a representative variation. This critical assessment of offline analytical techniques allowed for future researchers to better understand the results and develop a clearer methodology to evaluate the media performance/longevity.

µCT is still in its infancy for nonwoven filtration media analysis and prior to this exploratory study as not performed on industrially derived filtration media. This exploratory study demonstrated the impact that this analytical technique can have towards understanding the state of used filtration media. Furthermore, it proposed using the raw X-ray images, which have, until this study, been omitted from any analytics based on the literature search. The resultant porosity curves displayed a basis for future research, particularly when considering the difference between industrially used and virgin media under filtration assessment conditions. With further development around µCT operational conditions, image process, and method development, µCT analysis showed where and by how much the porosity changed and provided a definitive result to aid the explanation of larger global results.

7.4.3 Further Research

This preliminary study afforded an important insight into how the conduction of future research may occur. Give the observations made during the critical assessment of the two samples examined, the following points raised will guide and expand the current knowledge. This expansion will allow for a more accurate proposal towards the examination methodology for industrially used filtration media. As such, future research may choose to focus on the following observations made within this study:

1. Repetition of a new/virgin sample. This would ascertain if the parabolic nature suggested in Figure 60 was due to failure of the FAR or if new media does indeed exhibit this function. Given the industrially used media exhibited a clear exponential function, it seems unlikely, that the parabolic nature is true, but this needs confirmation before continuing.
2. The post clean method used within this study impacted the offline results. It would be more representative to first examine the sample in the post operational state, then

perform a pulse clean using site specific parameters. This clean would be a better representation of actual industrial practices. After pulse cleaning evaluation then the vacuum method could be used to evaluate the media only. Research around this subject, similar to that of Chapter 4, would ensure that the resultant offline data is more representative of actual conditions.

3. Causality examination as to why the used sample lasted longer than the new sample in terms of number of filtration cycles. This could be due to failure of the FAR, still requires an understanding of the difference between the new and industrially used sample. Whilst the results presented in this study suggested why, repetition of the same media or of a different site would ascertain not only if the failure resulted in this but allow for a clearer comparison between the samples in terms of online and offline data.
4. Offline data critiqued mass, thickness, air permeability, and porosity. However, given the sample must remain whole for air permeability, this contributed to the observed issues raised. The subsequent recommendation was to remove air permeability, in favour of sub sectioning which allowed for more sequential analysis as opposed to holistic. Although the obtained overall mean will still be holistic of the sample, accountability for a better variation representation would better describe the sample. The decision to remove air permeability would be based on the analyst. Research around this methodology would decide whether to remove it or not, or if it is necessary. If it is necessary to conduct air permeability, the machine will need upgrades to mitigate against accidental air ingress given the results shown in Figure 61 and Table 40.

Future modelling of the remaining longevity could use the chart idea previously mentioned or combine multiple industrially used samples to create a mathematical equation. Regardless, of the method, it would still require a sample to be evaluated in the FAR. This evaluation would need development to reduce the time required. As shown in Chapters 5 and 6, variation in parameters exists across the filtration bag. Therefore, this variation will also need to be examined, quantified, and an optimal model suggested to minimise the evaluation time, but still yield a confident result.

Chapter 8: Conclusions and Future Research Recommendations

8.1 Thesis Conclusion

The overall thesis aim was to examine various analytical techniques, such as air permeability, mass/density, and thickness, and enhance the understanding of the potential variation when examining industrially derived samples. In addition, a novel analytical technique, micro-computed tomography (μCT), was also explored using industrially derived samples. Overall, this thesis:

- Used industrial media from site B, to evaluate the cleaning methods stated in BS22031:2021 "Sampling and test method for cleanable filter media taken from filters of systems in operation" [16]. These stated methods, including one additional method: washing, were examined for the potential variation with the subsequent analysis after cleaning had been performed. Air permeability, sample mass/density, and thickness measurements were used to evaluate the various cleaning methods and showed that vacuuming the surface of the media provided the best recovery.
- High resolution mapping was performed on industrially derived samples for analytical techniques mass/density and thickness (site A) and air permeability (site B) to better understand the variation within a given sample size and any potential relationships. Results suggested that a relationship existed in the resultant data about the circumference of the filtration media. Whilst the mass/density and thickness relationship was best described as a Fourier type relationship, the air permeability appeared to be parabolic. When performing these analytical techniques, random sampling should be performed in order to improve the likelihood of obtaining a representative sample mean, given analysis in a fixed direction may yield the opposite and therefore impact data interpretation.
- Micro-computed tomography (μCT) was applied as an additional technique used during a preliminary longevity study which used industrially derived filter media (site C). This study demonstrated how the filter changed over an increasing number of filtration and cleaning cycles until it reached a pre-defined endpoint. The application of µCT demonstrated how the porosity of the filter media changed between it designated "new" state and post cleaned "final" state.

The sample mass/density, thickness, and air permeability studies demonstrated that fixed directional sampling may yield a statistically different mean than the global mean of the sample. However, it did show that fixed directional sampling could obtain more information about the sample, particularly about the circumference of the media. Analysis about the circumference of the media suggested regions of higher/lower values, which could impact the data analysis. Therefore, by performing higher resolution studies across various analytical techniques such as air permeability, mass/density, and thickness, a better understanding towards the potential variation was obtained.

8.2 Thesis Findings

The following findings are the outputs of the thesis:

- Whilst BS22031:2021 "Sampling and test method for cleanable filter media taken from filters of systems in operation" [16] allowed for any cleaning method to be used to convert the sample from the as received state to the post cleaned state, vacuuming should be recommended. This recommendation was based on the air permeability, sample mass and thickness analytical results determined when comparing various cleaning methods referred to in the standard such as brushing and scraping. An additional cleaning method: washing, was also evaluated, but due to the significant increase in sample turnaround time (due to the drying time), it is thought to be impractical at large scale.
- Fixed directional sampling for air permeability, sample mass/density, and thickness has the potential to yield a statistically different mean from the global mean which could adversely impact the subsequent analysis. Standards should be updated to explicitly specify this to promote a more representative mean.
- Fixed directional analysis for air permeability, sample mass/density, and thickness demonstrated a relationship which illustrated regions of higher/lower data values. Therefore, fixed directional analysis could provide more information about the filtration media in particular regions, as opposed to a global value. However, analysis in a fixed direction would need to be performed after random sampling, which would therefore increase the sample turnaround time and therefore have a potential impact downstream in terms of site operation and increased time required to understand the data.
- The critical evaluation of a longevity study is the first of its nature which used industrially used samples and new media. The study demonstrated that as the

difference between the baseline differential pressure and fixed cleaning differential pressure decreased, the time required for the baseline differential pressure to reach the cleaning differential pressure also decreased, which conformed to theory. If samples from the same site can be obtained with different operational times, a chart could be produced which could calculate the remaining longevity of future samples based on the analysis of subsequent samples. This ideology needs further study and exploration, however if possible, this could significantly improve the prediction of how long the media has left before reaching ultimate failure/ it's end of life point.

- µCT is a new and exciting analytical technique, which demonstrated the possibility to evaluate the porosity variation through industrially used and new samples of filtration media. The current literature which surrounds the use of µCT to evaluate industrially used filtration media is restricted, but the results obtained as part of this study demonstrated it is possible to obtain the overall porosity of the sample, as well as how the porosity changes through the thickness of the sample. In addition, the raw X-rays which are often omitted from analysis are capable of providing qualitative information about the density variation at both the face and side profile. Therefore, these should also be considered during evaluation of the µCT porosity results. Overall, the study demonstrated that µCT of filtration media is possible and can obtain results about how the media has changed during operation in terms of the resultant porosity variation.

8.3 Further Research

- Increasing the sample size of the mass/density and thickness study to incorporate a full, industrially used nonwoven filtration bag. This future study would continue to explore the possibility that a Fourier relationship exists about the circumference of the media. In addition, the data received from the study can explore the variation along the vertical height, similar to chapter 6.
- Industrially used samples could be obtained from different, known, positions within a cell and the locational variation evaluated. One of the limitations of this work is that it did not consider where the sample originated within the cell. BS22031:2021 "Sampling and test method for cleanable filter media taken from filters of systems in operation" [16] presented a method in which the sampling at different locations in the cell could be achieved. This study would aid to demonstrate if the observed

relationships about the circumference of the media, for chapters 5 and 6, where true across all spatial regions, or at a specific point within the cell.

- Whilst the full air permeability mapping showed the variation along the vertical height, it did not consider the operational time as a variable. Therefore, a study using multiple samples with different operational exposure times would aid to demonstrate how the air permeability evolved. The end point of this study would likely be at a point where cleaning becomes frequent, and the baseline differential pressure post cleaning is significantly higher. This study could also be done on sample mass/density and thickness.
- Further exploration of longevity prediction/modelling is needed, given the limited samples evaluated as part of chapter 7. If the remaining longevity of industrially used filtration media is able to be accurately predicted, then the use of multiple analytical techniques to evaluate the media will no longer be required. Initial testing suggested an exponential relationship existed between the new and industrially used sample, which if true, could lead to the publication of a site specific chart. The analyst would still have to run a test on the sample to determine where in the chart the sample is, but this would give an indication into how much longer the media could remain under normal operation.
- Further exploration of the use of µCT as an analytical technique to evaluate the condition of industrially used filtration media. Whilst the results in Chapter 7 demonstrated the application of µCT as an analytical technique, a more thorough methodology review is required in order to increase the accuracy of the resultant images produced and the results obtained. One barrier of µCT as an analytical technique is the expected cost to perform large scale analysis, particularly at an industrial scale. However, academic studies could demonstrate in a quantifiable way how the porosity and flow paths within a sample evolve over time, further aiding in predicting the longevity of the media.

References

[1] D. Curry, W. Nimmo, J. Howarth, and B. Dannatt, “High Resolution Permeability Study of Used Non-woven Filtration Media from A U.K. Energy from Waste Combustion Site,” in *Filtech 2022*, 2022, p. 15.

[2] D. F. Curry, B. Dannatt, B. Goulden, and W. Nimmo, “Testing air permeability in baghouse filtration,” *Filtr. + Sep.*, vol. 59, no. 2, pp. 20–22, 2022.

[3] E. Gültekin, H. İ. Çelik, S. Nohut, and S. K. Elma, “Predicting air permeability and porosity of nonwovens with image processing and artificial intelligence methods,” *J. Text. Inst.*, vol. 5000, 2020.

[4] T. Fukasawa, C. Kanaoka, T. Ishigami, and K. Fukui, “Effects of Surface Finish of Nonwoven Fabric Bag Filters on Filter Efficiency,” *Chem. Eng. Technol.*, vol. 45, no. 1, pp. 92–99, 2022.

[5] X. Liu, H. Shen, and X. Nie, “Study on the filtration performance of the baghouse filters for ultra-low emission as a function of filter pore size and fiber diameter,” *Int. J. Environ. Res. Public Health*, vol. 16, no. 2, pp. 1–19, 2019.

[6] M. Tang, D. Thompson, D. Q. Chang, S. C. Chen, and D. Y. H. Pui, “Filtration efficiency and loading characteristics of PM2.5 through commercial electret filter media,” *Sep. Purif. Technol.*, vol. 195, no. November 2017, pp. 101–109, 2018.

[7] J. Li, S. Li, and F. Zhou, “Effect of moisture content in coal dust on filtration and cleaning performance of filters,” *Physicochem. Probl. Miner. Process.*, vol. 52, no. 1, pp. 365–379, 2016.

[8] M. I. F. Rozy *et al.*, “A continuous-flow exposure method to determine degradation of polyphenylene sulfide non-woven bag-filter media by NO2 gas at high temperature,” *Adv. Powder Technol.*, vol. 30, no. 12, pp. 2881–2889, 2019.

[9] E. Çinçik and E. Koç, “The effect of blend ratio and process parameters on tensile properties of polyester/viscose blended needle-punched nonwovens,” *Fibers Polym.*, vol. 14, no. 6, pp. 1040–1049, 2013.

[10] G. Toscano, E. Leoni, T. Gasperini, and G. Picchi, “Performance of a portable NIR spectrometer for the determination of moisture content of industrial wood chips fuel,” *Fuel*, vol. 320, no. January, p. 123948, 2022.

[11] D. J. Jeanmonod, Rebecca, K. et al. Suzuki, and M. Hrabovsky, “An Assessment of Surface Properties and Moisture Uptake of Nonwoven Fabrics from Ginning By-products,” *Intech open*, vol. 2, p. 64, 2018.

[12] B. Suárez-Peña, L. Negral, L. Castrillón, L. Megido, E. Marañón, and Y. Fernández-Nava, “Imaging techniques and scanning electron microscopy as tools for characterizing a Si-based material used in air monitoring applications,” *Materials (Basel).*, vol. 9, no. 2, 2016.

[13] S. Y. Yeo, O. S. Kim, D. Y. Lim, S. W. Byun, and S. H. Jeong, “Effects of processing condition on the filtration performances of nonwovens for bag filter media,” *J. Mater. Sci.*, vol. 40, no. 20, pp. 5393–5398, 2005.

[14] N. Riefler, M. Ulrich, M. Morshäuser, and U. Fritsching, “Particle penetration in fiber filters,” *Particuology*, vol. 40, pp. 70–79, 2018.

[15] A. Jackiewicz, S. Jakubiak, and L. Gradoń, “Analysis of the behavior of deposits in fibrous filters during non-steady state filtration using X-ray computed tomography,” *Sep. Purif. Technol.*, vol. 156, pp. 12–21, 2015.

[16] British Standards Institution, “BS ISO 22031 : 2021 BSI Standards Publication Sampling and test method for cleanable filter media taken from filters of systems in operation,” 2021.

[17] D. for B. E. & I. Strategy, “UK Energy Trends: Section 1 - Total Energy,” no. September, pp. 1–63, 2022.

[18] CCC, “Reducing UK emissions - 2018 Progress Report to Parliament - Committee on Climate Change,” *Comm. Clim. Chang.*, no. June, 2018.

[19] L. Löfquist, “Is there a universal human right to electricity?,” *Int. J. Hum. Rights*, vol. 24, no. 6, pp. 711–723, 2020.

[20] G. M. J. Herbert and A. U. Krishnan, “Quantifying environmental performance of biomass energy,” *Renew. Sustain. Energy Rev.*, vol. 59, pp. 292–308, 2016.

[21] M. L. Bell and D. L. Davis, “Reassessment of the Lethal London Fog of 1952 : Novel Indicators of Acute and Chronic Consequences of Acute Exposure to Air Pollution Author (s): Michelle L . Bell and Devra Lee Davis Source : Environmental Health Perspectives , Vol . 109 , Supplement 3,” *Environ. Health Perspect.*, vol. 109, no. June, pp. 389–394, 2001.

[22] A. Grundy, “Low wind scuppers latest coal-free run as it ends at 55 days,” *Current*, pp. 1–8, 13-Aug-2020.

[23] R. Neate, “Great Britain heads for record coal-free period during lockdown,” *The Guardian*, pp. 1–6, 09-Jun-2020.

[24] Department for Business Energy and Industrial Strategy (BEIS), “End to coal power brought forward to October 2024,” 2021. [Online]. Available: https://www.gov.uk/government/news/end-to-coal-power-brought-forward-to-october-2024. [Accessed: 14-Nov-2022].

[25] Imperial College London, “Briefing Note : The best uses of natural gas within Paris climate targets,” London, 2021.

[26] C. Brogan, “Use of natural gas will decline if we are to achieve 1.5°C climate targets,” *Imperial College London*, no. October, London, p. 3, 13-Oct-2021.

[27] R. Harrabin, “Energy strategy: UK plans eight new nuclear reactors to boost production,” *BBC newsBbc*, p. 15, 07-Apr-2022.

[28] D. Palmer, R. Gottschalg, and T. Betts, “The future scope of large-scale solar in the UK: Site suitability and target analysis,” *Renew. Energy*, vol. 133, pp. 1136–1146, 2019.

[29] BEIS, “UK Rooftop Solar Behavioural Research (BEIS Research Paper Number 2021/018),” 2021.

[30] B. R. Naidu *et al.*, “SOLAR INTEGRATION IN THE UK AND INDIA : TECHNICAL BARRIERS.” Joint Virtual Clean Energy Centre (JVCEC), p. 84, 2021.

[31] G. Al Zohbi, P. Hendrick, and P. Bouillard, “Evaluation of the impact of wind farms on birds: The case study ofLebanon,” *Renew. Energy*, vol. 80, pp. 682–689, 2015.

[32] K. J. Boyle, J. Boatwright, S. Brahma, and W. Xu, “NIMBY, not, in siting community wind farms,” *Resour. Energy Econ.*, vol. 57, pp. 85–100, 2019.

[33] J. Firestone, A. Bates, and L. A. Knapp, “See me, Feel me, Touch me, Heal me: Wind turbines, culture, landscapes, and sound impressions,” *Land use policy*, vol. 46, pp. 241–249, 2015.

[34] C. Greenhalgh and A. Azapagic, “Review of drivers and barriers for nuclear power in the UK,” *Environ. Sci. Policy*, vol. 12, no. 7, pp. 1052–1067, 2009.

[35] J. M. West and L. E. McKinley, “Building confidence in the safe disposal of radioactive waste,” *Radioact. Environ.*, vol. 9, no. 2003, pp. 227–249, 2007.

[36] Z. Gu, “History review of nuclear reactor safety,” *Ann. Nucl. Energy*, vol. 120, pp. 682–690, 2018.

[37] M. V. Ramana, “Nuclear power and the public,” *Bull. At. Sci.*, vol. 67, no. 4, pp. 43–51, 2011.

[38] J. Wang and S. Kim, “Comparative analysis of public attitudes toward nuclear power energy across 27 European countries by applying the multilevel model,” *Sustain.*, vol. 10, no. 5, pp. 1–21, 2018.

[39] L. Rosendahl, *Biomass Combustion Science, Technology and Engineering*, 1st editio. Oxford: Woodhead Publishing Limited, 2013.

[40] S. Van Loo and J. Koppejan, *The Handbook of Biomass Combustion & Co-firing*, 1st editio. London: Earthscan, 2008.

[41] J. A. Ruiz, M. C. Juárez, M. P. Morales, P. Muñoz, and M. A. Mendívil, “Biomass logistics: Financial & environmental costs. Case study: 2MW electrical power plants,” *Biomass and Bioenergy*, vol. 56, pp. 260–267, 2013.

[42] P. Lauri, P. Havlík, G. Kindermann, N. Forsell, H. Böttcher, and M. Obersteiner, “Woody biomass energy potential in 2050,” *Energy Policy*, vol. 66, pp. 19–31, 2014.

[43] S. V. Vassilev, D. Baxter, L. K. Andersen, and C. G. Vassileva, “An overview of the chemical composition of biomass,” *Fuel*, vol. 89, no. 5, pp. 913–933, 2010.

[44] D. Carrington, “Burning imported wood in Drax power plant ‘ doesn’t make sense’, says Kwarteng,” *The Guardian*, London, pp. 1–5, 11-Aug-2022.

[45] A. Demirbas, “Potential applications of renewable energy sources , biomass combustion problems in boiler power systems and combustion related environmental issues,” vol. 31, pp. 171–192, 2005.

[46] R. L. Cordell *et al.*, “Evaluation of biomass burning across North West Europe and its impact on air quality,” *Atmos. Environ.*, vol. 141, pp. 276–286, 2016.

[47] L. J. R. Nunes, J. C. O. Matias, and J. P. S. Catalão, “Biomass combustion systems : A review on the physical and chemical properties of the ashes,” *Renew. Sustain. Energy Rev.*, vol. 53, pp. 235–242, 2016.

[48] European Parliament and Council, *Directive 2008/98/EC of the European Parliament and of the Council of 19 November 2008 on waste and repealing certain directives (Waste framework*. Europian Union, 2008, pp. 1–28.

[49] U.K. Government (DEFRA), “Guidance on Applying the Waste Hierarchy,” London, 2011.

[50] M. A. Habib, M. M. Ahmed, M. Aziz, M. R. A. Beg, and M. E. Hoque, “Municipal solid waste management and waste-to-energy potential from rajshahi city corporation in bangladesh,” *Appl. Sci.*, vol. 11, no. 9, 2021.

[51] I. Amber, D. M. Kulla, and N. Gukop, “Generation, characteristics and energy potential of solid municipal waste in Nigeria,” *J. Energy South. Africa*, vol. 23, no. 3, pp. 47–51, 2012.

[52] K. D. Sharma and S. Jain, “Municipal solid waste generation, composition, and management: the global scenario,” *Soc. Responsib. J.*, vol. 16, no. 6, pp. 917–948, 2020.

[53] J. Wang, A. Kusiak, R. W. Johnson, H. S. Cho, T. Fukuda, and G. Barbastathis, *AIR POLLUTION CONTROL TECHNOLOGY HANDBOOK*. 2002.

[54] A. Mukhopadhyay, “Pulse-jet filtration: An effective way to control industrial pollution Part I: Theory, selection and design of pulse-jet filter,” *Text. Prog.*, vol. 41, no. 4, pp. 195–315, 2009.

[55] B. Feng *et al.*, “High level of source-specific particulate matter air pollution associated with cardiac arrhythmias,” *Sci. Total Environ.*, vol. 657, pp. 1285–1293, 2019.

[56] M. B. Hadley, J. Baumgartner, and R. Vedanthan, “Developing a clinical approach to air pollution and cardiovascular health,” *Circulation*, vol. 137, no. 7, pp. 725–742, 2018.

[57] R. D. Brook *et al.*, “Particulate Matter Air Pollution and Cardiovascular Disease,” *Circulation*, vol. 121, no. 21, pp. 2331–2378, 2010.

[58] J. E. Fisher *et al.*, “Physical activity, air pollution, and the risk of asthma and chronic obstructive pulmonary disease,” *Am. J. Respir. Crit. Care Med.*, vol. 194, no. 7, pp. 855–865, 2016.

[59] P. Rajput, S. Izhar, and T. Gupta, “Deposition modeling of ambient aerosols in human respiratory system: Health implication of fine particles penetration into pulmonary region,” *Atmos. Pollut. Res.*, vol. 10, no. 1, pp. 334–343, 2019.

[60] R. Pérez-Padilla, A. Ramirez-Venegas, and R. Sansores-Martinez, “Clinical Characteristics of Patients With Biomass Smoke-Associated COPD and Chronic Bronchitis, 2004-2014.,” *Chronic Obstr. Pulm. Dis. (Miami, Fla.)*, vol. 1, no. 1, pp. 23–32, 2014.

[61] W. Feng *et al.*, “Short-term PM 10 and emergency department admissions for selective cardiovascular and respiratory diseases in Beijing, China,” *Sci. Total Environ.*, vol. 657, no. 10, pp. 213–221, 2019.

[62] S. Baldacci *et al.*, “Allergy and asthma: Effects of the exposure to particulate matter and biological allergens,” *Respir. Med.*, vol. 109, no. 9, pp. 1089–1104, 2015.

[63] Q. Deng, C. Ou, Y. M. Shen, Y. Xiang, Y. Miao, and Y. Li, “Health effects of physical activity as predicted by particle deposition in the human respiratory tract,” *Sci. Total Environ.*, vol. 657, pp. 819–826, 2019.

[64] M. B. Rice *et al.*, “Exposure to traffic and early life respiratory infection: A cohort study,” *Pediatr. Pulmonol.*, vol. 50, no. 3, pp. 252–259, 2015.

[65] X. Zhu *et al.*, “Risks of hospital admissions from a spectrum of causes associated with particulate matter pollution,” *Sci. Total Environ.*, vol. 656, pp. 90–100, 2019.

[66] N. T. T. Nhung, C. Schindler, T. M. Dien, N. Probst-Hensch, and N. Künzli, "Association of ambient air pollution with lengths of hospital stay for hanoi children with acute lower-respiratory infection, 2007–2016," *Environ. Pollut.*, vol. 247, pp. 752–762, 2019.

[67] J. A. Douglas, R. S. Archer, and S. E. Alexander, "Ecological determinants of respiratory health: Examining associations between asthma emergency department visits, diesel particulate matter, and public parks and open space in Los Angeles, California," *Prev. Med. Reports*, vol. 14, no. March, p. 100855, 2019.

[68] H. Yin, M. Pizzol, and L. Xu, "External costs of PM2.5 pollution in Beijing, China: Uncertainty analysis of multiple health impacts and costs," *Environ. Pollut.*, vol. 226, pp. 356–369, 2017.

[69] P. C. Goeminne *et al.*, "The economic burden of bronchiectasis - Known and unknown: A systematic review," *BMC Pulm. Med.*, vol. 19, no. 1, 2019.

[70] K. J. Foreman *et al.*, "Forecasting life expectancy, years of life lost, and all-cause and cause-specific mortality for 250 causes of death: reference and alternative scenarios for 2016–40 for 195 countries and territories," *Lancet*, vol. 392, no. 10159, pp. 2052–2090, 2018.

[71] J. D. Morris, "Mechanisms and mitigation of agglomeration during fluidized bed combustion of biomass," University of Sheffield, 2021.

[72] Northwoods, C. Park, Morpeth, and Northumberland, "The potential use of waste wood in the North East as an efficient biomass fuel source," *A Rep. Behalf Northwoods North East's Woodl. Imitative*, no. August, pp. 1–57, 2008.

[73] A. Bala-Litwiniak and D. Musiał, "Computational and Experimental Studies of Selected Types of Biomass Combustion in a Domestic Boiler," *Materials (Basel).*, vol. 15, no. 14, 2022.

[74] L. G. Florent, "Étude D'Un Dispositif De Traitement De Fumées Issues De L'Incinération De Déchets Industriels Spéciaux," vol. 104, 2012.

[75] N. Maeda, T. Katakura, T. Fukasawa, A. N. Huang, T. Kawano, and K. Fukui, "Morphology of woody biomass combustion ash and enrichment of potassium components by particle size classification," *Fuel Process. Technol.*, vol. 156, pp. 1–8, 2017.

[76] DUKES and ONS, *DUKES chapter 1: statistics on overall energy production and consumption*. 2018, p. 26.

[77] A. Demirbaş, "Heavy metal contents of fly ashes from selected biomass samples," *Energy Sources*, vol. 27, no. 13, pp. 1269–1276, 2005.

[78] R. Strobel, M. H. Waldner, and H. Gablinger, "Highly efficient combustion with low excess air in a modern energy-from-waste (EfW) plant," *Waste Manag.*, vol. 73, pp. 301–306, 2018.

[79] A. Johari, H. Hashim, R. Mat, H. Alias, M. H. Hassim, and M. Rozainee, "Generalization, formulation and heat contents of simulated MSW with high moisture content," *J. Eng. Sci. Technol.*, vol. 7, no. 6, pp. 701–710, 2012.

[80] S. V. Vassilev, C. G. Vassileva, and D. Baxter, "Trace element concentrations and associations in some biomass ashes," *Fuel*, vol. 129, pp. 292–313, 2014.

[81] A. Williams, J. M. Jones, L. Ma, and M. Pourkashanian, "Pollutants from the combustion of solid biomass fuels," vol. 38, 2012.

[82] L. S. Paraschiv, A. Serban, and S. Paraschiv, "Calculation of combustion air required for burning solid fuels (coal / biomass / solid waste) and analysis of flue gas composition," *Energy Reports*, vol. 6, no. September 2019, pp. 36–45, 2020.

[83] Q. Thabit, A. Nassour, and M. Nelles, "Flue Gas Composition and Treatment Potential of a Waste Incineration Plant," *Appl. Sci.*, vol. 12, no. 5236, p. 27, 2022.

[84] M. Edo, E. Björn, P. E. Persson, and S. Jansson, "Assessment of chemical and material contamination in waste wood fuels - A case study ranging over nine years," *Waste Manag.*, vol. 49, pp. 311–319, 2016.

[85] F. Bodénan and P. Deniard, "Characterization of flue gas cleaning residues from European solid waste incinerators: Assessment of various Ca-based sorbent processes," *Chemosphere*, vol. 51, no. 5, pp. 335–347, 2003.

[86] C. R. Yörük, A. Trikkel, and R. Kuusik, “Prediction of Flue Gas Composition and Comparative Overall Process Evaluation for Air and Oxyfuel Combustion of Estonian Oil Shale, Using Aspen Plus Process Simulation,” *Energy and Fuels*, vol. 30, no. 7, pp. 5893–5900, 2016.

[87] Y. C. Hsu, S. H. Chang, and M. B. Chang, “Emissions of PAHs, PCDD/Fs, dl-PCBs, chlorophenols and chlorobenzenes from municipal waste incinerator cofiring industrial waste,” *Chemosphere*, vol. 280, p. 130645, 2021.

[88] J. Vehlow, “Air pollution control systems in WtE units: An overview,” *Waste Manag.*, vol. 37, pp. 58–74, 2015.

[89] A. Dal Pozzo, R. Moricone, A. Tugnoli, and V. Cozzani, “Experimental Investigation of the Reactivity of Sodium Bicarbonate toward Hydrogen Chloride and Sulfur Dioxide at Low Temperatures,” *Ind. Eng. Chem. Res.*, vol. 58, no. 16, pp. 6316–6324, 2019.

[90] B. Walawska, A. Szymanek, A. Pajdak, and M. Nowak, “Flue gas desulfurization by mechanically and thermally activated sodium bicarbonate,” *Polish J. Chem. Technol.*, vol. 16, no. 3, pp. 56–62, 2014.

[91] Z. Wen, J. Di, S. Liu, J. Han, and J. C. K. Lee, “Evaluation of flue-gas treatment technologies for municipal waste incineration: A case study in Changzhou, China,” *J. Clean. Prod.*, vol. 184, pp. 912–920, 2018.

[92] A. T. Lima, L. M. Ottosen, A. J. Pedersen, and A. B. Ribeiro, “Characterization of fly ash from bio and municipal waste,” *Biomass and Bioenergy*, vol. 32, no. 3, pp. 277–282, 2008.

[93] A. Fuller *et al.*, *Fly ash formation and characteristics from (co-)Combustion of an herbaceous biomass and a Greek lignite (Low-Rank Coal) in a pulverized fuel pilot-scale test facility*, vol. 11, no. 6. 2018.

[94] R. W. Bryers, “Fireside slagging, fouling, and high-temperature corrosion of heat-transfer surface due to impurities in steam-raising fuels,” *Prog. Energy Combust. Sci.*, vol. 22, no. 1, pp. 29–120, 1996.

[95] A. A. Tortosa Masiá, B. J. P. Buhre, R. P. Gupta, and T. F. Wall, “Characterising ash of biomass and waste,” *Fuel Process. Technol.*, vol. 88, no. 11–12, pp. 1071–1081, 2007.

[96] S. V. Vassilev, D. Baxter, L. K. Andersen, C. G. Vassileva, and T. J. Morgan, “An overview of the organic and inorganic phase composition of biomass,” *Fuel*, vol. 94, pp. 1–33, 2012.

[97] R. Singh and A. Shukla, “A review on methods of flue gas cleaning from combustion of biomass,” *Renew. Sustain. Energy Rev.*, vol. 29, pp. 854–864, 2014.

[98] EPA, “Air Pollution Control Technology Fact Sheet. Flue Gas Desulfurization (FGD) - Wet, Spray Dry, and Dry Scrubbers,” pp. 1–6, 2002.

[99] J. Smid, Y. P. Chyou, and S. S. Hsiau, “An approximate theory for stresses in dust cake of ceramic candle filters,” *Powder Technol.*, vol. 203, no. 2, pp. 288–297, 2010.

[100] M. Schantz, J. Allen, C. Biehn, S. Glesmann, and G. Hunt, “Dry Sorbent Injection for Acid Gas Control : Process Chemistry , Waste Disposal and Plant Operational Impacts,” *Inst. clean air Co.*, no. July, pp. 1–22, 2016.

[101] Z. Xiong, Z. Ji, and X. Wu, “Development of a cyclone separator with high efficiency and low pressure drop in axial inlet cyclones,” *Powder Technol.*, vol. 253, pp. 644–649, 2014.

[102] S. K. Shukla, P. Shukla, and P. Ghosh, “The effect of modeling of velocity fluctuations on prediction of collection efficiency of cyclone separators,” *Appl. Math. Model.*, vol. 37, no. 8, pp. 5774–5789, 2013.

[103] Y. Li, G. Qin, Z. Xiong, Y. F. Ji, and L. Fan, “The effect of particle humidity on separation efficiency for an axial cyclone separator,” *Adv. Powder Technol.*, vol. 30, no. 4, pp. 724–731, 2019.

[104] H. Zhou, Z. Hu, Q. Zhang, Q. Wang, and X. Lv, “Numerical study on gas-solid flow characteristics of ultra-light particles in a cyclone separator,” *Powder Technol.*, vol. 344, pp. 784–796, 2019.

[105] J. Vehlow, “Air pollution control systems in WtE units: An overview,” *Waste Manag.*, vol. 37, pp. 58–74, 2015.

[106] A. E. De Oliveira and V. G. Guerra, “Electrostatic Precipitation of Nanoparticles and Submicron Particles: Review of Technological Strategies,” *Process Saf. Environ. Prot.*, vol. 153, pp. 422–438, 2021.

[107] P. V. Bush and T. R. Snyder, “Implications of particulate properties on electrostatic precipitator and fabric filter performance,” *Powder Technol.*, vol. 72, no. 3, pp. 207–213, 1992.

[108] A. Sarkar, S. Vishwakarma, H. Banichul, K. K. Mishra, and S. S. Roy, “A comprehensive analysis of the particle size and shape of fly ash from different fields of ESP of a super thermal power plant,” *Energy Sources, Part A Recover. Util. Environ. Eff.*, vol. 34, no. 5, pp. 385–395, 2012.

[109] K. V. George, C. V. Chalapati Rao, S. Manjunath, and A. M. Bopche, “Cyclone as a precleaner to esp - a need for indian coal based thermal power plants,” *Environ. Technol. (United Kingdom)*, vol. 24, no. 11, pp. 1425–1430, 2003.

[110] A. Jaworek, A. T. Sobczyk, A. Krupa, A. Marchewicz, T. Czech, and L. Śliwiński, “Hybrid electrostatic filtration systems for fly ash particles emission control. A review,” *Sep. Purif. Technol.*, vol. 213, no. August 2018, pp. 283–302, 2019.

[111] A. Jaworek, A. Marchewicz, A. T. Sobczyk, A. Krupa, and T. Czech, “Two-stage electrostatic precipitators for the reduction of PM2.5 particle emission,” *Prog. Energy Combust. Sci.*, vol. 67, pp. 206–233, 2018.

[112] K. Sutherland, *Filters and Filtration Handbook*. Butterworth-Heinemann, 2008.

[113] A. Mukhopadhyay, “Pulse-jet filtration: An effective way to control industrial pollution Part II: Process characterization and evaluation of filter media,” *Text. Prog.*, vol. 42, no. 1, pp. 1–97, 2010.

[114] I. M. Ward and D. L. M. Cansfield, *High-performance fibres*. 1992.

[115] L. K. Wang, C. Williford, and W. Chen, “Fabric Filtration,” in *Handbook of Environmental Engineering Volume 1: Air Pollution Control Engineering*, 1st ed., vol. 1, Humana Press, 2004, pp. 59–95.

[116] M. Wilcox, R. Kurz, and K. Brun, “Technology Review of Modern Gas Turbine Inlet Filtration Systems,” *Int. J. Rotating Mach.*, vol. 2012, no. October, pp. 1–15, 2012.

[117] Y. H. Joe, J. Shim, and H. S. Park, “Evaluation of the can velocity effect on a bag filter,” *Powder Technol.*, vol. 321, pp. 454–457, 2017.

[118] A. Mukhopadhyay and V. Pandit, “Control of industrial air pollution through sustainable development,” *Environ. Dev. Sustain.*, vol. 16, no. 1, pp. 35–48, 2014.

[119] A. C. Caputo and P. M. Pelagagge, “Economic comparison of pulsed electrostatic precipitators and fabric filters in coal-fired utility plants,” *Environ. Manag. Heal.*, vol. 10, no. 2, pp. 96–104, 1999.

[120] D. B. Purchas and K. Sutherland, “Non-woven Fabric Media,” in *Handbook of Filter Media*, 2nd ed., Oxford: Elsevier Science Ltd., 2002, pp. 81–116.

[121] J. H. Turner, A. S. Viner, R. E. Jenkins, W. M. Vatavuk, and J. D. McKenna, “Sizing and costing of fabric filters part ii: Costing considerations,” *J. Air Pollut. Control Assoc.*, vol. 37, no. 9, pp. 1105–1112, 1987.

[122] Y. Zhao, W. Qiu, and Z. Sun, “Removal of arsenic from flue gas using NaClO/NaClO 2 complex absorbent,” *Chem. Eng. Res. Des.*, vol. 144, pp. 505–511, 2019.

[123] M. Allen, “20 Economical Ways To Improve the Performance of a Baghouse Dust Collector,” *Iron Steel Technol.*, vol. 13, no. 5, pp. 50–58, 2016.

[124] A. C. Caputo and P. M. Pelagagge, “Baghouse System Design Based on Economic Optimization,” *Environ. Prog.*, vol. 19, no. 4, pp. 238–245, 2000.

[125] E. Kapeluszna, Ł. Kotwica, W. Pichór, and W. Nocuń-Wczelik, “Cement-based composites with waste expanded perlite - Structure, mechanical properties and durability in chloride and sulphate environments,” *Sustain. Mater. Technol.*, vol. 24, 2020.

[126] Z. Zhang, Y. Zhu, H. Zhu, Y. Zhang, J. L. Provis, and H. Wang, “Effect of drying procedures on pore structure and phase evolution of alkali-activated cements,” *Cem. Concr. Compos.*, vol. 96, no. November 2018, pp. 194–203, 2019.

[127] M. Khan and M. Ali, “Improvement in concrete behavior with fly ash, silica-fume and coconut fibres,” *Constr. Build. Mater.*, vol. 203, pp. 174–187, 2019.

[128] R. E. Ghosh *et al.*, “Fetal growth, stillbirth, infant mortality and other birth outcomes near UK municipal waste incinerators; retrospective population based cohort and case-control study,” *Environ. Int.*, vol. 122, no. July 2018, pp. 151–158, 2019.

[129] M. L. S. Oliveira, M. Izquierdo, X. Querol, R. N. Lieberman, B. K. Saikia, and L. F. O. Silva, “Nanoparticles from construction wastes: A problem to health and the environment,” *J. Clean. Prod.*, vol. 219, pp. 236–243, 2019.

[130] F. Mushtaq, M. Zahid, I. A. Bhatti, S. Nasir, and T. Hussain, “Possible applications of coal fly ash in wastewater treatment,” *J. Environ. Manage.*, vol. 240, no. February, pp. 27–46, 2019.

[131] J. C. Mycock, J. D. McKenna, and L. Theodore, *Handbook of Air Pollution Control Engineering and Technology*. CRC Press, 1995.

[132] M. Shadhin, R. Jayaraman, and M. Rahman, “Effect of Mat Design and Manufacturing Parameters on the Mechanical Properties of Needle-punched Flax Fiber-reinforced Composites.,” no. September, 2020.

[133] R. Roy and S. M. Ishtiaque, “Design and development of fibrous filter media induced by structural characteristics of needle punched nonwoven,” *J. Ind. Text.*, 2021.

[134] V. G. Nazarov and A. V. Dedov, “Application of Darcy’s Law for Modeling Air Permeability of Nonwoven Needle-Punched Fabrics,” *Fibre Chem.*, vol. 52, no. 2, pp. 112–116, 2020.

[135] Y. Bian, S. Wang, L. Zhang, and C. Chen, “Influence of fiber diameter, filter thickness, and packing density on PM2.5 removal efficiency of electrospun nanofiber air filters for indoor applications,” *Build. Environ.*, vol. 170, no. December 2019, p. 106628, 2020.

[136] E. H. Tanabe, P. M. Barros, K. B. Rodrigues, and M. L. Aguiar, “Experimental investigation of deposition and removal of particles during gas filtration with various fabric filters,” *Sep. Purif. Technol.*, vol. 80, no. 2, pp. 187–195, 2011.

[137] S. Li *et al.*, “Effects of cleaning mode on the performances of pulse-jet cartridge filter under varying particle sizes,” *Adv. Powder Technol.*, vol. 30, no. 9, pp. 1835–1841, 2019.

[138] C. Kanaoka, “Fine particle filtration technology using fiber as dust collection medium,” *KONA Powder Part. J.*, vol. 36, no. 36, pp. 88–113, 2019.

[139] D. Thomas, S. Pacault, A. Charvet, N. Bardin-Monnier, and J. C. Appert-Collin, “Composite fibrous filters for nano-aerosol filtration: Pressure drop and efficiency model,” *Sep. Purif. Technol.*, vol. 215, no. December 2018, pp. 557–564, 2019.

[140] J. Li, F. Zhou, and S. Li, “Experimental study on the dust filtration performance with participation of water mist,” *Process Saf. Environ. Prot.*, vol. 109, pp. 357–364, 2017.

[141] X. Simon, S. Chazelet, D. Thomas, D. Bémer, and R. Régnier, “Experimental study of pulse-jet cleaning of bag filters supported by rigid rings,” *Powder Technol.*, vol. 172, no. 2, pp. 67–81, 2007.

[142] W. G. Shin, S. Park, J. Shim, Y. H. Joe, and H. Park, “Non-uniform filtration velocity of process gas passing through a long bag filter,” *J. Hazard. Mater.*, vol. 365, no. November 2018, pp. 440–447, 2018.

[143] T. Rogoziński, “Pilot-scale study on the influence of wood dust type on pressure drop during filtration in a pulse-jet baghouse,” *Process Saf. Environ. Prot.*, vol. 119, pp. 58–64, 2018.

[144] J. U. Kim, J. Hwang, H. J. Choi, and M. H. Lee, “Effective filtration area of a pleated filter bag in a pulse-jet bag house,” *Powder Technol.*, vol. 311, pp. 522–527, 2017.

[145] C. R. N. Silva, V. S. Negrini, M. L. Aguiar, and J. R. Coury, “Influence of gas velocity on cake formation and detachment,” *Powder Technol.*, vol. 101, no. 2, pp. 165–172, 1999.

[146] M. L. Aguiar and J. R. Coury, “Cake formation in fabric filtration of gases,” *Ind. Eng. Chem. Res.*, vol. 35, no. 10, pp. 3673–3679, 1996.

[147] S. Kang, H. Lee, S. C. Kim, D. R. Chen, and D. Y. H. Pui, “Modeling of fibrous filter media for ultrafine particle filtration,” *Sep. Purif. Technol.*, vol. 209, no. July 2018, pp. 461–469, 2019.

[148] Q. Wang, X. Lin, and D. R. Chen, “Effect of dust loading rate on the loading characteristics of high efficiency filter media,” *Powder Technol.*, vol. 287, pp. 20–28, 2016.

[149] C. J. Chen, “Reducing pressure drop in a baghouse using flow distributors,” *J. Air Waste Manag. Assoc.*, vol. 51, no. 10, pp. 1471–1475, 2001.

[150] B. Alonso-Fariñas, M. Lupion, M. Rodriguez-Galan, and J. Martinez-Fernandez, “New candle prototype for hot gas filtration industrial applications,” *Fuel*, vol. 114, pp. 120–127, 2013.

[151] M. Lupion, B. Alonso-Fariñas, M. Rodriguez-Galan, and B. Navarrete, “Modelling pressure drop evolution on high temperature filters,” *Chem. Eng. Process. Process Intensif.*, vol. 66, pp. 12–19, 2013.

[152] Y. S. Chen and S. S. Hsiau, “Cake formation and growth in cake filtration,” *Powder Technol.*, vol. 192, no. 2, pp. 217–224, 2009.

[153] J.P.K. Seville, R. Clift, C.J. Withers, and W. Keidel, “Rigid ceramic media for filtering hot gases,” *Filtr. Sep.*, vol. 26, pp. 265 – 271, 1989.

[154] D. Hund, K. Schmidt, S. Ripperger, and S. Antonyuk, “Direct numerical simulation of cake formation during filtration with woven fabrics,” *Chem. Eng. Res. Des.*, vol. 139, pp. 26–33, 2018.

[155] C. Sen Wang and Y. Otani, “Removal of nanoparticles from gas streams by fibrous filters: A review,” *Ind. Eng. Chem. Res.*, vol. 52, no. 1, pp. 5–17, 2013.

[156] P. M. Barros, E. H. Tanabe, and M. L. Aguiar, “Performance of fibrous filters during nanoparticle cake formation,” *Sep. Sci. Technol.*, vol. 51, no. 6, pp. 1042–1052, 2016.

[157] S. Ergun, “Fluid Flow Through Packed Columns,” *Chem. Eng. Prog.*, vol. 48, no. 2, pp. 89–94, 1952.

[158] T.-C. Hsiao *et al.*, “Effects of temperature, dust concentration, and filtration superficial velocity on the loading behavior and dust cakes of ceramic candle filters during hot gas filtration,” *Sep. Purif. Technol.*, vol. 198, pp. 146–154, 2017.

[159] C. Tien and B. V. Ramarao, “Can filter cake porosity be estimated based on the Kozeny-Carman equation?,” *Powder Technol.*, vol. 237, pp. 233–240, 2013.

[160] A. F. Miguel, “Effect of air humidity on the evolution of permeability and performance of a fibrous filter during loading with hygroscopic and non-hygroscopic particles,” *J. Aerosol Sci.*, vol. 34, no. 6, pp. 783–799, 2003.

[161] M. Saleem, G. Krammer, and M. S. Tahir, “The effect of operating conditions on resistance parameters of filter media and limestone dust cake for uniformly loaded needle felts in a pilot scale test facility at ambient conditions,” *Powder Technol.*, vol. 228, pp. 100–107, 2012.

[162] R. Boudhan, A. Joubert, S. Durécu, K. Gueraoui, and L. Le Coq, “Influence of air humidity on particle filtration performance of a pulse-jet bag filter,” *J. Aerosol Sci.*, vol. 130, no. January, pp. 1–9, 2019.

[163] A. Joubert, J. C. Laborde, L. Bouilloux, S. Chazelet, and D. Thomas, “Modelling the pressure drop across HEPA filters during cake filtration in the presence of humidity,” *Chem. Eng. J.*, vol. 166, no. 2, pp. 616–623, 2011.

[164] Q. Ribeyre, A. Charvet, C. Vallières, and D. Thomas, “Impact of relative humidity on a nanostructured filter cake – Experimental and modelling approaches,” *Chem. Eng. Sci.*, vol. 161, pp. 109–116, 2017.

[165] J. F. Montgomery, S. I. Green, and S. N. Rogak, “Impact of relative humidity on HVAC filters loaded with hygroscopic and non-hygroscopic particles,” *Aerosol Sci. Technol.*, vol. 49, no. 5, pp. 322–331, 2015.

[166] O. Linderoth, P. Johansson, and L. Wadsö, “Development of pore structure, moisture sorption and transport properties in fly ash blended cement-based materials,” *Constr. Build. Mater.*, vol. 261, p. 120007, 2020.

[167] H. Jung, Y. J. Lee, and W. B. Yoon, “Effect of moisture content on the grinding process and powder properties in food: A review,” *Processes*, vol. 6, no. 6, pp. 6–10, 2018.

[168] W. C. Hinds, *Aerosol Technology*, 2nd ed. Los Angeles: John Wiley & Sons, INC, 1998.

[169] K. W. Lee and B. Y. H. Liu, “Theoretical study of aerosol filtration by fibrous filters,” *Aerosol Sci. Technol.*, vol. 1, no. 2, pp. 147–161, 1982.

[170] C. Y. Chen, “Filtration of Aerosols by Fibrous Media,” *Chem. Rev.*, vol. 55, no. 3, pp. 595–623, 1955.

[171] J. Steffens and J. R. Coury, “Collection efficiency of fiber filters operating on the removal of nano-sized aerosol particles: II-Heterogeneous fibers,” *Sep. Purif. Technol.*, vol. 58, no. 1, pp. 106–112, 2007.

[172] J. Visser, “Particle Adhesion and Removal: A Review,” *Part. Sci. Technol.*, vol. 13, no. 3–4, pp. 169–196, 1995.

[173] R. Lathrache and H. Fissan, “Enhancement of Particle Deposition in Filters Due To Electrostatic Effects.,” *Filtr. Sep.*, vol. 24, no. 6, 1987.

[174] A. Podgórski, A. Bałazy, and L. Gradoń, “Application of nanofibers to improve the filtration efficiency of the most penetrating aerosol particles in fibrous filters,” *Chem. Eng. Sci.*, vol. 61, no. 20, pp. 6804–6815, 2006.

[175] J. M. Lessard, A. Omran, A. Tagnit-Hamou, and R. Gagne, “Feasibility of using biomass fly and bottom ashes in dry-cast concrete production,” *Constr. Build. Mater.*, vol. 132, pp. 565–577, 2017.

[176] Y. Wang, B. C. Acarturk, L. Burris, R. D. Hooton, C. R. Shearer, and P. Suraneni, “Physicochemical characterization of unconventional fly ashes,” *Fuel*, vol. 316, no. February, p. 123318, 2022.

[177] G. Wang, T. Pinto, and M. Costa, “Investigation on ash deposit formation during the co-firing of coal with agricultural residues in a large-scale laboratory furnace,” *Fuel*, vol. 117, no. PART A, pp. 269–277, 2014.

[178] H. Wang, H. Zhao, K. Wang, Y. He, and C. Zheng, “Simulation of filtration process for multi-fiber filter using the Lattice-Boltzmann two-phase flow model,” *J. Aerosol Sci.*, vol. 66, pp. 164–178, 2013.

[179] W. C. Hinds, *Aerosol technology: Properties, Behavior, and Measurement of Airborne Particles*, 2nd ed. Hoboken, NJ: John Wiley & Sons. Inc., 1998.

[180] H. Förster, T. Thajudeen, C. Funk, and W. Peukert, “Separation of nanoparticles: Filtration and scavenging from waste incineration plants,” *Waste Manag.*, vol. 52, pp. 346–352, 2016.

[181] C.-J. Chen and M.-T. Cheng, “Effect of Flow Distributors on Uniformity of Velocity Profile in a Baghouse,” *J. Air Waste Manage. Assoc.*, vol. 55, no. 7, pp. 886–892, 2005.

[182] H. Yang, Y. Wang, M. Ren, and X. Yang, “Effect of the rectangular exit-port geometry of a distribution manifold on the flow performance,” *Appl. Therm. Eng.*, vol. 117, pp. 481–486, 2017.

[183] M. Porter, “Profiting from better air flow in baghouses,” *IEEE Cem. Ind. Tech. Conf.*, pp. 1–11, 2010.

[184] J. M. Hassan, T. A. Mohamed, W. S. Mohammed, and W. H. Alawee, “Modeling the Uniformity of Manifold with Various Configurations,” *J. Fluids*, vol. 2014, pp. 1–8, 2014.

[185] L. R. Da Vitória, F. A. R. Perreira, S. M. S. Rocha, R. Sartim, K. H. Simon, and D. C. Ribeiro, “Study of the influence of using bulkheads on the fabric filter performance,” *Chem. Eng. Trans.*, vol. 70, no. 2015, pp. 913–918, 2018.

[186] N. F. Nielsen, a S. Flsmidth, K. G. Skriver, and L. J. Castaño, “Fabric Filter Optimization using Computational Fluid Dynamics,” *Int. Conf. Electrost. Precip. ICESP XII*, pp. 239–243, 2011.

[187] E. I. Wedman and W. L. Gore, “A Practical Guide to Filter Media Failure Analysis,” no. 4673, 2009.

[188] L. Vásárhelyi, Z. Kónya, Kukovecz, and R. Vajtai, “Microcomputed tomography–based characterization of advanced materials: a review,” *Mater. Today Adv.*, vol. 8, pp. 1–13, 2020.

[189] S. S. R. Cirqueira, E. H. Tanabe, and M. L. Aguiar, “Experimental investigation of particle deposition in filter media during filtration cycles with regeneration by pulse jet cleaning,” *Process Saf. Environ. Prot.*, vol. 127, pp. 288–298, 2019.

[190] QAM, “Retrofitting Baghouse Pulse-Jet Dust Collectors,” 2007.

[191] O. Kurtz, J. Meyer, and G. Kasper, “The contribution of small leaks in a baghouse filter to dust emission in the PM2.5range—A system approach,” *Particuology*, vol. 30, pp. 40–52, 2017.

[192] J. Li, X. Lu, and W. F. Wang, “Leak monitoring and localization in baghouse filtration system using a distributed optical fiber dynamic air pressure sensor,” *Opt. Fiber Technol.*, vol. 57, no. March, 2020.

[193] L. M. Lo, D. R. Chen, and D. Y. H. Pui, “Experimental study of pleated fabric cartridges in a pulse-jet cleaned dust collector,” *Powder Technol.*, vol. 197, no. 3, pp. 141–149, 2010.

[194] C. F. Liu and S. M. Shih, “Effects of flue gas components on the reaction of Ca(OH)2 with so2,” *Ind. Eng. Chem. Res.*, vol. 45, no. 26, pp. 8765–8769, 2006.

[195] T. C. Keener and S. J. Khang, “Kinetics of the sodium bicarbonate-sulfur dioxide reaction,” *Chem. Eng. Sci.*, vol. 48, no. 16, pp. 2859–2865, 1993.

[196] O. Kurtz, J. Meyer, and G. Kasper, “The contribution of small leaks in a baghouse filter to dust emission in the PM2.5 range—A system approach,” *Particuology*, vol. 30, pp. 40–52, 2017.

[197] W. Qin, M. Dekermenjian, and R. J. Martin, “Prediction of particulate loading in exhaust from fabric filter baghouses with one or more failed bags,” *J. Air Waste Manag. Assoc.*, vol. 56, no. 8, pp. 1177–1183, 2006.

[198] D. M. Li, X. J. Gong, F. C. Wang, M. He, and G. P. Tang, “Study on the Mechanical Abrasion of the Filter Bags,” *Appl. Mech. Mater.*, vol. 321–324, pp. 205–208, 2013.

[199] B. Bach and E. Schmidt, “Influence of leaks in surface filters on particulate emissions,” *J. Hazard. Mater.*, vol. 144, no. 3, pp. 673–676, 2007.

[200] M. A. Saad and R. F. El-Newashy, “Effect of Fatigue on Welded and Sewn Nonwoven Filter Bags in Pulse-jet Air Filtration System,” *Am. Sci.*, vol. 8, no. 8, pp. 932–940, 2012.

[201] B. O. Andersen, N. F. Nielsen, and J. H. Walther, “Numerical and experimental study of pulse-jet cleaning in fabric filters,” *Powder Technol.*, vol. 291, pp. 284–298, 2016.

[202] BSI, “BS ISO 11057:2011 BSI Standards Publication Air quality - Test method for filtration characterization of cleanable filter media.” 2011.

[203] British Standards, “Test methods for evaluating degradation of characteristics of

cleanable filter media (ISO 16891:2016)," 2016.

[204] A. K. Maddineni, D. Das, and R. M. Damodaran, "Air-borne particle capture by fibrous filter media under collision effect: A CFD-based approach," *Sep. Purif. Technol.*, vol. 193, no. June 2017, pp. 1–10, 2018.

[205] J. Schuberth, G. Mauschitz, and W. Höflinger, "Clogging mechanisms involved in the aging process of cleanable filter media," *Sep. Purif. Technol.*, vol. 77, no. 2, pp. 196–201, 2011.

[206] C. Kanaoka and T. Kishima, "Observation of the process of dust accumulation on a rigid ceramic filter surface and the mechanism of cleaning dust from the filter surface," *Adv. Powder Technol.*, vol. 10, no. 4, pp. 417–426, 1999.

[207] B. C. Scoble, "The Three Biggest Food Dust Collector Problems and How to Avoid Them," 2009.

[208] J. Li, F. Zhou, and S. Li, "Effect of uniformity of the residual dust cake caused by patchy cleaning on the filtration process," *Sep. Purif. Technol.*, vol. 154, pp. 89–95, 2015.

[209] A. S. Viner, R. P. Donovan, D. S. Ensor, and L. S. Hovis, "Comparison of Baghouse Test Results with the GCA/EPA Design Model," *J. Air Pollut. Control Assoc.*, vol. 34, no. 8, pp. 872–880, 1984.

[210] J. Li, S. Li, and F. Zhou, "Effect of cone installation in a pleated filter cartridge during pulse-jet cleaning," *Powder Technol.*, vol. 284, pp. 245–252, 2015.

[211] P. Bulejko, "Numerical comparison of prediction models for aerosol filtration efficiency applied on a hollow-fiber membrane pore structure," *Nanomaterials*, vol. 8, no. 6, 2018.

[212] J. O. Litchwark, J. Winchester, and J. J. Nijdam, "Design of pulse-jet systems for milk powder baghouses," *Powder Technol.*, vol. 284, pp. 379–386, 2015.

[213] O. Kurtz, J. Meyer, and G. Kasper, "Influence of Filter Operating Parameters on Fine Dust Emissions from Pulse-Cleaned Filter Bags," *Chem. Eng. Technol.*, vol. 39, no. 3, pp. 435–443, 2016.

[214] E. Bakke, “Optimizing Filtration Parameters,” *J. Air Pollut. Control Assoc.*, vol. 24, no. 12, pp. 1150–1154, 1974.

[215] C. Yan, G. Liu, and H. Chen, “Effect of induced airflow on the surface static pressure of pleated fabric filter cartridges during pulse jet cleaning,” *Powder Technol.*, vol. 249, pp. 424–430, 2013.

[216] S. Li, F. Zhou, B. Xie, and F. Wang, “Influence of injection pipe characteristics on pulse-jet cleaning uniformity in a pleated cartridge filter,” *Powder Technol.*, vol. 328, pp. 264–274, 2018.

[217] J. Sievert and F. Löffler, “Fabric cleaning in pulse-jet filters,” *Chem. Eng. Process.*, vol. 26, no. 2, pp. 179–183, 1989.

[218] C. Huachang, Y. Liang, C. Joo-hong, and J. Zhongli, “Optimization of Nozzle Design for Pulse Cleaning of Ceramic Filter,” *Chinese J. Chem. Eng.*, vol. 16, no. 2, pp. 306–313, 2008.

[219] K. T. Hindy, “Influence of selected fixed parameters on pulse-jet fabric filter operation,” *Atmos. Environ.*, vol. 20, no. 8, pp. 1517–1521, 1986.

[220] S. Li *et al.*, “Experimental investigation of the optimization of nozzles under an injection pipe in a pulse-jet cartridge filter,” *Powder Technol.*, vol. 345, pp. 363–369, 2019.

[221] J. Cai, W. Hao, C. Zhang, J. Yu, and T. Wang, “On the forming mechanism of the cleaning airflow of pulse-jet fabric filters,” *J. Air Waste Manag. Assoc.*, vol. 67, no. 12, pp. 1273–1287, 2017.

[222] J. Li, D. Wu, Q. Wu, M. Luo, and J. Li, “Design and performance evaluation of novel colliding pulse jet for dust filter cleaning,” *Sep. Purif. Technol.*, vol. 213, no. November 2018, pp. 101–113, 2019.

[223] K. Fukui, G. Ichiba, M. I. F. Rozy, K. Ito, T. Fukasawa, and T. Ishigami, “Effects of NO2 gas concentration on the degradation of polyphenylene sulfide non-woven bag filter at high temperature,” *Adv. Powder Technol.*, vol. 32, no. 9, pp. 3278–3287, 2021.

[224] M. Pham, C. Clark, and J. McKenna, “The evolution and impact of testing baghouse filter performance,” *J. Air Waste Manag. Assoc.*, vol. 62, no. 8, pp. 916–923, 2012.

[225] K. Hoppe *et al.*, “Modeling the separation performance of depth filter considering tomographic data,” *Environ. Prog. Sustain. Energy*, vol. 39, no. 5, pp. 1–11, 2020.

[226] B. Yang, Q. Huang, M. Chen, Y. Shen, and S. Zhu, “Mn-Ce-Nb-O x /P84 catalytic filters prepared by a novel method for simultaneous removal of particulates and NO,” *J. Rare Earths*, vol. 37, no. 3, pp. 273–281, 2019.

[227] C. Akduman, V. Demirel, and F. Tezcan, “Filter life comparison of different levels of nanofiber coated cleanable-surface filter for gas turbine,” *J. Appl. Polym. Sci.*, vol. 138, no. 33, 2021.

[228] S. Dolny, T. Rogozinski, and S. Dobak, “Methodology of pilot-scale studies on pulse-jet filtration of air polluted with wood dust,” *Wood Res.*, vol. 64, no. 2, pp. 325–334, 2019.

[229] British Standards Institution, “BS EN ISO 9237:1995 - Determiantion of the permeability of fabrics to air.” p. 16, 1995.

[230] BSI, “BS EN 29073-1:1992 Nonwovens — Part 1: Determination of mass per unit area.” London, p. 10, 1992.

[231] BSI, “BS EN 29073-2:1997 Nonwovens — Part 2: Determination of thickness,” *Management*. London, p. 14, 1997.

[232] British Standards Institution, “BS EN 9073-15:2008 Test methods for nonwovens-Part 15: Determination of air permeability,” 2008.

[233] M. E. Ince, “Air permeability characterization of glass fiber nonwoven fabric for liquid composite molding applications,” *IOP Conf. Ser. Mater. Sci. Eng.*, vol. 459, no. 1, 2018.

[234] S. Y. Yeo, D. Y. Lim, S. W. Byun, J. H. Kim, and S. H. Jeong, “Design of filter bag media with high collection efficiency,” *J. Mater. Sci.*, vol. 42, no. 19, pp. 8040–8046, 2007.

[235] M. A. Ali, R. Umer, K. A. Khan, S. Bickerton, and W. J. Cantwell, “Non-destructive evaluation of through-thickness permeability in 3D woven fabrics for composite fan blade applications,” *Aerosp. Sci. Technol.*, vol. 82–83, pp. 520–533, 2018.

[236] G. Zhu, D. Kremenakova, Y. Wang, and J. Militky, “Air permeability of polyester nonwoven fabrics,” *Autex Res. J.*, vol. 15, no. 1, pp. 8–12, 2015.

[237] T. Fukasawa, C. Kanaoka, I. Kimura, L. Bao, T. Ishigami, and K. Fukui, “Distributions of Fiber Mass, Air Permeability, and Filter Efficiency in Nonwoven Fabric Bag Filters,” *Chem. Eng. Technol.*, vol. 44, no. 3, pp. 535–541, 2021.

[238] D. Q. Chang, C. Y. Tien, C. Y. Peng, M. Tang, and S. C. Chen, “Development of composite filters with high efficiency, low pressure drop, and high holding capacity PM2.5 filtration,” *Sep. Purif. Technol.*, vol. 212, no. August 2018, pp. 699–708, 2019.

[239] E. Sikorska, J. M. Gac, and L. Gradoń, “Performance of a depth fibrous filter at particulate loading conditions. Description of temporary and local phenomena with structure development,” *Chem. Eng. Res. Des.*, vol. 132, pp. 743–750, 2018.

[240] J. S. Kim and M. H. Lee, “Measurement of effective filtration area of pleated bag filter for pulse-jet cleaning,” *Powder Technol.*, vol. 343, pp. 662–670, 2019.

[241] K. Liu, Y. Zhao, L. Jia, R. Hao, and D. Fu, “A novel CFD-based method for predicting pressure drop and dust cake distribution of ceramic filter during filtration process at macro-scale,” *Powder Technol.*, vol. 353, pp. 27–40, 2019.

[242] J. Steffens and J. R. Coury, “Collection efficiency of fiber filters operating on the removal of nano-sized aerosol particles: I-Homogeneous fibers,” *Sep. Purif. Technol.*, vol. 58, no. 1, pp. 99–105, 2007.

[243] W. Cai and G. Hu, “Oxidation degradation of polyphenylene sulfide needle felt at different sulfuric acid dew point temperatures,” *High Perform. Polym.*, vol. 27, no. 1, pp. 94–99, 2015.

[244] J. Yang, M. Huang, J. Peng, and J. Shi, “Rapid determination of the moisture content of milk powder by microwave sensor,” *Meas. J. Int. Meas. Confed.*, vol. 87, pp. 83–86, 2016.

[245] D. Naviglio, S. Conti, L. Ferrara, and A. Santini, “Determination of Moisture in Powder and Lyophilised Saffron (Crocus sativus L.) by Karl Fischer Method,” *Open Food Sci. J.*, vol. 4, no. 1, pp. 1–6, 2010.

[246] T. Rizvi, P. Xing, M. Pourkashanian, L. I. Darvell, J. M. Jones, and W. Nimmo, "Prediction of biomass ash fusion behaviour by the use of detailed characterisation methods coupled with thermodynamic analysis," *Fuel*, vol. 141, pp. 275–284, 2015.

[247] University of Dundee, "Modern Fly Ashes in Concrete Construction," no. May, 2015.

[248] M. M. Content, C. Quality, and M. Formation, "Determination of Moisture Content 1.," pp. 1–6, 2015.

[249] A. P. Keerthipala, F. Science, and T. Series, *Appendix A : Moisture Analysis*, vol. 18, no. 6. 2018.

[250] A. Rawal, "Structural analysis of pore size distribution of nonwovens," *J. Text. Inst.*, vol. 101, no. 4, pp. 350–359, 2010.

[251] S. C. Kim, J. Wang, W. G. Shin, J. H. Scheckman, and D. Y. H. Pui, "Structural properties and filter loading characteristics of soot agglomerates," *Aerosol Sci. Technol.*, vol. 43, no. 10, pp. 1033–1041, 2009.

[252] O. Mahmoud, H. A. Nasr-El-Din, Z. Vryzas, and V. C. Kelessidis, "Characterization of Filter Cake Generated by Nanoparticle-Based Drilling Fluid for HP/HT Applications," no. March, 2017.

[253] T. C. Esteves, R. Rajamma, D. Soares, A. S. Silva, V. M. Ferreira, and J. A. Labrincha, "Use of biomass fly ash for mitigation of alkali-silica reaction of cement mortars," *Constr. Build. Mater.*, vol. 26, no. 1, pp. 687–693, 2012.

[254] Z. Değirmenci and E. Çoruh, "Investigating the effects of weight variation and patterning on strength of nonwoven products," *Tekst. ve Konfeksiyon*, vol. 28, no. 4, pp. 280–286, 2018.

[255] M. Šešlija, A. Rosić, N. Radović, M. Vasić, M. Đogo, and M. Jotić, "Laboratory Testing of Fly Ash," *Teh. Vjesn.*, vol. 23, no. 6, pp. 1839–1848, 2016.

[256] A. Omran, N. Soliman, A. Xie, T. Davidenko, and A. Tagnit-Hamou, "Field trials with concrete incorporating biomass-fly ash," *Constr. Build. Mater.*, vol. 186, pp. 660–669, 2018.

[257] L. Sutter, R. D. Hooton, and S. Schlorholtz, *Methods for Evaluating Fly Ash for Use in Highway Concrete*. 2013.

[258] A. Wardhono, "Comparison Study of Class F and Class C Fly Ashes as Cement Replacement Material on Strength Development of Non-Cement Mortar," *IOP Conf. Ser. Mater. Sci. Eng.*, vol. 288, no. 1, pp. 1–7, 2018.

[259] T. W. C. Pereira, F. B. Marques, F. D. A. R. Pereira, D. D. C. Ribeiro, and S. M. S. Rocha, "The influence of the fabric filter layout of in a flow mass filtrate," *J. Clean. Prod.*, vol. 111, pp. 117–124, 2016.

[260] A. Kumar, T. Staedler, and X. Jiang, "Role of relative size of asperities and adhering particles on the adhesion force," *J. Colloid Interface Sci.*, vol. 409, pp. 211–218, 2013.

[261] A. Kavouras and G. Krammer, "Deriving cake detachment versus cake area load in a jet pulsed filter by a mechanistic model," *Powder Technol.*, vol. 133, no. 1–3, pp. 134–146, 2003.

[262] F. ORCAN, "Parametric or Non-parametric: Skewness to Test Normality for Mean Comparison," *Int. J. Assess. Tools Educ.*, vol. 7, no. 2, pp. 236–246, 2020.

[263] P. J. Curran, S. G. West, and J. F. Finch, "The Robustness of Test Statistics to Nonnormality and Specification Error in Confirmatory Factor Analysis," *Psychol. Methods*, vol. 1, no. 1, pp. 16–29, 1996.

[264] Simon (missing) - University of Cambridge, "FAQ / Simon - CBU statistics Wiki Testing normality including skewness and kurtosis," 2018. [Online]. Available: https://imaging.mrc-cbu.cam.ac.uk/statswiki/FAQ/Simon. [Accessed: 20-Jul-2022].

[265] P. H. Westfall, "Kurtosis as Peakedness, 1905–2014. R.I.P.," *Am. Stat.*, vol. 68, no. 3, pp. 191–195, 2014.

[266] N. C. Davis, "Factors Influencing the Air Permeability of Felt and Felt-Like Structures," *Text. Res. J.*, vol. 28, no. 4, pp. 318–324, 1958.

[267] S. A. Hosseini and H. Vahedi Tafreshi, "Modeling particle-loaded single fiber efficiency and fiber drag using ANSYS-Fluent CFD code," *Comput. Fluids*, vol. 66, pp. 157–166, 2012.

[268] H. Wang, H. Zhao, Z. Guo, and C. Zheng, “Numerical simulation of particle capture process of fibrous filters using Lattice Boltzmann two-phase flow model,” *Powder Technol.*, vol. 227, pp. 111–122, 2012.

[269] R. Przekop, A. Moskal, and L. Gradoń, “Lattice-Boltzmann approach for description of the structure of deposited particulate matter in fibrous filters,” *J. Aerosol Sci.*, vol. 34, no. 2, pp. 133–147, 2003.

[270] P. Soltani, M. Zarrebini, R. Laghaei, and A. Hassanpour, “Prediction of permeability of realistic and virtual layered nonwovens using combined application of X-ray MCT and computer simulation,” *Chem. Eng. Res. Des.*, vol. 124, pp. 299–312, 2017.

[271] M. Rahimi-Gorji, O. Pourmehran, M. Gorji-Bandpy, and T. B. Gorji, “CFD simulation of airflow behavior and particle transport and deposition in different breathing conditions through the realistic model of human airways,” *J. Mol. Liq.*, vol. 209, pp. 121–133, 2015.

[272] R. G. W. Vasconcelos, N. Beaudoin, A. Hamilton, N. C. Hyatt, J. L. Provis, and C. L. Corkhill, “Characterisation of a high pH cement backfill for the geological disposal of nuclear waste: The Nirex Reference Vault Backfill,” *Appl. Geochemistry*, vol. 89, no. October 2017, pp. 180–189, 2018.

[273] E. N. Landis and D. T. Keane, “X-ray microtomography,” *Mater. Charact.*, vol. 61, no. 12, pp. 1305–1316, 2010.

[274] M. B. Afifi, A. Abdelrazek, N. A. Deiab, A. I. Abd El-Hafez, and A. H. El-Farrash, “The effects of CT x-ray tube voltage and current variations on the relative electron density (RED) and CT number conversion curves,” *J. Radiat. Res. Appl. Sci.*, vol. 13, no. 1, pp. 1–11, 2020.

[275] T. M. Buzug, *Computed tomography*, 1st ed., vol. 1. Springer, 2008.

[276] L. Li *et al.*, “Study on the origin of linear deviation with the Beer-Lambert law in absorption spectroscopy by measuring sulfur dioxide,” *Spectrochim. Acta - Part A Mol. Biomol. Spectrosc.*, vol. 275, p. 121192, 2022.

[277] T. Hagita, S. Shiotani, N. Toyama, N. Tominaga, H. Miyazaki, and N. Ogasawara, "Correlation between Hounsfield Unit values of blood in CT on immediate postmortem CT after cardiopulmonary resuscitation and antemortem hemoglobin levels," *Forensic Imaging*, vol. 30, no. August, p. 200515, 2022.

[278] P. Xue *et al.*, "Effective lung ventilation estimation based on 4D CT image registration and supervoxels," *Biomed. Signal Process. Control*, vol. 79, no. February 2022, 2023.

[279] T. B. Hunter and M. S. Taljanovic, "Foreign Bodies," *Radiographics*, vol. 23, no. 3, pp. 731–757, 2003.

[280] M. Saps, J. M. Rosen, and J. Ecanow, "X-ray detection of ingested non-metallic foreign bodies," *World J. Clin. Pediatr.*, vol. 3, no. 2, p. 14, 2014.

[281] Y. Liu, I. Straumit, D. Vasiukov, S. V. Lomov, and S. Panier, "Prediction of linear and non-linear behavior of 3D woven composite using mesoscopic voxel models reconstructed from X-ray micro-tomography," *Compos. Struct.*, vol. 179, pp. 568–579, 2017.

[282] Z. Cheng and J. Wang, "Investigation of the fabric evolution and the stress-transmission behaviour of sands based on X-ray μCT images," *Adv. Powder Technol.*, vol. 30, no. 9, pp. 1858–1869, 2019.

[283] W. Huang, P. Causse, V. Brailovski, H. Hu, and F. Trochu, "Reconstruction of mesostructural material twin models of engineering textiles based on Micro-CT Aided Geometric Modeling," *Compos. Part A Appl. Sci. Manuf.*, vol. 124, no. June, 2019.

[284] N. Sandler, K. Reiche, J. Heinämäki, and J. Yliruusi, "Effect of moisture on powder flow properties of theophylline," *Pharmaceutics*, vol. 2, no. 3, pp. 275–290, 2010.

[285] N. Otsu, "A Threshold Selection Method from Gray-Level Histograms," *IEEE Trans. Syst. Man. Cybern.*, vol. SMC-9, no. 1, pp. 62–66, 1979.

[286] A. Charvet, S. Rolland Du Roscoat, M. Peralba, J. F. Bloch, and Y. Gonthier, "Contribution of synchrotron X-ray holotomography to the understanding of liquid distribution in a medium during liquid aerosol filtration," *Chem. Eng. Sci.*, vol. 66, no. 4, pp. 624–631, 2011.

Appendices

Appendix A: Material Datasheets of New Nonwoven Filtration Media

The following data sheets pertain to the filtration media used within this thesis.

Media in Chapter 5:

GUTSCHE Textile Engineering

TECHNICAL DATA / TECHNISCHE DATEN

GUTSCHE *porotex*® PT

Type: PT083RA08X2.020

PTFE needlefelt on PTFE scrim,
dustside is made of white and brown PTFE (brown part > 20%)
with special treatment *membratex* ®
PTFE Nadelfilz auf PTFE Stützgewebe,
Anströmseite aus weißem und braunem PTFE (Braunanteil > 20%)
mit Spezialausrüstung membratex ®

Area weight *Flächengewicht*	DIN EN	29073 - part 1	830	g/m²
Thickness *Dicke*	DIN EN ISO	9073 - part 2	1,3	mm
Density *Dichte*			0,64	g/cm³
Air permeability *Luftdurchlässigkeit*	DIN EN ISO	9237	80	l/dm²min at 2 mbar (20 mm W.G./WS)
Tensile strength *Höchstzugkraft*	DIN EN	29073 - part 3		
	machine direction /	*längs*	> 65	daN/5cm
	cross direction /	*quer*	> 60	daN/5cm

continuous temperature, normal/max. 240/260 °C
Dauertemperaturbeständigkeit, normal/max.

Acid resistance *Säurebeständigkeit*	very good *sehr gut*
Alkali resistance *Alkalibeständigkeit*	very good *sehr gut*
Hydrolysis resistance *Hydrolysebeständigkeit*	very good *sehr gut*

The a.m. technical information is for indication only and subject to alteration, usual tolerances apply. Such data is to the best of our knowledge at the time of print. Admissible operating temperatures may have to be reduced according to actual operating conditions. Please get on to your contact person at GUTSCHE.
Die vorstehenden technischen Daten sind Anhaltspunkte, Änderungen und übliche Toleranzen behalten wir uns vor. Alle Angaben entsprechen bestem Wissen. Temperaturbeständigkeiten sind je nach Einsatzbedingung auch niedriger anzusetzen. Ihr GUTSCHE-Ansprechpartner informiert Sie gerne.

Revision 0, October 2012

MGF Gutsche GmbH & Co.KG
Hermann-Muth-Str. 8, D - 36039 Fulda, Germany,
Phone +49 661 83 84-0, Fax +49 661 83 84-38

GUTSCHE *porotex*®

Media in Chapter 4 and 6:

Lydall Industrial Filtration
Textile Mfg EMEA Ltd.
Hareholme Mill
Bacup Road
Rawtenstall
Rossendale
BB4 7JL
UK

T: +44 (0) 1706 214 001
F: +44 (0) 1706 830 003
www.lydallif.com
ifinfotmemea@lydall.com

Lydall
Industrial Filtration Textile Mfg EMEA
Pioneers in Global Textile Filter Media

Customer: [redacted]
Our Order Ref.: [redacted]

Customer Order No.: [redacted]
Project Ref./Name: [redacted]

Filter Bag Datasheet

Lydall Filter Bag Part No:	[redacted]	**LAB GmbH Drawing No.**	[redacted]
Product Code (Media):	[redacted]		
Fibre Blend:	P84	**Scrim Type:**	PTFE
Finish:	SINGED		
Chemical Treatment:	CR1 - A powerful fluorocarbon treatment providing liquid repellency, a certain degree of improved chemical resistance and can help control certain dust cakes		
Weight:	550g/m^2	**Thickness:**	2.75mm
Permeability:	175 $dm^3/dm^2/min$ @200Pa	**Electrical Resistance:**	N/A
	Machine Direction	**Cross Direction**	
Strength N/5cm	725	1500	
Strain at 50N / 5cm (%)	1.0	2.0	
Strain at Peak (%)	55.0	45.0	
Shrinkage at 200°C (%)	2.5	1.5	
Filter Bag Description:	Nom 6000mm o/a long x 130mm nom diameter . Open top with glass bead profile snapband in PTFE felt cuff, Single base disc with 90mm bumper reinforcement, collection outside. No welding of seams.		
Stitching thread:	PTFE		
Cell Plate:	Snapband designed to suit cell plate hole size 130mm dia (-0, +0.5) x 5mm thick		
Filter Cage:	Designed for use with filter cage, Lydall item number MC002 [redacted]		

Media in Chapter 7:

GUTSCHE
Textile Engineering

TECHNICAL DATA | TECHNISCHE DATEN

optivel® TF

Type: TP063RA12S2.260

PTFE/Polyimide needlefelt on PTFE scrim, with special treatment *membratex* ® and *antafin* ®
PTFE/Polyimid Nadelfilz auf PTFE-Stützgewebe, mit Spezialausrüstung membratex® und antafin®

Area weight *Flächengewicht*		630	g/m²	DIN EN 29073 - part 1
Thickness *Dicke*		1,6	mm	DIN EN ISO 9073 - part 2
Density *Dichte*		0,39	g/cm³	
Air permeability *Luftdurchlässigkeit*		120	l/dm²min (20 mm W.G./WS)	DIN EN ISO 9237
Tensile strength *Höchstzugkraft*	*machine direction/längs* *cross direction/quer*	> 80 > 60	daN/5cm daN/5cm	DIN EN 29073 - part 3
Continuous temperature (normal/max.) *Dauertemperaturbeständigkeit (normal/max.)*		240/260	°C	
Acid resistance *Säurebeständigkeit*		very good *sehr gut*		
Alkali resistance *Alkalibeständigkeit*		good *gut*		
Hydrolysis resistance *Hydrolysebeständigkeit*		very good - good *sehr gut - gut*		

The a.m. technical information is for indication only and subject to alteration, usual tolerances apply. Such data is to the best of our knowledge at the time of print. Admissible operating temperatures may have to be reduced according to actual operating conditions. Please get on to your contact person at Lydall Gutsche.

Die vorstehenden technischen Daten sind Anhaltspunkte, Änderungen und übliche Toleranzen behalten wir uns vor. Alle Angaben entsprechen bestem Wissen. Temperaturbeständigkeiten sind je nach Einsatzbedingung auch niedriger anzusetzen. Ihr Lydall Gutsche Ansprechpartner informiert Sie gerne.

Revision 10, February 2019

Lydall Gutsche GmbH & Co. KG
Hermann-Muth-Str. 8, D - 36039 Fulda, Germany,
Phone +49 661 83 84-0, Fax +49 661 83 84-38

GUTSCHE *porotex*®

Appendix B: Air Permeability Mapping of New Nonwoven Filtration Bag

Noticeable variation in the mass and thickness presented in the new media used within Chapter 5 led to the proposition that the new nonwoven filtration media, would also exhibit an unspecified degree of locational variation. Given the provision of new filtration media for Chapter 5, a 30cm by 100cm swath removal of a random position along the filtration bag occurred. Upon the completion of an incision about the stitch point, this allowed the media to become flat and provided feasibility towards the conduction of air permeability analysis across the sample size. Analysis occurred at five centimetre intervals across the machine and cross direction of the sample, which yielded a total of one hundred individual sample points, each with its own unique spatial location. Conduction of the air permeability assessment was at 200Pa and at a sample surface area size of 20cm2 as per the standard and methodology presented in Chapter 6.

Discussed at length in Chapter 6, previous studies of similar methodologies cover the advantages and limitations of the performance of this method, and subsequent consideration against used nonwoven filtration media. The aim therefore of this study was to ascertain two points: The value reported within the datasheet was 80ldm^{2}min^{-1}, is this representative of the random samples? And secondly, what is the anticipated variation? Figure 73 presented the standard distribution of the obtained data and demonstrated the gaussian distribution expected following the results obtained in Chapters 5 and 6. Two outliers appeared within the data, which led to the accountability of 98% of the data within the distribution. The subsequent mean was determined at 94.91±32.81 ldm^{2}min^{-1}. At the lower and upper maximum bounds, a repeat of this within a different sample would expect the resultant mean to be between 62.10-127.72 ldm^{2}min^{-1}.

This result demonstrated that it would be possible to achieve a mean air permeability of 80 ldm^{2}min^{-1}, as stated within the standard. However, given that the referenced methodology only required three different surface areas, the accuracy, in comparison to this study is lower. Whilst the manufacturer may have evaluated more, their omission of the exact number led to the assumption that the minimum required repeats happened. This may not be true, but the omission of any other indication led to difficulties in determining this. These studies mean at an increased difference of 14.91 ldm^{2}min^{-1}, is more representative of the media, however, if locational variation in the machine direction occurred, it could be that this result is artificially higher/lower than the global average. As show in Chapter 6 for used media, the air permeability varied along the machine direction. This study used industrially used filtration

media, but it demonstrated the potential variation afforded in the machine direction. As such, a repeat of this study across the full used nonwoven filtration media bag would provide a more representative mean, accounting for the variation across the full machine direction. Although, given the unambiguity surrounding the standard and the compliance to the same testing methodology for the studies sample, the resultant mean of the study is more representative of the new nonwoven filtration media, due to the increased sample size.

Consequently, the first aim can be summarised as such: Although the material datasheets air permeability is comparatively representative, the difference between it and the studies mean and variation questioned the value. Without knowing more about the sample selection method, it is difficult to validate the use without the conduction of a full assessment of air permeability in the machine direction. Therefore, in terms of absolute means, the studies mean of 94.91 ldm^2min^{-1} represented new nonwoven filtration media in internal reports and analysis of used nonwoven filtration media from the manufacturer and product.

The determined variation happened at ±32.81 ldm^2min^{-1} following analysis of 100 distinct positions on the sample. The original datasheet omitted any value which surrounded variation. This answered the second aim by demonstrating the variation in the air permeability. Utilisation of this value would occur as part of the analysis, which would provide a more detailed information about the samples received as discussed in Chapter 6.

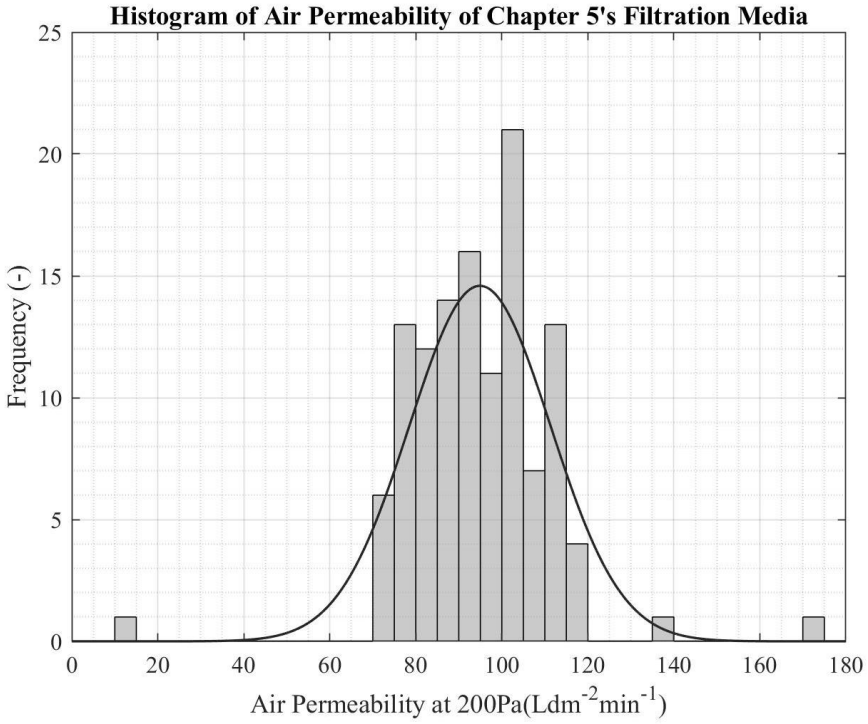

Figure 73: Histogram Distribution of the Air Permeability of New Nonwoven Filtration Media (Chapter 5's Media)

Similar to Chapter 6, given the locational information about each datapoint was known, it allowed for mapping of the air permeability to ascertain visually any variation. Figure 74 illustrated the resultant map of the air permeability. Chapter 6 disregarded direct mapping of new air permeability against the new air permeability map due to the inability to specify exactly what the air permeability was at a given point on the bag in the new condition. This led to the use of a global mean. Consequently, the air permeability map only visualised the variation. As chapter 5 did not afford an air permeability study, analysis in any fixed direction was unnecessary. However, critical analysis of the aforementioned standard in the datasheet, in collaboration with this data, would ascertain any localised variation in the fixed direction, and any potential variation in random sampling. Therefore, future studies surrounding this media and industrially used filtration media, would require the analysis performed in Chapter 6 before conclusion of a decision about the applicability of the standard, or any regions of statistically significance.

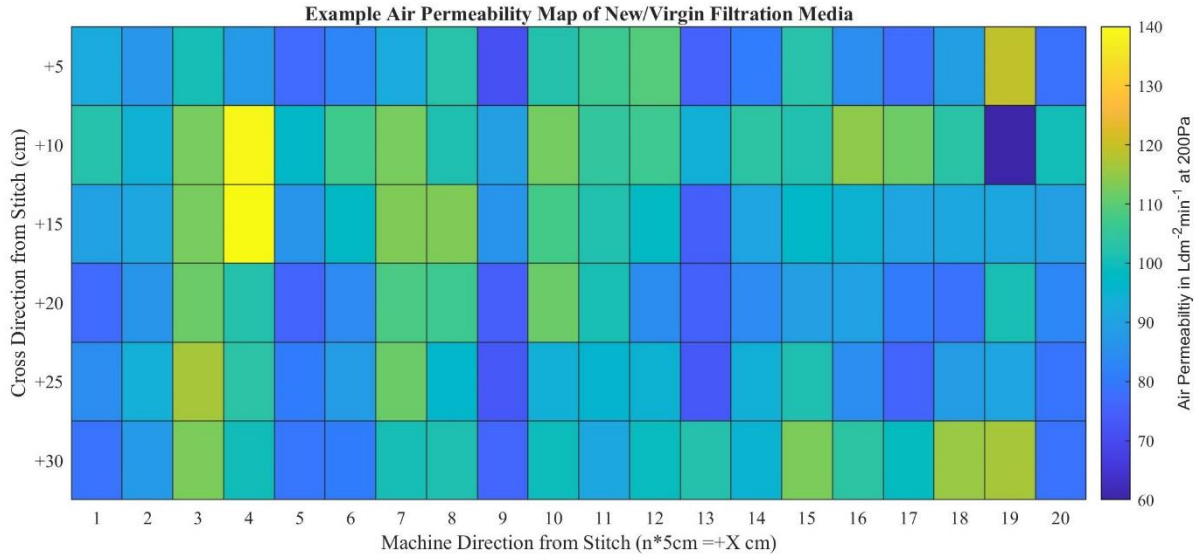

Figure 74: Air Permeability Map of New Nonwoven Fitlration Media (Chapter 5's Media)

Appendix C: µCT Images

A detailed discussion about the use of microcomputed tomography is available in Chapter 7. Prior to the analysis of the samples generated in this chapter, new and industrially used nonwoven filtration media occurred using this technique. Found below, are example tomographs with relevant descriptions attached to each example. The original datafiles are available upon request. A selection of this data appeared in the FERIA conference paper, with the preliminary results reported internally before being authorised for the conference.

Figure 75 and Figure 76 portrayed the X-ray's taken of the AR and PC samples side profile. In these X-rays, the darker the region, the denser the region. These X-ray images detailed the scrim location, and how it changed through the sample, suggesting the warp and weft directions of the scrim. The filtrate evolution through the sample appeared to vary from the regions. Of particular note was the N=3 AR sample which exhibited large deposits at the surface. In both the AR N=2 and N=3 samples, the extent of depth filtration was more prominent. Once cleaned, Figure 76 suggested that the extent of this depth filtration, given the removal of the filtrate above the surface of the media. Minimal change in the X-rays between AR and PC N=1 suggested that the majority of the filtrate deposition was depth filtration. N=2 recovered slightly, but the best overall recovery was the N=3, which upon cleaning suggested only a marginal extent of depth filtration.

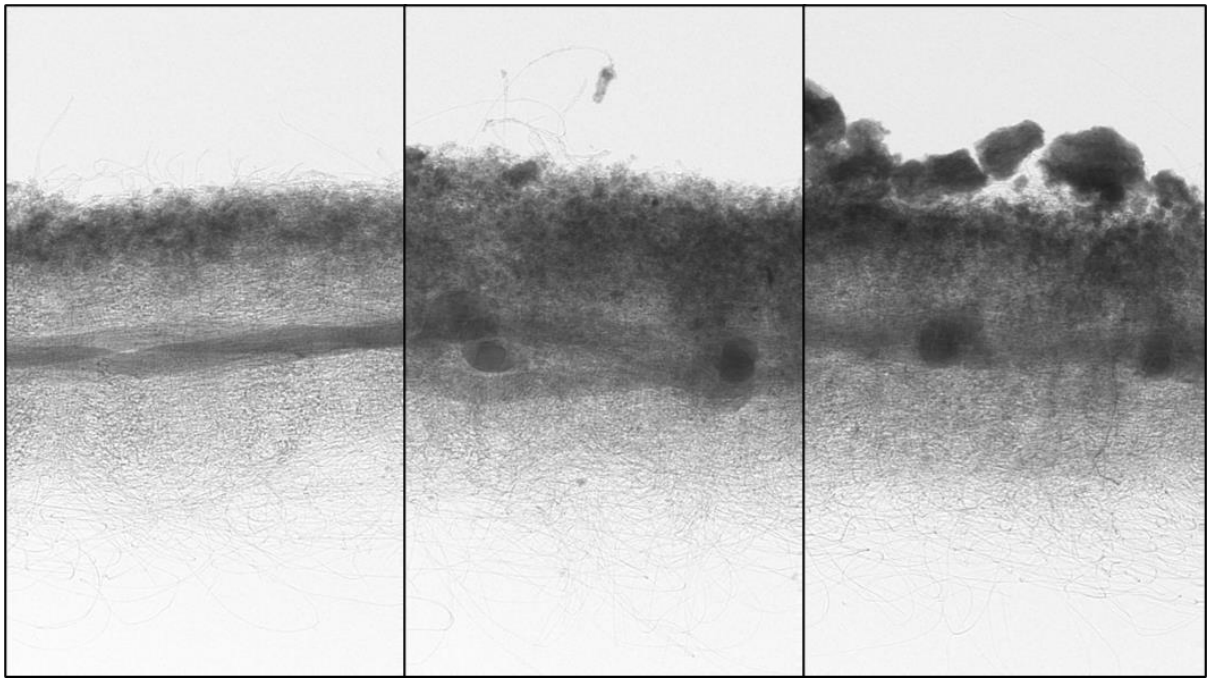

Figure 75: X-ray Images of N=1 (Left), N=2 (Middle), and N=3 (Right) of An AR State Sample from a Biomass Combustion Site (Site C). Note: The Air Entry Side is at the Top of the Image. Darker Regions Represent a Denser Material Present

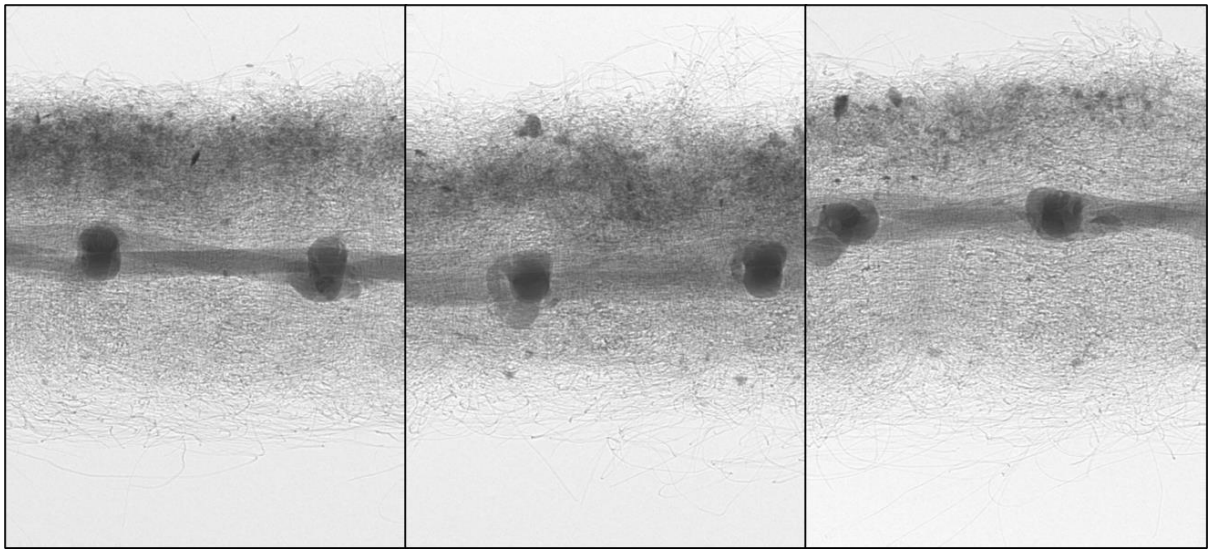

Figure 76: X-ray Images of N=1 (Left), N=2 (Middle), and N=3 (Right) of An PC State Sample from a Biomass Combustion Site (Site C). Note: The Air Entry Side is at the Top of the Image. Darker Regions Represent a Denser Material Present

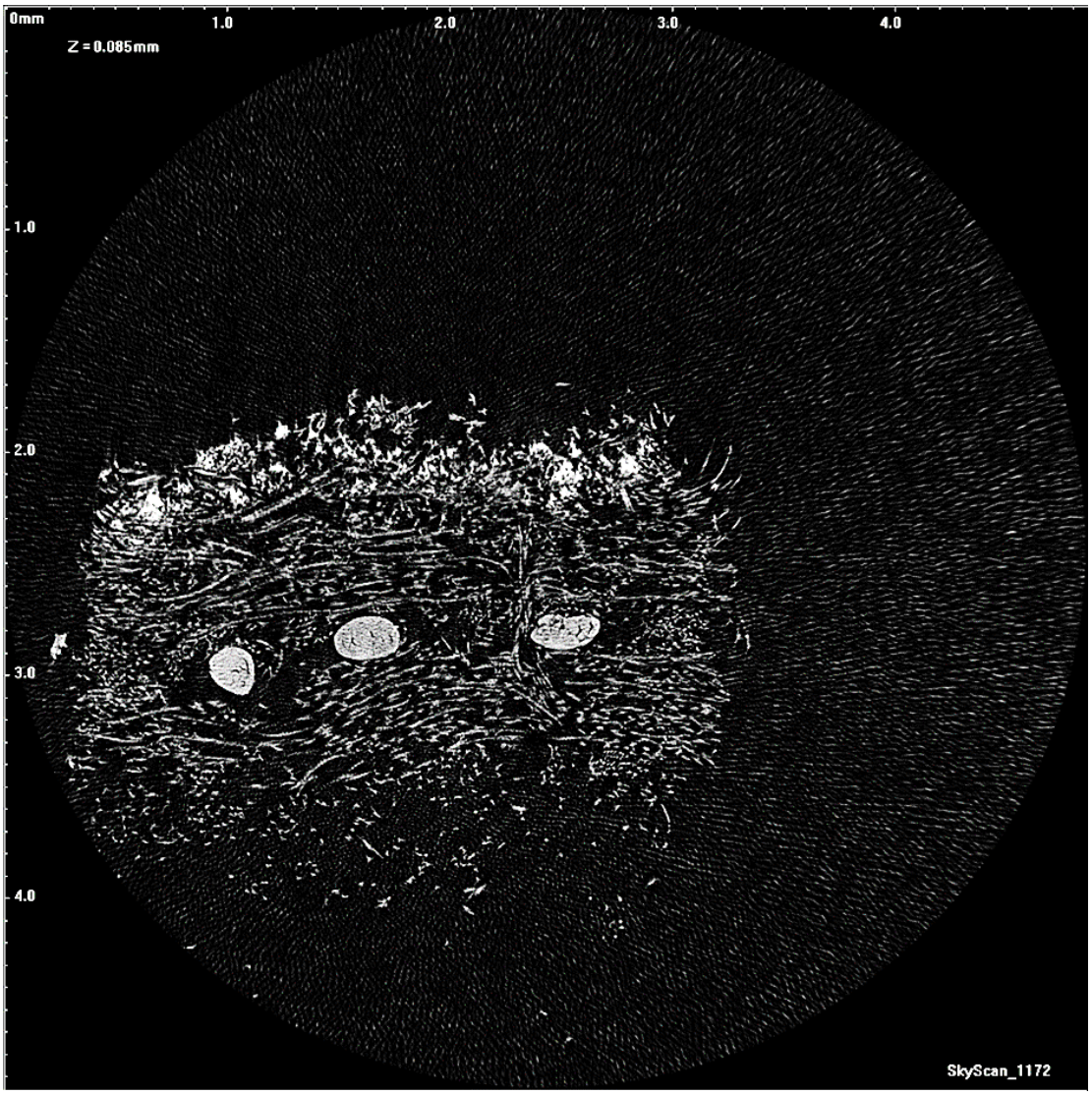

Figure 77: Tomographic Example of AR N=1 from Site C. Note: Air Entry Side is at the Vertical Top of the Tomograph

Figure 77 provided an example of the tomograph for an as received N=1 sample from Site C. The resultant tomograph illustrated the porosity within the sample. Three cylindrical like fibres represented the PTFE scrim. Micropores exhibited within these apparent cylinders, which would affect the overall porosity of the sample. At the air entry side, the deposition of filtrate is more noticeable. At the micro level, the extent of the deposition is dependent on the how density of the filtrate packing, how the filtrate has reacted, and how the filtrate interacts when deposited. At varying levels across the z-plane, the extent of deposition can be variable. As such, it is necessary to perform analysis over multiple tomographs to obtain an average.

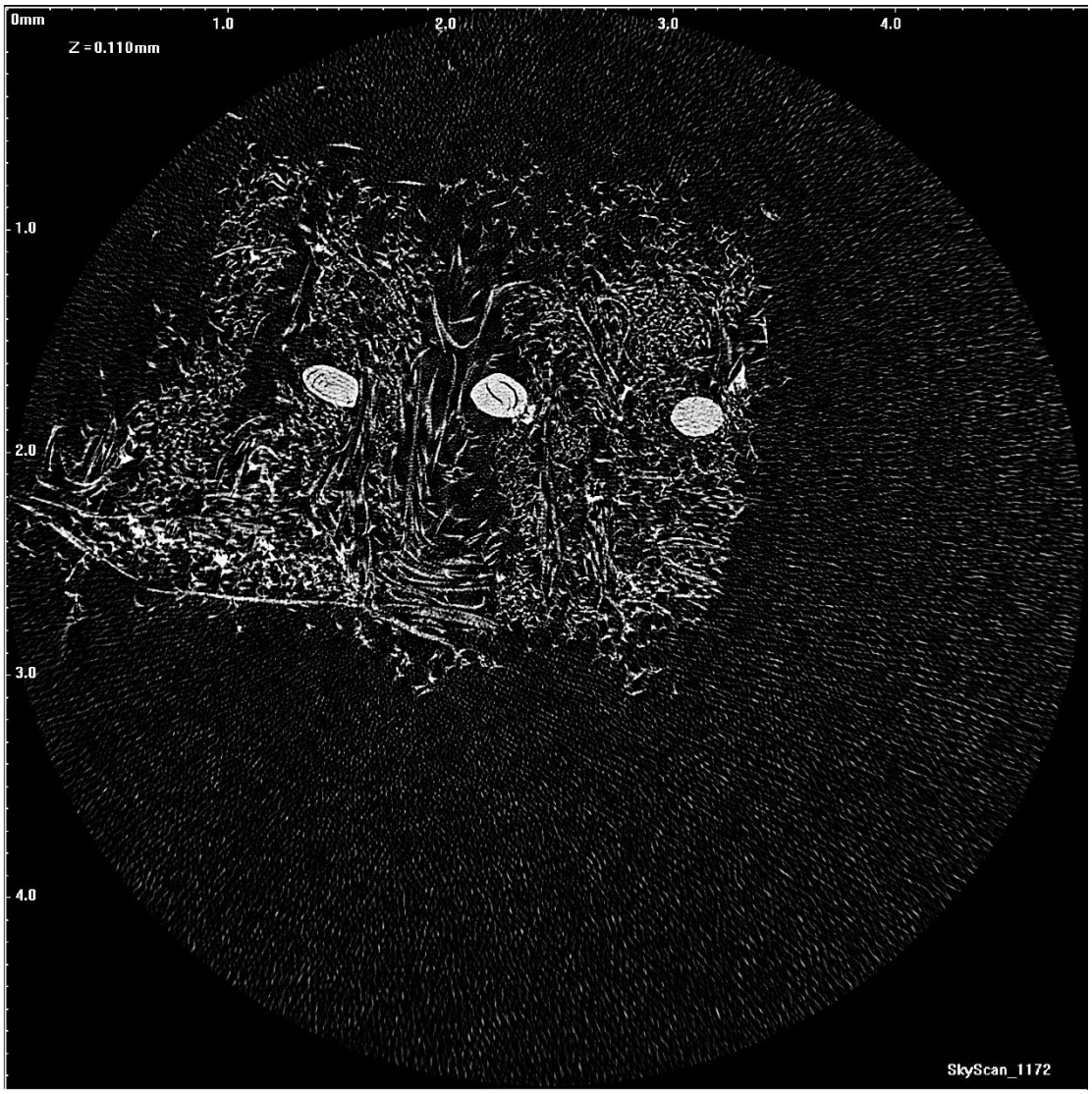

Figure 78:Tomographic Example of AR N=1 from Site C. Note: Air Entry Side is at the Vertical Bottom of the Tomograph

Figure 78 presented the PC N=1 sample. Unlike the AR N=1 cycle the filtrate was less pronounced. This is due to the cleaning method employed to remove the filtrate. Although removal of the surface filtrate appeared successful visually, a small proportion remained just below the surface, which demonstrated the depth filtration that had taken place. Indeed,

throughout the sample, evidence of internal deposition pockets at different depths. Like the AR sample, large pores near the scrim points where shown. For both Figure 78 and Figure 77, the thickness of the media appeared significantly larger than the original media presented in Figure 79.

Figure 79 illustrated the new media, detailing a profile X-ray of the sample, and a tomograph slice which demonstrated the cross piece of the scrim.

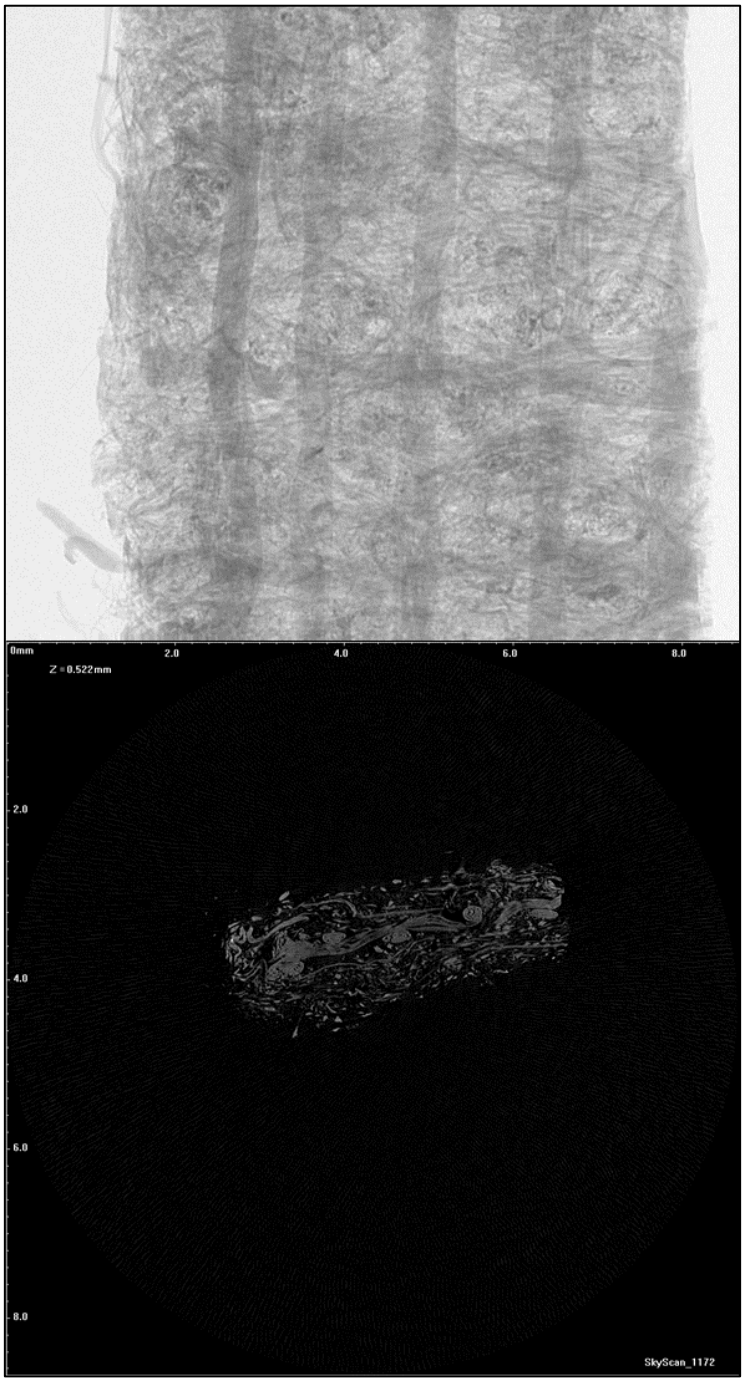

Figure 79: Example of Combustion Site C's Non-Woven Filtration Media X-ray (top) and Tomograph (Bottom)

Appendix D: SEM Images

During the project, a selection of SEM imaging and SEM-EDX analysis, conducted on new/used filtration media and fly ash from various combustion sites within the U.K., occurred. Presented below is a selection of these results, presented into two constituent parts: Images and EDX results. Likewise in Appendix C, the original images and data are available upon request.

Part A: SEM Images

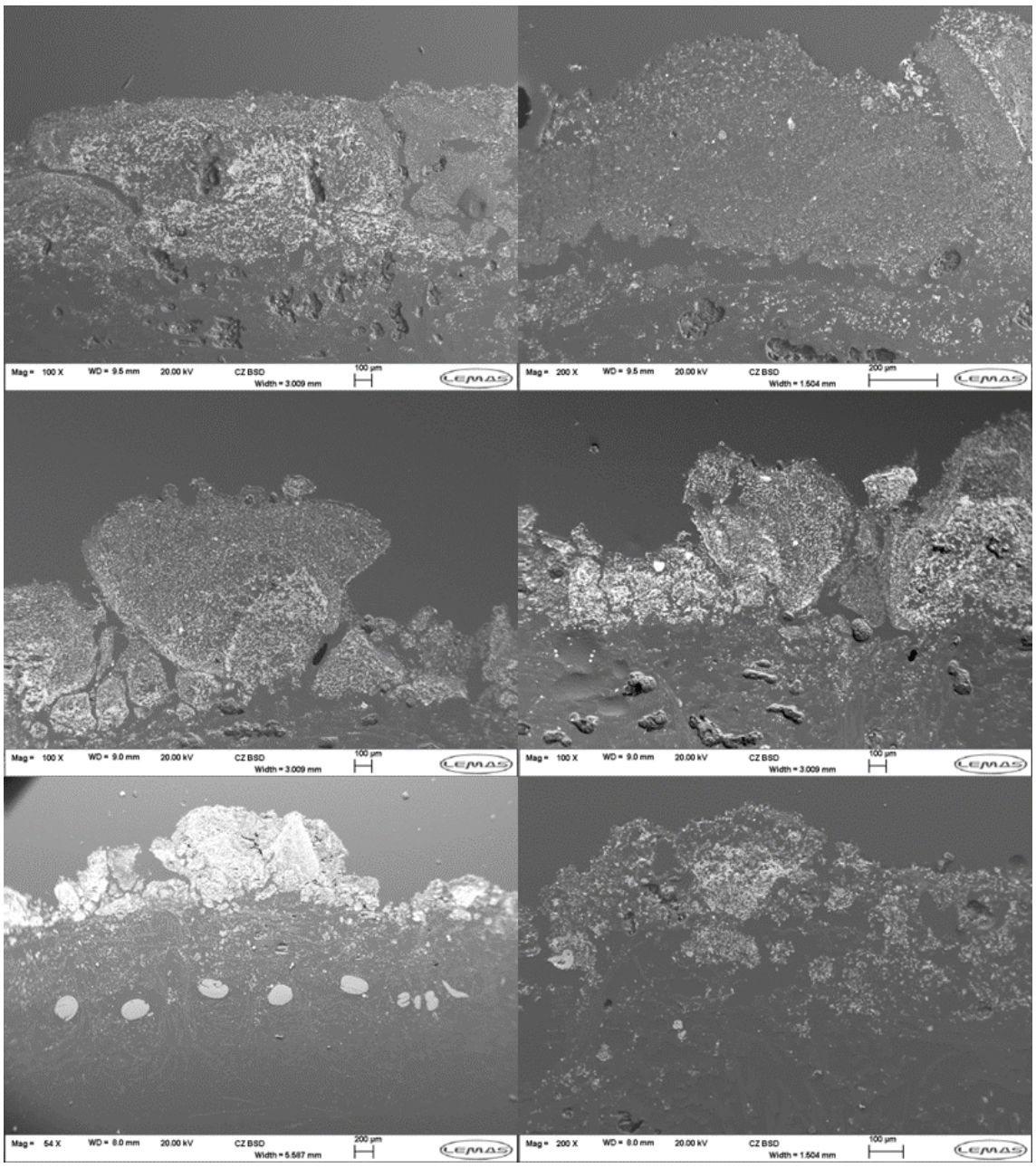

The above images represent the filtrate deposition at and above the surface of the media. Each row represented the vertical top middle and bottom (1,2, and 3) respectively. These SEM images detail the variation of the filtrate on the surface for Site B at a given plane.

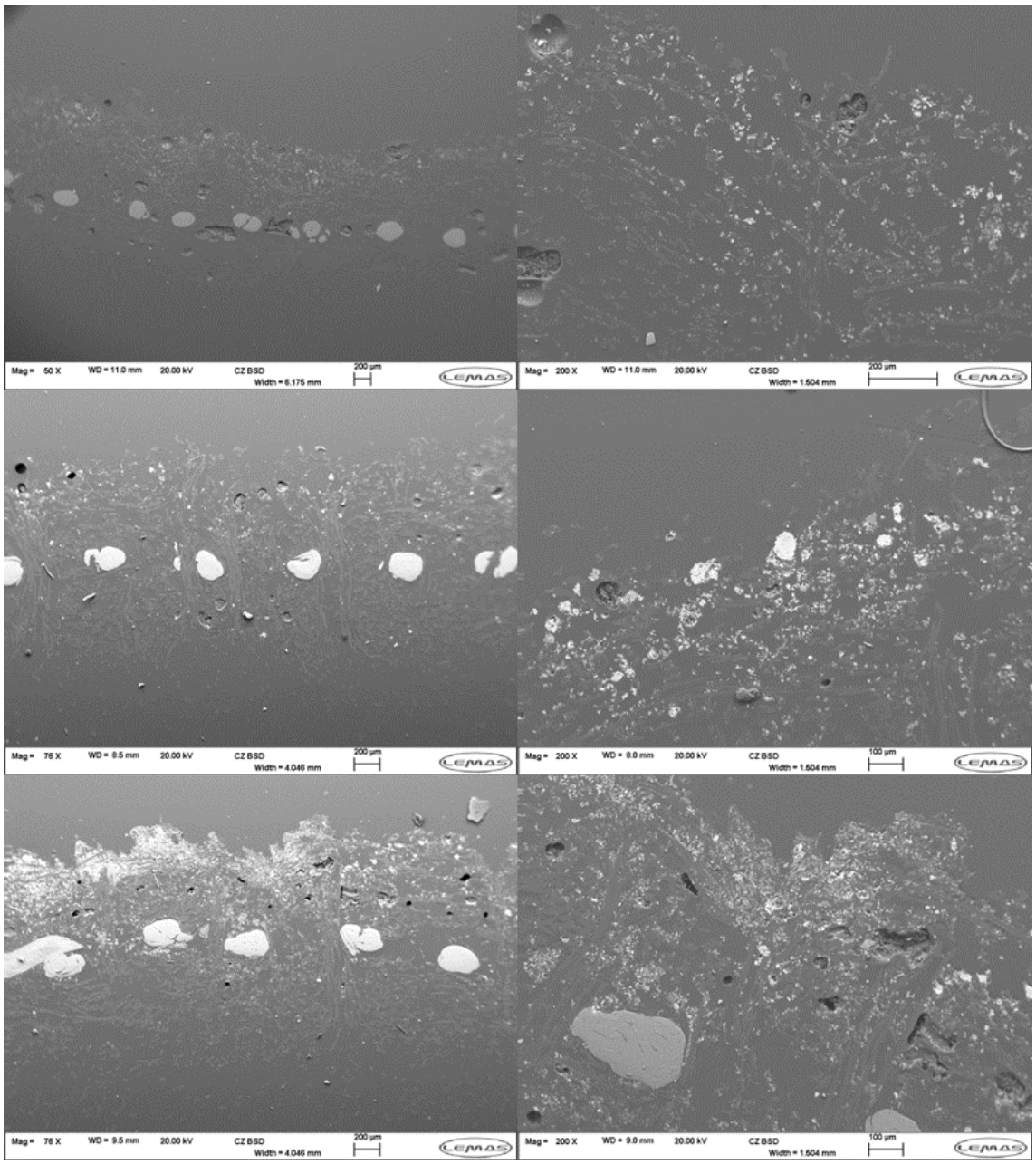

The samples, from the same site and layout as the previous group are the PC state version. As defined in Chapter 4, which used the same filtration media as that presented in these two figures, the employed cleaning method was vacuuming to remove the filtrate. Following cleaning, whilst filtrate remained for the N=1 and N=2 samples, as shown just below the surface, a larger proportion remained for the N=3.

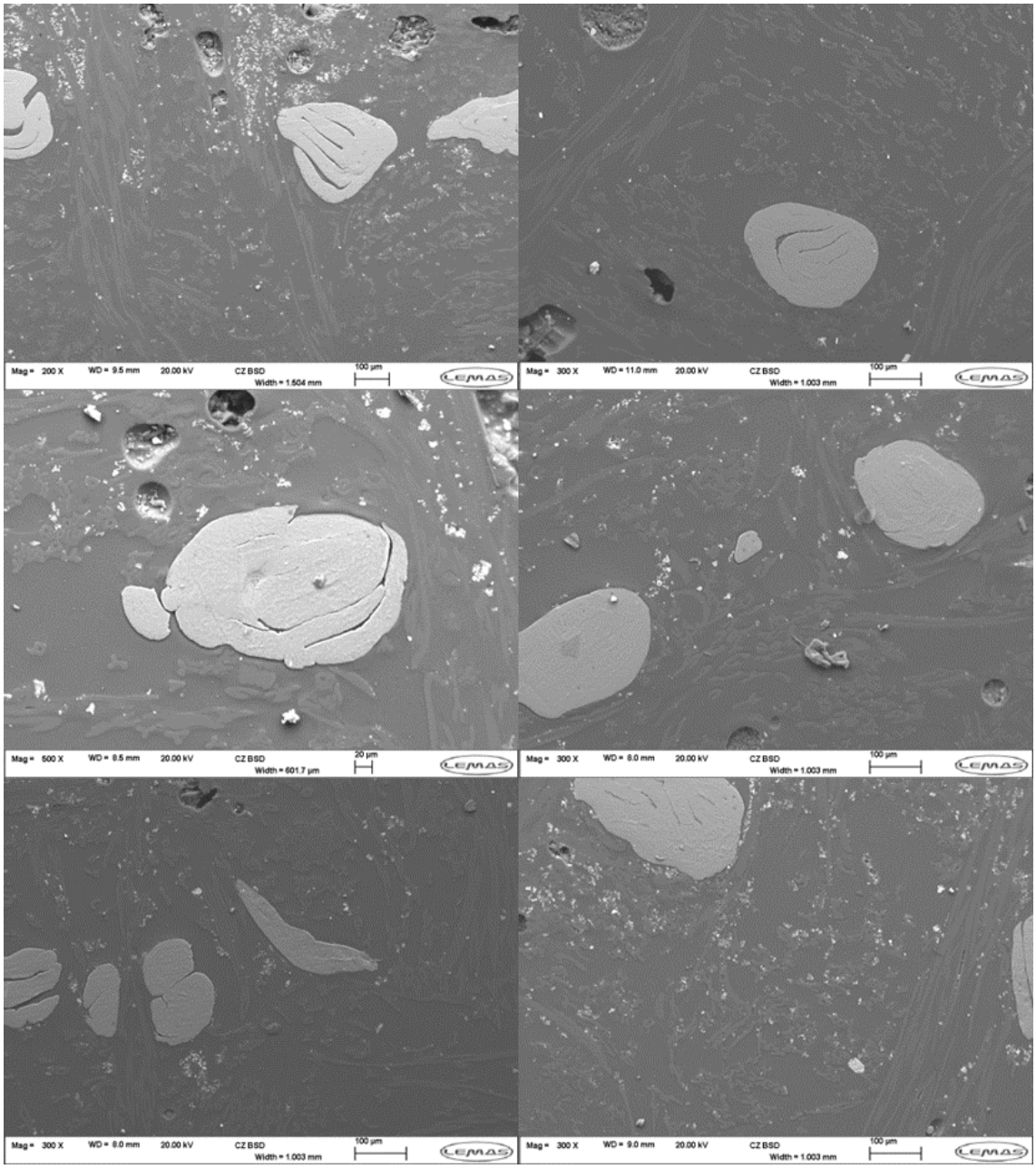

Images above detailed the variation in scrim shape. Assumed near cylindrica, it is evident that the resultant shape can vary drastically. Scrim points exhibited a branch like structure, which could originate from the manufacture process of the scrim itself, or during the manufacture of the final product. The SEM image on the bottom left showed the needle of the fibres going through the scrim itself, which suggested it had divided. Internal deposition about the scrim occurred. The SEM image on the top left of the above group showed a two needlepoints and cold suggest that filtrate began to “flow” through this point more readily than the surrounding media. The next SEM image provided a clearer image of this potential phenomenon at a different location.

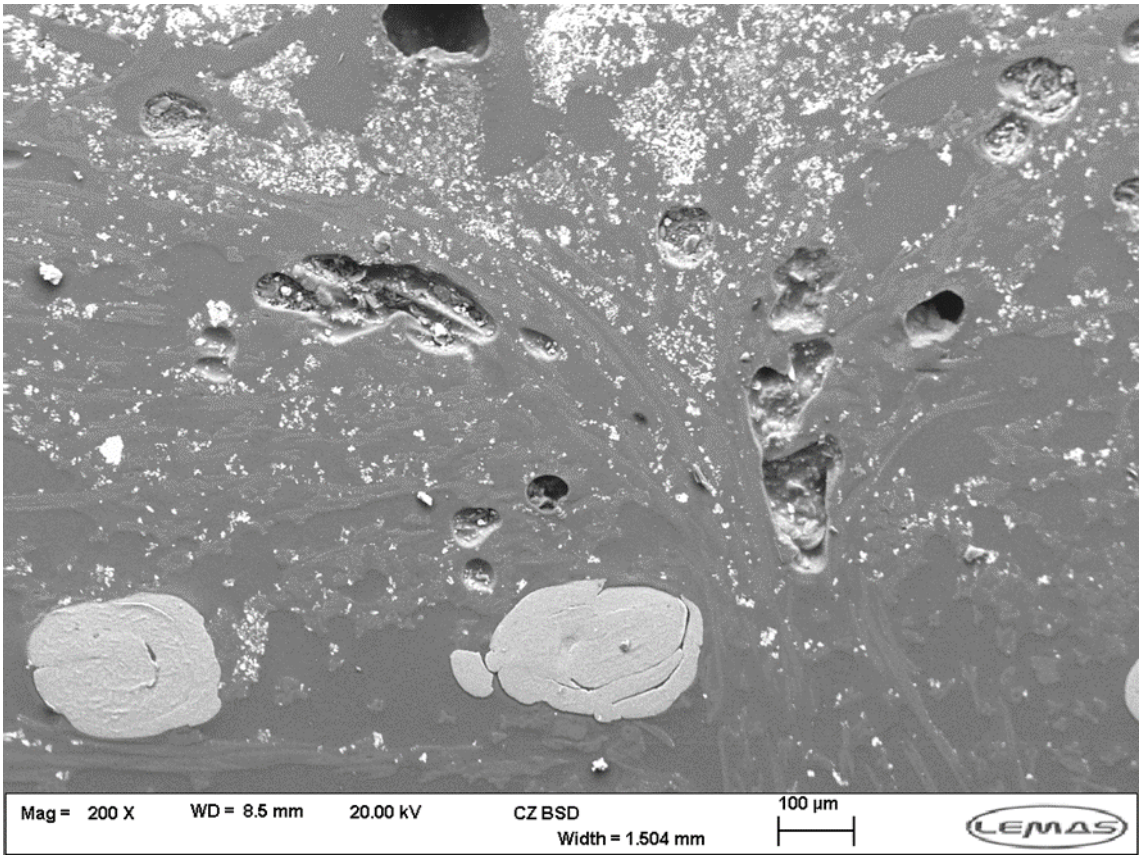

Further examination of any available stitch point positions within a fixed sample demonstrated comparable results, to varying extents as the above image. Here, the stitch point at the air entry side of the sample has transitioned through the media, as required. It appeared that one of the side effects of this is the creation of a channel like structure within the media. As the channel reached the air entry surface, it appeared to curve off towards the left and right side, which created a large groove within the surface. On nonwoven filtration media that is needle felted, the appearance visually of this is a darker, round mark on the surface. Under SEM examination of this effect using industrially derived (used) media, is possible. In the above SEM image, the filtrate appeared to flow more readily into the channel, which severely affected the amount of filtrate deposited internally. On all the Filtration samples evaluated from comparable sites and media, there was no recorded incident where this channel was fully saturated through the entire thickness of the media. Though the observations made would suggest the possibility of this occurring. Evaluation of the same site, over different operational periods would aid in identification of this phenomenon and attempt to determine when filtrate has fully transitioned through the media and contributing to emissions.

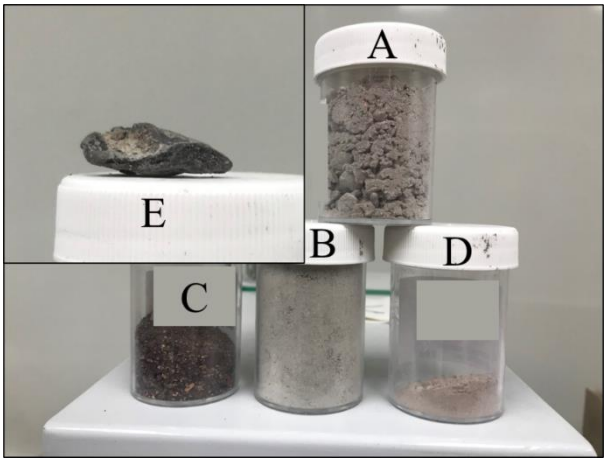

Figure 80: Samples A-E for SEM and SEM-EDX Analysis

Five additional samples where ran as part of an internal report to aid in quantifying the structure and chemical composition of the samples. The above image, labelled A through E provided a visual example of these samples. Apart from sample E, these samples appeared in a powder form. Samples A, B, and D where fly ash from two different sites. Samples B and D where from the same site, but from various locations. Sample C was debris found in the vertical bottom of the filtration bag. Samples from different sites presented this debris also. Sample E was one of multiple significantly large agglomerates of fly ash on the air entry side of a filtration bag. These agglomerates where heavy and unseen before. Figure 81 through to Figure 85 illustrated some of the obtained images of the samples shown in Figure 80.

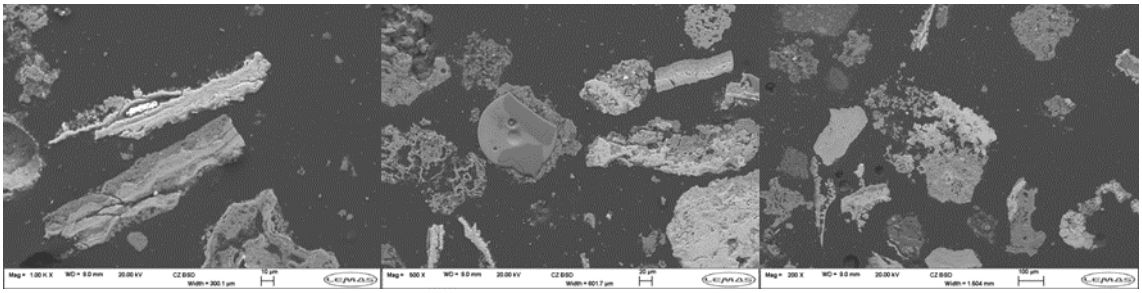

Figure 81: Sample A Images

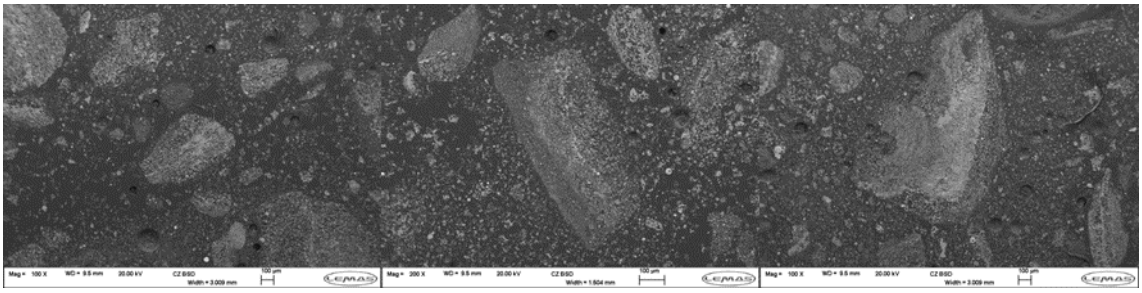

Figure 82: Sample B Images

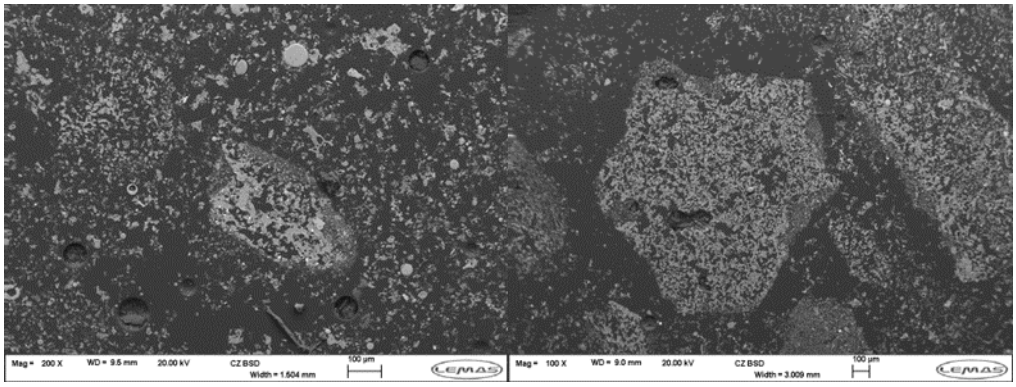

Figure 83: Sample C Images

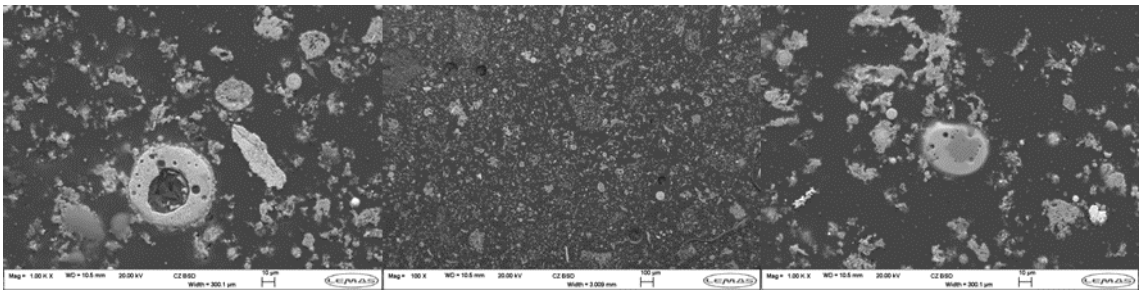

Figure 84: Sample D Images

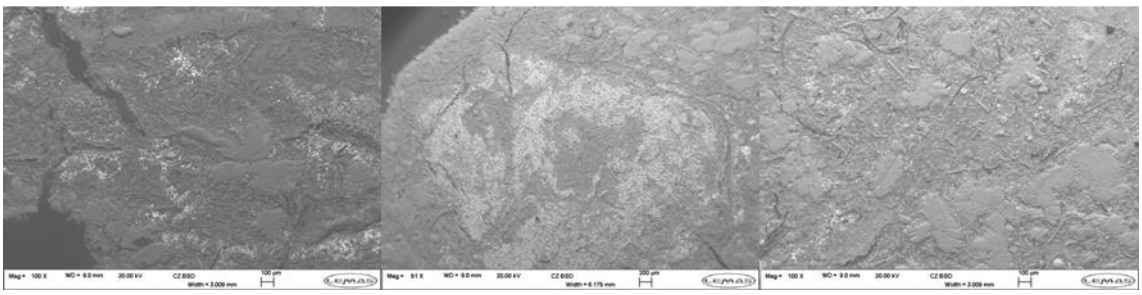

Figure 85:Sample E Images

Part B: SEM-EDX Analysis

The following table demonstrated the range of results obtained from spectral analysis across each of the samples illustrated in Figure 80.

	Sample				
Element	D	B	C	E	A
C	31.05	52.62	40.02	47.30	30.58
O	39.75	28.52	36.32	23.27	38.25
F	0.09	0.00	0.18	0.02	1.41
Na	1.96	1.47	2.18	2.27	0.61
Mg	0.98	0.07	0.65	0.28	0.23
Al	2.16	0.63	1.08	0.42	0.36
Si	5.72	0.74	6.54	2.86	3.63
P	1.40	0.01	0.03	0.12	0.51
S	2.69	5.94	4.82	3.25	2.09
Cl	0.44	1.12	0.73	9.55	0.58
K	1.34	1.82	2.21	2.18	0.29
Ca	8.32	6.43	4.33	5.85	6.76
Sc	0.00	0.06	0.00	0.08	0.00
Ti	0.42	0.01	0.08	0.01	0.07
V	0.00	0.01	0.13	0.00	0.00
Cr	0.00	0.00	0.00	0.01	2.65
Mn	0.05	0.00	0.00	0.00	0.23
Fe	3.28	0.09	0.30	0.08	11.01
Ni	0.00	0.00	0.00	0.00	0.60
Cu	0.00	0.00	0.01	0.00	0.00
Zn	0.41	0.51	0.51	0.94	0.12
Ba	0.00	0.00	0.00	0.11	0.00
Pb	0.00	0.00	0.00	1.50	0.00

Table 45: Average Percentile of all Spectral Analysis Taken for Samples A to E

	Sample				
Element	D	B	C	E	A
C	14.66	38.2	15.27	25.83	15.3
O	20.91	20.8	20.99	9.64	24.2
F	0	0	0	0	0
Na	0	0	0.14	0	0
Mg	0	0	0	0	0
Al	0	0	0	0	0
Si	0	0.21	0.19	0	0
P	0	0	0	0	0
S	0	0	0	0	0
Cl	0	0.07	0	0.2	0
K	0	0	0.34	0	0
Ca	0	2.15	0	0.7	0
Sc	0	0	0	0	0
Ti	0	0	0	0	0
V	0	0	0	0	0
Cr	0	0	0	0	0
Mn	0	0	0	0	0
Fe	0	0	0	0	0
Ni	0	0	0	0	0
Zn	0	0.26	0	0	0
Ba	0	0	0	0	0
Pb	0	0	0	0	0

Table 46: Minimum Percentile of all Spectral Analysis Taken for Samples A to E

	Sample				
Element	D	B	C	E	A
C	66.28	68.78	69.11	60.82	63.63
O	52.69	36.09	53.68	48.11	56.41
F	1.79	0	2.16	0.29	24.05
Na	11.23	3.72	7.59	10.67	5.37
Mg	9.22	0.19	7.31	3.55	2.11
Al	14.81	4.75	6.59	1.79	4.24
Si	21.98	3.91	23.56	31.83	28.28
P	10.57	0.11	0.24	1.68	8.3
S	11.75	10.89	11.15	12.3	10.11
Cl	2.11	2.08	2.17	20.45	1.1
K	8.76	5.15	9.23	16.37	0.88
Ca	22.83	16.77	12.52	13.55	23.53
Sc	0	0.42	0	1.21	0
Ti	4.65	0.06	0.64	0.11	1
V	0	0.09	1.53	0	0
Cr	0	0	0	0.09	11.8
Mn	0.53	0	0	0	0.91
Fe	32.75	0.5	2.79	0.57	37.69
Ni	0	0	0	0	2.93
Zn	1.28	0.78	1.53	2.77	0.82
Ba	0	0	0	1.65	0
Pb	0	0	0	22.56	0

Table 47: Maximum Percentile of all Spectral Analysis Taken for Samples A to E

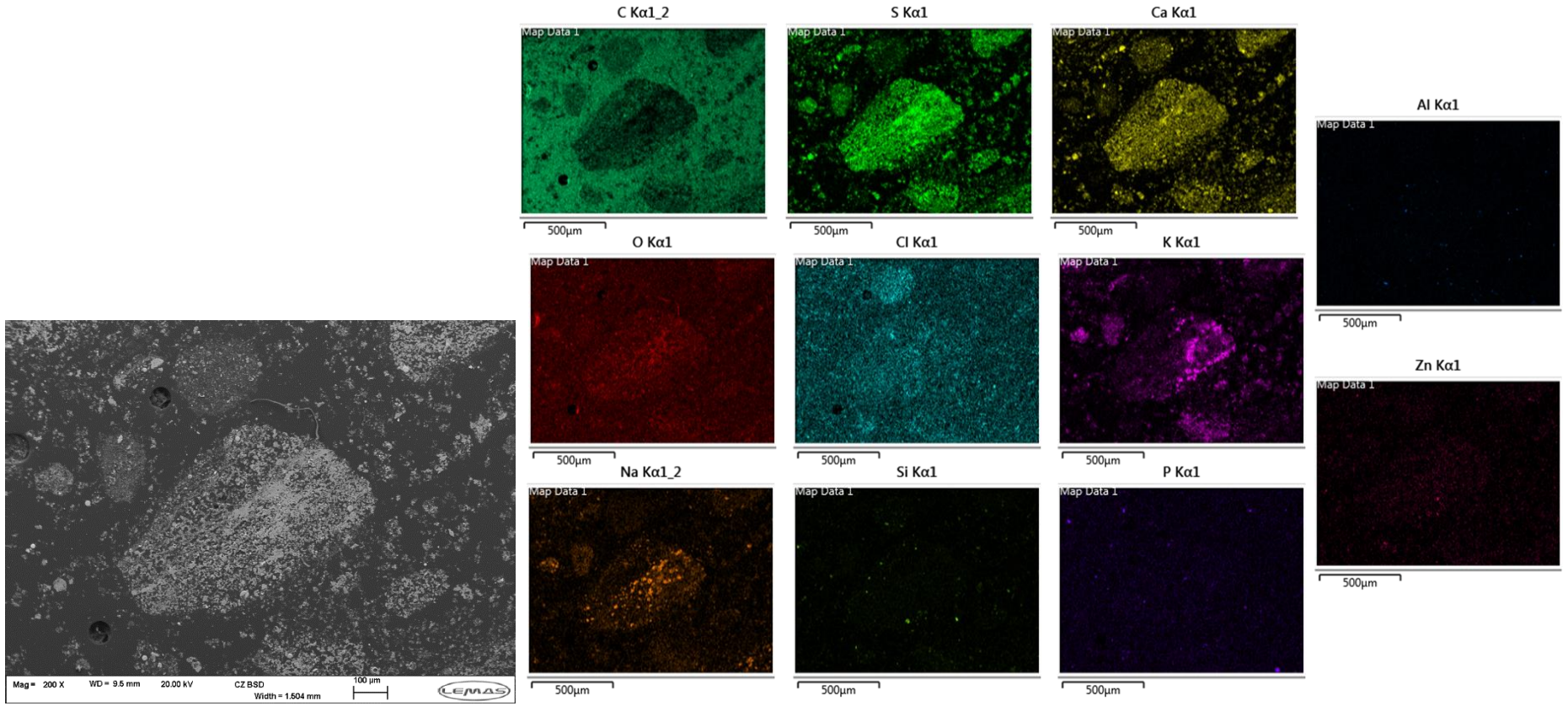

Figure 86: Sample A EDX Elemental Mapping

Figure 86 provided an illustrative elemental map of the observable elements within the defined region.

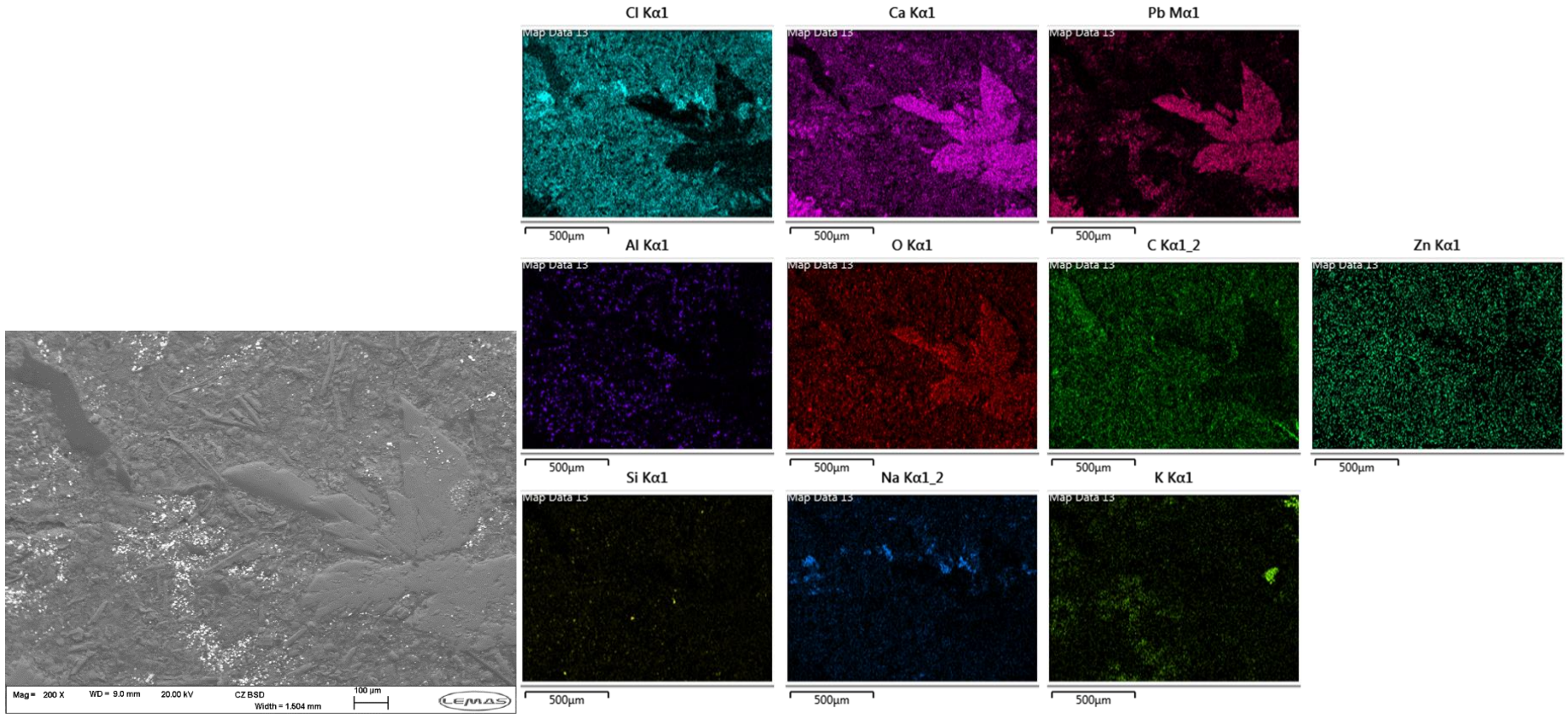

Figure 87: Sample E EDX Elemental Mapping

Figure 87 provided an illustrative elemental map of the observable elements within the defined region.

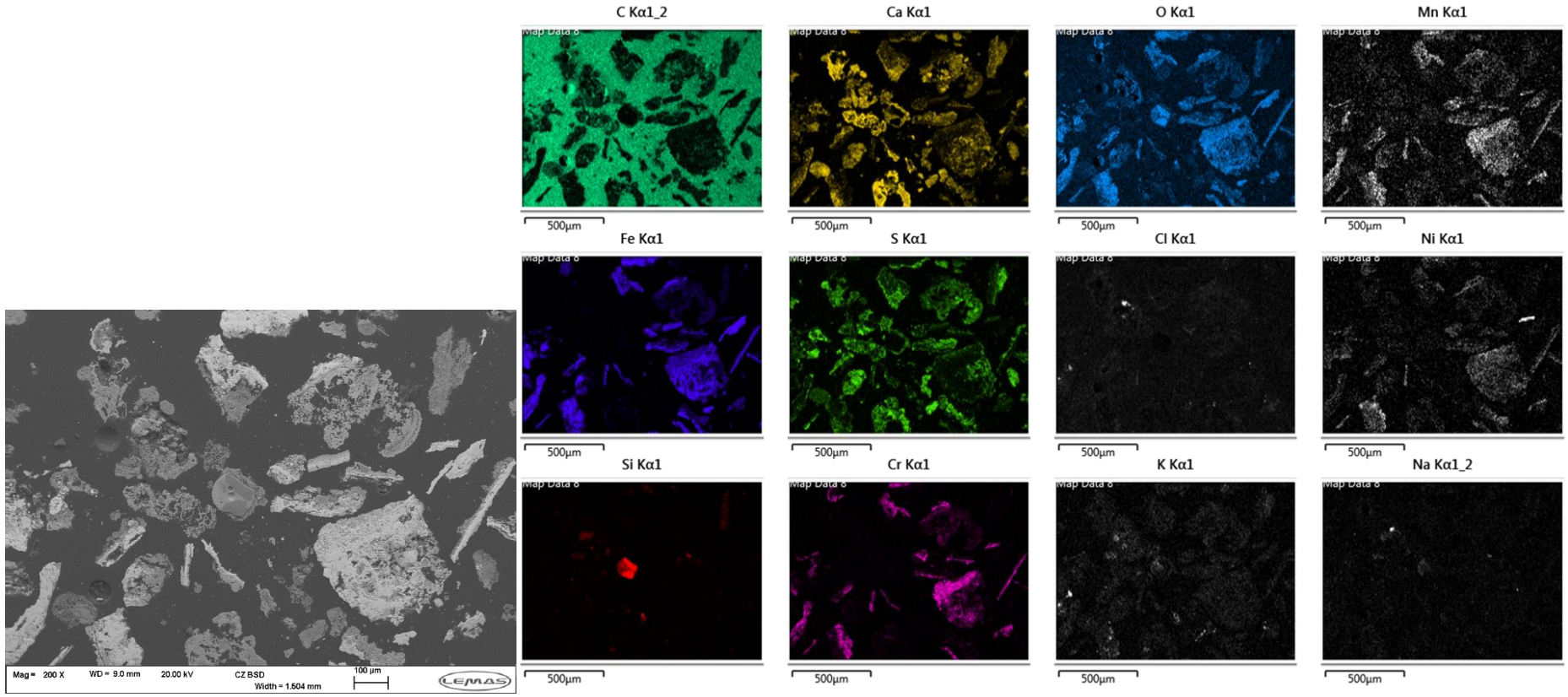

Figure 88: Sample A EDX Elemental Mapping

Figure 88 provided an illustrative elemental map of the observable elements within the defined region.

Appendix E: Industrial Contribution Reports/ Executive Summaries

During the four years of this project, the author has made a considerable number of industrial contributions. A summary of the key reports presented to the industrial partner, including submission dates are in the table below. These internal reports helped to guide, support, and develop techniques at the industrial partners laboratory. As such, redaction of specifics protected customers, but still allowed for the demonstration of the contribution. Reflection of this redaction is visible in the labels used to represent different sites or customers through the use of different letters for each specific site or customer.

Title	Date	Description
Particle Size Distribution Study	31/07/2019	Particle size distribution in the wet and dry phase of seven samples from distinct locations.
VOC Analysis using GC-MS	23/08/2019	Analysis of six samples using GC-MS to determine the presence of specific VOC's and general composition.
Site D Analysis	30/06/2021	Six filtration bags from industry required standard laboratory analysis. A draft version of the report was handed over internally for review before publishing to the customer.
Conceptual Air Permeability Study	08/07/2021	An air permeability study using two sections of remaining filtration media not used during standard analysis. This developed the methodology and idea for Chapter 6.
Site F Analysis	19/08/2021	Five filtration bags from industry required standard laboratory analysis. A draft version of the report was handed over internally for review before publishing to the customer.
Site B Analysis	05/10/2021	Twenty-four filtration bags from industry required standard laboratory analysis. A draft version of the report was handed over internally for review before publishing to the customer.
Site B SEM-EDX Analysis	13/10/2021	Samples taken from the bulk media remaining from standard testing underwent SEM-EDX analysis to further understanding and suggest variations within the vertical height of the used filtration media.
Free Lime	02/11/2021	Continual improvements of the laboratory led to the

Determination Methodology and Analysis (Site G) Free Lime Determination Methodology and Analysis (Site G) [Continued…]		request to extend the available testing facilities to offer and include free lime determination. Following a review of literature and potential methods found, deployment of identified experimental apparatus and consumables, and set up, and method evaluation using known samples, an SOP for industrial derived samples occurred. This facilitated towards the development of the laboratory and widened the range of analytical services available. Site G underwent evaluation of free lime of five different samples to demonstrate the results.
Moisture Determination Methodology	16/11/2021	Continual improvements of the laboratory led to the request to extend the available testing facilities to offer and include moisture determination. Following a review of literature and potential methods found, deployment of identified experimental apparatus and consumables, and set up, and method evaluation using known samples, an SOP for industrial derived samples occurred. This facilitated towards the development of the laboratory and widened the range of analytical services available. Following development, multiple samples underwent moisture evaluation, including both ash and filtration media.
Site H Analysis	16/11/2021	Six filtration bags from industry required standard laboratory analysis. A draft version of the report was handed over internally for review before publishing to the customer.
Site I Weight Determination Analysis	01/12/2021	Analysis of a used filtration bag which presented with a significantly wet filtrate on the surface which was clay like. Weight analysis demonstrated the difference between a "normal" sample from the same site and compartment.
Site J Moisture	06/12/2021	Conduction of moisture analysis on six filtrate samples,

Analysis		three each from two filtration bags.
Site D and E SEM-EDX Analysis	07/01/2022	Detailed review of All samples shown in Figure 80 See appendix D
Various Laboratory Tasks/Analysis	01/02/2022 To 31/12/2022	Performed analysis using various analytical methods across a wide range of samples.

Table 48: List of Internal Reports/Analysis Performed Over the Duration of the Project